PROGNOSTICATION AND PREDICTION OF CANCER PATIENT OUTCOMES USING AI-BASED CLASSIFIERS

von der Fakultät Energie-, Verfahrens- und Biotechnik der Universität Stuttgart
und dem Stuttgart Center for Simulation Science
zur Erlangung der Würde eines
Doktors der Naturwissenschaften (Dr. rer. nat.) genehmigte Abhandlung

Vorgelegt von
Cristiano Guttà
aus Bari, Italien

Hauptberichter: **Prof. Dr. Markus Morrison (Rehm)**

Mitberichter: **Prof. Dr. Nicole Radde**

Prof. Dr. Thomas Sauter

Tag der mündlichen Prüfung: 17.05.2023

Institut für Zellbiologie und Immunologie der Universität Stuttgart

2023

A Papà, che mi ha insegnato a "non perdere mai la Strada Maestra".

CONTENTS

ERKLÄRUNG

Hiermit erkläre ich, dass die vorliegende Arbeit von mir persönlich ohne unrechtmäßige Hilfe angefertigt wurde. Verwendete Daten, Grafiken und Informationen, die nicht von mir stammen wurden entsprechend gekennzeichnet.

DECLARATION

I hereby declare, that this thesis was prepared by myself without illegal help. Where information has been derived from other sources, I confirm that this has been elucidated in the thesis.

Stuttgart, 16.01.2023

Cristiano Guttà

SUMMARY

In recent years, it has been unanimously recognized that a “one size fits all” approach cannot be applied to cancer patient management, due to the extreme inter-individual variability and intra-tumor heterogeneity. For these reasons, prevention, diagnosis, prognosis and treatment interventions are based on the analysis of several parameters. Readily available information like family history and lifestyle or environmental factors are integrated with quantitative data including, among others, gene and protein expression, which require high expertise and costly procedures to be generated. Given the complexity, non-linearity and high dimensionality of these data, classical statistical approaches may be insufficient to confidently identify patterns correlating e.g. with treatment response or patient survival. In addition, the advances in computing hardware performance together with the increasing quality and quantity of high-throughput data, have boosted the interest in artificial intelligence (AI) application to oncology. In particular, machine learning (ML) and deep learning (DL) methods have shown unprecedented potential when applied to a wide variety of data, ranging from medical imaging to multi-omics datasets. In particular, ML is a subset of AI methods designed to make decisions on unseen samples based on the experience gained on training data. DL is a subfield of ML based on artificial neural networks, algorithms designed to resemble human cognition, and can be used to solve tasks too challenging for classic ML algorithms.

In this work, the development and application of AI-based classification frameworks to generate case-specific predictions in three use-cases is described. Different levels of complexity are considered, upscaling from pathway-specific data generated from cell lines to patient biopsies and full transcriptome profiles. Each of the presented approaches showcase the potential of ML/DL pipelines in aiding and informing clinical decision making. The first two approaches focus on the cellular process of apoptosis, the main cell death modality often deregulated in cancer. Targeting this pathway in otherwise resistant tumors may represent a promising treatment strategy if appropriate patient selection is performed. To reach this goal, the baseline expression of key regulators was analyzed to identify signatures predictive for treatment efficacy or correlated with patient prognosis.

In the first study, a data-driven modelling pipeline was devised to predict the response of melanoma cell lines to a novel apoptosis inducing treatment strategy. The protein

expression of 19 key apoptosis regulators was quantified in 16 melanoma cell lines together with responses to IZI1551, a hexavalent tumor necrosis factor (TNF)-related apoptosis-inducing ligand (TRAIL) receptor agonist, in combination with the inhibitor of apoptosis (IAP) antagonist Birinapant. These data were used to train a pattern recognition framework for predicting case-specifically synergistic behaviors and identifying putative responders. When challenged to predict the response of tumor cell spheroids and cells isolated from melanoma metastases, the classifier achieved >80% accuracy, demonstrating its potential as a prototype tool for patient selection. A similar modelling approach was used to prognosticate progression free survival (PFS) of advanced melanoma patients based on the expression of nine apoptosis regulators. After immunohistochemical staining of tissue micro arrays constructed from tumor biopsies, the markers expression was assessed both digitally and manually. Surprisingly, high expression of the pro-apoptotic proteins Bax, Bak and Smac correlated with worse prognosis, and this trend was further validated at mRNA level in an independent melanoma cohort. A supervised classifier was built based on the expression of the three-proteins signature and achieved an AUC>0.79 discriminating long term (PFS>12 months) vs. short term survivors (PFS<12 months). These results highlighted a counterintuitive correlation between the expression of pro-apoptotic proteins and prognosis of patients treated with chemotherapy. While the first two studies focused on a limited number of proteins related to a specific pathway of interest, the third classification framework presented here aims at identifying breast cancer patients likely to experience disease progression or recurrence, based on their full transcriptome profiles. Two of the largest and best annotated publicly available datasets (TCGA and METABRIC) were identified as suitable candidates to train and test a DL pipeline based on generative adversarial networks (GAN). This approach addresses the common problem of data scarcity in clinical datasets, where the amount of variables far outnumbers the patients, generating synthetic individuals to enrich the original training data. Moreover, taking advantage of the generalization capability of this method, high stratification performance was achieved without any prior patient selection, which is a typical limitation of established prognostic tests currently in use.

In conclusion, this work demonstrates how different AI-based methods driven by domain knowledge can assist translationally relevant tasks such as patient selection for novel treatment strategies, prognostication of survival based on biomarker signatures and identification of high risk patients.

ZUSAMMENFASSUNG

In den letzten Jahren wurde einstimmig anerkannt, dass ein “one size fits all” Ansatz nicht auf das Management von Krebspatienten angewendet werden kann. Grund dafür sind die sehr starke, interindividuelle Variabilität und Heterogenität von Tumoren. Deswegen wurden in Prävention, Diagnose, Prognose und Behandlung heutzutage verschiedene Faktoren berücksichtigt. Diese reichen von leicht verfügbaren Informationen wie Lebensstil, Umfeld oder Familiengeschichte bis hin zu quantitativen Daten, wie unter anderem Gen- und Proteinexpression. Da diese Daten sehr komplex, nicht-linear und hochdimensional sind, reichen klassische, statistische Ansätze oft nicht aus, um Muster zu erkennen, welche z.B. mit dem Ansprechen auf die Behandlung oder dem Überleben des Patienten korrelieren. Fortschritt in Rechenleistung und verbesserte Qualität und Quantität von Hochdurchsatzdaten haben das Interesse an künstlicher Intelligenz (KI) zur Anwendung in der Onkologie gesteigert. Speziell maschinelles Lernen (ML) ist eine KI-Methode, die entwickelt wurde, um Entscheidungen bei unbekannten Daten auf Grundlage der Erfahrung von bekannten Trainingsdaten zu treffen. Dabei ist Deep Learning (DL) eine Untergruppe der ML-Algorithmen basierend auf künstlichen, neuronalen Netzwerken. Diese ähneln menschlicher Wahrnehmung und können für Aufgaben genutzt werden, die zu anspruchsvoll für klassische ML-Algorithmen sind.

In dieser Arbeit wird die Entwicklung and Anwendung von KI-basierter Klassifizierung beschrieben, um fallspezifische Vorhersagen in drei verschiedenen Anwendungsfällen zu treffen. Diese beinhalten das Hochskalieren von pfadspezifischen Daten aus Krebszelllinien, die Biopsie von Patienten und vollständige Transkriptomprofile. Jeder dieser Anwendungsfälle zeigt das Potential der ML/DL Analysen, klinische Entscheidungen zu unterstützen. Die ersten beiden Ansätze konzentrieren sich auf die zellulären Prozesse der Apoptose, der wichtigste Zelltodmechanismus, der bei Krebszellen oft dereguliert ist. Zielt man auf diesen Prozess in sonst resistenten Tumoren, könnte dies eine vielversprechende Behandlungsstrategie darstellen, falls eine passende Auswahl des Patienten durchgeführt wurde. Außerdem wurde die Grundexpression der wichtigsten Regulatoren analysiert, um Korrelationen mit dem Überleben von Patienten zu identifizieren, welche mit Apoptose-induzierenden Medikamenten behandelt wurden, wie z.B. Chemotherapeutika. In der ersten Studie wurde eine datengesteuerte Pipeline entwickelt, um die Antwort von Melanomzelllinien

auf eine neuartige Behandlung zur Apoptoseinduktion vorherzusagen. Die Proteinexpression von 19 Schlüsselregulatoren der Apoptose wurde in 16 Melanomzelllinien quantifiziert und genutzt, um die synergistische Antwort auf IZI1551, ein hexavalenter tumor necrosis factor (TNF)-related apoptosis-inducing ligand (TRAIL) Rezeptor Agonist, in Kombination mit Birinapant, dem Antagonist des Inhibitors der Apoptose (IAP) vorherzusagen. Dies gelang mit 81.25 prozentiger Genauigkeit. Für die Vorhersage der Antwort bei Tumorzell-Sphäroiden und isolierten Zellen aus Melanommetastasen erreichte der Klassifikator eine Genauigkeit von über 80%, was das Potential zur Patientenauswahl demonstriert. Ein ähnlicher Ansatz wurde genutzt um folgenfreies Überleben (PFS) von fortgeschrittenen Melanompatienten auf Grundlage von neun Apoptose Proteinen zu prognostizieren. Diese neun Marker wurden durch Micro Arrays aus Tumorbiopsien isoliert und durch immunhistochemische Färbung digitalisiert und manuell quantifiziert. Hohe Expression der pro-apoptotischen Proteine Bax, Bak und Smac korrelierte mit einer schlechten Prognose. Dieser Trend wurde zusätzlich auf mRNA Ebene in einer unabhängigen Melanomkohorte bestätigt. Ein überwachter Klassifikator wurde auf Grundlage der Expression der drei Proteine entwickelt und erreichte bei der Vorhersage von verlängertem Überleben (PFS > 12 Monate) eine AUC > 0.79. Dies hebt eine kontraintuitive Korrelation zwischen der Expression von pro-apoptotischen Proteinen und der Prognose von Patienten, die durch Chemotherapie behandelt wurden, hervor. Während sich die ersten beiden Studien auf eine beschränkte Anzahl an Proteinen eines bestimmten Pfads konzentriert haben, nutzt dritte Klassifikationsnetzwerk komplette Transkriptomprofile. Dadurch sollen Brustkrebspatienten erkannt werden, bei denen ein Fortschreiten oder Wiederauftreten der Krankheit wahrscheinlich ist. Zwei der größten und am besten kommentierten, öffentlichen Datensätze wurden als geeignete Kandidaten befunden, um eine DL-Pipeline zu trainieren und testen. Diese Pipeline basiert auf generative, generischen Netzwerken (GAN). Dieser Ansatz verdeutlicht das allgemeine Problem von Datenknappheit in klinischen Datensätzen, in denen die Anzahl der Variablen um einiges größer ist als die Anzahl der Patienten. Das Erzeugen von künstlichen Individuen hilft dabei, die originalen Trainingsdaten zu vergrößern. Nutzt man außerdem die Fähigkeit zur Generalisierung dieser Methode, erreicht man eine hohe Schichtungsleistung ohne vorherige Patientenauswahl, was eine typische Limitierung in aktuell etablierten Prognosetests ist.

Zusammengefasst demonstriert diese Arbeit wie verschiedene KI-basierte Methoden, angetrieben durch Fachwissen, wichtige Aufgaben wie Patientenauswahl für neuartige Behandlungen, Prognose von überlebensbasierten Biomarkersignaturen und Identifizierung von Hochrisikopatienten unterstützen kann.

ACKNOWLEDGEMENTS

First and foremost, my thank you goes to the cancer patients who donated their information to the scientific community. This work, together with hundreds of other dissertations and papers, would have not been possible without their generous contribution and the joint effort of the institutions making the data freely accessible.

Thank you to my supervisor, Prof. Markus Morrison, for guiding me through this intense journey. Thanks for stepping in when my overenthusiastic nature was leading me off track. Thank you to Prof. Nicole Radde and Prof. Thomas Sauter for taking part in the evaluation of this thesis and for the experience shared through the SimTech and Mel-Plex projects. Thanks to Dr. Roman Fischer, who gave me the chance to start working at the IZI. Thank you to Dr. Christoph Morhard for the great collaboration and our "networking dinners".

Thank you Gavin, it really takes some effort to share the office with someone like me for over six years! Thank you for your endless and selfless support, thank you for being my friend. Thanks to the people who were part of the many Isengard "iterations", Christian on top. We had a great time together and our after-work beers and conversations at the station in Feuerbach won't be forgotten.

Thanks to all the present and past members of the Morrison group for spending unforgettable moments together. Thanks to Cathrin, Nadine, Vesna, Biswa, Josip, Nivetha and Tabea for being more than colleagues. Thanks to my students, Lara, Cedric and Tine, for letting me learn through teaching. Thanks to Nats, not everyone knows that my very first day at the IZI she supervised me. Thanks to Fabi, the newcomer who won me with a Wegbier on our first night out together. Thanks Gabi, for reconsidering your first opinion on me. And Dani, just thank you. Thanks to all the other members that I am not mentioning here because, well… you know me. I am sure you won't get angry!

Thanks to the guys from my block in Bari, "Il Cortile", my special supporters since we were kids. Thanks to the W.C.R.A., my martial arts association. It's always good to come back, have a friendly spar and feel like I never left the Academy.

Thanks to Yoshimura, my motorcycle, for putting a smile on my face every single time I turn the ignition key and turn the throttle. We have seen a lot and a long road is still waiting ahead, full of people to meet and places to discover.

Thank you Milvio for being my best friend, for supporting every decision I take, especially the bad ones.

Thanks to my wife Ornella for being a reliable, unmovable pillar.

Thanks to my family, far but always close. Thanks to my Mother, for hanging in there. Thanks to my Dad, for making me the man I am now. Thanks for teaching me how to orient myself in the night following the stars, how to read the wind and decide how far from the shore I could swim. Thank you for teaching me that a man is really done for when he stops being amazed in front of the stormy sea or the summer sunset. And you never stopped.

Stay tuned folks! This chapter may be closed, but the rest of my story is far from been over.

PUBLICATIONS, CONFERENCE CONTRIBUTIONS AND AWARDS

First-author publications

The research articles presented in this dissertation were published or submitted to peer reviewed journals:

Vetma, V.*, **Guttà, C.***, Peters, N., Praetorius, C., Hutt, M., Seifert, O., Meier, F., Kontermann, R., Kulms, D., & Rehm, M. (2020). Convergence of pathway analysis and pattern recognition predicts sensitization to latest generation TRAIL therapeutics by IAP antagonism. *Cell Death and Differentiation*, 27(8), 2417–2432. https://doi.org/10.1038/s41418-020-0512-5

*Contributed equally

Guttà, C., Rahman, A., Aura, C., Dynoodt, P., Charles, E. M., Hirschenhahn, E., Joseph, J., Wouters, J., de Chaumont, C., Rafferty, M., Warren, M., van den Oord, J. J., Gallagher, W. M., & Rehm, M. (2020). Low expression of pro-apoptotic proteins Bax, Bak and Smac indicates prolonged progression-free survival in chemotherapy-treated metastatic melanoma. *Cell Death & Disease*, 11(2), 124. https://doi.org/10.1038/s41419-020-2309-3

Guttà, C.✉, Morhard, C., Rehm, M.✉ (2022) Applying GAN-based data augmentation to improve transcriptome-based prognostication in breast cancer. Submitted to *PLOS Computational Biology* (in revision). Available as preprint on *medRxiv*. https://doi.org/10.1101/2022.10.07.22280776

✉ Corresponding authors.

Co-authorship publications

Rožanc, J., Sakellaropoulos, T., Antoranz, A., **Guttà, C.**, Podder, B., Vetma, V., Rufo, N., Agostinis, P., Pliaka, V., Sauter, T., Kulms, D., Rehm, M., & Alexopoulos, L. G. (2019). Phosphoprotein patterns predict trametinib responsiveness and optimal trametinib sensitisation strategies in melanoma. *Cell death and differentiation*, *26*(8), 1365–1378. https://doi.org/10.1038/s41418-018-0210-8

Podder, B., **Guttà, C.**, Rožanc, J., Gerlach, E., Feoktistova, M., Panayotova-Dimitrova, D., Alexopoulos, L. G., Leverkus, M., & Rehm, M. (2019). TAK1 suppresses RIPK1-dependent cell death and is associated with disease progression in melanoma. *Cell death and differentiation*, *26*(12), 2520–2534. https://doi.org/10.1038/s41418-019-0315-8

Fullstone, G., **Guttà, C.**, Beyer, A., & Rehm, M. (2020). The FLAME-accelerated signalling tool (FaST) for facile parallelisation of flexible agent-based models of cell signalling. *NPJ systems biology and applications*, 6(1), 10. https://doi.org/10.1038/s41540-020-0128-x

Fullstone, G., Bauer, T. L., **Guttà, C.**, Salvucci, M., Prehn, J., & Rehm, M. (2020). The apoptosome molecular timer synergises with XIAP to suppress apoptosis execution and contributes to prognosticating survival in colorectal cancer. *Cell death and differentiation*, *27*(10), 2828–2842. https://doi.org/10.1038/s41418-020-0545-9

Vera, J., Lai, X., Baur, A., Erdmann, M., Shailendra Gupta, S., **Guttà, C.**, Heinzerling, L., Heppt, M., Kazmierczak, P. M., Kunz, M., Lischer, C., Pützer, B., Rehm, M., Ostalecki, C., Retzlaff, J., Witt, S., Wolkenhauer, O., & Berking, C. (2022). Melanoma 2.0. Skin cancer as a paradigm for emerging diagnostic technologies, computational modelling and artificial intelligence. *Briefings in Bioinformatics*, bbac433, https://doi.org/10.1093/bib/bbac433

Conference contributions

Additionally, parts of this work have been presented at international conferences as posters or talks:

9th Swiss Apoptosis Meeting. September 2016, Bern (CH)
Poster: *A systems–level analysis of autophagy as a potential novel approach towards melanoma prognosis*

25th European Cell Death Organization Conference. September 2017, Leuven (BE)
Poster: *Data driven modeling predicts responsiveness to TRAIL/Smac mimetic combinations in malignant melanoma*

11th European Workshop on Cell Death. May 2018, Fiuggi (IT)
Poster: *Bax and Bak are prognostic marker candidates in metastatic melanoma, with low expression indicating better prognosis*

10th Swiss Apoptosis Meeting. September 2018, Bern (CH)
Poster and flash talk: *Bax, Bak and Smac are prognostic marker candidates in metastatic melanoma with low expression indicating better prognosis*

30th German Skin Cancer Congress, September 2020 (Virtual)
Invited talk: *Pattern recognition to identify prognostic signatures in TMA protein profiles*

e:Med Meeting on Systems Medicine. November 2020 (Virtual)
Poster and flash talk: *Convergence of pathway proteome analysis and pattern recognition predicts sensitization to latest generation TRAIL therapeutics by IAP antagonism*

EMBO Workshop: Dying in self-defense. May 2022, Crete (GR)
Poster and flash talk: *High-throughput proteomics-based modelling for case-specific BH3 mimetics efficacy prediction*

8th Conference on Systems Biology of Mammalian Cells. May 2022, Heidelberg (DE)
Poster: *Applying generative adversarial networks for data augmentation improves transcriptomic datasets interoperability and breast cancer prognostication*

Awards

Best talk award*:* *Mathematical systems modelling of melanoma: translational potential and mechanistic understanding*.
11th PhD Workshop on Molecular Mechanisms and Therapeutic Approaches in Cancer. September 2017, Freudenstadt (DE)

Best poster award*:* *Bax, Bak and Smac are prognostic marker candidates in metastatic melanoma with low expression indicating better prognosis*.
12th PhD Workshop on Molecular Mechanisms and Therapeutic Approaches in Cancer. September 2018, Freudenstadt (DE)

SimTech Master Thesis Challenge for Doctoral Students award for the best master thesis project proposal: *Melanoma as a perturbation of the "human model": integration and standardization of patient -omics data for personalized medicine*.
11th SimTech Status Seminar. December 2018, Bad Boll (DE)

NaWik Communication Award for the best and most creative flash talk: *Convergence of pathway proteome analysis and pattern recognition predicts sensitization to latest generation TRAIL therapeutics by IAP antagonism*.
e:Med Meeting on Systems Medicine. November 2020 (Virtual)

TRAINING AND SECONDMENTS

Courses, Workshops and Summer Schools

Transferable skill course: Personal Effectiveness & Conflict Management, Gender Balance in Science, Statistics in Biomedical Research, Writing skills for Biomedical Research. Katholieke Universiteit Leuven. May 2016, Leuven (BE)

Summer School: Anglo-German Research Training Initiative "Putting your research into context". King's College London. July 2016, London (UK)

Training Course: Concepts and Methods in Programmed Cell Death and Autophagy. Graduate School for Cellular and Biomedical Sciences of the University of Bern. September 2016, Bern (CH)

Commercialisation Bootcamp and Thesis Writing Course. Organized by Oncomark Ltd and Systems Biology Ireland, held at NovaUCD (University College of Dublin). October 2017, Dublin (IE)

Workshop: Quantitative Biophotonics for Translational Systems Biology. Danish Cancer Society Research Center, January 2017, Copenhagen (DK)

Workshop: Image Processing with ImageJ. Organized by the Bioimaging Center of the University of Konstanz and held at the University of Stuttgart. April 2017, Stuttgart (DE)

Training Course: Concepts and Methods in Programmed Cell Death and Autophagy. Graduate School for Cellular and Biomedical Sciences of the University of Bern and Life Sciences Switzerland. September 2018, Bern (CH)

Secondments

Part of the results presented in this thesis were generated during the following secondments:

Oncomark Ltd. September – October 2017, Dublin (IE)
Supervisor: Prof. Dr. William M. Gallagher

Institute of Pharmacology, University of Bern. May – July 2018, Bern (CH)
Supervisor: Prof. Dr. Hans-Uwe Simon

LIST OF ABBREVIATIONS AND ACRONYMS

ABC	Area between curves
AC-GAN	Auxiliary classifier generative adversarial network
ADAM	Adaptive moment estimation
AI	Artificial intelligence
ANN	Artificial neural network
ANOVA	Analysis of variance
APAF-1	Apoptotic protease activating factor-1
API	Average positive intensisty
AUC	Area under the curve
Bad	Bcl-2-associated agonist of cell death
Bak	Bcl-2 homologous antagonist/killer
Bax	Bcl-2-associated X protein
Bcl-2	B-cell lymphoma 2
Bcl-w	B cell lymphoma W
Bcl-xL	B cell lymphoma extra large
Bfl-1	Bcl-2-related isolated from fetal liver 1
BH	BCL-2 homology
Bid	BH3-interacting domain death agonist
Bim	Bcl-2-interacting mediator of cell death
BRAF	B-rapidly accelerated fibrosarcoma
BRCA	Breast cancer
BSA	Bovine Serum Albumin
CD95	Cluster of differentiation 95
CDK4	cyclin-dependent kinase 4
CDKN2A	cyclin-dependent kinase inhibitor 2A
cFLIP	Cellular FLICE-like inhibitory protein
$cFLIP_L$	cFLIP long
$cFLIP_S$	cFLIP short
CGAN	conditional generative adversarial network
cIAP1	Cellular inhibitor of apoptosis protein 1
cIAP2	Cellular inhibitor of apoptosis protein 2
cNLP	Clinical natural language processing
CNN	Convolutional neural network
CT	Computed tomography
CTLA-4	Cytotoxic T-lymphocyte antigen 4
CV	Cross validation
DAMPS	damage-associated molecular patterns
DD	death domain
DED	Death effector domain
DIABLO	Direct inhibitor of apoptosis-binding protein with low pi
DISC	death-inducing signaling complex
DL	Deep learning
DMEM	Dulbecco's modified eagle medium
DNN	Deep neural network

DR	Death receptor
DSS	Disease specific survival
DTIC	Dimethyltriazeno-imidazol carboxamide
ER	Estrogen receptor
FACS	Fluorescence activated cell sorting
FADD	FAS-associated death domain
Fas	Fibroblast associated surface antigen
Fas-L	Fas ligand
FBS	Fetal bovine serum
Fc	Fragment crystallizable
FDA	Food & Drugs Administration
FFPE	Formalin fixed paraffin-embedded
FITC	Fluorescein isothiocyanate
FLICE	FADD-like interleukin-1β-converting enzyme
FN	false negative
FP	False positive
FPKM	Fragments per kilobase per million mapped fragments
GAN	Generative adversarial networks
GDAC	Genome Data Analysis Center
GDC	Genomic Data Commons
GEP	Gene expression profiling
GES	Gene expression signature
GFP	Green fluorescent protein
GP	Gradient penalty
H&E	Hematoxylin and eosin
HER2	Human epidermal growth factor receptor 2
HR	Hazard ratio
Hrk	Harakiri
H-Score	Histoscore
IAP	Inhibitor of apoptosis
IgG	immune globulin G
IHC	Immunohistochemistry
IRES	internal ribosome entry site
KM	Kaplan-Meier
kPCA	Kernel principal component analysis
LDA	Linear discriminant analysis
LOOCV	Leave one out cross validation
LUBAC	linear ubiquitin chain assembly complex
MAPK	mitogen-activated protein kinase
MB	Molecular Taxonomy of Breast Cancer International Consortium
Mcl-1	Myeloid cell leukaemia 1
MCTS	Multi-cellular tumour spheroid
MEK	mitogen-activated protein kinase
METABRIC	Molecular Taxonomy of Breast Cancer International Consortium
mIHC	Multiplex Immunoistochemistry
ML	Machine learning

MOM	Mitochondrial outer membrane
MOMP	Mitochondrial outer membrane permeabilization
MRI	Magnetic resonance imaging
MTIC	3-methyl-(triazen-1-yl)imidazole-4-carboxamide
NF-1	Neurofibromin 1
NF-κB	nuclear factor 'kappa-light-chain-enhancer' of activated B-cells
NIH	National Institutes of Health
NLP	Natural language processing
NRAS	Neuroblastoma RAS viral oncogene homolog
OS	Overall survival
PAM50	Prediction Analysis of Microarray 50
PARP	Poly (ADP-ribose) polymerase
PBS	Phosphate-buffered saline
PC	Principal component
PCA	Principal component analysis
PD-1	Programmed death protein 1
PD-L	PD ligand
PFI	Progression free interval
PFS	Progression free survival
PI	propidium iodide
PI3K	Phosphoinositide 3-kinase
PR	Progesterone receptor
PTEN	Phosphatase and TENsin homolog
PUMA	p53 upregulated modulator of apoptosis
Q-VD-OPh	Quinoline-Val-Asp-Difluorophenoxymethylketone
QA	Quality assurance
QI	Quality improvement
RAC1	Ras-related C3 Botulinum Toxin Substrate 1
RELU	Rectified linear unit
RF	Random forest
RING	Really interesting new gene
RL	Reinforcement learning
RNA-Seq	RNA sequencing
ROC	Receiver operating characteristic
ROR-P	Risk of recurrence - proliferation score
RPMI	Roswell Park Memorial Institute
scTRAIL	single chain TRAIL
SKCM	Skin cutaneous melanoma
SL	Supervised learning
SMAC/Smac	Second mitochondria-derived activator of caspases
SMOTE	Synthetic minority oversampling technique
SN	Sensitivity
SP	Specificity
SVM	Support vector machines
t-SNE	t-distributed stochastic neighbor embedding
tBid	truncated BH3-interacting domain death agonist

TBST	Tris-buffered saline with Tween20
TCGA	Tge Cancer Genome Atlas
TERT	Telomerase reverse transcriptase
T-GAN-D	Trained GAN discriminator
TMA	Tissue micro array
TN	True negative
TNBC	Triple negative breast cancer
TNF	Tumor necrosis factor
TNFRSF	Tumor necrosis factor receptor superfamily
TNFα	Tumor necrosis factor α
TNM	Tumor, node, metastasis
TP	true positive
TP53	Tumor protein 53
TPP	Total percent positive
TRAIL	TNF-related apoptosis-inducing ligand
TRAIL-R1	Tumour necrosis factor-related apoptosis-inducing ligand receptor 1
TRAIL-R2	Tumour necrosis factor-related apoptosis-inducing ligand receptor 2
USD	United States Dollars
UCSC	University of California, Santa Cruz
UL	Unsupervised learning
UQ	Upper quartile
UV	ultraviolet
WEKA	Waikato Environment for Knowledge Analysis
WGAN	Wasserstein generative adversarial network
XIAP	X-linked inhibitor of apoptosis protein

LIST OF FIGURES

LIST OF SUPPLEMENTARY FIGURES

LIST OF TABLES

LIST OF SUPPLEMENTARY TABLES

1 INTRODUCTION

The introduction of this thesis is structured to provide a comprehensive background for the three original publications presented in Section 2. Firstly, the basic concepts of Artificial Intelligence (AI) and its integration in the field of medical research are discussed (Section 1.1). Since the main focus of this work is the development and application of binary classifiers to cancer patient data, the subsequent sections delve into the categorization and evaluation of these specific algorithms (Section 1.1.1, 1.1.2). Given the challenges posed by limited data availability in clinical settings, common techniques to handle data scarcity, such as feature selection, dimensionality reduction, and data augmentation, aiming to optimize algorithm performance, are described in Section 1.1.3. Two disease settings were selected as use cases for the three research articles presented in this thesis: melanoma and breast cancer. Section 1.2 reports mechanisms of melanoma formation and progression, along with information about staging and state-of-the-art treatment strategies. In this context, the controlled cell death pathway of apoptosis is introduced (Section 1.3) as a suitable druggable target to eliminate cancer cells. Breast cancer pathophysiology and patient management are illustrated in Section 1.4, with a particular focus on multi-gene expression signatures for patient prognostication. Finally, Section 1.5 states the objectives of this thesis, focused on the development of AI-based classifiers aimed at assisting clinical decision making.

1.1 Artificial Intelligence

The term “Artificial Intelligence” (AI) was coined by John McCarty, who in his proposal for the 1956 Dartmouth College Conference theorized that any aspect of learning could be simulated and executed by a machine (McCarthy *et al.*, 2006). McCarty and colleagues believed that human prerogatives such as solving problems or learning through experience could be transferred to automatic calculators if opportunely programmed. The concept of “thinking machines” was not completely new, but formalized a few years earlier by Alan Turing: if a machine was capable of holding a

conversation without being distinguished from a human being, this could be defined as “thinking” (Turing, 1950). The very first successful implementation of such a concept was a program able to play the game checkers, developed by Christopher Strachey in 1951 (Strachey, 1952).

The field has drastically progressed over the past seventy years thanks to the availability of cheaper and higher-performance computing hardware, advanced machine learning (ML) methods and amount of data generated in different fields. The oversimplified concept of these technologies is that an algorithm can be trained on a set of data and use this experience to solve specific tasks that may be either too repetitive or too complex for a human. AI finds currently application in numerous domains, such as marketing and financial services, e-commerce, facial recognition, autonomous driving vehicles and many more. Recently, the increasing availability and routine acquisition and digitalization of cancer patients data has encouraged the repurposing and application of AI techniques to medicine and in particular to oncology (Wallis, 2019). The type of data related to cancer patients is diverse, complex and large. Imaging (e.g. radiology or pathology), -omics data (e.g. genomics, transcriptomics) together with companion clinic-pathological and follow-up information need appropriate processing techniques in order to be analyzed and address specific questions. Different AI algorithms have shown their potential when applied to cancer detection and diagnosis, subtype classification, treatment optimization, identification of new therapeutic targets, drug discovery and drug repositioning (Elemento *et al.*, 2021).

Despite the increasing academic and private sector interest for AI applications to oncology, with more than 5,500 articles published in 2022, the adoption of these technologies in clinical practice remains still limited. According to a review carried out in 2020, 64 AI-based algorithms or devices were approved by the US Food & Drugs Administration (FDA), only 6 of which applied to cancer diagnostics. The main obstacles to the implementation of such methods into the clinics include transparency of the software, security of the data and the underlying bias of the data the models are fed with. Moreover, the regulation of the use and maintenance of such technologies represents a critical point (Benjamens *et al.*, 2020).

1.1.1 Categorization of machine learning algorithms

ML is the process by which a machine learns to perform a particular task and improve from experience. The learning process is defined by algorithms aimed at extracting

patterns from representative examples (or training data) and subsequently using them to make decisions on previously unseen data (or test data). Depending on the type of data and the task that the algorithm has to solve, ML methods can be divided into three broad categories: (i) supervised learning (SL), (ii) unsupervised learning (UL) and (iii) reinforced learning (RL) (**Figure 1.1-1**) (Shao *et al.*, 2022). In cancer research, several studies have applied these techniques, even though mostly retrospectively (Eckardt *et al.*, 2021), to diverse types of data including gene and protein expression, methylation data, copy number alterations, mutations and, more recently, images (Liñares-Blanco *et al.*, 2021). ML models have found several promising applications in cancer diagnosis and early detection. Other tasks include tumor classification and staging or treatment response predictions (Bertsimas and Wiberg, 2020).

SL algorithms are used to generate predictions and solve either classification or regression tasks. Classification algorithms are trained on a set of previously labeled data to predict the category of unlabeled data of a test set (e.g. low vs. high risk patient, benign vs. malignant sample). Random Forest (RF) and Support Vector Machines (SVM) are among the most widely used, especially when applied to gene expression data. In contrast, regression algorithms are used to predict a continuous real variable (e.g. survival times or level of expression of a specific gene). Popular methods are, among others, linear regression and *K*-nearest neighbors (Liñares-Blanco *et al.*, 2021). While supervised models aim at predicting a specific discrete or continuous outcome, UL's goal is identifying underlying structures in unlabeled data. Clustering is the most common unsupervised task addressed in cancer research, with *K*-means and hierarchical clustering among the most used. (Bertsimas and Wiberg, 2020). These methods can be used to identify groups of patients with specific clinical outcomes belonging to clusters (or subtypes) generated from genomic data (Awada *et al.*, 2021). Finally, RL algorithms are the least commonly used in the field. These models are trained to take decisions in a specific sequence and are based on a penalty/reward system. For example, in a precision medicine setting, these models can learn to indicate the dose adjustment of a drug that may induce toxicity or anti-tumor response, and can be rewarded or penalized depending on the clinical outcome and the severity of the adverse effects. Therefore, the model learns to indicate interventions over a certain period of time that maximize the long-term reward (Eckardt *et al.*, 2021).

Deep learning (DL) is a subset of ML techniques based on deep artificial neural networks (DNN) (**Figure 1.1-1**). A DNN is constructed of interconnected neurons

organized in consecutive layers and can be used to solve classification tasks. The first layer, or input layer, is presented with a sample together with its class. The information is then passed to the first hidden layer and subsequently to multiple other layers, which in turn manipulate the input several times. Each layer has the task of encoding features relevant for the classification. This information is ultimately transferred to the last layer of the architecture, or output layer, that generates a prediction. During the training process, the network will adapt the weights and thresholds given to certain features in order to generate the best predictions for the known set of data. In addition, during the learning process, the algorithm also learns which features should be placed on which layer to optimize the performance. Based on these parameters, a test sample will be evaluated by the different layers of the network and will be assigned to a class (Tran *et al.*, 2021). Convolutional neural networks (CNN) are deep neural networks that take advantage of convolutional layers for features extraction. Other than representing the most popular architectures used for image analysis in cancer diagnosis, CNNs also showed satisfactory performance when analyzing unstructured data such as gene expression or proteomics data (Bhinder *et al.*, 2021). DL has also recently become the major framework of natural language processing (NLP). NLP systems handle, augment and transform free texts into computable representations (Yim *et al.*, 2016). Applied to the healthcare environment, clinical NLP (cNLP) algorithms were used for example to extract timelines (e.g date of surgery or treatment) or cancer phenotypes from pathology and radiology reports. Consequently, the digitalized information is readily available for integration with -omics data or additional clinical records. This process not only reduces the time required for manual annotation of clinical datasets, but ensures that information recorded in text form is not neglected when automated predictive or prognostic tools are employed (Savova *et al.*, 2019).

Since the focus of this thesis is the development and application of binary ML and DL classifiers, the following sections will present the most relevant techniques to evaluate and optimize the performance of these particular algorithms.

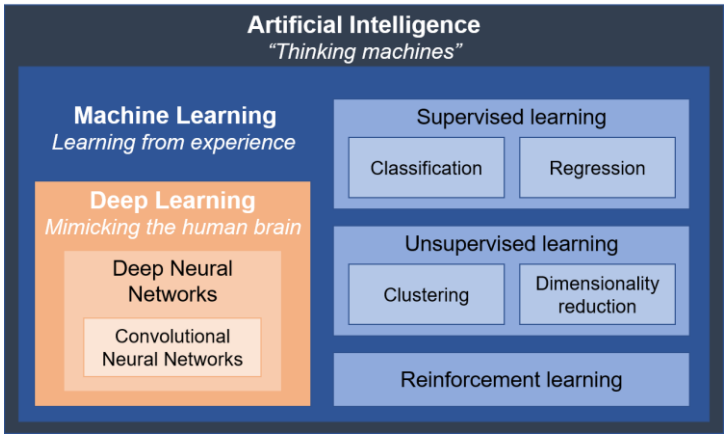

Figure 1.1-1: The taxonomy of AI.

Venn diagram representing the relationships between artificial intelligence, machine learning, deep learning and their sub-categories.

1.1.2 Evaluating a binary classifier

In order to evaluate the performance of a binary classifier or compare algorithms, different metrics can be computed. Here, the most widely used parameters in the biomedical field are presented. The first and simplest one is accuracy, calculated as the number of correct predictions divided by the total number of predictions. In some cases, the overall accuracy may not well represent the model performance, especially in case of imbalanced classes. In this case, the construction of a confusion matrix can offer better insight into the model performance. A binary classifier can produce four possible outcomes: correct positive prediction (true positive [TP]), a correct negative prediction (true negative [TN]), an incorrect positive prediction (false positive [FP]) or an incorrect negative prediction (false negative [FN]). The confusion matrix is a 2×2 table in which the columns represent the actual classes and the rows the predicted classes, and it is populated by the four aforementioned values (**Figure 1.1-2A**). Sensitivity ([SN] or true positive rate), and specificity ([SP] or true negative rate), are two of the metrics calculated from the confusion matrix values and are useful to evaluate the ability of a model to identify TPs and avoid FNs or identify TNs and avoid FPs respectively and are calculated as follows (Bishop, 2006):

$$Sensitivity = TP/(TP + FN)$$

$$Specificity = TN/(TN + FP)$$

Translated into clinical terms, using a simple example of a pipeline predicting if a patient will experience cancer recurrence or not, a high SN indicates that the classifier is particularly good at identifying real high-risk patients. Conversely, high SP indicates that the prognostic test is well suited for identifying low-risk patients (Trevethan, 2017). Additionally, it is possible to calculate SN and SP of a binary classifier at different classification thresholds. Considering an oversimplified example, one could infer if a patient belongs to the high risk or low risk class based on the value of a single continuous variable. SN and 1-SP can be calculated at each decision boundary and plotted as a receiver operating characteristic (ROC) curve (**Figure 1.1-2B**). ROC curves are popular representations of overall model performance and the different threshold results can be summarized by the area under the curve (AUC). As the name suggests, the AUC is a single scalar value calculated as the area underneath the ROC curve. This value can range from 0 to 1, with 1 representing a perfect classifier and 0.5 a random classifier. The analysis of ROCs has been widely used to assess the performance of

cancer diagnostic, prognostic and predictive classifiers (Moi *et al.*, 2018; Weiss *et al.*, 2003).

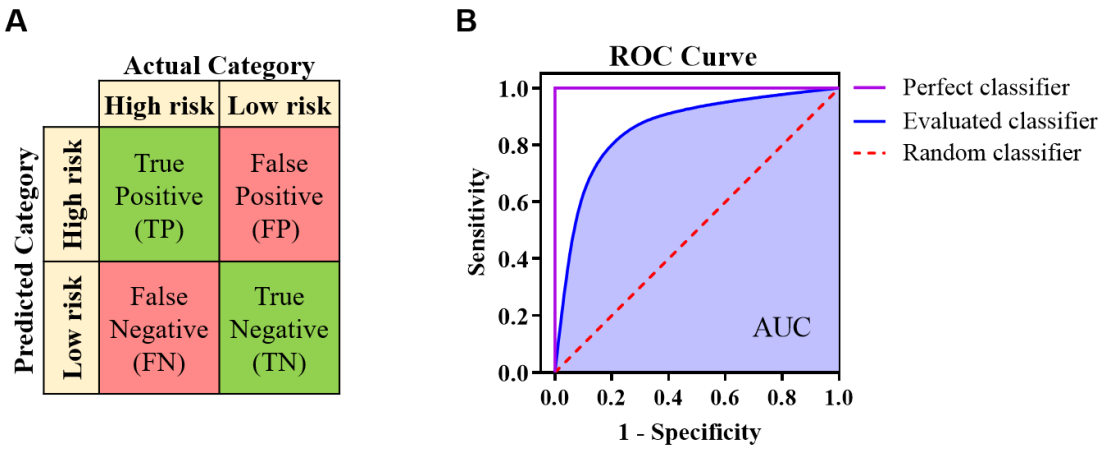

Figure 1.1-2: Common metrics for the evaluation of binary classifiers.A Confusion matrix of a hypothetical binary classifier aimed at discriminating high vs low risk patients. **B** Receiver operating characteristic (ROC) curve of a classifier (blue line) generated using sensitivity and specificity values computed at different classification thresholds. The area under the ROC curve (AUC) is commonly used to summarize the model performance.

1.1.3 Handling data scarcity

Medical and -omics datasets are often characterized by a high number of variables (e.g. thousands of genes) and small sample size (e.g. a few hundred patients). While several supervised classifiers have the potential to be applied to such datasets to solve different tasks, these models were originally not designed to cope with a high amount of irrelevant or redundant variables, which degrade model accuracy (Saeys *et al.*, 2007). Moreover, limited training data and imbalanced datasets (e.g. the majority of patients experience recurrence in a cohort) make the training of the model difficult, causing overfitting and poor generalization (Abu-Mostafa, 1989; Bansal *et al.*, 2022). The challenge of high dimensionality is commonly tackled using feature selection methods, dimensionality reduction (Janecek and Gansterer, 2008) or data augmentation (Yousefi *et al.*, 2019).

1.1.3.1 Feature selection

Feature selection aims at selecting subsets of informative variables from high-dimensional datasets to improve model performance and reduce computing times. Supervised feature selection techniques are applied when the classes of the samples are known and can be divided into three categories depending on their interaction with the classifier. Univariate filter techniques (e.g. t-test, analysis of variance- [ANOVA] or information gain-based) assess the importance of each feature individually, usually

providing a relevance score from which the top scoring features can be selected. The main disadvantage of these univariate methods is that the interdependency of the different features is ignored, thereby retaining possibly redundant variables. To circumvent this problem, multivariate methods that consider these dependencies (e.g. correlation-based), can be used at the expense of higher computational complexity. Both univariate and multivariate filter selections are performed before using the classifier, making them independent from the modelling algorithm. Conversely, wrapper methods select features iteratively training and testing a specific classifier and evaluating its performance at each iteration with different subsets of variables. Compared to univariate filter methods, wrappers always take into account feature dependencies, but, since the variables are selected to obtain the best performance with a specific classifier, the identified subsets may be suboptimal when transferred to other models. These methods are usually computationally expensive since the classifier is recursively challenged and are more prone to overfitting. The third class is represented by embedded techniques, where the selection of an optimal subset of features is built into the classifier itself (e.g. random forest, support vector machines) (Saeys *et al.*, 2007). Feature selection methods have been applied to a large variety of -omics data, including transcriptomics (Díaz-Uriarte and Alvarez de Andrés, 2006; Guyon *et al.*, 2002), proteomics (Shi *et al.*, 2021) and metabolomics (Grissa *et al.*, 2016) to improve model performance.

1.1.3.2 Dimensionality reduction

Alternatively, the attribute space can be reduced using dimensionality reduction. Instead of discarding features, these techniques combine the initial set of features into new attributes, losing only a small amount of information contained in the original dataset. The most widely used technique is principal component analysis (PCA, **Figure 1.1-3A, B**), which produces linear combinations of all original features into a new set of attributes, called principal components (PC), ordered by the amount of variance that they explain (Jollife and Cadima, 2016). Usually, a relatively small number of PCs, compared to the initial number of features, is sufficient to capture most of the variance of the initial dataset, therefore reducing the dimensionality of input data that classifiers have to process (Shi *et al.*, 2021). The main disadvantage of PCA, compared to feature selection methods, is the difficulty of interpreting the contribution of an attribute to the linear combinations, making a ranking of features based on their importance not accessible (Janecek and Gansterer, 2008). PCA followed by classification has been

successfully applied e.g. to gene expression data for patient classification (Hsu *et al.*, 2014) or multi-omics data for cancer subtyping (Hira *et al.*, 2021).

Linear discriminant analysis (LDA) is closely related to PCA since it also aims at identifying linear combinations that explain the variance of the initial dataset (**Figure 1.1-3C**). Differently from PCA, LDA considers the class of each sample to compute linear discriminants (LD), axes of a new orthogonal space, that maximize the separation between the classes whilst minimizing the variability within each class. While commonly listed as a dimensionality reduction algorithm, LDA finds wide application in supervised classification problems, since the linear decision boundary computed with a training dataset can be used to predict the class of new unseen samples. In cancer research, LDA was applied for generating e.g. diagnosis, subtyping, and risk group predictions (Huang *et al.*, 2009; Ni *et al.*, 2020; Tapak *et al.*, 2019).

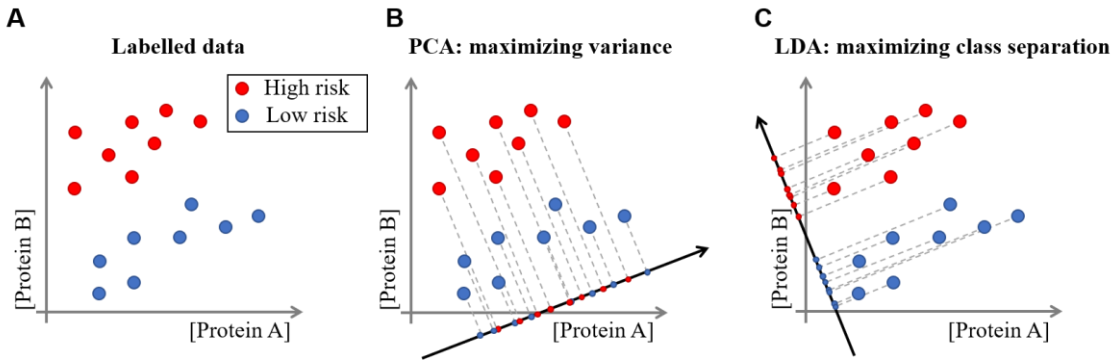

Figure 1.1-3: Graphical representation of PCA and LDA projections.A Scatter plot representing a hypothetical dataset composed of n = 16 patients and m = 2 variables. **B** Principal component analysis (PCA) does not consider the category labels and aims to find a lower dimensional representation of the initial dataset maximizing the variance. A principal component (black arrow) is a new axis onto which the original data points are projected. **C** Linear discriminant analysis (LDA) aims to maximize the separation between the categories to find a lower dimensional discriminative representation of the initial dataset. A linear discriminant (black arrow) is a new axis onto which the original data points are projected.

1.1.3.3 Re-sampling

Class imbalance is a problem related to data scarcity. Biomedical datasets can be composed of a high number of samples belonging to one category, or majority class, and only a few samples representing a second, underrepresented category, or minority class. When applied to these datasets, AI methods have the tendency to generate predictions geared towards the majority class, reducing the contribution of the minority class towards the class definition (Tasci *et al.*, 2022). Although no universal solution exists to address this issue, several strategies can be used to alleviate the imbalance ratio. Among these, the most common ones are data-level methods based on re-sampling, which aims at either increasing the sample size of the minority class (over-

sampling) or decreasing the sample size of the majority class (under-sampling). In the first case, samples from the minority class are randomly duplicated and added to the training dataset. In the latter, random samples are excluded to reduce the majority class instances. While under-sampling raises the problem of discarding potentially relevant information excluding samples, over-sampling comes with the potential of overfitting. The synthetic minority oversampling technique (SMOTE) may reduce overfitting, generating new samples through interpolation of several data points from the minority class. The second popular group of approaches is cost-sensitive learning. These techniques require a model to be adapted, so that the classifier is more heavily penalized when a sample from the minority class is misclassified. Even though cost-sensitive methods show good performance, their use is limited by the complexity of the implementation and the optimal definition of a penalty score (Gnip *et al.*, 2021). Re-sampling methods have been widely applied to medical imaging dataset balancing, e.g. for enhancing glioblastoma prognosis or glioma grading from radiological images (Liu, Hall, *et al.*, 2017; Suárez-García *et al.*, 2020), or RNA-seq datasets, for example for improving breast cancer subtyping (Yu, Wang, *et al.*, 2020).

1.1.3.4 Data augmentation

The objective of data augmentation is increasing the amount of samples creating slightly modified copies of the original or generating new synthetic ones (Shorten and Khoshgoftaar, 2019). This concept is intuitive when applied to images. For example, to increase the number of pictures in a dataset, it is possible to flip, rotate, scale, translate or add noise to them. A classifier exposed to such an increased training set may perform better in a canonical cross validation approach, but may fail to achieve satisfactory performance when exposed to new unseen test samples. The lack of generalization ability can be explained by the fact that the model training has been highly affected by similar images that share common underlying patterns, that may not be present in the new test set. In the clinical environment, especially when dealing with unstructured data (e.g. gene or protein expression datasets) the acquisition of new samples to expose the model to a wider variety of training instances may be unfeasible. Therefore, generative models can be employed to generate synthetic samples and enrich scarce training datasets. Generative adversarial networks (GAN) are DL-based generative models able to produce new samples starting from a random noise vector. GANs are widely used in virtual image generation and were recently employed to produce synthetic medical images (e.g. computer tomography and magnetic resonance images), electronic health

records and -omics data. The concept of GAN was introduced in 2014 by Goodfellow et al. (Goodfellow *et al.*, 2014). A GAN consists of two artificial neural networks, called the generator and the discriminator, competing with each other. The generator produces new synthetic samples taking a random noise vector as input (Aldausari *et al.*, 2022). These samples are then passed to the discriminator, which tries to distinguish real from fake samples. The process proceeds reiteratively until the generator produces fake samples that cannot be distinguished from real ones by the discriminator (**Figure 1.1-4A**). The ability to selectively generate samples belonging to a particular class or category was achieved with the development of the conditional GAN (CGAN) (Mirza and Osindero, 2014). In a CGAN, the discriminator expects from the generator to produce samples belonging to a specific class, penalizing not only the generation of unrealistic samples, but also the presence of features not belonging to a specific category (**Figure 1.1-4B**). An extension of this concept is the auxiliary classifier GAN (AC-GAN), published in 2016 (Odena *et al.*, 2016). In this architecture, the discriminator is not aware of the class of the generated samples, and has the additional task to predict the category itself (**Figure 1.1-4C**). Such a trained discriminator lends itself to be used as a standalone classifier in a transfer learning setting (Saha and Sheikh, 2021). The Wasserstein GAN (WGAN) was presented in 2017 to improve training stability and quality of the output. In this implementation, the discriminator has an additional "critic" task which assigns a score representing the distance between the distribution of the fake samples compared to the distribution of the real training data (Arjovsky *et al.*, 2017).

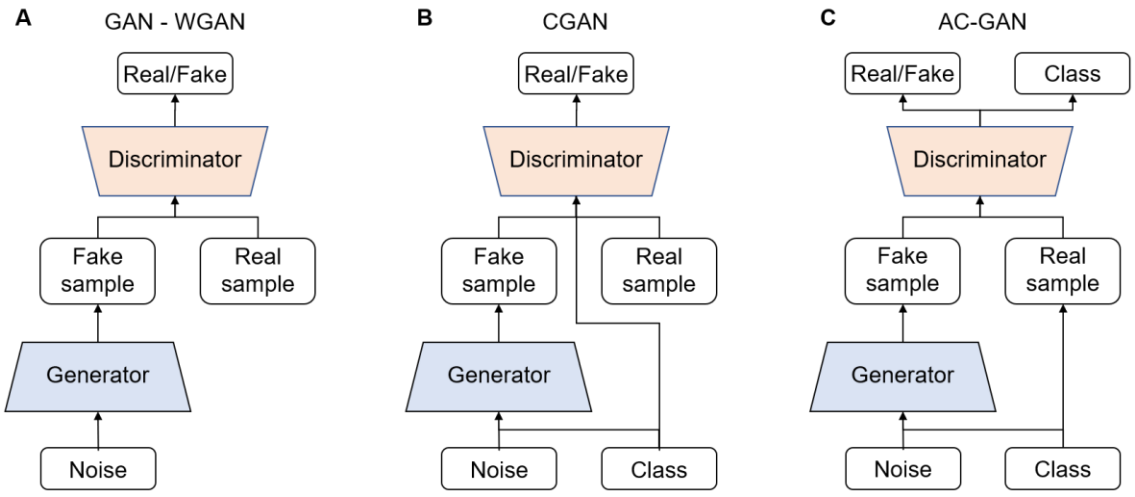

Figure 1.1-4: Evolution of GAN architectures. A The original (also known as "vanilla") GAN implementation and the WGAN architectures aim at generating high quality synthetic images. **B** CGAN is used to generate samples belonging to a specific class. **C** The prediction of the class of generated samples is an additional task of the ACGAN architecture.

Several other GAN architectures were developed to address specific problems. Cycle-GAN was developed to generate paired images from two different but related domains, such as magnetic resonance imaging (MRI) and computed tomography (CT) scans. Wolterink et al. used paired CT and MRI images of brain tumors to generate the missing image of patients that underwent only one of the two diagnostic procedures (Wolterink *et al.*, 2017). medGAN is an extension of the original implementation able to generate electronic health records, which include both continuous and discrete variables (e.g. stage or treatment information) (Choi *et al.*, 2017). Applied to single-cell RNA-seq, an implementation of the CGAN was developed to generate distinct immune cell types (Marouf *et al.*, 2020).

In this thesis, two disease settings were used as use cases for the application of AI-based classifiers. In the next sections, malignant melanoma and breast cancer will be introduced, discussing unmet clinical needs that ML and DL algorithms can contribute to tackling.

1.2 Melanoma

Cutaneous melanoma originates from melanocytes, the pigment-producing cells of the skin. When these cells are exposed to ultraviolet (UV) radiation, they can accumulate mutations that lead to uncontrolled proliferation and apoptosis evasion (Broussard *et al.*, 2018). Despite accounting for only 1% of all skin cancers, melanoma is the cause of 60% of all cutaneous malignancies related deaths (Vera *et al.*, 2022). In addition to UV exposure, other factors such as genetic predisposition, number of congenital and acquired melanocytic nevi, genetic and family history, play a role in melanoma development (Leonardi *et al.*, 2018). When detected in its early stage, melanomas are surgically removed and patients usually do not experience further complications, with 5-year survival rates of over 95% (Keung and Gershenwald, 2018). However, melanoma rapidly metastasizes and when diagnosed in its advanced stage the survival rate after 5 years decreases to less than 20% (Sandru *et al.*, 2014). One of the major risk factors for melanoma development is exposure to UV radiation. Even a few episodes of severe sunburns may double the risk of developing melanoma (Weinstock *et al.*, 1989). Moreover, excessive amounts of melanocytic nevi, especially if acquired later in life, represent an indicator for potential melanoma development (Batistatou *et al.*, 2007). Given the nature of the major risk factors, prevention and regular screenings are crucial to avoid the onset of the disease. Melanoma diagnosis is largely carried out by direct

observation of the skin lesion usually aided by a dermoscope. The clinician assesses the presence of morphological traits such as asymmetry, irregular borders, color variations, diameter and elevation of the surface of the nevi. In addition, several studies have shown the potential of DL in recognizing malignant lesions (Navarrete-Dechent *et al.*, 2018) reaching human expert-level diagnosis performance (Han *et al.*, 2018).

1.2.1 Staging

Melanoma staging is based on four systems. The Clark scale and the Breslow thickness describe how deeply the cancer has grown into the skin layers. The Clark scale has five levels which refer to the main layers of the skin that are affected by the disease. A level 1 melanoma, or melanoma *in situ*, involves only the epidermis, the outer level of the skin, while a level 5 melanoma has completely invaded the dermis reaching the underlying fat level that also contains the blood vessels. Instead, the Breslow thickness is measured in millimeters (mm) from the skin surface to the deepest point of the tumor. This value is also integrated into the TNM (Tumor, Node, Metastasis) system, which considers thickness, ulceration and spread of malignant cells to lymph nodes and to other organs. Finally, the clinical staging integrates this information into a 0 to IV staging system. Stage 0 represents an *in situ* lesion while Stage IV describes a cancer spread to lymph nodes and other tissues and body sites which commonly include lungs, liver or brain (Keung and Gershenwald, 2018). 80% of melanomas are diagnosed at Stage I, meaning that the cancer has reached 2 mm of thickness but has not spread to lymph nodes or distant organs. Notably, the majority of melanoma-related deaths occur in patients diagnosed with localized tumors. This suggests that among these patients exist a subpopulation of individuals at high-risk of recurrence or metastases who may benefit from more frequent screenings after the excision. Therefore, prognostication based on the clinical staging only, may not be sufficient for adequate patient management (LeQuang, 2022). Gene Expression Profiling (GEP) can improve prognostication and involves the analysis mRNA panels. Encouragingly, these tests have shown great potential in identifying early stage patients at higher risk of experiencing metastases or disease progression. Several of these prognostic tests are currently available (e.g. Decision-Dx Melanoma, Melagenix, Merlin) but none are routinely used in the clinics (Bollard *et al.*, 2021).

1.2.2 Driver mutations

Melanoma is one of the cancers with the highest mutational burden (Shao *et al.*, 2020) with hundreds of genes mutated in a single tumor (Scatena *et al.*, 2021). The two most frequent alterations are activating mutations in B-rapidly accelerated fibrosarcoma (*BRAF*) and neuroblastoma RAS viral oncogene homolog (*NRAS*). These mutations are found in about 50% and 20% of melanomas, respectively (Liu and Sheikh, 2014). Both genes encode for proteins implicated in the mitogen-activated protein kinase (MAPK) pathway, and constitutively active BRAF and NRAS promote cell growth and proliferation. In addition, as a consequence of *NRAS* mutation, the phosphoinositide 3-kinase (PI3K) pathway can be hyperactivated, promoting proliferation and survival. A similar effect is achieved through the loss of phosphatase and TENsin homolog (*PTEN*), a negative regulator of the PI3K pathway implicated in the development of 30-60% of melanomas (Milella *et al.*, 2015). Additionally, NRAS can be hyperactivated as a consequence of neurofibromin (*NF*)-1 mutations (present in 10-15% melanomas) (Mehnert and Kluger, 2012). Melanogenesis and melanocyte cell division are also promoted by mutations in *c-KIT*, which encodes a tyrosine kinase transmembrane receptor modulating both the PI3K and the MAPK pathways. Additional genes reported to be implicated in melanoma development are tumor protein 53 (*TP53*), telomerase reverse transcriptase (*TERT*), Ras-related C3 Botulinum Toxin Substrate 1 (*RAC1*), cyclin-dependent kinase inhibitor 2A (*CDKN2A*), cyclin-dependent kinase 4 (*CDK4*) (Scatena *et al.*, 2021).

1.2.3 Management

As mentioned above, surgical removal of the tumor may be curative in the majority of cases when performed in the early stage of the disease. Once melanoma metastasizes, metastasectomy may be performed, followed by other treatment interventions. Until recently, chemotherapy has been the only treatment option for metastatic melanoma. In particular, dimethyltriazeno-imidazol carboxamide (DTIC) or dacarbazine is the only FDA approved monochemotherapy since 1974. DTIC is processed in the liver generating its metabolite 3-methyl-(triazen-1-yl)imidazole-4-carboxamide (MTIC), which can alkylate the DNA and therefore induce mutations and prevent DNA replication (Liu and Sheikh, 2014). Even though no substantial survival improvement is observed and new therapeutic options are nowadays available, chemotherapy remains the only treatment option in poorly funded healthcare environments and in case of refractory, progressive or relapsed melanomas (Domingues *et al.*, 2018). The management scenario changed drastically from 2011 with the approval of new treatment

approaches. In particular, tumors harboring BRAF activating mutations can be treated with kinase-inhibiting drugs such as the BRAF inhibitors vemurafenib and dabrafenib. These drugs lead to improved clinical response rates and prolonged survival, but the advantage may be limited by acquired resistance mechanisms. Combination treatments with dual specificity mitogen-activated protein kinase inhibitors (MEK- inhibitors), such as trametinib and cobimetinib, have shown potential to circumvent this limitation (Davis *et al.*, 2019). About 50% of patients do not qualify for targeted therapies but can be considered for treatment with immune checkpoint inhibitors, targeting the cytotoxic T-lymphocyte antigen 4 (CTLA-4) and programmed death protein 1 (PD-1) in order to activate T-cells. Antibodies against CTLA-4 or PD1 stimulate the immune response by preventing binding of ligands suppressing T-cell activation present on dendritic cells (B7) and melanoma cells (PD-L1/2) (Heppt *et al.*, 2016). Immunotherapy showed improved overall and progression free survival compared to chemotherapy, reaching unprecedented efficacy when combining CTLA-4 and PD-1 blockade (Switzer *et al.*, 2022). Despite these advantages, check point inhibitors are expensive, have shown satisfactory response in only limited subsets of patients and a significant portion of individuals experienced severe side effects. Taking all of these into account, finding biomarkers related to prognosis or predictive for patient response emerges as a priority, together with the identification of novel treatment options. One promising therapeutic target is the apoptosis pathway, since its deregulation contributes to melanoma progression and cell death evasion mechanisms (Broussard *et al.*, 2018).

1.3 Apoptosis

Apoptosis is a highly regulated and conserved form of programmed cell death essential for development and aging as a homeostatic mechanisms to regulate cell populations in tissues (Elmore, 2007). In addition, cells may commit to apoptosis in response to several stimuli or stress signals, such as, among others, viral or bacterial infection, DNA damage, hypoxia or metabolic stress. After its first discovery by Carl Vogt in 1842, who reported cell death in the notochord and adjacent cartilage of metamorphic toads, many studies collected evidence of the involvement of this process in different organisms and tissues (Clarke and Clarke, 1996). Only over one century after its first report, Kerr and colleagues named the process *apoptosis* (from Ancient Greek: ἀπόπτωσις, falling off), formally defining the mechanism as "*controlled cell deletion*" (Kerr *et al.*, 1972). Cells dying by apoptosis show characteristic morphological features, such as rounding and

shrinking followed by chromatin condensation and DNA fragmentation. Afterwards, cell membrane blebbing is followed by the disruption of the cell into apoptotic bodies, smaller vesicles which are subsequently eliminated by phagocytes responding to the "*Find me*" and "*Eat me*" signals (Ravichandran, 2010). During the entire process the membrane remains intact, avoiding the release of damage-associated molecular patterns (DAMPs) and therefore limiting immunogenic or inflammatory responses.

Apoptosis exerts a key role in preventing cancer. Many tumorigenic stresses such as uncontrolled proliferation or DNA damage can trigger apoptosis and contribute to eliminating aberrant cells. Cancer cells can evade apoptosis in a variety of ways, including upregulation of apoptosis inhibitors, downregulation of pro-apoptotic proteins or loss of tumor suppressive function of sensor proteins. Understanding the complex interplay of apoptosis regulators and considering their expression patterns can help identifying points of intervention to restore susceptibility to cell death. Therefore, apoptosis represents a desirable target for treatment interventions (Lopez and Tait, 2015).

The apoptotic machinery can be activated by intra- or extracellular signals triggering the intrinsic or mitochondrial pathway such as oxidative stress, irradiation, or treatment with cytotoxic drugs (**Figure 1.3-1**). The intrinsic pathway converges on the mitochondrial outer membrane permeabilization (MOMP), an event which is tightly regulated by the interplay of the members of the B-cell lymphoma 2 (Bcl-2) family of proteins. Alternatively, the extrinsic or death receptor (DR) pathway is activated when extracellular ligands such as TNF (tumor necrosis factor), Fas-L (fibroblast associated surface antigen ligand) or TRAIL (TNF-related apoptosis-inducing ligand) bind to the extracellular domain of the type 1 TNF receptor (TNFR1), Fas (also called CD95/Apo-1) and TRAIL receptors 1/2 (TRAIL-R1/2), respectively (Jan and Chaudhry, 2019). Both signaling cascades converge on the activation of initiator and effector cysteine-dependent aspartate-directed proteases (caspases) expressed as inactive zymogens (procaspases). Initiator caspases (e.g. Caspase 8 and Caspase 9) are monomers activated after recruitment and dimerization on activation platforms. These in turn cleave dimeric effector caspases (e.g. Caspase 3 and Caspase 7), forming active heterotetramers (Lavrik *et al.*, 2005). Activated executioner caspases subsequently cleave hundreds of different target proteins (e.g. Poly (ADP-ribose) polymerase [PARP] and lamin), ultimately leading to cell death (Taylor *et al.*, 2008).

1.3.1 Apoptosis intrinsic pathway

As stated above, cells can activate the intrinsic apoptosis pathway in response to different apoptotic stimuli. The signaling cascade is regulated by the interplay of the Bcl-2 family of proteins, represented by pro-apoptotic and pro-survival (or anti-apoptotic) proteins, each containing at least one of four Bcl-2 homology (BH) domains. As a consequence of upstream death inducing signals, "activator" BH3-only pro-apoptotic proteins are upregulated (such as Bcl-2-interacting mediator of cell death [Bim] or p53-upregulated modulator of apoptosis [PUMA]) or activated through cleavage (BH3-interacting domain death agonist [Bid] to form the active, truncated tBid). The activators can bind and activate the pore-forming proteins Bcl-2-associated X protein (Bax) or Bcl-2 antagonist/killer (Bak). As a result of this binding, Bax and Bak undergo a conformational change that allows the formation of oligomers forming macropores in the outer mitochondrial membrane. While Bak is anchored to the mitochondrial outer membrane (MOM) (Brouwer *et al.*, 2014), Bax mainly resides in the cytosol of non-apoptotic cells and translocates to the MOM to be activated (Czabotar *et al.*, 2014). To antagonize this process, pro-survival Bcl-2 family proteins such as Bcl-2; B cell lymphoma extra large (Bcl- xL); B cell lymphoma W (Bcl-w); Bcl-2-related isolated from fetal liver 1 (Bfl-1), and myeloid cell leukaemia 1 (Mcl-1), bind and sequester activators and pore forming proteins. Additional BH3-only proteins known as "sensitizers" (e.g. Bcl-2-associated agonist of cell death [Bad], activator of apoptosis harakiri (Hrk) and Noxa [Latin for 'damage']) can indirectly promote apoptosis by inhibiting anti-apoptotic Bcl-2 proteins.

The balance between pro-apoptotic and anti-apoptotic Bcl-2 family proteins is crucial for determining whether a cell will execute MOMP and diverse stimuli can influence the abundance and activity of key regulators. For example, genotoxic damage (induced by ionizing radiation or treatment with cytotoxic chemotherapies) induces the activation of the transcription factor p53, increasing the transcription of Bax, PUMA and Noxa whilst repressing Bcl-2. Similarly, Bim and Bax mRNA levels are elevated as a consequence of high expression of the oncogene MYC (Fairlie and Lee, 2021).

As a result of MOMP, proteins residing in the intermembrane space including second mitochondria-derived activator of caspases (SMAC), serine protease OMI and cytochrome-c are released in the cytosol. Cytochrome-c forms an heptameric complex together with apoptotic protease activating factor-1 (APAF-1) and deoxyadenosine triphosphate/adenosine triphosphate, which serves the role of activation platform for

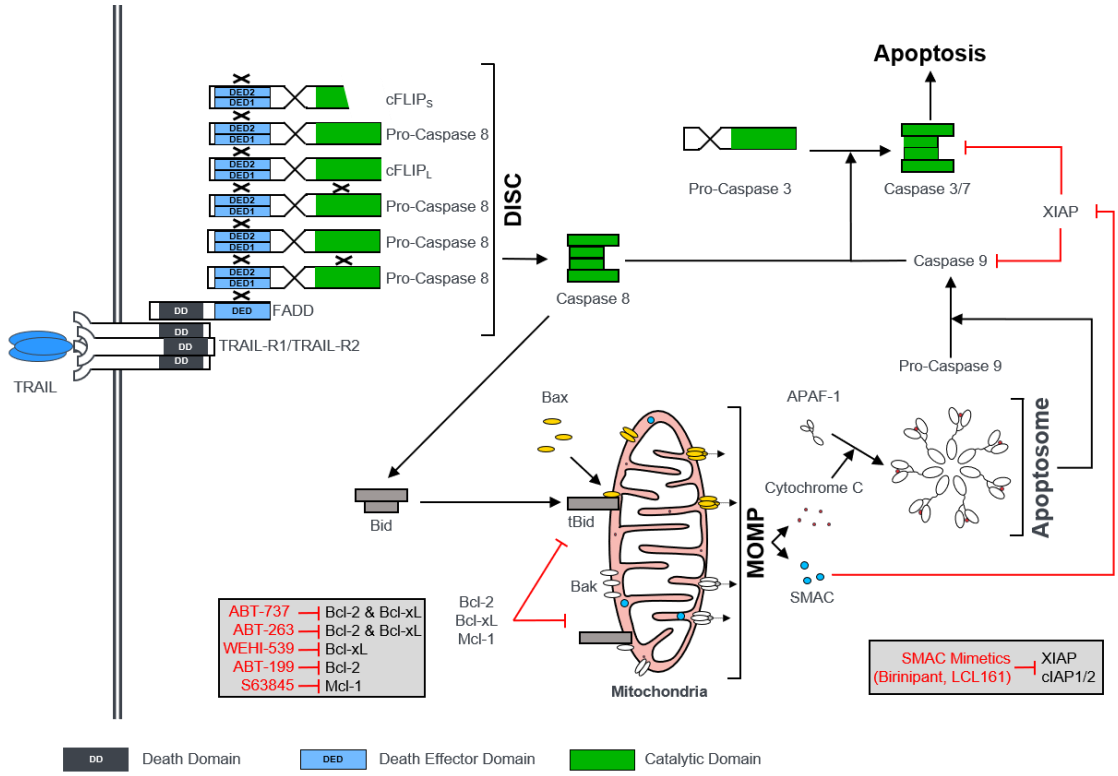

Figure 1.3-1: Schematics of TRAIL-induced apoptosis. Following TRAIL binding to TRAIL-R1/2, the receptors trimerize allowing the formation of the DICS. Pro-Caspase 8 is recruited and activated within this complex and can subsequently cleave and activate effector Caspase 3, executing cell death. In type II cells, an additional level of signal amplification involves mitochondria. Caspase 8 cleaves Bid, which in turn activates pore-forming proteins Bax and Bak, resulting in the release of Smac and Cytochrome C from mitochondria. Cytochrome C forms an activation platform for Pro-Caspase 9 together with APAF-1 and dATP/ATP. Activated Caspase 9 cleaves and activates executioner caspases, IAPs and pro- and anti-apoptotic family members provide additional levels of regulation of the signalling pathway. Several compounds have been developed to target IAPs and anti-apoptotic Bcl-2 proteins and induce apoptosis, alone or in combination with TRAIL (grey boxes). Schematics adapted from the original designed by Gavin Fullstone.

Pro-Caspase 9. While bound to the apoptosome, active Caspase 9 cleaves and activates the executioner caspases driving apoptosis. Caspase 9 and effector caspases activation can be blocked by the X-linked inhibitor of apoptosis protein (XIAP) which is in turn is inhibited by SMAC and OMI, released during MOMP. In addition, Caspase 3, can cleave both Pro-Caspase 9 and self-cleaved Caspase 9 (p35/p12) into the p37/p10 and p35/p10 forms, respectively, originating a positive feedback loop through the removal of the high affinity domain for XIAP (Denault *et al.*, 2007; Wu *et al.*, 2016). While XIAP directly inhibits caspase activity, cellular inhibitor of apoptosis 1 and 2 (cIAP1/2) are also able to bind caspases and influence cell fate. cIAP1/2 may promote ubiquitination through their really interesting new gene (RING) domains and subsequent proteasomal degradation of caspases. Alternatively, the two proteins can promote survival contributing to the activation of nuclear factor 'kappa-light-chain-

enhancer' of activated B-cells (NF-κB) and mitogen-activated protein kinase (MAPK) signaling (Sharma *et al.*, 2017).

1.3.2 Apoptosis extrinsic pathway

The second branch of the apoptotic pathway, known as the extrinsic pathway, involves the activation of cell surface death receptors. Death receptors possess a death domain (DD) on their cytoplasmic side that allows the recruitment of additional proteins and the formation of the death-inducing signaling complex (DISC). In particular, when stimulated with TRAIL, TRAIL-R1 and TRAIL-R2 oligomerize and undergo a conformational change that exposes their DDs (**Figure 1.3-1**). The adaptor molecule FAS-associated death domain (FADD) contains a DD at the C-terminus and a death effector domain (DED) at the N-terminus. FADD binds the receptors via homotypic interactions of the respective DDs and, through its DED, recruits Pro-Caspase 8 to the DISC, binding its DED1. Further Pro-Caspase 8 monomers are then recruited at the DISC through DED2-DED1 homotypic interactions, forming filaments that facilitate the dimerization and subsequent auto catalytic cleavage of Pro-Caspase 8. The resulting active Caspase 8 heterotetramer is released into the cytosol and can cleave and activate Caspase 3 and 7 (Dickens *et al.*, 2012). In addition to further Pro-Caspase 8 molecules, cellular FLICE-like inhibitory protein (cFLIP, FADD-like interleukin-1β-converting enzyme [FLICE]) can be recruited at the DISC. cFLIP also contains two DEDs and can modulate the activation of Pro-Caspase 8 binding at the DISC. The isoform cFLIP short ($cFLIP_S$) lacks the protease domain and disrupts Pro-Caspase 8 filaments, thereby preventing Pro-Caspase 8 activation. The long isoform of cFLIP instead ($cFLIP_L$) promotes Caspase 8 catalytic activity but was shown to inhibit extrinsic apoptosis when expressed in high amounts (Hughes *et al.*, 2016).

The intrinsic and extrinsic pathways cross-talk through Caspase 8. Cells able to achieve sufficient effector caspases activation by Caspase 8 after DR stimulation are termed Type I and can execute apoptosis independently of the mitochondrial pathway. Type II cells instead require a second level of amplification and rely on Caspase 8 cleaving Bid into tBid, its active and truncated form, subsequently engaging the intrinsic pathway (Scaffidi *et al.*, 1998).

1.3.3 Mechanisms of resistance

Resisting cell death is one of the hallmarks of cancer and tumor cells show a variety of mechanisms to limit or evade apoptosis (Hanahan and Weinberg, 2011). The extrinsic pathway can be impaired by reducing the surface expression of death receptors. This can be achieved for example by downregulating the expression of a receptor (e.g. CD95 in leukemia or neuroblastoma cells) or impairing the transport of TRAIL-Rs to the cell membrane from the endoplasmic reticulum (e.g. in colon carcinoma cells). In addition, epigenetic changes such as hypermethylation of gene promoters can reduce the expression of death receptors (Fulda, 2010). The intrinsic pathway can be impaired by upregulating anti-apoptotic Bcl-2 proteins or down-regulating pro-apoptotic ones. In the first case, various mechanisms, including copy number amplification, enhanced transcription or reduction of microRNAs suppressing pro-survival Bcl-2 protein expression can favor cell survival. The expression of pro-apoptotic proteins such as PUMA, Noxa and Bax is reduced as a consequence of p53 loss. In addition, it was reported in various tumors that Bim, PUMA or Noxa expression can be silenced either by promoter methylation or deletion. Additionally, the levels of the apoptosome components can be lowered through epigenetic silencing or inhibitory phosphorylation of APAF-1 and ubiquitination and proteasome-dependent degradation of cytochrome-c (Lopez and Tait, 2015). Moreover, increased expression of IAPs can inhibit apoptosis. In particular, XIAP and cIAP1 are translated via an internal ribosome entry site (IRES) which allows their production despite the breakdown of translation initiation factors from active caspases (Fulda, 2010).

1.3.4 Targeting apoptosis in cancer therapy

Many anti-cancer therapies are aimed at eliciting apoptosis in indirect ways. Chemotherapeutic drugs can induce cell death by causing DNA damage or cell cycle arrest, however cancer cells can be insensitive to these treatments or develop resistance. In addition, normal cells also suffer from the toxicity of these drugs, resulting in patients experiencing side effects (Pan *et al.*, 2016). However, the mechanistic insights into apoptotic signaling that accumulated over the last three decades allowed the development of therapeutic strategies aimed at inducing cell death by directly targeting the regulators of apoptosis. These include BH3 mimetics, inhibiting anti-apoptotic Bcl-2 family members, SMAC-mimetics, antagonizing IAPs, and death-receptor agonists, triggering the extrinsic pathway (Lopez and Tait, 2015).

1.3.4.1 BH3 mimetics

BH3 mimetics are small molecules that mimic the binding of BH3-only pro-apoptotic proteins to anti-apoptotic Bcl-2 family members. The first small molecule designed to bind Bcl-2, Bcl-xL and Bcl-w was ABT-737 (Oltersdorf *et al.*, 2005), which initially proved its potential as a single agent against lymphoma and small cell lung carcinoma cell lines. The promising results encouraged the development of its orally bioavailable successor ABT-263 (navitoclax) which, despite the response rates observed in chronic lymphocytic leukemia, caused thrombocytopenia in platelets caused by Bcl-xL inhibition (Tse *et al.*, 2008). ABT-199 (venetoclax) circumvented this problem by selectively inhibiting Bcl-2, reaching an overall response rate of 79% in the phase I study including chronic lymphocytic leukemia patients (Roberts *et al.*, 2016; Souers *et al.*, 2013). However, treatment with venetoclax was reported to cause tumor lysis syndrome, especially in patients with high tumor burden, which was attenuated with a different dose schedule (Davids *et al.*, 2018). Resistance to Bcl-2/Bcl-xL inhibitors is often associated with the expression levels of Mcl-1, which was additionally shown to be frequently amplified in several cancer types (Wertz *et al.*, 2011; Zack *et al.*, 2013). The Mcl-1 inhibitors VU661013 and S63845 showed synergistic effects with ABT-199 in venetoclax-resistant xenograft models of acute myeloid leukemia (Prukova *et al.*, 2019), suggesting that the combination or sequential treatment with different BH3-mimetics may result in improved responses. Analyzing the expression levels of Bcl-2 family proteins and BH3 profiling can help identifying the addiction of cancer cells to a specific anti-apoptotic protein and aid predicting the response to this increasing number of therapeutic candidates (Carneiro and El-Deiry, 2020; Fraser *et al.*, 2019; Lopez and Tait, 2015).

1.3.4.2 SMAC mimetics

IAP proteins are overexpressed in several cancer types, with high expression correlating with poor patient survival (Fulda and Vucic, 2012). Three members of the IAP family are well characterized for their roles in preventing apoptosis. XIAP can prevent caspase activation by binding to Caspase 3, 7 and 9. cIAP1 and cIAP2 do not directly bind caspases, but can induce pro-survival responses ubiquitylating the components of the canonical and non-canonical NF-κB signaling pathways (Yu, Lin, *et al.*, 2020). SMAC mimetics are small molecules that mimic the IAP-Binding Motifs or natural IAPs antagonists, such as SMAC or OMI. These molecules can bind to XIAP preventing caspase inhibition and promote cIAPs auto-ubiquitylation and proteasomal degradation

(Morrish *et al.*, 2020). Birinapant (TL32711) is one of the most clinically progressed SMAC mimetic. It has higher affinity for cIAP1 than cIAP2 and XIAP and this characteristic may contribute to its good tolerability (Condon *et al.*, 2014). As a single agent, birinapant showed high anti-tumor efficacy in preclinical studies including ovarian, colorectal, skin cancer and head and neck squamous cell carcinoma (Benetatos *et al.*, 2014; Eytan *et al.*, 2016; Krepler *et al.*, 2013). Clinical trials with patients affected by advanced solid tumors or lymphoma, acute myeloid leukemia and ovarian cancer, did not show significant clinical responses but highlighted the good safety profile, suggesting the potential of this drug for combination treatments (Amaravadi *et al.*, 2015; Frey *et al.*, 2014; Noonan *et al.*, 2016). Birinapant is currently tested in combination with anti PD-1 immunotherapy in solid tumors (Amaravadi *et al.*, 2015) and with radiation therapy in head and neck cancer patients (NCT03803774). Additional compounds such as LCL161 and Debio have also progressed into the clinic. Similar to Birinapant, they promote cIAP1 degradation whilst exhibiting a lower affinity for cIAP2 and XIAP but still exhibit limited clinical efficacy. The on-target effect and the potential to synergize with other drugs (e.g. immunotherapy) makes this class of molecules attractive therapeutic candidates for cancer treatment (Morrish *et al.*, 2020).

1.3.4.3 TRAIL receptor ligands

The extrinsic apoptotic pathway is triggered by the activation of DRs, transmembrane proteins members of the TNF receptor superfamily (Green and Llambi, 2015). In particular, TRAIL-R1/2 are activated by TRAIL, a transmembrane trimeric glycoprotein that can be cleaved and released as a soluble ligand. Various cells of the immune system, amongst them natural killer cells, T cells, natural killer T cells, dendritic cells and macrophages, express TRAIL to modulate immune responses (Falschlehner, Schaefer, *et al.*, 2009). TRAIL has gained attention due to its ability of selectivity killing cancer cells while sparing normal ones in preclinical studies (Falschlehner, Ganten, *et al.*, 2009), avoiding liver toxicity and pro-inflammatory responses observed with Fas ligand (CD95 agonists) and TNF, respectively. In the early 2000s, recombinant human TRAIL and agonistic monoclonal antibodies against TRAIL-R1/2 started to be evaluated in the clinic, unfortunately with limited success (Carneiro and El-Deiry, 2020). Recombinant TRAIL did not show significant activity in clinical trials due to short half-lives, limited ability to induce receptor clustering, binding to decoy receptors and lack of biomarkers to inform patient selection (Ashkenazi, 2015). Subsequently,

agonist monoclonal antibodies against TRAIL-R1 and TRAIL-R2 were engineered towards longer half-lives and higher order of receptor clustering. These constructs showed significant preclinical activity but limited clinical efficacy, in particular when administered as single agents. Several strategies have been developed to improve TRAIL's therapeutic activity. First, the generation of single-chain variants (scTRAIL) by fusion of the extracellular part via short peptide linkers avoids the dissociation of the homotrimer. Moreover, fusing TRAIL to antibody fragments, such as the fragment crystallizable (Fc) part of human immunoglobulin G1 (IgG1) can further increase its half-life. Additionally producing dimeric scTRAIL fusion proteins with higher valency results in higher receptor clustering (Hutt *et al.,* 2017). A representative example of a construct incorporating these characteristics is the hexavalent Fc-scTRAIL receptor agonist IZI1551. The agonist consists of two scTRAIL monomers with a single glycine residue as linker to connect three protomers, fused to the C-terminus of a human IgG1 Fc region. The two monomers are covalently linked via disulfide bonds in the Fc region, forming the hexavalent dimer. It was shown that the increased receptor clustering induced by hexavalent TRAIL-receptor agonists caused more potent induction of apoptosis signaling and increased cytotoxicity against cancer cells. (Hutt *et al.*, 2018). Another hexavalent TRAIL construct, ABBV-621, is currently under evaluation in clinical trials as single agent or in combination therapies (NCT04570631, NCT03082209).

1.4 Breast cancer

Breast cancer is the most frequent malignancy across women, with 2.1 million new cases diagnosed worldwide in 2018 and 626,679 deaths caused by the disease (Bray *et al.*, 2018). When the cancer is still confined to the breast or has spread only to the axillary lymph-nodes, it is curable in 70-80% of the patients. Conversely, the metastatic disease can only be treated to manage the symptoms and prolong survival. Breast cancer originates in the functional units of the breast called duct lobular units. Depending on the site of origin, two histological subtypes can be distinguished: invasive ductal carcinoma, and invasive lobular carcinoma developing from their in situ counterparts named ductal carcinoma in situ and lobular carcinoma in situ, respectively. Both invasive subtypes can invade the surrounding breast tissues and spread to other parts of the body, most frequently to the bones, liver, lungs and brain (Harbeck *et al.*, 2019). The exact mechanism of breast cancer initiation is still debated, but two main models

were reported to contribute to cancer formation and progression. According to the clonal evolution model, a population of cells start to accumulate mutations and undergo epigenetic changes and the “fittest” cancer cells are selected and proliferate. In the cancer stem cell model the precursor cancer cells are responsible for the disease initiation and progression (Bombonati and Sgroi, 2011). Independent of the initiation mechanism, at the molecular and histological level, breast cancer is a highly heterogenous disease. Several classification methods have been developed to categorize the tumors in subtypes and therefore streamline patient management.

1.4.1 Prognostic factors and subtyping

Surrogate intrinsic subtypes are the most common categorization method for breast cancer classification and have been shown to be informative for prognostication and treatment planning. The subtyping is based on several factors including the status of three specific receptors, the histological grade and proliferation characteristics. The status of three main markers is universally recognized as indispensable for the appropriate management of the patients and is routinely tested at diagnosis: the expression of estrogen receptor (ER), progesterone receptor (PR), and human epidermal growth factor receptor 2 (HER2). The expression is assessed by immunohistochemistry (IHC) on formalin-fixed paraffin-embedded (FFPE) tissue samples obtained from pre-surgical biopsies. Tumors expressing ER and/or PR are defined hormone receptor-positive; while tumors not expressing any of the three markers are termed triple-negative, with the latter being the most aggressive (Waks and Winer, 2019). The histological grade is assessed according to the Elston- and Ellis- modified Scarff–Bloom–Richardson system, which considers the percentage of tubule formation, the degree of nuclear pleomorphism and the mitotic count of the tumor. The three parameters are summarized in a three class grading system demonstrated to be a reliable prognostic factor representing tumor aggressiveness (Elston and Ellis, 1991). The Ki67 index is also measured by IHC and quantifies the proportion of proliferating cells in breast cancer. Even if no international consensus for scoring and thresholding has been reached yet, it has shown prognostic value in ER- positive, HER2-negative tumors (Zhang *et al.*, 2021).

An increasing body of literature suggests that classic IHC based signatures are in some cases less informative compared to novel gene expression signature (GES) (Wang et al., 2021). The Prediction Analysis of Microarray 50 (PAM50) is a 50-gene signature

initially proposed in 2010 that classifies tumors into four intrinsic molecular subtypes. The least aggressive is the luminal A subtype, followed by luminal B (expressing ER), human HER2-enriched and basal-like (without ER expression), the most aggressive. These subtypes were associated with specific relapse-free and overall survival outcomes, allowing the identification of a subset of patients at high risk of experiencing disease progression or recurrence (Kensler *et al.*, 2019).

1.4.2 Gene expression signatures and patient management

Currently, four GES are available on the market and integrated into the clinical decision process, depending on the availability of the required analysis infrastructure and national reimbursement regulations. First generation tests are performed directly by the companies owning the technology. OncotypeDX (Genomic Health Inc., Redwood City, CA, USA) and Mammaprint (Agendia BV, Amsterdam, The Netherlands) are a 21- and a 70-GES respectively, belonging to this category. Both are prognostic for risk of early relapse in early stage ER-positive, HER2-negative tumors with 0 to 3 involved lymph nodes. Instead, second generation tests can be performed locally on dedicated devices. Similar to the previous two methods, Endopredict (Myriad Genetics Inc, Salt Lake City, UT, USA) and Prosigna (NanoString Technologies, Seattle, WA, USA) are recommended for ER-positive, HER2-negative tumors, but include tumor extension and the degree of spread to regional lymph nodes as parameters. Moreover, second generation tests are prognostic not only for early, but also late recurrence. When anatomo-pathological criteria are not conclusive, GES can aid in identifying individuals for whom chemotherapy may be beneficial, whilst avoiding adverse effects of unnecessary treatments for low risk patients (Foulon *et al.*, 2020). Despite surgery representing the first or second line of treatment for early stage patients with undetectable metastases, the removal of the primary tumor can be preceded (neoadjuvant) or followed (adjuvant) by systemic chemotherapeutic treatment. Planning neoadjuvant or adjuvant interventions at this stage is often informed by the results of GES-based tests. In addition to chemotherapy, endocrine therapy is administered to block the effect of estrogen in ER positive tumors. In triple-negative and HER2 positive tumors, neoadjuvant therapy is always administered before surgery. In case pathological complete response is not achieved, systemic therapy can be prolonged.

Advanced breast cancer is generally uncurable, especially when distant metastases are present, but several treatment schedules were developed to treat the symptoms and slow

cancer progression. Luminal-like (HER2 negative, ER and/or PR positive) tumors are treated with endocrine therapy alone or in combination with cycline dependent kinase (CDK) 4/6 inhibitors. For triple negative tumors, chemotherapy is the main therapeutic option unless immune cells expressing PD-L1 are detected, suggesting the use of immunotherapy. In case of rapid disease progression, chemotherapy represents the last line of treatment for both subtypes. For HER2 positive tumors, anti-HER2 agents are continuously administered independently from progression, together with chemotherapy. Despite the steps forward in patients management, the overall survival of patients with distant metastases rarely exceeds 2-3 years, therefore avoiding late diagnosis and identifying patients at high risk of recurrence remains a priority (Harbeck *et al.*, 2019).

1.5 Aim of the thesis

Despite the advances in prevention, diagnosis and management, cancer has been the cause of death for approximately ten million patients worldwide in 2020. While the number of new cancer diagnoses increases every year, mortality has followed an opposite trend over the last two decades. Early diagnosis, new treatment options and prognostic tools have improved patient handling, supported by technologies capable of producing immense amount of data. While the role of AI in clinical practice is a matter of heated debate, ML and DL technologies are widely incorporated into diverse domains of oncology research. They have proven their ability of processing high dimensional data and the potential for assisting in decision making. In this thesis, three translationally relevant problems were tackled applying ML and DL-based pipelines to datasets of increasing complexity.

First, it was tested if apoptosis protein expression profiles were sufficient to predict the response of melanoma cell lines to the TRAIL-receptor agonist IZI1551 in combination with Birinapant. Hereby, cell death measurements and expression data of nineteen apoptosis regulators were used to train a prototype classification framework, subsequently tested for its predictive potential in two validation settings, using 3D tumor spheroids and cells derived from patient biopsies. Finally, an *in silico* clinical trial was designed to assess the response of a wider cohort of melanoma patients to the proposed combination treatment.

Expression data from apoptosis regulators were also collected in the second study, aimed at predicting the survival of metastatic melanoma patients treated with DTIC.

While new targeted therapies and immunotherapies have improved melanoma patient management, chemotherapy is still in use as last line of treatment of in poorly funded healthcare environments. Therefore, the identification of signatures prognostic for these groups of patients remains of high relevance. The expression of nine key proteins of the intrinsic apoptosis pathway was estimated by digital analysis of tissue micro arrays stained by immunohistochemistry and integrated into a dataset with follow-up information. Survival analyses were conducted to identify potential correlations with patient prognosis and independently validated in a separate cohort. Finally, a classifier was trained to discriminate long and short-term survivors and to compare the prognostic potential of the full protein panel against the putative biomarker signature.

In the last study, DL and GAN architectures were used to analyze full transcriptome profiles of breast cancer patients. The identification of high-risk patients is crucial when planning adjuvant or neoadjuvant treatment interventions, especially to avoid the side effects of unnecessary treatments for low-risk patients and the costs related to the therapy. Classical ML algorithms may be inadequate for the analysis of high-dimensional and imbalanced datasets, in particular when the number of features largely surpasses the number of samples. Gene expression datasets are usually affected by these limitations, but data augmentation methods can circumvent these problems creating new synthetic samples and enriching training datasets. In this work, the applicability of generative algorithms originally designed for image analysis to mRNA expression data was tested. To address the need of generally applicable prognostic tools, a GAN-based classifier was developed to identify high and low-risk patients. The data were retrieved from two independent publicly available datasets to test robustness and transferability. Finally, the classifier was compared to classical clinical biomarkers and an established GES for its stratification capability.

2 ORIGINAL PUBLICATIONS

2.1 Convergence of pathway analysis and pattern recognition predicts sensitization to latest generation TRAIL therapeutics by IAP antagonism

The following manuscript was published in *Cell Death and Differentiation* in 2020 and licensed under a Creative Commons Attribution 4.0 International License (http://creativecommons.org/licenses/by/4.0/). To facilitate reading, the manuscripts were reformatted and the figures positioned in the corresponding result subsections.

Vetma, V.*, **Guttà, C.***, Peters, N., Praetorius, C., Hutt, M., Seifert, O., Meier, F., Kontermann, R., Kulms, D., & Rehm, M. (2020). Convergence of pathway analysis and pattern recognition predicts sensitization to latest generation TRAIL therapeutics by IAP antagonism. *Cell death and differentiation*, 27(8), 2417–2432. https://doi.org/10.1038/s41418-020-0512-5.

* These authors contributed equally

Authors contribution:

VV*: designed and performed the experiments, performed the data analysis, drafted the manuscript and designed the figures.

CG*: processed the experimental data, designed and performed the data analysis, drafted the manuscript and designed the figures.

NP: designed and performed the experiments, contributed to the final version of the manuscript.

CP: contributed to sample preparation and characterization, discussed the results and approved the manuscript.

MH: contributed in IZI1551 production and dosage definition, discussed the results and approved the manuscript.

OS: contributed in IZI1551 production and dosage definition, discussed the results and approved the manuscript.

FM: contributed to sample preparation and characterization, discussed the results and approved the manuscript.

RK: contributed to study supervision, discussed the results and approved the manuscript.

DM: contributed to study supervision, sample preparation, discussed the results and approved the manuscript.

MR: supervised the project, drafted the manuscript and designed the figures.

Research article

Convergence of pathway analysis and pattern recognition predicts sensitization to latest generation TRAIL therapeutics by IAP antagonism

Vesna Vetma[1,2,*],Cristiano Guttà[1,*], Nathalie Peters[1], Christian Praetorius[4,5], Meike Hutt[1], Oliver Seifert[1], Friedegund Meier[5,6,7], Roland Kontermann[1,8], Dagmar Kulms[4,5,9], Markus Rehm[1,2,3,8,10]

1 Institute for Cell Biology and Immunology, University of Stuttgart, Stuttgart, Germany

2 Department of Physiology & Medical Physics, Royal College of Surgeons in Ireland, Dublin, Ireland

3 Stuttgart Centre for Simulation Science (SC SimTech), University of Stuttgart, Germany

4 Center for Regenerative Therapies, Technical University Dresden, Dresden, Germany

5 Skin Cancer Center at the University Cancer Centre, Department of Dermatology, Faculty of Medicine, University Hospital Carl Gustav Carus, Technical University Dresden, Germany

6 National Center for Tumor Diseases (NCT), Dresden, Germany

7 German Cancer Research Center (DKFZ), Heidelberg, Germany

8 Stuttgart Research Center Systems Biology, University of Stuttgart, Stuttgart, Germany

9 Experimental Dermatology, Department of Dermatology, Technical University Dresden, Dresden, Germany

10 Centre for Systems Medicine, Royal College of Surgeons in Ireland, Dublin, Ireland

*These authors contributed equally to this work

Running title: Predicting TRAIL/IAP antagonist responses

Keywords: TRAIL, Birinapant, Biomarker, Cell death, Apoptosis, Melanoma

Conflict of interest: R.E.K. is a named inventor on patent applications covering the scTRAIL technology (IZI1551). All remaining authors declare that they have no conflict of interest.

To whom correspondence should be addressed:

Prof Dr Markus Rehm

Institute for Cell Biology and Immunology

University of Stuttgart

Allmandring 31, 70569 Stuttgart, Germany

Phone: +49 711 685-66987

E-mail: markus.morrison@izi.uni-stuttgart.de

2.1.1 Abstract

Second generation TRAIL-based therapeutics, combined with sensitizing co-treatments, have recently entered clinical trials. However, reliable response predictors for optimal patient selection are not yet available. Here, we demonstrate that a novel and translationally relevant hexavalent TRAIL receptor agonist, IZI1551, in combination with Birinapant, a clinically tested IAP antagonist, efficiently induces cell death in various melanoma models, and that responsiveness can be predicted by combining pathway analysis, data-driven modelling and pattern recognition. Across a panel of 16 melanoma cell lines, responsiveness to IZI1551/Birinapant was heterogeneous, with complete resistance and pronounced synergies observed. Expression patterns of TRAIL pathway regulators allowed us to develop a combinatorial marker that predicts potent cell killing with high accuracy. IZI1551/Birinapant responsiveness could be predicted not only for cell lines, but also for 3D tumour cell spheroids and for cells directly isolated from patient melanoma metastases (80-100% prediction accuracies). Mathematical parameter reduction identified 11 proteins crucial to ensure prediction accuracy, with x-linked inhibitor of apoptosis protein (XIAP) and procaspase-3 scoring highest, and Bcl-2 family members strongly represented. Applied to expression data of a cohort of n = 365 metastatic melanoma patients in a proof-of-concept *in silico* trial, the predictor suggested that IZI1551/Birinapant responsiveness could be expected for up to 30% of patient tumours. Overall, response frequencies in melanoma models were very encouraging, and the capability to predict melanoma sensitivity to combinations of latest generation TRAIL-based therapeutics and IAP antagonists can address the need for patient selection strategies in clinical trials based on these novel drugs.

2.1.2 Introduction

The immune system can eliminate cancer cells by activating cell surface apoptosis-inducing death receptors, such as tumour necrosis factor-related apoptosis-inducing ligand receptors 1 and 2 (also known as death receptors 4 and 5 (DR4/5)). Many cancer cells, including melanoma, over-express these TRAIL-Rs, possibly due to an additional role these receptors can play in supporting cellular proliferation and invasion by autonomous TRAIL/TRAIL-R signalling (von Karstedt *et al.*, 2015). Developing TRAIL-based therapeutics has been a highly active but only moderately successful translational research field for many years, but recent progress in designing superior TRAIL-based biologics and an improved mechanistic understanding of drug-induced

TRAIL-sensitization now provide novel avenues for new anti-cancer therapies (Von Karstedt *et al.*, 2017). Latest generation TRAIL-derived therapeutics overcome limitations of previous formulations by significantly improving TRAIL receptor oligomerisation and activation by higher valency, and by exerting significantly prolonged serum half-lives. Highly promising variants are hexavalent fusion proteins that couple two single-chain TRAIL trimers and that outperform soluble human TRAIL and TRAIL-R-targeting antibodies (Gieffers *et al.*, 2013; Hutt *et al.*, 2017; Morgan-Lappe, 2017). Cellular inhibitor of apoptosis proteins (cIAPs) 1 and 2 can prevent TRAIL-induced cell death by recruiting components of the linear ubiquitin chain assembly complex (LUBAC) to aggregated TRAIL-Rs. The activitiy of LUBAC promotes pro-survival signalling and suppresses both apoptosis and necroptosis signalling cascades (Lafont *et al.*, 2017). Synthethic IAP antagonists, such as Birinapant (TL32711), BV6 or LCL-161, therefore potently sensitize cells to TRAIL-induced caspase-8 activation and apoptosis (Benetatos *et al.*, 2014; Fulda and Vucic, 2012). IAP antagonists bind to cIAPs and cause conformational changes that allow dimerisation of cIAP RING domains, auto-ubiquitylation and subsequent proteasomal degradation (Darding *et al.*, 2011). In cells capable of activating caspase-8, the cleavage of the Bcl-2 family protein Bid initiates the formation of Bax/Bak pores in the outer mitochondrial membrane, followed by activation of downstream caspases-9, -3, -7 and subsequent cell death (Taylor *et al.*, 2008). Birinapant also binds to and inhibits x-linked inhibitor of apoptosis protein (XIAP), a major antagonist of caspases-9, -3 , -7 that is also involved in upstream regulation of cell death signalling, with nM affinity (Allensworth *et al.*, 2013; Holcik and Korneluk, 2001; Vucic, 2018). Inducing apoptosis through the TRAIL pathway can proceed without the need for transcriptional responses or protein neo-synthesis, processes required for cell death induction by the majority of cytotoxic therapeutics. This suggests that pre-treatment amounts of proteins regulating apoptotic TRAIL signalling might suffice to derive predictors for treatment responsiveness.

Especially in highly heterogeneous cancers, such malignant melanoma, predictive markers and validated companion diagnostic tests developed from such markers will be necessary to identify those patients likely to respond to treatment (Caberlotto and Lauria, 2015; Goossens *et al.*, 2015). The incidence of cutaneous melanoma continues to rise rapidly (Whiteman *et al.*, 2016). While chemotherapy-based treatments provide little benefit for patients with metastatic melanoma, more recent treatment options such as targeted immuno-therapeutics, BRAFV600 and MEK inhibitors, and combinations

thereof in many cases can prolong survival or, less frequently, induce lasting disease remission (Domingues *et al.*, 2018; Hogan *et al.*, 2018). However, substantial numbers of patients do not qualify for these treatments or experience disease relapse, so that additional treatment options, for example those building on TRAIL-based therapeutics and IAP antagonists, can be attractive alternatives should it become possible to reliably predict treatment responsiveness.

Here we can report that expression profiles of TRAIL pathway regulators can serve to predict responsiveness to the combination of IZI1551, a prototypical example of a translationally relevant latest generation TRAIL-based biologic (Hutt *et al.*, 2017), and Birinapant (TL32711), a well-characterised example for a translationally relevant IAP antagonist (Benetatos *et al.*, 2014). Across a diverse and heterogeneous melanoma cell line panel, 3D multi-cellular tumour spheroids and melanoma cells isolated from patient metastases, we achieved >80% prediction accuracy. A proof of concept *in silico* trial based on a cohort of 365 metastatic melanoma patients indicates that IZI1551/Birinapant responsiveness could be expected for up to 30% of tumours.

2.1.3 Materials and methods

2.1.3.1 Materials

TL32711 (Birinapant) was obtained from Active Biochem, Germany. IZI1551 was produced and purified as described before (Hutt *et al.*, 2017). QVD-OPh was bought from Selleckchem, Germany. cIAP1 and cIAP2 recombinant proteins, required to determine absolute expression amounts in melanoma cells, were bought from R&D, Germany.

2.1.3.2 Melanoma cell lines and freshly isolated melanoma cells

Melanoma cell lines SkMel5 (ATCC; HTB-70), Malme 3M (ATCC; HTB-64), SkMel2 (ATCC; HTB-68), SkMel147 (Memorial Sloan Kettering Cancer Center; NY), WM3060 (Wistar; WC00126), WM1791c (Wistar; WC00086), MeWo (ATCC; HTB-65), Mel Juso (DSMZ; ACC74), WM1366 (Wistar; WC00078), WM115 (ATCC; CRL-1675), WM35 (Wistar; WC00060), WM3211 (Wistar, WC00045), WM793 (Wistar, WC00062), WM852 (Wistar, WC00065), WM1346 (Wistar, WC00121), and WM3248 (Wistar, WC00081) were purchased from ATCC (Mannasas, VA, USA), DSMZ (Braunschweig, Germany) or the Wistar Institute (Philadelphia, PA, USA). Six cell lines carried activating BRAF mutations (WM35, WM793, WM3248, WM115,

SkMel5, and Malme 3M), six cell lines NRAS mutations (WM1366, WM1346, SkMel147, SkMel2, Mel Juso, WM3060), one cell line a CDK4 mutation (WM1791c), one cell line carried a c-KIT mutation (WM3211), one cell line carried both NRAS and BRAF mutations (WM852) and one cell line was BRAF/NRAS/c-KIT/CDK4 wildtype (MeWo). All cell lines were purchased as authenticated STR-profiled stocks directly from the vendors. Freshly isolated melanoma cells (M10, M20, M32, M34, M45) were obtained from metastases and prepared for experiments by the Department of Dermatology, University of Dresden, Germany. Two metastases carried BRAF activating mutations (M10 and M45), while three carried activating NRAS mutations (M20, M32, and M34). Further materials (M51_1, M52_2 and M54) were obtained for extended validation (M54, BRAF/NRAS wildtype; M51_1, M51_2 carried BRAF activating mutations). Cell isolates were obtained as part of routine resections at University Hospital Dresden, under the auspices of the local Ethics Committee (ethical approval number EK335082018). Informed consent was obtained from all subjects. Cells were maintained in RPMI-1640 (Thermo Fisher Scientific, Germany) supplemented with 10% (v/v) FBS Brazil One (PAN Biotech, Germany) at 37˚C and 5% CO_2. Mycoplasma testing was regularly conducted.

2.1.3.3 Culturing of 3D spheroids

Cells were harvested and diluted to the concentration of 10^4 cells/mL in RPMI-1640/10% FBS with the addition of 0.24% Methyl Cellulose (Sigma Aldrich, Germany). 250 cells per drop were placed into the lid of a Petri dish filled with PBS. Spheroids were incubated for 10 days at 37˚C and 5% CO_2. The medium was exchanged every other day. Slower growing Malme 3M cells and freshly obtained metastatic melanoma cells (M34) were seeded at 500 cells per drop and incubated for two weeks.

2.1.3.4 Flow cytometry

Semi high-throughput cell death measurements. Cells were washed, trypsinised and stained with propidium iodide (PI, Sigma Aldrich, Germany) at 1.33 µg/mL for 10 minutes. The measurements were performed on a high throughput flow cytometer (BD LSRII SORP) using the 488 nm laser for excitation, while emission was recorded at 617 nm. Flow cytometry data were analysed using Cyflogic v. 1.2.1 (CyFlo Ltd, Finland). All experiments were performed in triplicates and in n = 3 independent repeats.

Annexin V-GFP or APC / PI staining. Cells were harvested and washed in PBS and Annexin V Binding buffer (Biolegend, Germany). Cells were stained with Annexin V-APC (Biolegend, Germany) (0.1%) or Annexin V-GFP (made in-house, 0.1%) and PI (Biolegend, Germany) (1 µg/mL). Measurements were conducted on a BD FACS Canto II flow cytometer using 561 nm excitation (emission from 600 to 620 nm) (PI) or 640 nm excitation (emission from 655 to 685 nm) (APC). Alternatively, measurements were conducted with a MacsQuant flow cytometer using 488 nm excitation (emission from 655-730 nm (PI), and emission from 500-550 nm (GFP)). Flow cytometry data were analysed either with the BD FACS Diva software (BD Biosciences, USA) or with Flowing software (Turku Centre for Biotechnology, Finland).

TRAIL receptor measurements. Cells were harvested and blocked in ice-cold PBA buffer (1 x PBS, 0.25 % BSA and 0.02 % Sodium Azide). Surface death receptors were probed with the following antibodies for 1 h at 4°C: mouse anti-TRAIL R1/TNFRSF 10 A (1:100, R&D Systems), mouse anti-TRAIL R2/TNFRSF 10B (1:100, R&D Systems), mouse anti-TRAIL R3/TNFRSF 10C (1:100, R&D Systems) mouse anti-TRAIL R4/TNFRSF 10D (1:100, R&D Systems), purified mouse IgG1 (1:100, R&D Systems) and purified mouse IgG2b (1:100, R&D Systems). Secondary goat anti-mouse FITC conjugated antibody (1:50, Dako, Biozol, Germany) was added for 45 min at 4°C. Cells were analysed in a MacsQuant flow cytometer using 488 nm excitation (emission was recorded at 500-550 nm). The surface expression of death receptors was calculated by calibration against quantification beads (QIFIKIT, Biozol, Germany), comparing the mean FITC signal of cells to calibration signals. Data were analysed with Flowing Software.

2.1.3.5 Western blot analysis

Protein quantification. Cells were trypsinised, washed in PBS, centrifuged and lysed in lysis buffer (150 mM NaCl, 1 mM EDTA, 20 mM TRIS, 1% Triton x-100, pH=7.6) with addition of phosphatase inhibitor (PhosSTOP, 20x, Roche, Germany) and protease inhibitor cocktails (cOmplete, 20x, Roche, Germany). Spheroids were additionally sonicated. The total protein concentration was determined with Bradford assay. 20 µg of protein were resolved on Nu-PAGE™ 4-12% Bis-Tris Midi gels (Invitrogen, Thermo Fisher Scientific, Germany) at 200 V, 400 mA for 40 min, followed by transfer to nitrocellulose membranes using an iBlot device (Invitrogen, Thermo Fisher Scientific, Germany). The membranes were blocked in 0.5x Blocking Solution (Roche, Germany) for 1 h at room temperature. The following primary antibodies were used for overnight

incubations at 4°C: mouse anti-Apaf-1 (1:1000; BD Transduction Laboratories), rabbit anti-Bak (1:1000; CST), rabbit anti-Bax (1:1000, CST), mouse anti-Bcl2 (1:1000; BD Transduction Laboratories) rabbit anti-Bcl-xL (1:1000, CST), mouse anti-Bid (1:1000, BD Transduction Laboratories), rabbit anti-Caspase 3 (1:1000; CST), mouse anti-Caspase 8 (1:1000; CST), rabbit anti-Caspase 9 (1:1000, CST), rabbit anti-cIAP1 (1:1000, Abcam), rabbit anti-cIAP2 (1:1000, Abcam), mouse anti-cFLIP (1:500, Abcam), mouse anti-cFLIP (1:500, Enzo), mouse anti-Cytochrome C (1:1000, BD Transduction Laboratories), rabbit anti-FADD (1:1000, Santa Cruz), rabbit anti-Mcl1 (1:1000, CST), mouse anti-PARP (1:1000, BD Transduction Laboratories), mouse anti-SMAC/DIABLO (1:1000, BD Transduction Laboratories), mouse anti-XIAP (1:1000, BD Transduction Laboratories), mouse anti-XIAP (1:1000, CST), mouse anti-actin (1:10000, CST). Subsequently, membranes were washed 3 x 10 min in TBST and incubated with secondary antibody (goat anti-rabbit IRDye 680 (1:10000) or goat anti-mouse IRDye 800 (1:5000) (LI-COR Biosciences) for 15 min at room temperature, followed by 10 min washing with TBST. Signals were captured on an Odyssey LiCor Imaging System. The quantification of proteins was performed on raw 16 bit images using Odyssey V3.0 software (LI-COR Biosciences). The intensities of the fluorescent signals were corrected for loading.

2.1.3.6 Data processing and analysis for predictor identification

All data processing and analysis was performed using a customised version of a previously developed pipeline (Rožanc *et al.*, 2019). The script was developed for MATLAB 2017b (The Mathworks, UK), equipped with the statistical toolbox. Prior to statistical analysis, protein data were mean-centered and scaled, dividing by the respective standard deviation. A principal component analysis (PCA) was performed on the standardised dataset and the PCs with an eigenvalue >1 were used for subsequent analyses. Linear discriminant analysis (LDA) was applied to objectively assess the accuracy of response class separation in the space defined by the first six PCs. Then, leave-one-out cross-validation (LOOCV) was applied iteratively to the 16-cell line panel to assess predictive capacity. For each iteration, data from 15 cell lines were used as a training set to define the PC space, and one test cell line was subsequently positioned according to its protein expression profile. LDA was then applied to determine if the test cell line was placed in the correct responsiveness sub-space. The response of 3D grown and patients-derived primary cell lines was predicted with the same workflow, using the predictor obtained from the data set of the 16-cell lines panel.

The optimal predictive protein subset (reduced predictor) was determined using the *Select attributes* panel of the WEKA workbench (Version 3.8.2, (Frank *et al.*, 2004)). A ranking of the proteins was obtained using the *CorrelationAttributeEval* attribute evaluator with *Ranker* search method and 10-fold cross-validation mode. This attribute selection method evaluates the *merit* of each protein individually by calculating the Pearson's correlation between the individual protein and the responsiveness class. The attribute selection step was performed using the proteins quantified in the 2D cell lines panel. The complete prediction pipeline was iteratively applied taking into account the first six PCs, and removing the protein with the lowest rank at each iteration. Statistical analyses not described above were performed with GraphPad Prism 7 (GraphPad Software).

2.1.3.7 *In silico* trial

The protein expression patterns of the melanoma cell line panel were used to estimate the protein expression profiles in melanoma tumours of 472 patients for which transcriptome data are deposited in the cancer genome atlas melanoma cohort (TCGA-SKCM). Normalised mRNA expression data (Upper Quartile normalised Fragments per Kilobase of transcript per Million mapped read, log2(FPKM-UQ+1)) generated by the Genomic Data Commons (GDC-NIH) were downloaded from the UCSC-XENA browser (Available at: https://xena.ucsc.edu/. Accessed: 4th February 2019). Data interpolation was performed using *Point-to-point* curve creation in GraphPad Prism 7 (GraphPad Software). Standard curves were generated using minimum and maximum values of protein expression range (cell line panel) and TCGA-SKCM back transformed mRNA expression data. For response predictions, PCA was applied to the data for the n = 11 predictor proteins in the cell lines dataset, followed LDA-based definition of responsiveness and resistant subspaces, and subsequent positioning of n = 365 TCGA derived melanoma metastases in the PC space according to their estimated protein values.

2.1.4 Results

2.1.4.1 IAP antagonist Birinapant sensitizes a subset of melanoma cell lines to apoptosis induced by the 2nd generation TRAIL-based biologic IZI1551

To study the responsiveness and the response heterogeneities of melanoma cells to IZI1551, a novel and translationally relevant hexavalent TRAIL receptor agonist (Hutt *et al.*, 2017), to the IAP antagonist TL32711/Birinapant, a compound currently evaluated in clinical trials (Fulda, 2015), or combinations thereof, we employed a diverse set of sixteen cell lines (see materials and methods). For each cell line, cell death was determined at 15 treatment conditions, using semi-high throughput flow cytometry. Cell lines varied in their response to the treatments, ranging from high resistance to high sensitivity (**Figure 2.1-1A**). Many cell lines responded synergistically to the combination treatment (synergistic responders; WM1366, SkMel5, SkMel2, Malme3M, Mel Juso, WM3060, WM115, WM35, SkMel147, WM793, WM1346, WM3248), as determined using Webb's fractional product method, whereas others (WM3211, MeWo, WM1791c, WM852 cells) failed to do so (low responders) (**Figure 2.1-1B**).

Birinapant had on-target activity in both synergistic responders and low responders, since cIAP1 protein amounts were efficiently and rapidly lost upon single agent and combination treatments (**Figure 2.1-1C**). Neither single nor combination treatment induced detectable amounts of TNFα secretion (**Supplementary Figure 2.1-1**), a response to IAP antagonists that in rare cases can contribute to autocrine cell death induction (Krepler *et al.*, 2013). The amounts of XIAP remained largely unchanged, except for the combination treatment in synergistically responding Mel Juso cells (**Figure 2.1-1C**). XIAP is a known caspase-3 substrate (Deveraux *et al.*, 1999), and correspondingly caspase inhibitor Q-VD-OPh restored XIAP amounts, indicating that IZI1551/Birinapant induces apoptosis in responder cell lines such as Mel Juso (**Figure 2.1-1C**). This was further supported by the processing of procaspases 8 and 3, and by the caspase-dependent cleavage of Bid and PARP in Mel Juso cells (**Figure 2.1-1D**). In poorly responding MeWo cells, instead, PARP cleavage was modest and detectable only as a transient pulse (**Figure 2.1-1D, E**). In line with these observations, caspase inhibitor Q-VD-OPh prevented IZI1551 and IZI1551/Birinapant induced cell death in Mel Juso cells and other synergistic responders, such as SkMel2 and Malme 3M (**Figure 2.1-1E**).

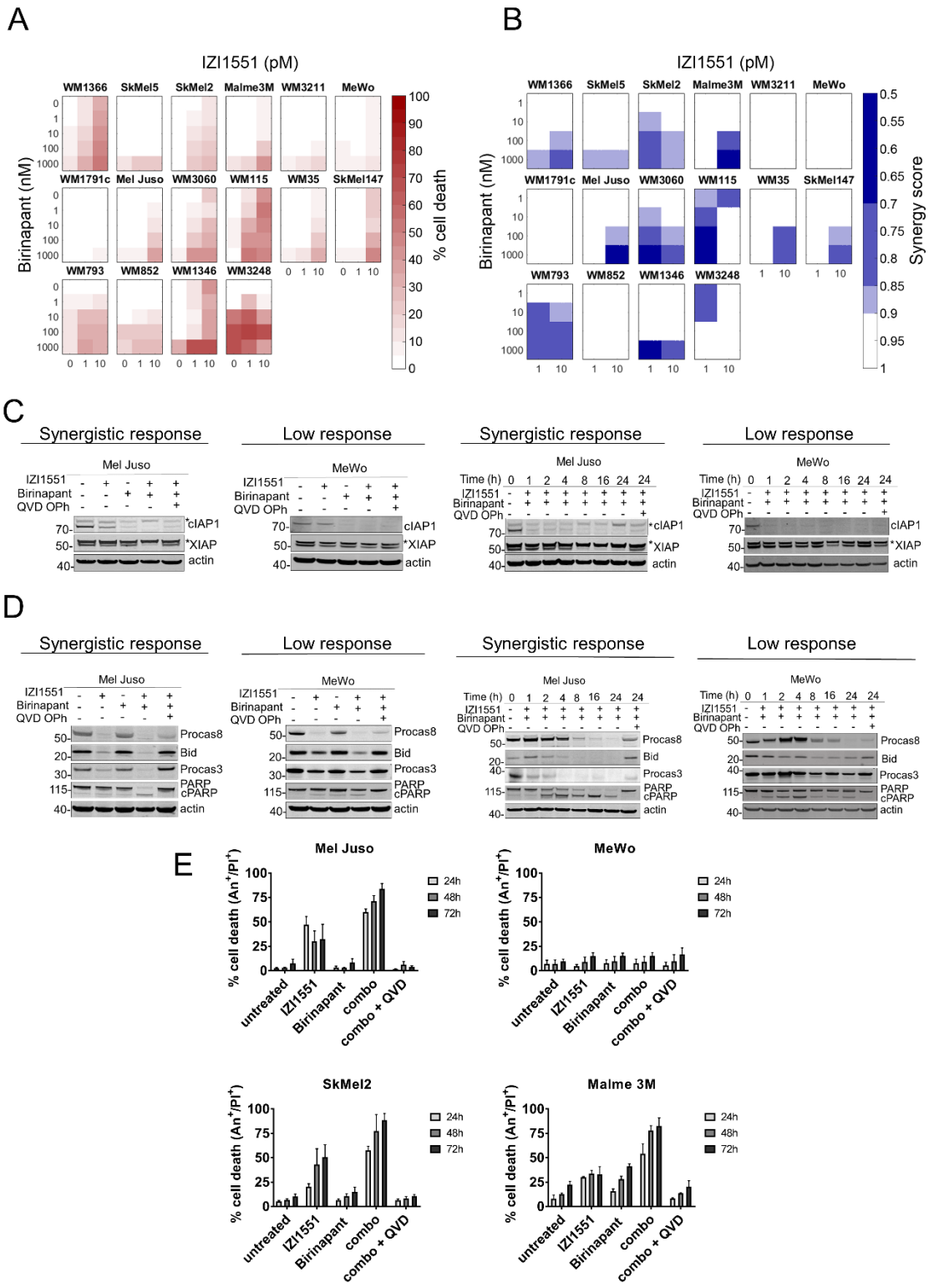

Figure 2.1-1: IAP antagonist Birinapant sensitizes a subset of melanoma cell lines to IZI1551-induced apoptosis. A Melanoma cell lines respond heterogeneously to single and combination treatment of IZI1551 and Birinapant. Cells were treated for 72 h followed by flow cytometric determination of cell death (propidium iodide positivity). Data shown are means from n = 3 independent experiments. **B** Synergy scores for treatment combinations, as calculated by Webb's fractional product method. **C** Treatment-induced changes in IAP amounts, analyzed by Western blotting. Actin served as loading control. Asterisks indicate unspecific bands. Representative results from n = 3 independent experiments are shown. **D** Apoptotic signalling was studied 24 h after single and combination treatment with IZI1551, Birinapant and QVD OPh (30 µM). Actin served as a loading control. Representative results from n = 3 independent experiments are shown. **E** Melanoma cell lines die by apoptosis upon combination treatment.

Cell lines were treated with 1 nM IZI1551, 1 µM Birinapant, with or without 30 µM QVD OPh. Cells were stained with PI and Annexin V-APC and analysed by flow cytometry. Shown are mean values + SD of three independent experiments.

Taken together, these results show that Birinapant sensitizes a subset of human melanoma cell lines to cell death induced by IZI1551, a 2nd generation TRAIL-based therapeutic, and that apoptosis appears to be the primary cell death modality in synergistic responders.

2.1.4.2 Expression patterns of apoptosis proteins allow predicting IZI1551/Birinapant responsiveness

The combination of IZI1551/Birinapant can induce apoptotic cell death without the need for protein neo-synthesis. We therefore next explored if baseline expression amounts of apoptosis proteins carry information on the responsiveness of melanoma cell lines to the combination of IZI1551/Birinapant. Pre-treatment amounts of 19 key pro- and anti-apoptotic players that regulate the apoptotic TRAIL signalling pathway were determined by quantitative immunoblotting at high dynamic range or, for death receptors, by cell surface staining (**Figure 2.1-2A**; **Supplementary Figure 2.1-2**). Expression patterns varied considerably between the proteins and across the cell lines. To explore possible correlations between protein expression patterns, we conducted a principal component analysis (PCA). A total of six principle components (PCs), all with an eigenvalue >1 and thus fulfilling the Kaiser criterion (Kaiser, 1960), were required to capture approximately 80% of the data variance **(Figure 2.1-2B**), highlighting that pre-treatment expression patterns were highly heterogeneous. Similarly, the associated weight coefficients indicated that individual proteins contributed heterogeneously to the first six PCs, without obvious positive or negative correlations between pro- and anti-apoptotic proteins (**Figure 2.1-2C**). A visualisation of the cell line positions within the space defined by the first three PCs correspondingly failed to identify visually distinct clusters of cell lines (**Figure 2.1-2D**). In conclusion, these data demonstrate high expression heterogeneity between proteins and between the cell lines.

Interestingly, colour coding the cell lines according to synergistic or low responsiveness indicated that synergistically responding and poorly responding cell lines occupy distinct regions within the plotted space (**Figure 2.1-2E**). Linear discriminant analysis (LDA) confirmed this visual impression, with 14/16 cell lines (88%) correctly separated into their respective response categories. These results, therefore, indicate that even though apoptosis protein expression is highly heterogeneous across the cell lines, the

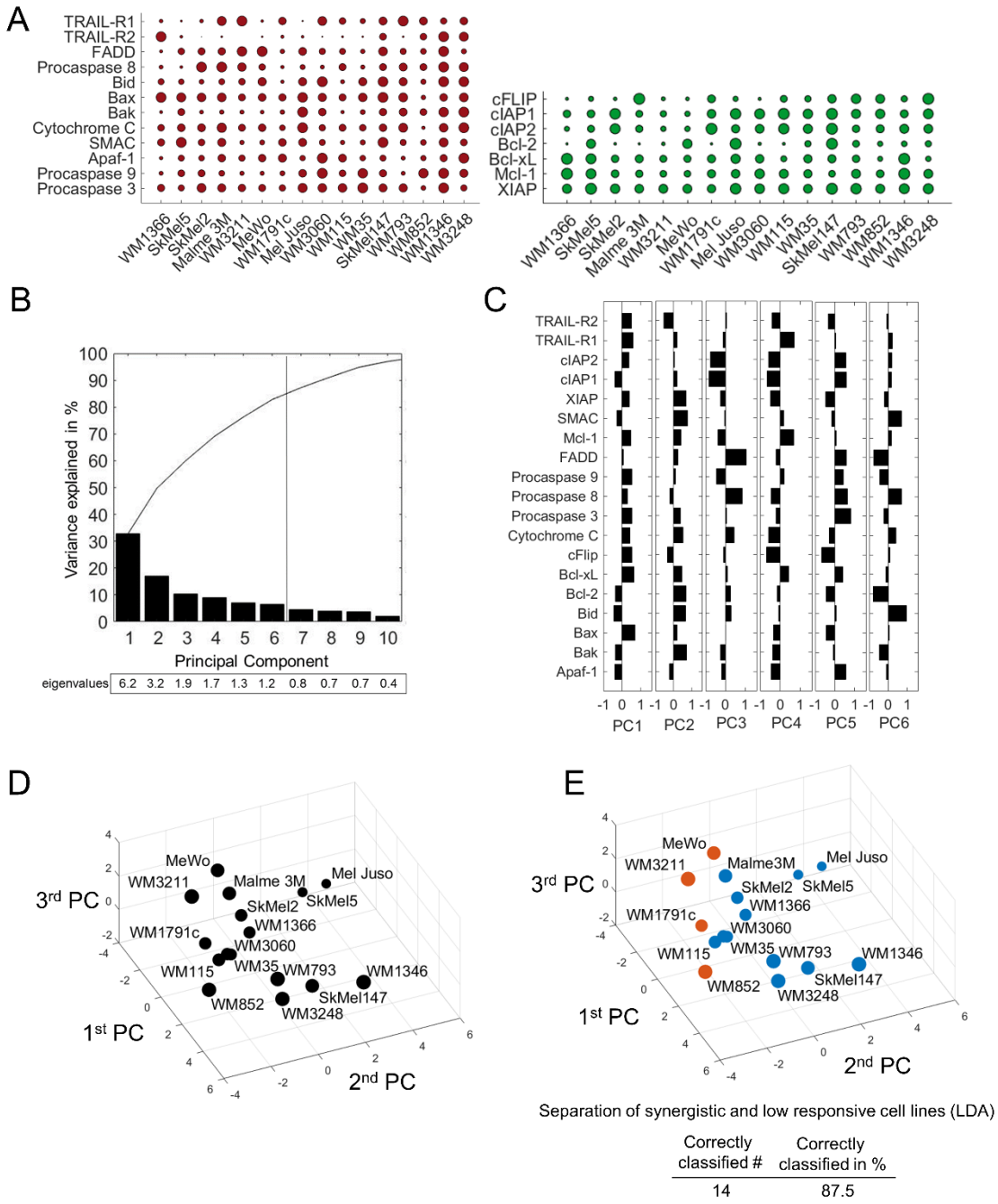

Figure 2.1-2: Expression patterns of apoptosis proteins separate resistant from synergistically responding cell lines. **A** Baseline expression of pro- and anti-apoptotic proteins of the TRAIL pathway. Circles summarize 684 quantifications, and circle sizes represent relative expression amounts of the proteins between cell lines. Protein amounts are provided in **Supplementary Table 2.1-1**. **B** Percentage of the variance of the original dataset explained by PCs. PCs with an eigenvalue >1 were retained for further analysis. Accumulated "variance explained" is plotted in black. **C** Weight coefficient table. Bars represent the contributions of the respective proteins to the different PCs. **D** Cell lines positioned in a multidimensional space according to their individual protein expression profiles. The PC space shown was defined by the first three PCs. Circle sizes decrease with distance from the observer to aid in 3D visualization. **E** Colour coding indicates responsiveness of cell lines to IZI1551/Birinapant (orange = low response; blue = synergistic response). Table insert indicates accuracy of spatial segmentation between low and synergistic responders.

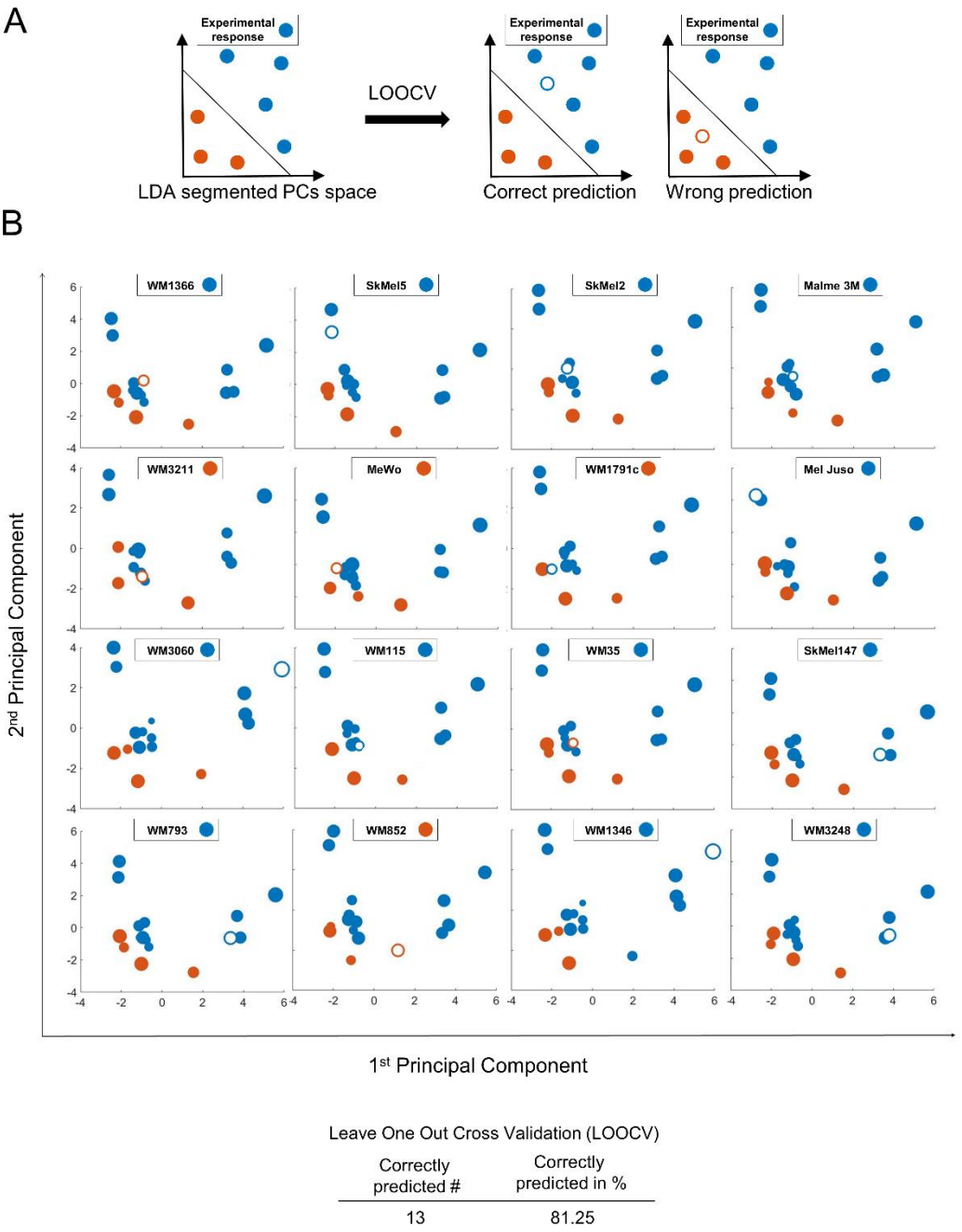

Figure 2.1-3: Expression patterns of apoptosis proteins allow predicting IZI1551/Birinapant responsiveness. A Simplified 2D schematic showing the workflow for determining prediction accuracy by combined PCA/LDA/LOOCV. Following PCA, an LDA separates the PC space into areas for synergistic responsiveness and low responsiveness. A cell line of unknown responsiveness (empty circle) is then placed into the segmented PC space according to its protein expression profile, with the positioning serving as the response prediction. Experimental responsiveness data served to validate predictions. **B** 2D projection of LOOCV results for the 16 cell lines. The responsiveness of the test cell line was predicted (blue for synergistic, orange for low responsive). The empty circle represents the test cell line being placed into the PC space. Circle sizes decrease with distance from the observer to aid 3D visualization. Table insert summarises prediction accuracy.

expression patterns nevertheless carry information on the capability to respond synergistically to the combination of IZI1551/Birinapant. We next tested if the protein expression patterns would be sufficient to predict responsiveness or resistance to IZI1551/Birinapant in melanoma cell lines. To this end, we performed leave-one-out

cross-validation (LOOCV) based on the approach described above. PCAs were conducted for sets of 15 cell lines, followed by LDAs to define the hyperspace regions of responsiveness and resistance. Missing cell lines were subsequently positioned into the LDA-segmented PC spaces according to their individual expression patterns of apoptosis regulators. If the tested cell line positioned into the correct response region, the prediction was considered successful (**Figure 2.1-3A**). Overall, LOOCV was sufficient to correctly predict the responsiveness of 13 out of 16 cell lines (81%) (**Figure 2.1-3B**), indicating that the measured protein panel allows predicting responsiveness to IZI1551/Birinapant on a case-by-case basis with high accuracy.

2.1.4.3 Responses to IZI1551/Birinapant can be predicted for 3D growth conditions

We next studied if responsiveness to IZI1551/Birinapant can be predicted for cells grown as multi-cellular tumour spheroids (MCTS). While more demanding as a cell culturing method, spheroids provide the advantage of higher microenvironmental complexity at nevertheless well-controlled experimental conditions (Vörsmann *et al.*, 2013). Protein quantification from spheroids of five cell lines able to form MCTS demonstrated that the transition from 2D cell culture to 3D spheroid culture substantially affected protein expression patterns (**Figure 2.1-4A, B**, **Supplementary Figure 2.1-3**). A number of pro- as well as anti-apoptotic proteins were considerably downregulated, such as Bid, Bcl-2, Procaspase 3, FADD and Mcl-1. cFLIP and TRAIL-R1, instead, appeared to accumulate, and a number of other proteins changed heterogeneously in their expression amounts across spheroids of different cell lines (**Figure 2.1-4B**). While a reductionist reasoning based on individual protein changes would intuitively suggest that IZI1551/Birinapant responsiveness of 3D MCTS should differ from 2D cultures, the combined complexity of altered protein expression prevents drawing conclusions prior to experimental validation. We therefore used the PCA/LDA-based approach to generate testable predictions on MCTS responsiveness. Positioning the MCTS forming cell lines into the PC space according to their respective pathway proteome revealed that their coordinates differed substantially from their 2D cultivated counterparts (**Figure 2.1-4C**). Interestingly, despite the substantial changes in relative protein amounts, all cell lines were predicted to remain within their respective response class (**Figure 2.1-4C)**, color-coded open circles). To test these *in-silico* predictions, we measured cell death in spheroids treated with IZI1551, Birinapant or the combination thereof. Indeed, the predictions could be confirmed for all five cell lines, with SkMel2,

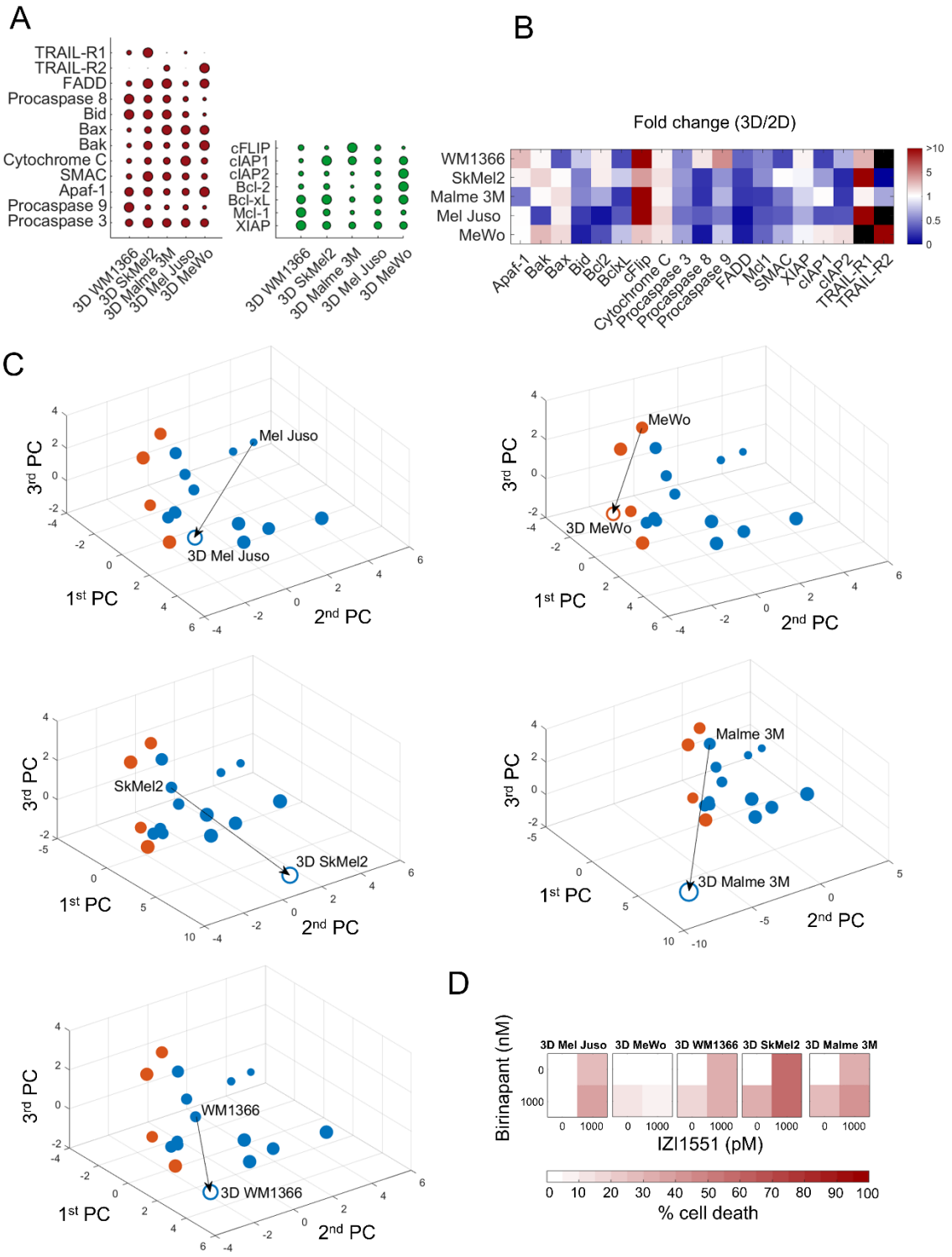

Figure 2.1-4: Responses to IZI1551/Birinapant can be predicted for 3D growth conditions. **A** Quantification of pro- and anti-apoptotic proteins in cell lines grown as MCTS (red and green, respectively). Circles summarize 285 quantifications and circle sizes represent mean protein quantities determined from at least n = 3 independent experiments. Protein amounts are provided in **Supplementary Table 2.1-1**. **B** Heatmap showing the fold change in protein expression between 3D and 2D culture. Black colour indicates absence in either 2D or 3D conditions. **C** Positioning of cell lines grown in 3D in the PC space defined by 2D cultured cell lines. Empty circles indicate positions of cell lines grown in 3D. Arrows indicate the change of position in the PC space caused by altered protein expression between 2D to 3D growth conditions. Circle colours reflect expected responsiveness (blue) or resistance (orange), based on the LDA segmented PC space. The circle size decreases with distance from the observer to aid 3D visualization. **D** Experimental validation of MCTS responsiveness to IZI1551/Birinapant treatment.

MCTS of cell lines were treated with IZI1551 (1 nM) and Birinapant (1 µM) or their combination for 24 h. Cell death was measured by flow cytometry (PI uptake). Data show means of n = 3 measurements.

WM1366, Mel Juso and Malme 3M responding to the combination treatment of IZI1551/Birinapant, and MeWo cells remaining resistant in the 3D growth scenario (**Figure 2.1-4D**). TNFα was not secreted upon growth in 3D or in response to the treatments, as tested for Mel Juso and MeWo cells (not shown). Overall, we therefore conclude that a PCA/LDA-based prediction framework, parameterised with protein expression and treatment responsiveness data from 2D cell cultures, is sufficient to predict responses to IZI1551/Birinapant for 3D spheroid growth conditions.

2.1.4.4 Responses to IZI1551/Birinapant can be predicted for melanoma cells freshly isolated from metastases

For a translationally more relevant setting, we next tested if IZI1551/Birinapant responses can be predicted for melanoma cells freshly isolated from metastases. Following quantification of apoptosis regulatory proteins (**Figure 2.1-5A**, **Supplementary Figure 2.1-4**), cells were positioned into the PC space. Predictions were generated as described above and cells were colour coded according to their expected IZI1551/Birinapant responsiveness. M10, M20, M32, and M45 cells were predicted to respond to IZI1551/Birinapant combination treatment, whereas M34 cells were expected to respond poorly (**Figure 2.1-5B**). Validation experiments confirmed the predictions on high responsiveness of M10, M32 and M20 cells and poor responsiveness of M34 cells (**Figure 2.1-5C**). We therefore conclude that high predictions accuracies can also be achieved for cells freshly isolated from clinical materials.

2.1.4.5 A reduced predictor maintains performance and estimates response prevalence to IZI1551/Birinapant in metastatic melanoma

The framework to predict responsiveness to IZI1551/Birinapant builds on an otherwise unbiased selection of nineteen regulators known to be involved in canonical apoptosis signal transduction for this treatment combination. We next determined the contribution of the individual protein variables towards accurate predictions. To do so, we used the attribute selection feature of the WEKA workbench (Frank *et al.*, 2004) to compute the "merit" of each protein, based on the protein expression profiles and the responsiveness data of the melanoma cell line panel. From this, we obtained a ranking of protein variables according to the degree of association with treatment responsiveness (in sequence of decreasing merit: XIAP, Procaspase 3, Cytochrome C, Mcl-1, cIAP1, Bax,

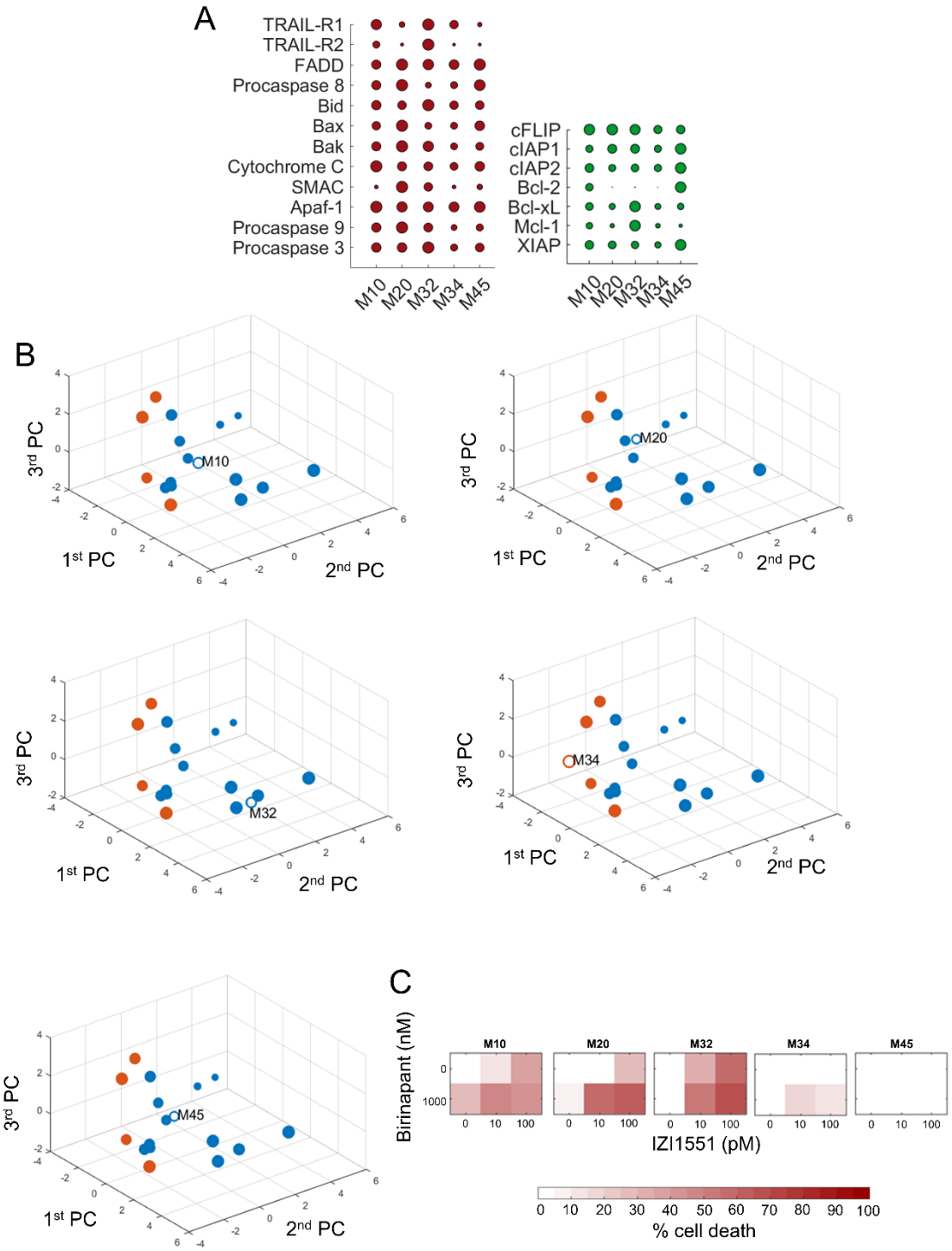

Figure 2.1-5: Responses to IZI1551/Birinapant can be predicted for cells isolated from melanoma metastases. A Quantification of apoptosis regulatory proteins in cells derived from melanoma metastases. Red coloured circles represent pro-apoptotic and green circles anti-apoptotic proteins. Circles summarize 285 quantifications, and circle sizes represent mean protein quantities determined from at least n = 3 independent experiments. Protein amounts are shown in **Supplementary Table 2.1-1**. **B** Positioning of melanoma cells from patient metastases in the PC space defined by 2D cultured cell lines. Empty circles indicate positions of patient cells. Circle colours reflect expected responsiveness (blue) or resistance (orange), based on the LDA segmented PC space. The circle size decreases with distance from the observer to aid 3D visualization. **C** Experimental validation of primary melanoma cell responsiveness to IZI1551/Birinapant treatment. Cells were treated as indicated for 24 h. Cell death was measured by flow cytometry (PI uptake). Heat maps show the mean of n = 3 independent experiments.

Bid, Bcl-xL, Smac, FADD, Bak, cIAP2, TRAIL-R1, Procaspase 9, Apaf-1, TRAIL-R2, Procaspase 8, cFLIP and Bcl-2). We then iteratively performed predictions for the cell line panel, with the protein with the lowest merit removed upon each iteration.

Performance was largely maintained (14/16 correct predictions for the cell line panel) when limiting the predictor to the eleven proteins with the highest merit (**Figure 2.1-6A**). The reduced predictor correctly determined treatment responsiveness in 4/5 MCTS growth scenarios and in 4/5 biopsy-derived fresh melanoma cells (**Figure 2.1-6B, C**). Further validation of the reduced predictor was conducted using nine additional and independently analysed samples, including three 2D and six 3D growth scenarios. Also in these samples prediction accuracies of approx. 80% were achieved (**Figure 2.1-6D-F, Supplementary Figure 2.1-5**). Overall, we noted strong influences of XIAP and procaspase-3, direct interactors and regulators of type I signalling competency during extrinsic apoptosis (Aldridge *et al.*, 2011; Wilson *et al.*, 2009), and various members of the Bcl-2 family in the predictor (**Figure 2.1-6A**). The ability to predict responsiveness to IZI1551/Birinapant in cell lines and *ex vivo* cultures raises the question if responses can be expected in patients, and if so, how frequent such responses might be. We therefore estimated the clinical response prevalence under the assumption that favourable drug pharmacokinetics and pharmacodynamics allow both drugs to reach their targets. Expression profiles of predictor variables were deduced from transcriptome data of metastatic melanoma patients (n = 365, TCGM-SKCM cohort, **Supplementary Table 2.1-2**) by mapping to protein expression ranges measured experimentally. Following positioning into the LDA segmented PC space defined by the predictor, 111 out of 365 patients were expected to respond to treatment (**Figure 2.1-6G**). The expectation of approx. 30% responders needs to be interpreted in the context of predictor accuracy. The 80% prediction accuracy achieved in the cell line panel is composed of a predictor sensitivity of 92% and a specificity of 75%, so that the predictor strength lies in recalling true positives. Taken together, these results demonstrate that highly accurate predictions can be made for IZI1551/Birinapant responsiveness with a reduced set of input variables, and that in up to 30% of clinical cases an on target responsiveness could be expected, as estimated from a representative cohort of metastatic melanoma patients.

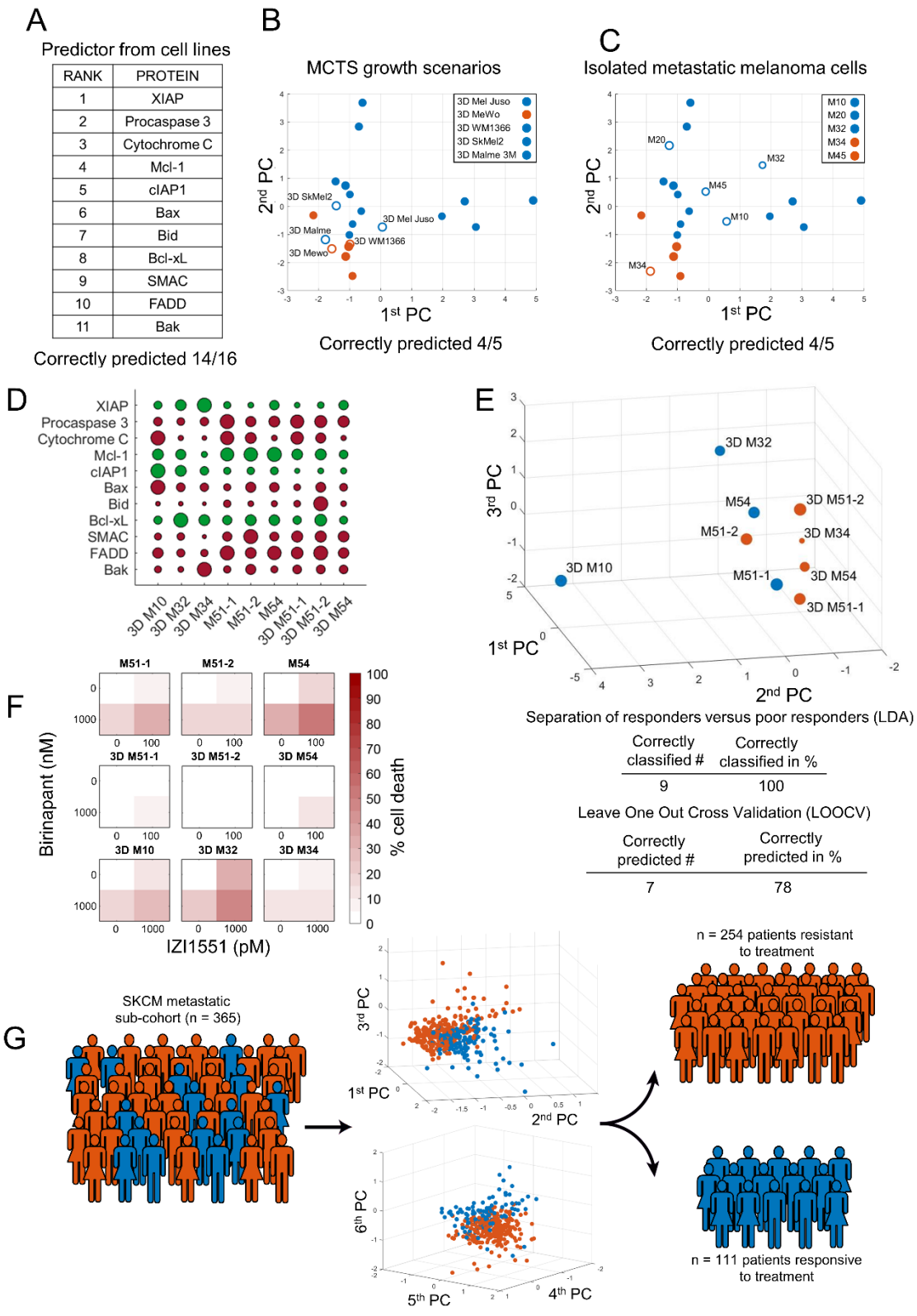

Figure 2.1-6: A reduced predictor maintains performance and estimates response prevalence to IZI1551/Birinapant in metastatic melanoma. A Ranking of variables in a reduced predictor, as obtained by computed merit. **B** and **C** Responsiveness predictions and prediction accuracies for MCTS growth scenarios and for metastatic melanoma cells isolated from patients. The PC space is shown as a two-dimensional projection. Filled circles represent training data from the melanoma cell line panel. Open circles highlight positions of MCTS (B) or cells isolated from melanoma metastases (C). **D** Quantities of apoptosis regulators in additional validation samples. Circle sizes represent relative protein amounts. Protein amounts are listed in **Supplementary Table 2.1-1**. Western blots are shown in **Supplementary Figure 2.1-5**. **E** Validation samples positioned in the PC space obtained by the reduced predictor. Color-

coding indicates responsiveness. Table inserts display accuracy of spatial segmentation and prediction accuracy. **F** Experimental responsiveness of validation samples. Cells were treated as indicated for 24 h. Cell death was measured by flow cytometry (PI uptake). Heat maps show the mean of n = 3 independent experiments. **G** Estimation of response prevalence in a hypothetical trial. Estimated protein expression profiles of metastatic melanoma patients (n = 365) were used to predict responsiveness (blue, n = 111) or resistance (orange n = 254) to IZI1551/Birinapant combination treatment. 3D graphs show arrangement of predicted responders and non-responders in the predictor space.

2.1.5 Discussion

Here, we report that protein expression signatures of TRAIL pathway regulators can serve to predict responsiveness to the combination of IZI1551 and Birinapant, targeted therapeutics with high translational relevance (Fulda and Vucic, 2012; de Miguel *et al.*, 2016). High accuracies for response predictions were achieved for melanoma cell lines, for 3D multi-cellular melanoma spheroids and for cells newly isolated from melanoma metastases (approx. 80% prediction accuracy). Protein prioritization resulted in a reduced marker that, when applied in a proof of concept *in silico* trial, suggests that IZI1551/Birinapant responsiveness could be expected in up to 30% of tumours in patients with metastatic melanoma.

Previous TRAIL-based therapeutics were tested in translational settings and performed unsatisfactorily (de Miguel *et al.*, 2016). Among the reasons for limited efficacy of TRAIL-R agonistic antibodies in the clinic were short serum half-lives and the requirement for immune cell-mediated, Fcγ-dependent clustering of therapeutic antibodies to induce efficient TRAIL-R1/R2 oligomerisation and caspase-8 activation (Wilson *et al.*, 2011). 2nd generation TRAIL-based therapeutics address these problems, for example by increased valency and by using Fc regions as dimerization and half-life extension modules (Gieffers *et al.*, 2013; Hutt *et al.*, 2017; de Miguel *et al.*, 2016). IZI1551, consisting of two tri-valent single-chain TRAIL fragments cross-linked via the Fc part of an IgG antibody, is a prototypical example for this principle and potently induces apoptosis *in vivo* in cells moderately responsive to traditional TRAIL-based therapeutics (Hutt *et al.*, 2017). However, in many cases sensitizing co-treatments are required to ensure efficient apoptosis induction following TRAIL-R1/R2 activation. IAP antagonists are potent sensitizers to extrinsic apoptosis (Fulda, 2015), suppressing the formation of LUBAC and the associated initiation of pro-survival signalling. IAP antagonists also sensitize to apoptosis induced by intrinsic cytotoxic stimuli, such as genotoxic therapeutics in pancreatic, colon and brain cancer (Crawford *et al.*, 2018; Dineen *et al.*, 2010; Ziegler *et al.*, 2011), where cIAPs likely impair caspase-8 binding and activation on cytosolic ripoptosomes (Feoktistova *et al.*, 2011; Tenev *et al.*, 2011).

While both 2nd generation TRAIL-R1/R2 agonists as well as IAP antagonists are currently tested in clinical trials (NCT03082209, (Fulda, 2015; Morgan-Lappe, 2017)), currently no studies test their combination. In addition, validated biomarkers predictive of treatment responsiveness do not exist for TRAIL-based therapeutics, IAP antagonists or the combination of both. The lack of reliable molecular markers to predict responses to TRAIL might indeed have contributed to the poor performance of TRAIL based therapeutics in the clinical setting, since no patient selection could be performed (Lemke *et al.*, 2014). The absence of response predictors for IAP antagonists likewise affects current clinical trials based on this class of therapeutics (Fulda, 2015). Notably, for both TRAIL-R1/R2 agonists as well as for IAP antagonists, the expression amounts of their direct molecular targets, i.e. TRAIL-R1/R2 amounts and cIAP proteins, appear insufficient to derive response biomarkers (Fulda, 2015; Wagner *et al.*, 2007; Zakaria *et al.*, 2016). This indicates that treatment efficacy is determined further downstream within the signal transduction network and/or too complex to be captured by traditional or reductionist biomarker discovery approaches.

With IAP antagonists removing the apical suppression of extrinsic apoptosis induction, we hypothesized that the expression amounts of key regulatory proteins of the TRAIL signal transduction network can serve to predict responsiveness. Indeed, predictions on IZI1551/Birinapant responses, based on the expression patterns of key TRAIL pathway regulators, were highly accurate. Being able to predict responsiveness also in a micro-environmentally more complex 3D setting and in cells newly isolated from patients indicates that concerns about using continuously cultured cell lines to develop a predictor for IZI1551/Birinapant responsiveness can be alleviated, possibly because protein expression alone is sufficient to derive treatment responsiveness. Complex genetic characterisations and careful selection of cell line and *in vivo* models might however be warranted for studies on treatment scenarios that are highly dependent on disease-relevant mutations, and accordingly the genetic representation of the disease (Fang and Eglen, 2017; Garman *et al.*, 2017; Luebker *et al.*, 2017).

We initiated our study using 19 proteins considered key regulators of IZI1551/Birinapant induced signal transduction. We could reduce this panel to an 11 protein signature which, compared to traditional biomarkers, still seems rather large. However, this likely reflects the complexity of apoptosis signal transduction and regulation, as well as the disease heterogeneity observed in melanoma. The development of complex protein quantity-based biomarkers for routine clinical

application still faces major technological challenges (Panis *et al.*, 2016; Petricoin *et al.*, 2002). Traditional immunohistochemical analyses of tumour biopsies typically provides insufficient dynamic range and limited calibration possibilities to derive reliable quantitative data. Alternative approaches, such as reverse phase protein arrays and mass spectrometric analyses of clinical specimen can overcome these hurdles, but are difficult to embed into routine pathology and laboratory workflows in the clinical environment. To take intra-tumour cell-to-cell heterogeneity into account, an aspect likely crucial to refine our predictor in a translational setting, technology such as mass cytometry could provide the possibility to capture multiplexed protein markers at the single cell level (Spitzer and Nolan, 2016). However, this technology is difficult to apply to tissue specimen. Developments in the field of high dynamic range fluorescence-based analysis of FFPE materials, coupled to multiplexing technologies that allow re-staining of tissue slices (Gerdes *et al.*, 2013; Schubert *et al.*, 2006), might more conveniently and routinely allow obtaining quantitative protein expression data, especially where entire cellular proteomes are not required.

It is noteworthy that none of the melanoma models studied lacked TRAIL-R1/R2 or caspase-8 expression, and TRAIL-Rs or caspase-8 amounts did not appear crucial to predict responsiveness. The amounts of these proteins therefore possibly do not limit IZI1551/Birinapant responsiveness in melanoma. A recent study in models of non-small-cell lung cancer and pancreatic ductal adenocarcinoma interestingly indicates that cancer cells might become addicted to TRAIL receptor expression, with autonomous TRAIL-R signalling contributing to disease progression (von Karstedt *et al.*, 2015). Additionally, proliferating cells might rely on a cell death-independent role of caspase-8 in contributing to chromosome alignment during mitosis (Liccardi *et al.*, 2019). In the predictor, the expression of XIAP and caspase-3 strongly contributed to accurate response predictions. Both proteins play crucial roles in controlling cellular life/death decisions during apoptosis execution (Rehm *et al.*, 2006; Taylor *et al.*, 2008). XIAP additionally holds in check the “type I” link by which caspase-8 can activate caspase-3 (Aldridge *et al.*, 2011; Jost *et al.*, 2009; Wilson *et al.*, 2009). However, kinetically the mitochondrial route still seems preferred in cells capable to die by type I signalling (Aldridge *et al.*, 2011), most likely due to the strong amplification of apoptosis signalling by Bcl-2 family-dependent mitochondrial outer membrane permeabilisation and apoptosome formation. Indeed, various Bcl-2 family members, such as Mcl-1, Bax, Bid, Bcl-xL and Bak, display prominently in the predictor. Mcl-1 and Bcl-xL negatively

regulate Bax/Bak pore formation, while Bid is a primary substrate of both caspase-8 and caspase-3, with truncated Bid inhibiting Mcl-1 and Bcl-xL, and activating Bax and Bak (Hantusch *et al.*, 2018). Taken together, the interplay of caspases-3, XIAP and Bcl-2 family members, initiated by non-limiting amounts of TRAIL receptors and caspase-8, appears to play a central role in melanoma cell death upon exposure to IZI1551/Birinapant.

Taken together, this study represents a successful proof-of-concept for developing a stratification marker for malignant melanoma in response to a novel, clinically relevant combination treatment based on a 2nd generation hexavalent TRAIL variant (IZI1551) and a representative IAP antagonist, Birinapant. This can form the basis for future translational and clinical studies in which combination treatments of 2nd generation TRAIL-based therapeutics and IAP antagonists will be tested and for which optimal patient selection strategies are required.

2.1.6 Acknowledgments and funding information

The authors kindly acknowledge support by the European Union's Horizon 2020 research and innovation programme under the Marie Skłodowska-Curie grant agreement #642295 (MEL-PLEX). MR and CG are funded by the Deutsche Forschungsgemeinschaft (DFG, German Research Foundation) under Germany's Excellence Strategy - EXC 2075 – 390740016. MR also receives support from the German Research Foundation (FOR2036 (MO 3226/1-1)) and the European Union's Horizon 2020 research and innovation programme (grant agreement #766069 (GLIO-TRAIN)) and the Health Research Board Ireland (HRA POR 2015 1091). The authors thank Doris Göttsch, Beatrice Reiser and Alexandra Kraske for technical assistance.

2.1.7 Supplementary material

Supplementary Table 2.1-1: Protein data obtained from melanoma cell lines and cells isolated from metastases.

	DR4 [cell surface antigen density]	*DR5 [cell surface antigen density]*	*FADD [µM]*	*Procaspase 8 [µM]*	*Bid [µM]*	*Bax [µM]*
WM1366	3655	1086	0.044	0.049	0.141	0.310
SkMel5	311	374	0.184	0.028	0.190	0.257
SkMel2	18	1145	0.213	0.303	0.197	0.237
Malme 3M	148	6593	0.230	0.305	0.183	0.240
WM3211	0	8017	0.384	0.224	0.064	0.155
MeWo	132	642	0.415	0.136	0.115	0.192
WM1791c	398	4675	0.088	0.040	0.097	0.170
Mel Juso	269	209	0.263	0.080	0.192	0.296
WM3060	65	6366	0.171	0.051	0.081	0.213
WM115	160	3656	0.159	0.159	0.068	0.160
WM35	127	2347	0.088	0.058	0.061	0.232
SkMel147	2689	7976	0.294	0.125	0.074	1.823
WM793	213	12188	0.148	0.161	0.052	1.467
WM852	2532	7889	0.131	0.122	0.022	0.391
WM1346	5638	4987	0.379	0.246	0.078	1.088
WM3248	4680	7299	0.102	0.207	0.075	1.442
3D WM1366	13361	0	0.016	0.089	0.101	0.098
3D SkMel2	56479	7	0.049	0.059	0.091	0.250
3D Malme	200	4000	0.048	0.058	0.089	0.492
3D Mel juso	4968	0	0.016	0.027	0.043	0.434
3D MeWo	0	10000	0.043	0.012	0.012	0.431
M10	2730	3369	0.035	0.087	0.047	0.435
M20	561	1047	0.052	0.132	0.040	0.764
M32	6797	3981	0.046	0.039	0.067	0.291
M34	478	2267	0.039	0.053	0.038	0.293
M45	528	651	0.053	0.122	0.040	0.573
3D M10			0.026		0.027	1.606
3D M32			0.016		0.026	0.629
3D M34			0.013		0.018	0.585
M51_1			0.046		0.066	0.422
M51_2			0.028		0.039	0.848
M54 2D			0.043		0.044	0.747
3D M51_1			0.032		0.054	0.379
3D M51_2			0.045		0.228	0.803
3D M54			0.026		0.039	0.509

	Bak [µM]	*Cytochrome C [µM]*	*SMAC [µM]*	*Apaf-1 [µM]*	*Procaspase 9 [µM]*	*Procaspase 3 [µM]*
WM1366	0.467	3.860	0.278	0.091	0.002	0.199
SkMel5	2.420	5.239	0.534	0.262	0.007	0.146
SkMel2	0.764	5.451	0.240	0.234	0.007	0.301
Malme 3M	0.944	7.565	0.364	0.402	0.005	0.251
WM3211	0.865	4.342	0.105	0.287	0.003	0.212
MeWo	0.725	5.045	0.136	0.396	0.003	0.194
WM1791c	1.032	2.895	0.320	0.464	0.004	0.161
Mel Juso	4.784	8.539	0.348	0.212	0.009	0.318
WM3060	2.778	3.657	0.198	0.686	0.014	0.289
WM115	0.622	4.336	0.108	0.440	0.006	0.288
WM35	1.222	3.837	0.143	0.228	0.013	0.377
SkMel147	0.403	6.618	0.288	0.113	0.014	0.404
WM793	0.468	9.289	0.111	0.052	0.005	0.426
WM852	0.349	1.479	0.095	0.089	0.024	0.146
WM1346	0.662	8.711	0.232	0.157	0.027	0.608
WM3248	0.726	11.420	0.135	0.293	0.018	0.243
3D WM1366	0.564	5.579	0.076	0.300	0.012	0.099
3D SkMel2	1.887	10.453	0.231	0.314	0.004	0.165
3D Malme	1.020	10.533	0.165	0.174	0.003	0.130
3D Mel juso	1.201	20.377	0.120	0.206	0.004	0.132
3D MeWo	2.485	9.128	0.088	0.368	0.002	0.115
M10	1.899	10.348	0.095	0.290	0.004	0.173
M20	2.869	6.829	0.791	0.246	0.006	0.175
M32	2.445	6.509	0.463	0.229	0.004	0.242
M34	1.096	5.119	0.102	0.229	0.002	0.098
M45	1.466	7.574	0.207	0.265	0.002	0.147
3D M10	0.937	18.787	0.165			0.081
3D M32	0.633	2.787	0.190			0.065
3D M34	3.674	2.249	0.060			0.079
M51_1	1.021	16.753	0.281			0.211
M51_2	1.930	11.460	0.638			0.114
M54 2D	0.952	3.249	0.267			0.128
3D M51_1	1.453	14.838	0.405			0.187
3D M51_2	1.469	9.813	0.408			0.156
3D M54	1.393	2.804	0.378			0.137

	cFLIP [µM]	*cIAP1 [µM]*	*cIAP2 [µM]*	*Bcl-2 [µM]*	*Bcl-xL [µM]*	*Mcl-1 [µM]*	*XIAP [µM]*
WM1366	0.041	0.035	0.017	0.139	0.164	0.081	0.049
SkMel5	0.087	0.037	0.031	2.270	0.138	0.067	0.070
SkMel2	0.130	0.070	0.064	0.184	0.076	0.040	0.052
Malme 3M	0.165	0.029	0.033	0.135	0.089	0.036	0.044
WM3211	0.104	0.025	0.018	0.356	0.068	0.030	0.046
MeWo	0.127	0.018	0.019	2.385	0.072	0.030	0.046
WM1791c	0.093	0.046	0.075	0.155	0.091	0.046	0.041
Mel Juso	0.089	0.068	0.043	3.272	0.120	0.050	0.066
WM3060	0.129	0.062	0.049	0.301	0.099	0.062	0.055
WM115	0.155	0.074	0.067	0.224	0.050	0.055	0.061
WM35	0.134	0.056	0.053	1.092	0.095	0.047	0.045
SkMel147	0.215	0.035	0.095	0.570	0.308	0.042	0.075
WM793	0.270	0.025	0.044	0.223	0.253	0.075	0.068
WM852	0.240	0.026	0.052	0.133	0.117	0.055	0.051
WM1346	0.118	0.018	0.066	0.152	0.546	0.111	0.063
WM3248	0.356	0.029	0.062	0.186	0.136	0.076	0.063
3D WM1366	1.164	0.009	0.011	0.211	0.046	0.039	0.065
3D SkMel2	0.577	0.039	0.010	0.283	0.056	0.020	0.046
3D Malme	3.156	0.029	0.007	0.083	0.019	0.008	0.034
3D Mel juso	1.147	0.020	0.013	0.254	0.039	0.015	0.041
3D MeWo	0.374	0.029	0.040	0.705	0.050	0.011	0.041
M10	0.129	0.027	0.020	0.944	0.137	0.074	0.058
M20	0.130	0.041	0.014	0.005	0.088	0.034	0.049
M32	0.121	0.041	0.016	0.013	0.259	0.200	0.044
M34	0.077	0.027	0.014	0.002	0.083	0.038	0.032
M45	0.084	0.058	0.030	1.850	0.096	0.020	0.090
3D M10		0.030			0.089	0.037	0.064
3D M32		0.018			0.254	0.032	0.115
3D M34		0.011			0.154	0.012	0.195
M51_1		0.008			0.113	0.052	0.052
M51_2		0.009			0.154	0.055	0.033
M54 2D		0.010			0.147	0.060	0.090
3D M51_1		0.004			0.092	0.035	0.032
3D M51_2		0.005			0.178	0.037	0.044
3D M54		0.006			0.083	0.023	0.089

Supplementary Table 2.1-2: Patient demographics and clinical information of the metastatic SKCM-TCGA sub-cohort (n = 365 patients).

Patients demographics and clinical information		
Age at diagnosis (years)		
Mean	56.2	
Median	56	
Range	15 - 87	
Gender	**Value**	**%**
Female	136	37.26
Male	229	62.74
Ethnicity	**Value**	**%**
White (non-Hispanic or Latino)	342	93.70
White (Hispanic or Latino)	7	1.92
White (ethnicity not reported)	4	1.10
Asian	5	1.37
Black or African American	1	0.27
Not reported	6	1.64
Disease stage at initial diagnosis	**Value**	**%**
Stage 0 - II	164	44.93
Stage III - IV	165	45.21
Not reported	36	9.86
Clark level at initial diagnosis	**Value**	**%**
I - III	83	22.74
IV - V	159	43.56
Not reported	123	33.70
Overall survival from initial diagnosis (months)		
Median	80.6	
Range	2.6 - 357.1	

A

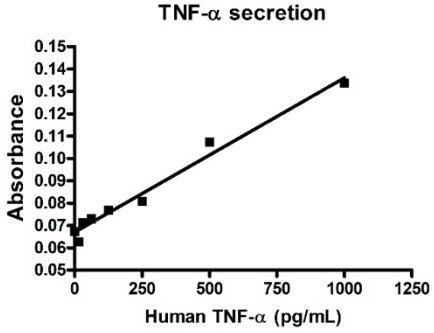

B

3D Mewo	
control	Below detecting limit
IZI1551	Below detecting limit
Birinapant	Below detecting limit
combo	Below detecting limit
Hela positive control	30.09 pg/mL

3D Mel Juso	
control	Below detecting limit
IZI1551	Below detecting limit
Birinapant	Below detecting limit
combo	Below detecting limit
Hela positive control	30.09 pg/mL

C

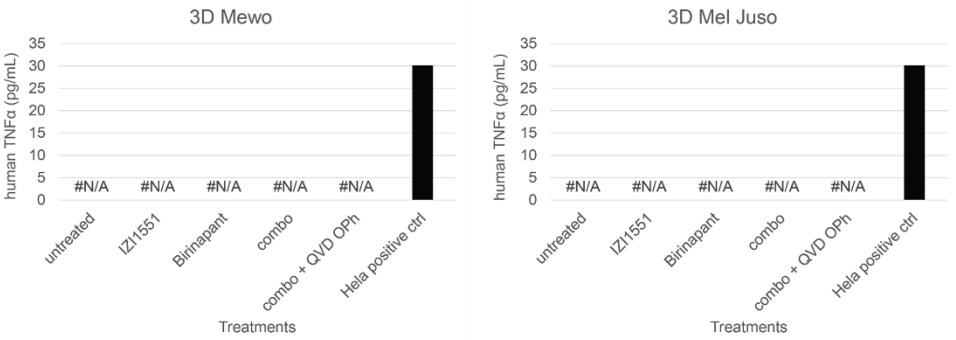

Supplementary Figure 2.1-1: Cell lines MeWo and Mel Juso do not secrete TNF-α when treated with IZI1551, Birinapant or their combination. A Titration of recombinant standard TNF-α using Human TNF-α DuoSet ELISA. **B** Cell lines MeWo and Mel Juso do not secrete TNF-α. 3D MeWo and Mel Juso were treated with 1 µM IZI1551, 1 µM Birinapant or their combination for 24 h. Hela cells were exposed to 15 s 30 mJ UVB and treated for 24 h with 10 ng/mL IL-1 for the production of TNF-α that served as a positive control. 100 µl of each supernatant was tested for TNF-α secretion. **C** Histogram of the data presented in **B**.

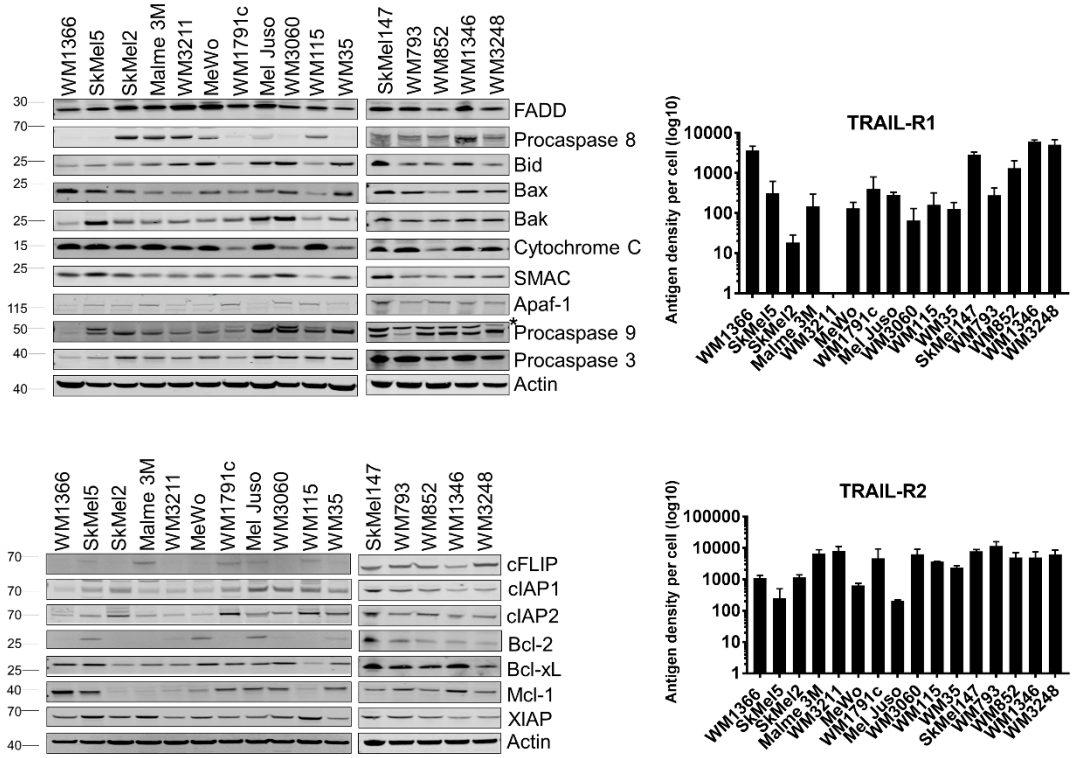

Supplementary Figure 2.1-2: Apoptosis proteins are heterogeneously expressed in melanoma cell lines. Intracellular pro- and anti-apoptotic proteins were detected by western blotting at high dynamic range. Actin served as loading control. Representative 8 bit converted images are shown from at least n = 3 repeat experiments. Death receptors were measured by surface staining and flow cytometry. Bars show mean of antigen density (TRAIL-R1,TRAIL-R2) per cell + SD from n = 3 repeat experiments.

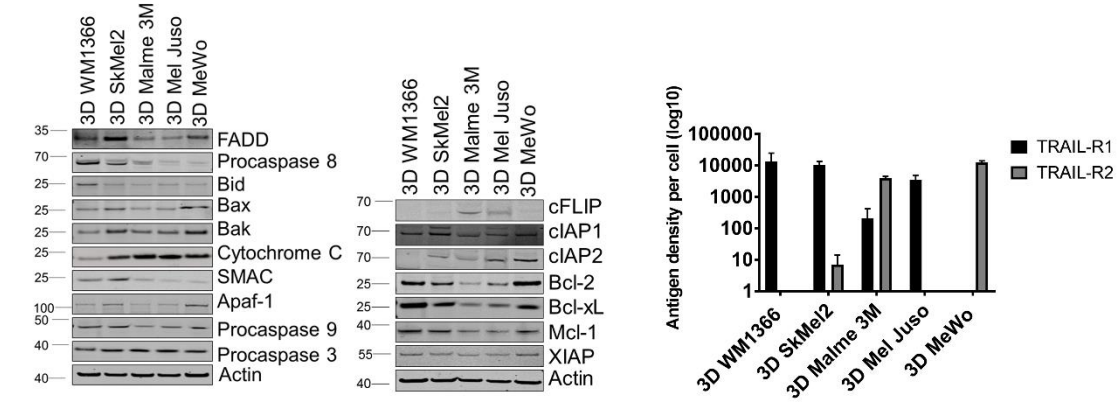

Supplementary Figure 2.1-3: Protein expression in melanoma MCTS. Cell lines grown as MCTSs were analysed for intracellular pro- and anti-apoptotic protein expression by western blotting. Actin served as loading control. Representative 8 bit converted images are shown from at least n = 3 repeat experiments. Death receptors were measured by surface staining and flow cytometry. Bars show mean of antigen density (TRAIL-R1, TRAIL-R2) per cell + SD from n = 3 repeat experiments.

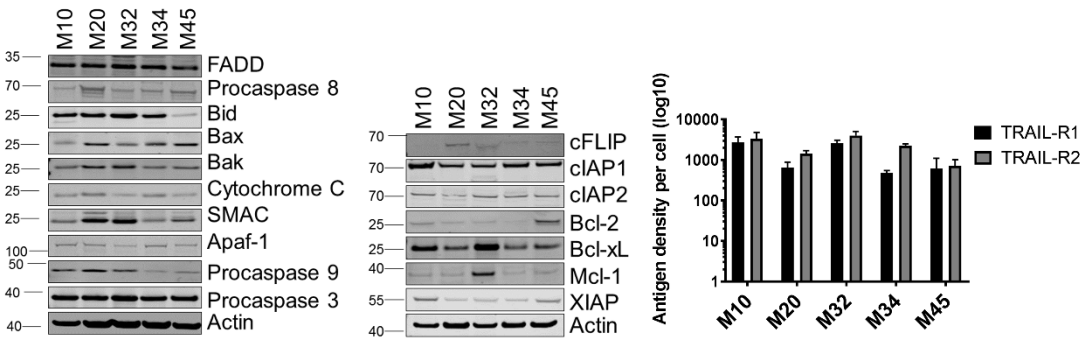

Supplementary Figure 2.1-4: Protein expression in melanoma cells isolated from patient metastases. Intracellular pro- and anti-apoptotic protein expression was determined by western blotting. Actin served as loading control. Representative 8 bit converted images are shown from at least n = 3 repeat experiments. Death receptors were measured by surface staining and flow cytometry. Bars show mean of antigen density (TRAIL-R1, TRAIL-R2) per cell + SD from n = 3 repeat experiments.

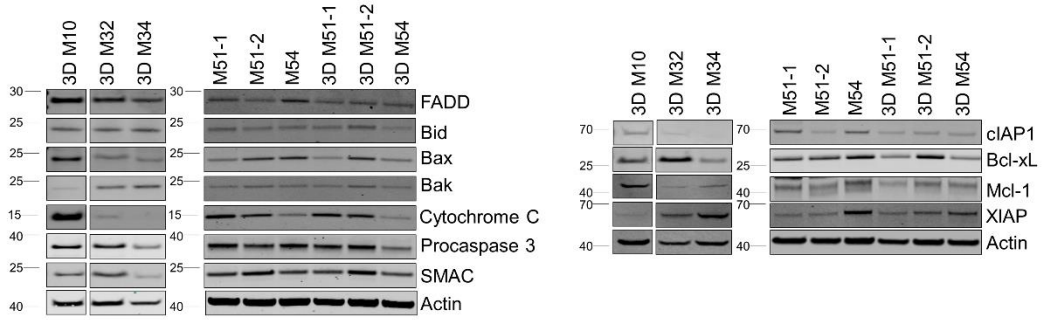

Supplementary Figure 2.1-5: Protein expression in additional melanoma samples, as required for further validation of the reduced predictor. Intracellular pro- and anti-apoptotic protein expression was determined by western blotting. Actin served as loading control. Representative 8 bit converted images are shown.

2.2 Low expression of pro-apoptotic proteins Bax, Bak and Smac indicates prolonged progression-free survival in chemotherapy-treated metastatic melanoma

Guttà, C., Rahman, A., Aura, C., Dynoodt, P., Charles, E. M., Hirschenhahn, E., Joseph, J., Wouters, J., de Chaumont, C., Rafferty, M., Warren, M., van den Oord, J. J., Gallagher, W. M., & Rehm, M. (2020). Low expression of pro-apoptotic proteins Bax, Bak and Smac indicates prolonged progression-free survival in chemotherapy-treated metastatic melanoma. *Cell death & disease*, *11*(2), 124. https://doi.org/10.1038/s41419-020-2309-3.

Author contributions:

CG: processed the IHC and clinical data, performed the data analysis, curated the IHC and clinical datasets, drafted the manuscript and designed the figures.

AR: performed IHC on TMAs and CPAs, antibody validation, manually scored the tissue samples, performed the digital image analysis, revised and approved the manuscript.

CA: manually scored the tissue samples, performed the quality control of the tissue samples, revised and approved the manuscript.

PD: contributed to digital image analysis and data acquisition, antibody validation, contributed to the datasets curation, revised and approved the manuscript.

EMC: preprocessed the IHC and clinical data, curated the IHC and clinical datasets, revised and approved the manuscript.

EH: contributed to IHC data collection and integration, revised and approved the manuscript.

JJ: parametrized and performed the digital image analysis, revised and approved the manuscript.

JW: contributed to digital image analysis, antibody validation, revised and approved the manuscript.

CD: contributed to cell-based analyses, revised and approved the manuscript.

MRA: co-supervised antibody validation and digital imaging, revised and approved the manuscript.

MW: manually scored samples, supervised scoring and TMA analyses, discussed the results, contributed to the IHC dataset curation.

JV: contributed to sample collection and preparation and characterization, supervised scoring, discussed the results and revised and approved the manuscript.

WG: Supervised antibody validation and digital imaging, discussed the results, revised and approved the manuscript.

MRE: conceived and supervised the project as a whole, drafted the manuscript and designed the figures.

Research article

Low expression of pro-apoptotic proteins Bax, Bak and Smac indicates prolonged progression free survival in chemotherapy-treated metastatic melanoma

Cristiano Guttà[1], Arman Rahman[2,3], Claudia Aura[2,3,4], Peter Dynoodt[2,5], Emilie M. Charles[4,6,7], Elodie Hirschenhahn[4,6,7], Jesuchristopher Joseph[2,6], Jasper Wouters[2,5,8,9], Ciaran de Chaumont[2,6], Mairin Rafferty[2], Madhuri Warren[4], Joost J. van den Oord[5], William M. Gallagher[2,3], Markus Rehm[1,6,7,10,11]

1 Institute of Cell Biology and Immunology, University of Stuttgart, Stuttgart, Germany;

2 Oncomark Ltd., Nova UCD, Dublin 4, Ireland.

3 UCD School of Biomolecular and Biomedical Science, UCD Conway Institute, University College Dublin, Dublin 4, Ireland;

4 Pathology Diagnostics Ltd., Stirling House Business Centre, Waterbeach, Cambridge, UK;

5 Translational Cell and Tissue Research, KU Leuven (University of Leuven), Leuven, Belgium.

6 Department of Physiology and Medical Physics, Royal College of Surgeons in Ireland, Dublin 2, Ireland;

7 Centre for Systems Medicine, Royal College of Surgeons in Ireland, Dublin 2, Ireland;

8 VIB-KU Leuven Center for Brain & Disease Research, KU Leuven, Leuven, Belgium;

9 Department of Human Genetics, KU Leuven (University of Leuven), Leuven, Belgium

10 Stuttgart Research Center Systems Biology, University of Stuttgart, Stuttgart, Germany;

11 Stuttgart Center for Simulation Science (SC SimTech), University of Stuttgart, Stuttgart, Germany;

Running title: Role of Bax, Bak and Smac in melanoma prognosis

Keywords: Melanoma, Bax, Bak, Smac, Apoptosis

Competing interests: The authors declare that they have no conflict of interests.

To whom correspondence should be addressed.
Prof. Dr. Markus Rehm
Institute for Cell Biology and Immunology
University of Stuttgart
Allmandring 31, 70569 Stuttgart, Germany
Phone: +49 711 685-66987
E-mail: markus.morrison@izi.uni-stuttgart.de

2.2.1 Abstract

Despite the introduction of novel targeted therapies, chemotherapy still remains the primary treatment for metastatic melanoma in poorly funded healthcare environments or in case of disease relapse, with no reliable molecular markers for progression free survival (PFS) available. Since chemotherapy primarily eliminates cancer cells by apoptosis, we here evaluated if the expression of key apoptosis regulators (Bax, Bak, Bcl-2, Bcl-xL, Smac, Procaspase-9, Apaf-1, Procaspase-3 and XIAP) allows prognosticating PFS in stage III/IV melanoma patients. Following antibody validation, marker expression was determined by automated and manual scoring of immunohistochemically stained tissue micro arrays (TMAs) constructed from treatment-naïve metastatic melanoma biopsies. Interestingly and counter-intuitively, low expression of the pro-apoptotic proteins Bax, Bak and Smac indicated better prognosis (log-rank $p<0.0001$, $p=0.0301$ and $p=0.0227$ for automated and $p=0.0422$, $p=0.0410$ and $p=0.0073$ for manual scoring). These findings were independently validated in the TCGA metastatic melanoma cohort (TCGA SKCM) at transcript level (log-rank $p=0.0004$, $p=0.0104$ and $p=0.0377$). Taking expression heterogeneity between the markers in individual tumor samples into account allowed defining combinatorial Bax, Bak, Smac signatures that were associated with significantly increased PFS ($p=0.0002$ and $p=0.0028$ at protein and transcript level, respectively). Furthermore, combined low expression of Bax, Bak and Smac allowed predicting prolonged PFS (>12 months) on a case-by-case basis (ROC AUC=0.79). Taken together, our results therefore suggest that Bax, Bak and Smac jointly define a signature with potential clinical utility in chemotherapy-treated metastatic melanoma.

2.2.2 Introduction

Melanoma, an aggressive neoplasm originating from the malignant transformation of melanocytes, rapidly metastasizes if not surgically removed at an early stage. While novel and costly targeted treatment options and immunotherapies have significantly improved the management of metastatic disease (Domingues *et al.*, 2018; Heppt *et al.*, 2016; Margolin, 2016), patients in poorly funded healthcare environments still rely on chemotherapy as the primary first line treatment. Likewise, chemotherapy remains in frequent use as a 2nd or last line treatment option in otherwise refractory or in recurrent disease. Even though treatments based on the DNA alkylating agent dacarbazine have been the chemotherapeutic standard of care for metastatic melanoma for more than 30

years, chemotherapy may benefit only few patients (Gupta *et al.*, 2017; Lui *et al.*, 2007). The median survival of patients treated with dacarbazine-based chemotherapy lies in the range of 6-9 months (Atkins *et al.*, 2008; Bedikian *et al.*, 2006; Middleton *et al.*, 2000) with no reliable molecular markers available that would allow to identify those patients in which disease progression is substantially delayed and which therefore might have benefited from this treatment.

Apoptosis is the main cell death mechanism by which the body tries to eliminate transformed and therefore potentially cancerous cells. Apoptosis likewise is the primary cell death modality induced by dacarbazine and other DNA alkylating agents. DNA alkylation induces the intrinsic apoptosis pathway, as was shown experimentally in various melanoma model systems (Anvekar *et al.*, 2012; Sanada *et al.*, 2007). Pro- and anti-apoptotic Bcl-2 family members, such as Bax, Bak and Bcl-2, Bcl-xL, respectively, regulate the mitochondrial apoptosis signaling hub (Czabotar *et al.*, 2014). Activated Bax and Bak form pores in the outer mitochondrial membrane, leading to the release of pro-apoptotic factors, such as Smac, into the cytosol (Tait and Green, 2010). Subsequently, the execution phase of apoptosis is initiated, during which proteases such as initiator caspase-9 and effector caspase-3 are activated in an Apaf-1 dependent manner. These proteases then rapidly execute apoptotic death, but can be inhibited by the anti-apoptotic protein XIAP, which itself is targeted by Smac (Hellwig *et al.*, 2011). Impaired apoptosis signaling is a hallmark of cancer (Hanahan and Weinberg, 2011), based on which it is reasonable to assume that melanoma cells are highly apoptosis resistant. Indeed, experimental studies suggest that melanoma cells either are highly chemoresistant or acquire resistance and thereby evade apoptotic cell death (Lev *et al.*, 2004; Soengas and Lowe, 2003). However, it is less clear if perturbed expression of apoptosis regulators is indeed associated with patient prognosis in the clinical scenario. Various studies immunohistochemically assessed individual apoptosis regulators as potential protein biomarkers for melanoma progression and patient survival (Anvekar *et al.*, 2011; Charles and Rehm, 2014). Unfortunately though, the majority of studies lack controls and validation information that would support the specificity of the used reagents and staining protocols. Not surprisingly, results obtained so far remained largely inconclusive or even contradictory (Charles and Rehm, 2014). Additionally, apoptosis regulators at key signaling hubs frequently act cooperatively and redundantly, so that it can be speculated that single molecule makers might not be sufficiently robust for clinical use.

In this study, we therefore assessed the expression of nine apoptosis regulators (Bax, Bak, Bcl-2, Bcl-xL, Smac, Procaspase-9, Apaf-1, Procaspase-3 and XIAP) in metastatic melanoma tissues by IHC, using antibodies that passed rigorous validation. Interestingly, low expression of Bax, Bak and Smac associated with prolonged PFS, a finding confirmed at transcriptional level in an independent cohort. Combining Bax, Bak and Smac expression with a pattern recognition approach allowed predicting individual patient PFS with high accuracy. Taken together, our results identified a putative combinatorial prognostic signature with potential clinical utility for chemotherapy treated metastatic melanoma.

2.2.3 Materials and Methods

2.2.3.1 Ethics approval and consent to participate

The use of the patient cohort was approved by the Medical Ethical Committee and Institutional Review Board (OG032) of the University Hospitals of KU Leuven (reference number ML10659) and by the UZ Leuven Biobank (reference number S56609).

2.2.3.2 Antibodies

The following antibodies were used for immunoblotting and immunohistochemistry. A rabbit polyclonal beta Actin antibody (Santa Cruz Biotechnology; sc-81178); Apaf-1 (Cell Signalling; D5C3), Bak (Abcam; ab32371), Bax (Millipore; ABC11), Bcl-2 (Dako; MO887), Bcl-xL (BD labs; 610212), Procaspase-3 (Cell Signalling; 9662), Procaspase-9 (Cell Signalling; 9502), Smac (Cell Signalling; 2954), XIAP (BD labs; 610762).

2.2.3.3 Cell culturing

For antibody validation, the following human cancer cell lines were used: A375, HCT-116, HCT-116 (Bax/Bak)$^{-/-}$, HCT-116 Smac$^{-/-}$, HCT-116 XIAP$^{o/-}$, HeLa, Jurkat Casp-9$^{-/-}$, MCF-7, PM-WK, Preyer, SK-Mel-94. Cell lines were obtained from ATCC, DSMZ or provided by colleagues (Prof Martin Leverkus, University of Heidelberg; Prof Richard Youle, National Institutes of Health, USA; Prof Richard Vogelstein, The Johns Hopkins University School of Medicine, USA; Prof Ingo Schmitz, University of Braunschweig, Germany; Prof Sebastian Wesselborg, University of Düsseldorf, Germany; Prof Maria Soengas, National Cancer Research Centre, Spain) and described before (Cummins *et al.*, 2004; Geserick *et al.*, 2008; Kohli *et al.*, 2004; Samraj *et al.*, 2006; Soengas *et al.*,

2001; Wang and Youle, 2012). Cell lines were cultured in RPMI-1640 medium (Sigma-Aldrich) or DMEM (Lonza, Slough, UK) supplemented with 4 mM L-glutamine, 4.5 g/l glucose, 10% (w/v) heat-inactivated fetal bovine serum (Sigma-Aldrich), 100 U/ml penicillin and 100 µg/ml streptomycin (Sigma-Aldrich). Cells were grown at 5% CO_2 and 37°C.

2.2.3.4 Immunoblotting

For whole cell extracts, cells were collected at 400 *g* for 3 min and washed with phosphate-buffered saline. Cells were re-suspended in lysis buffer (62.5 mM Tris-HCl, pH 6.8, 10% (v/v) glycerin, 2% (w/v) SDS, 1 mM phenylmethylsulfonyl fluoride, 1 µg/ml pepstatin A, 1 µg/ml leupeptin, and 5 µg/ml aprotinin) and heated at 95°C for 20 min. Protein content was determined with the Pierce Micro-BCA protein assay (Pierce, Northumberland, UK). An equal amount of protein (20 µg) was loaded onto SDS-polyacrylamide gels. Proteins were separated at 100 V for 2.5 h and then blotted to nitrocellulose membranes (Protean BA 83; 2 µm; Schleicher & Schuell) in transfer buffer (25 mM Tris, 192 mM glycine, 20% methanol (v/v), and 0.01% SDS) at 18 V for 60 min. The blots were blocked with 5% non fat dry milk in TBST (15 mM Tris-HCl, pH 7.5, 200 mM NaCl, and 0.1% Tween 20) at room temperature for 1 h. Membranes were incubated with the primary antibodies at room temperature for 2 h or overnight at 4°C. Membranes were washed with TBST three times for 5 min and incubated with peroxidase-conjugated secondary antibodies (Jackson Laboratories) for 1 h. Blots were washed and developed using the enhanced chemiluminescence detection reagent (Millipore, Ireland).

2.2.3.5 Preparation of cell pellets for IHC

Cells were grown to a confluence of 50-75%. Cells were then detached and suspended in 10% phosphate-buffered formalin at room temperature and fixed for 4-6 hours. Fixed cells were centrifuged at 500 x g for 3 min, washed once with 1x PBS and pelleted again. A 1% agarose solution was prepared in 1x PBS and cooled down to 40°C in a water bath. The cell/agarose mixtures were transferred into plugs and let solidify. The agarose plugs were processed into paraffin blocks using standard tissue processing. Cell pellet samples (typically 0.6 mm in diameter) were then used for analysis.

2.2.3.6 Tissue Micro Arrays (TMAs)

TMAs of formalin fixed paraffin-embedded (FFPE) tumor samples derived from 74 melanoma patients treated with Dacarbazine (alone or in combination with Cisplatin or

Carboplatin), were generated. The TMA contained duplicate cores obtained from 14 primary melanomas, 62 metastatic melanomas and adjacent normal tissue. Demographics, clinical and follow-up information were available for the entire cohort. A total of n = 58 samples, representing untreated metastatic melanoma patients, were analyzed for this study (Table 1).

2.2.3.7 Immunohistochemistry

IHC staining on formalin-fixed, paraffin-embedded (FFPE) cell pellets and tissue microarrays (TMA) was performed using an automated IHC platform (Link-48, Dako, Glostrup, Denmark) according to the manufacturer's instructions. Sections (4 µm in thickness) were deparaffinised and antigen retrieval was performed at 95°C for 15 min in appropriate buffer (high pH buffer, pH 9.0; low pH buffer, pH 6.0) using the PT-Link module (Dako, Glostrup, Denmark). A polymer-based detection system (EnVision Flex, Dako) was used with Permanent Red as the chromogen, resulting in a red colour endpoint that contrasted well with brown melanin. Sections were counterstained with haematoxylin. Positive and negative controls (omission of the primary antibody and replacement with the IgG-2a isotype control, mouse-ab18443; IgG isotype control, rabbit-ab208334, Abcam, Cambridge, UK) were included in each run. In addition, a Haematoxylin and Eosin (H&E) staining was performed for all slides of the TMAs, enabling pathologists to check for TMA core integrity, quality, and tumour content.

2.2.3.8 Core quality assessment

A pathological review of the H&E stained sections and TMA blocks was conducted to define the quality of individual tissue cores and to assess the percentage of tumour tissue in each core. Each core was individually observed to determine if there were any tissue artifacts (poorly fixed tissue, folded tissue, no tumour present, no tissue present, foreign material introduced at embedding, poor tissue microscopic details) or staining artifacts (knife marks across section, holes, clumps of stain precipitate, air bubbles) which would have compromised either the manual or automated image analysis. All quality assessments were independently validated by a second pathologist. Cores with compromising artifacts or with insufficient percentage of tumour cells were excluded from further analyses.

2.2.3.9 Manual and automated scoring

IHC materials were first viewed at low power to judge overall quality and distribution of staining. Subsequently, staining frequency (total % stained cells) and staining

intensity (intensity of stained cells; 0 = no staining, 1+ = weak staining, 2+ = moderate staining, 3+ = strong staining) were determined. Histoscores (H-Scores) were then calculated as follows:

$$\text{H-Score} = 1 \times \%_{\text{cells } 1+} + 2 \times \%_{\text{cells } 2+} + 3 \times \%_{\text{cells } 3+}$$

The manual scoring was performed on images acquired with the Aperio ScanScope XT slide scanner (Aperio Technologies, Vista, CA) used at 20x magnification with a maximum pixel resolution of 0.5 µm. ImageScope analysis software (Aperio Technologies, Vista, CA) was used for viewing and analysing digital images. Aperio Spectrum software was used to generate individual tissue spot images for automated analysis. The Colour Deconvolution algorithm (Aperio Technologies) was used to obtain quantitative values for Average Positive Intensity (API) (average intensity of pixels positively stained, graded from 0, 1, 2, 3) and Total Percent Positive (TPP) (percentage of positive stained area in relation to total area of the core). Histoscores were calculated as described above.

2.2.3.10 Survival analysis

Progression free survival (PFS) was calculated as the time between the surgery that procured the sample and the date of disease progression or of a new metastatic event in a different location. Pathologist's and automated H-Score were used to separate patients with high (above median) and low (below median) expression of each marker protein included in this study. In case more than one tissue core with satisfactory quality was available for a single patient, the average H-Score was considered. Log-rank testing was used to compare the two groups over a follow-up time of 36 months. Log-rank testing for trends was used when comparing three groups. Kaplan-Meier survival curves were generated and compared using GraphPad Prism (version 4.03). For analysis of data stored in the cancer genome atlas (TCGA), normalized mRNA expression data (Upper Quartile normalized Fragments per Kilobase of transcript per Million mapped read, $\log_2$(FPKM-UQ+1)) generated by the Genomic Data Commons (GDC-NIH) were

downloaded from the UCSC-XENA browser[1] (Goldman *et al.*, 2019). The SKCM cohort, unlike other TCGA datasets, contains mainly metastatic samples (Liu *et al.*, 2018) (370 out of 477), some of which were collected a long time after initial diagnosis of the primary melanoma (Akbani *et al.*, 2015). In order to correlate mRNA expression to progression of metastatic disease, the "*new tumour event free survival*" was calculated as the time between sample collection and the first new tumour event (in case of multiple new tumour events during the follow-up time) or, in case of no new tumour events, death. If a new tumour event was reported before the date of sample collection, the patient was excluded from the sub-cohort. Follow-up data and associated clinical records were downloaded from Broad GDAC Firehose (Broad Institute TCGA Genome Data Analysis Center, 2016) (new tumor event time from initial diagnosis) and UCSC-XENA browser (Goldman *et al.*, 2019) (overall survival from initial diagnosis), respectively. Sample collection information are available through the GDC data portal[2] (Grossman *et al.*, 2016) (time from initial diagnosis to sample collection). Since treatment information are not routinely available for all deposited metastatic melanoma cases, we downselected the cohort to stage III/IV melanoma patients diagnosed with metastatic melanoma before 2010, to ensure that chemotherapy-based treatment options would have been the standard first line of treatment (n = 79 patients). An optimized chi-square based cut-off was determined to divide patients with high and low *BAX*, *BAK1* and *DIABLO* (Smac) mRNA amounts, and the two groups were compared by log-rank test. The cut-off for each marker was obtained by selecting the cohort separation that resulted in the highest chi-squared value with the function *survdiff* of the library *survival* in R (version 3.4.0). Median cut-off based results are reported in **Supplementary Figure 2.2-4**. Log-rank test for trend was used when comparing three groups. Kaplan-Meier survival curves were generated and compared using GraphPad Prism (version 4.03).

[1] UCSC Xena Functional Genomics Browser: https://xena.ucsc.edu/

[2] GDC Data Portal: https://portal.gdc.cancer.gov/

2.2.3.11 Data driven modelling and pattern recognition

A data-driven modelling approach based on a previously published method (Passante *et al.*, 2013) was developed to predict patients' PFS using H-Scores generated by automated image analysis as input. The pipeline was developed for MATLAB (version 2016a, The Mathworks, UK), equipped with the statistical toolbox. Prior to the analysis, patients with a complete protein panel (n = 50) were divided into two PFS categories: PFS >12 months (n = 17) and PFS<12 months (n = 33). After standardization of the initial dataset, a principal component analysis (PCA) was performed and the principal components (PC) with an eigenvalue >1 were considered for subsequent analyses. The patients were positioned in the 3D space defined by the first three PCs according to the scores computed by PCA, and linear discriminant analysis (LDA) was used to test the class segmentation accuracy. To evaluate the predictive potential of the framework, leave one out cross validation (LOOCV) followed by LDA was applied iteratively to the dataset, using 49 patients as training set and one patient as test at each iteration. LDA was also applied to a dataset reduced to three proteins (Bax, Bak and Smac), skipping the initial dimensionality reduction step. PCA and LDA were performed using the functions *pca* and *classify*, respectively. The predictive performance of the two classification models was compared by computing the area under the curve (AUC) with the function *perfcurve*.

2.2.4 Results

2.2.4.1 Low expression of pro-apoptotic proteins Bax, Bak and Smac correlates with increased progression free survival (PFS) in chemotherapy-treated metastatic melanoma

Genotoxic chemotherapy based on DNA-alkylating agents such as dacarbazine induces intrinsic apoptosis, preferentially in proliferating cells such as cancer cells. Intrinsic apoptosis is governed by the family of Bcl-2 proteins and the subsequent signalling network of the apoptosis execution phase. We therefore tested key players of this apoptosis signalling modules as potential prognostic markers in metastatic melanoma. In total, we analysed the expression of six pro-apoptotic (Bax, Bak, Smac, Procaspase-9, Apaf-1, Procaspase-3) and three anti-apoptotic proteins (Bcl-2, Bcl-xL, XIAP) in metastatic melanoma samples spotted on tissue micro arrays (TMAs). Only treatment naïve samples from metastases were used for subsequent analyses. Information such as patient demographics, histopathology and staging, treatment and follow-up are provided as **Supplementary Table 2.2-1** and are summarized in **Table 2.2-1**. Following

comprehensive antibody validation (**Supplementary Figure 2.2-1A-D**), IHC stains for n = 58 tumour metastases matching the inclusion criteria were analysed from the TMAs. Only tissue samples passing independent pathologist quality control for tissue integrity and staining artifacts were considered for subsequent analyses (**Supplementary Table 2.2-2**). TMAs scans were then used to generate mark-up images of the tissue cores, followed by automated quantification of staining intensities (see methods). The dynamic range of the staining intensities allowed to confidently define quartiles of negative, low, medium and high staining for protein expression (see **Figure 2.2-1A** for examples for Bax, Bak and Smac). From these, H-Scores were calculated for each tumour sample (**Figure 2.2-1B**), thereby allowing comparison to best practice manual scoring (see **Figure 2.2-2**). To test if protein expression amounts and patient prognosis correlate, we

Table 2.2-1: Summary of demographics and clinical information of the patients included in the study.

Characteristics		
Gender	***Value***	***%***
Male	30	51.7
Female	28	48.3
Age at surgery (years)	***Value***	***%***
<65	44	75.9
≥ 65 and < 75	8	13.8
> 75	6	10.3
Metastatic melanoma location	***Value***	***%***
Distant skin site	10	17.2
Distant organ	17	29.3
Distant lymph node	28	48.3
Distant subcutaneous site	3	5.2
Metastasis Stage	***Value***	***%***
M1a	8	13.8
M1b	8	13.8
M1c	42	72.4
Primary melanoma type	***Value***	***%***
Cutaneous	46	79.3
Mucosal	1	1.7
Ocular	2	3.4
Unknown	9	15.5
Treatment	***Value***	***%***
Dacarbazine	3	5.2
Dacarbazine, Cisplatin	54	93.1
Dacarbazine, Carboplatin	1	1.7
Overall survival	***t_0 = sample collection***	***t_0 = chemotherapy start***
Median (range) in months	19 (2-126)	11 (0-87)
Progression-free survival	***t_0 = sample collection***	***t_0 = chemotherapy start***
Median (range) in months	10 (1-100)	4 (0-83)

performed survival analyses for all nine apoptosis regulatory proteins. Kaplan-Meier curves representing progression free survival (PFS) from the date of sample procurement showed that low amounts of pro-apoptotic proteins Bax, Bak and Smac significantly correlated with better prognosis (**Figure 2.2-1C**). With the exception of Procaspase-9, which associated with better prognosis in this analysis, none of the other proteins (Bcl-2, Bcl-xL, Apaf-1, XIAP and Procaspase-3) individually correlated with better or worse prognosis (**Supplementary Figure 2.2-2**). Overall, these results surprisingly indicate that low amounts of apoptosis inducing proteins Bax, Bak and Smac are linked to a better prognosis in chemotherapy treated metastatic melanoma.

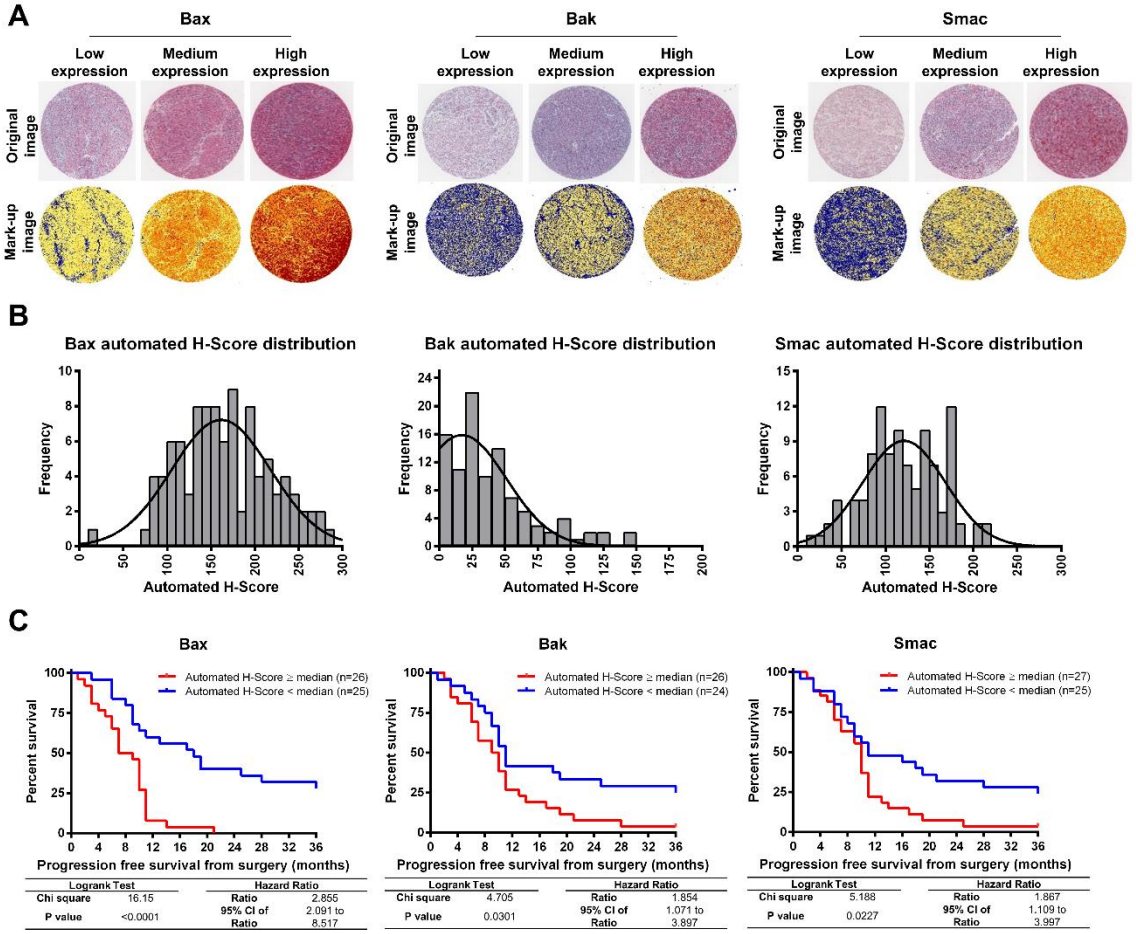

Figure 2.2-1: Low expression of pro-apoptotic proteins Bax, Bak and Smac correlates with increased progression free survival (PFS) in chemotherapy-treated metastatic melanoma. A Tissue cores stained by IHC for Bax, Bak and Smac. Representative original (left panels) and mark-up images (right panels) of cores with low, medium and high expression of the three proteins are shown. The mark-up images were quantified to compute automated H-Scores. Table insert shows cohort information. **B** Distribution of H-Scores across the analysed melanoma tissue cores. Only stained cores that passed the quality control were retained for subsequent analyses (Bax n = 100 cores from 52 patients, Bak n = 100 cores from 51 patients, Smac n = 104 cores from 53 patients,). **C** Survival analysis based on H-scores for Bax, Bak and Smac. Median H-Scores were used as cut-off to separate the patients with high (red line) and low (blue line) expression of each protein. Log-rank test was used to compare the Kaplan-Meier curves for progression free survival from the date of sample procurement.

2.2.4.2 Manual scoring confirms association of low Bak, Bax and Smac protein expression with improved PFS

To further validate our findings, we next conducted best-practice manual scoring of the stained TMAs. H-scores for all marker candidates were obtained from two independent pathologists, both blinded to patient PFS. Plotting H-Scores obtained by automated analysis against manual H-Scores, we noted that manual scores strongly clustered at values of approximately 200, whereas automated scoring provided higher granularity across the entire dynamic range (**Figure 2.2-2A, Figure 2.2-1B, Supplementary Table 2.2-2**). This highlights that manual scoring appears limited in differentiating within the range of medium staining intensities and frequencies. Nevertheless, median separation of patient samples based on manual H-Scores provided survival curves for Bax, Bak and Smac staining that were very similar to those obtained by automated scoring (**Figure 2.2-2B**). In contrast, the manual scores for all other proteins failed to separate patients with high and low PFS (**Supplementary Figure 2.2-3**). These results therefore demonstrate that the Bax, Bak and Smac signatures are robust enough to also be captured in routine manual IHC-based biomarker discovery workflows.

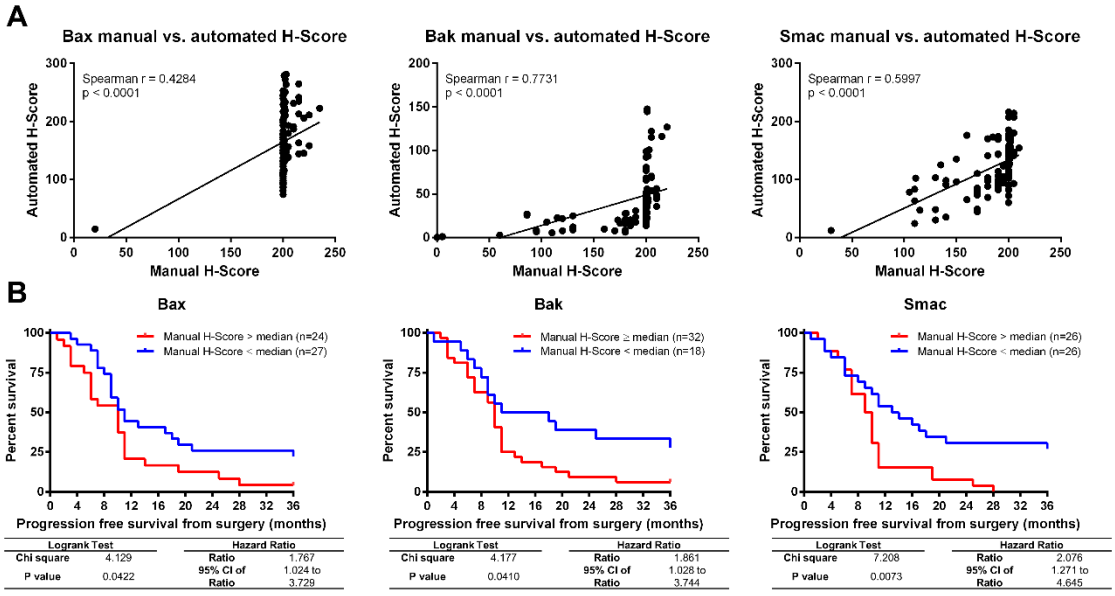

Figure 2.2-2: Manual scoring confirms association of low Bak, Bax and Smac protein expression with improved PFS. A Correlation between automated and manual H-Scores. Manual scores were obtained from two independent pathologists blinded to patient follow up. Correlation was analysed using Spearman's rank correlation coefficient. **B** Median H-Scores were used as cut-off to separate the patients with high (red line) and low (blue line) expression of each protein. Log-rank test was used to compare the Kaplan-Meier curves for progression free survival from the date of sample procurement.

2.2.4.3 Combined low expression of Bax, Bak and Smac is a combinatorial marker candidate for improved progression free survival

During apoptosis, Bax and Bak form pores in the outer mitochondrial membrane, leading to Smac release into the cytosol. Due to the significant correlation of the single proteins with PFS and their direct relationship within the apoptosis signal transduction cascade, we checked if combinations of the three markers could improve prognostication of PFS. For the n = 50 patients for which H-Scores for Bax, Bak and Smac were available, we noted that combined low or high staining for all three markers was restricted to subsets of the tumour samples (**Figure 2.2-3A**). We therefore divided the cohort into three groups of combined high expression, heterogeneous expression and combined low expression. PFS-based survival analysis of the three groups demonstrated that patients harbouring tumours with combined low expression of Bax, Bak and Smac showed significantly improved PFS, extending beyond 36 months for 50% of this subgroup (**Figure 2.2-3B**). In contrast, when only one or two markers where expressed in low amounts, PFS improved only slightly (median PFS = 10 months vs. 8.5 months when all three markers were highly expressed) (**Figure 2.2-3B**). Overall, this shows that Bax, Bak and Smac could jointly define a signature that strongly associates with PFS, with combined low expression indicating improved PFS.

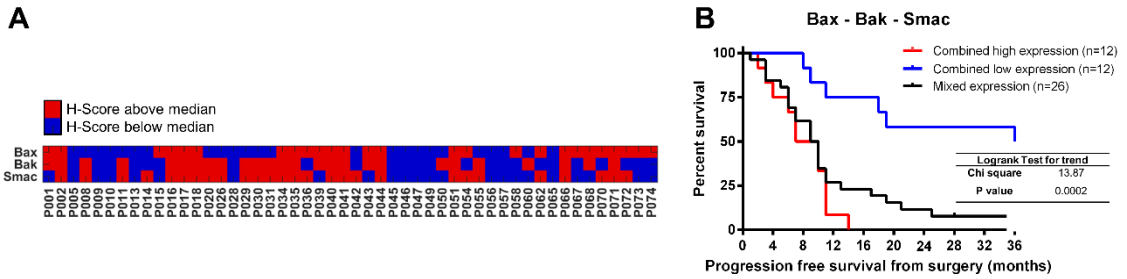

Figure 2.2-3: Combined low expression of Bax, Bak and Smac is a combinatorial marker candidate for improved progression free survival. A Expression profiles based on the H-Scores of Bax, Bak and Smac (blue: automated H-Score below median, red: above median) in n = 50 patients. **B** Survival analysis for the cohort based on the expression profiles shown in a. Log-rank test for trend was used to compare three Kaplan-Meier curves representing patients with low Bax, Bak and Smac H-Scores (blue) vs. mixed and high expression (black and red, respectively).

2.2.4.4 TCGA SKCM-based analysis validates the prognostic Bax, Bak, Smac signature

To independently validate the prognostic potential of Bax, Bak and Smac expression, we analysed transcriptome data of n = 79 metastatic melanoma patients from the TCGA-SKCM cohort (**Table 2.2-2**). The survival analysis revealed that low *BAX*, *BAK1* and *DIABLO* (*SMAC*) mRNA amounts significantly correlate with better prognosis (**Figure 2.2-4A**). As previously observed at protein level, the expression

Table 2.2-2: Patient demographics and clinical information of the metastatic SKCM-TCGA sub-cohort.

Characteristics		
Age at diagnosis (years)		
Mean	55.5	
Median	55	
Range	18 - 87	
Gender	***Value***	***%***
Female	32	40.51
Male	47	59.49
Ethnicity	***Value***	***%***
White (non-Hispanic or Latino)	79	100
Disease stage at initial diagnosis	***Value***	***%***
Stage III	68	86.08
Stage IV	11	13.92
Overall survival from initial diagnosis (months)		
Mean	35.1	
Range	2.6 - 175.2	
Overall survival from sample procurement (months)		
Mean	15.9	
Range	1.1 - 64.9	

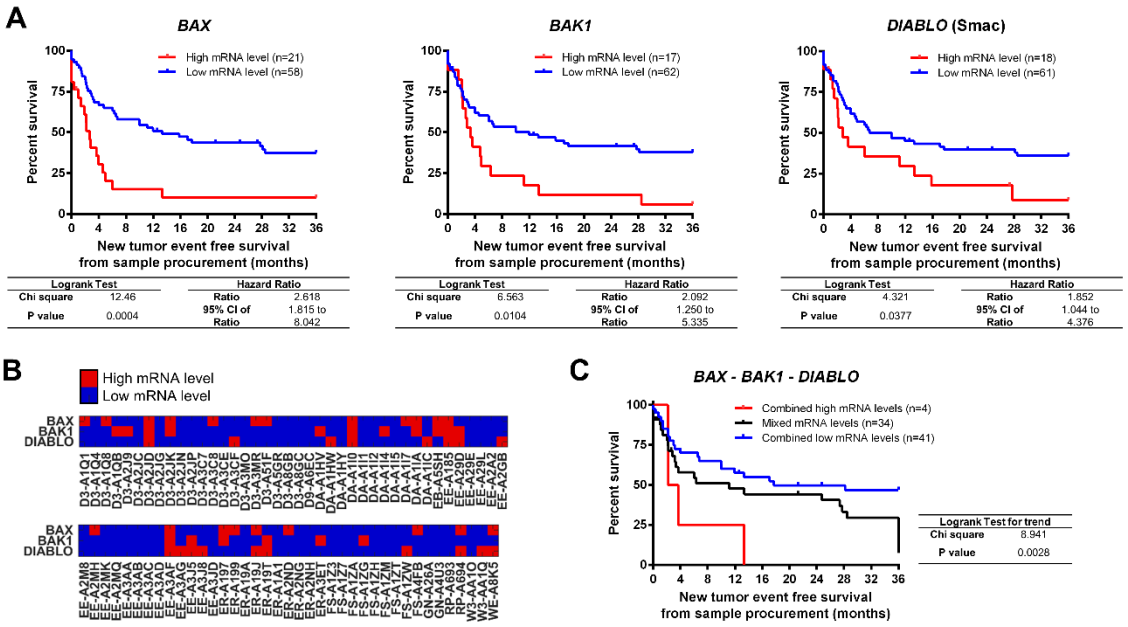

Figure 2.2-4: TCGA SKCM-based analysis validates the prognostic Bax, Bak, Smac signature. Independent validation of the prognostic signature at transcriptome level in the SKCM-TCGA metastatic sub-cohort. **A** Survival analysis in the SKCM-TCGA sub-cohort (n = 79 patients diagnosed with stage III or IV metastatic melanoma before 2010). An optimized chi-square based cut-off was determined to divide patients with high (red) and low (blue) normalised *BAX*, *BAK1* and *DIABLO* (Smac) expression (log_2(FPKM-UQ+1)). Kaplan-Meier curves (follow-up from sample procurement) were compared by log-rank test. **B** mRNA amounts for *BAX*, *BAK1* and *DIABLO* (Smac) (blue: mRNA level below cut-off, red: mRNA level above cut-off). **C** Survival analysis in the metastatic TCGA-SKCM sub-cohort based on the expression profiles in Fig. 4b. Log-rank test for trend was used to compare three Kaplan-Meier curves representing patients with combined low *BAX*, *BAK1* and *DIABLO* (Smac) expression (blue), combined high expression (red) or with mixed expression (black).

pattern between *BAX*, *BAK1* and *DIABLO* was heterogeneous across the cohort (**Figure 2.2-4B**). Patients with low tumour mRNA amounts across all three markers had a significantly better prognosis than patients in which at least one marker was highly expressed (**Figure 2.2-4C**). Taken together, these results recapitulate in an independent cohort the trends observed at protein level, confirming the prognostic potential of Bax, Bak and Smac as a combinatorial marker in chemotherapy-treated metastatic melanoma.

2.2.4.5 Pattern recognition allows predicting patient prognosis

We next applied a data-driven pattern recognition approach to study if the Bax, Bak, Smac signature would be sufficiently strong to predict patient PFS from protein expression profiles (Passante *et al.*, 2013). First, H-Scores from automated TMA analysis for all marker candidates were subjected to a principal component analysis (PCA) (applied to the 50 patient samples for which the complete nine protein panel was available). Patient tumours were positioned into a 3D space defined by the first three principal components (PCs) and colour-coded to represent high or low PFS (PFS>12 months and PFS<12 months). Visually inspecting the scatter plot, we noticed a tendency of patients with high or low PFS to occupy distinct sub-regions of the PC space (**Figure 2.2-5A**). To objectively assess the quality of this segregation, we applied linear discriminant analysis (LDA). LDA segmentation encouragingly separated 72% of the patients into their correct prognosis sub-space. Next, we tested if these patterns were sufficiently strong to also predict the PFS category on a case-by-case basis. To do so, we performed leave one out cross validation (LOOCV). At each iteration, the PFS category of one patient was predicted after using the remaining 49 patients as a training set that defined the PCA subspaces for high and low PFS. The panel of nine apoptosis regulatory proteins allowed to correctly predict high or low PFS in 74% of patients. Since our previous survival analyses (**Figure 2.2-1**) showed that only Bax, Bak and Smac consistently correlated with PFS, we likewise tested if a similarly good or even better performing classifier can be derived from those three markers alone. Indeed, cluster segmentation and prediction accuracy tended to improve to 80% and 78% accuracy, respectively (**Figure 2.2-5B**). In conclusion, as highlighted by the comparison of receiver operating characteristic (ROC) curves (**Figure 2.2-5C**), classification based on the Bax-Bak-Smac signature alone is sufficient to obtain high prediction accuracies for patient PFS, whereas the remaining protein markers do not carry meaningful information to improve these predictions. Overall, this strengthens the evidence for low Bax, Bak and Smac expression being associated with better prognosis in metastatic

melanoma and points out a route by which pattern recognition allows generating predictions for patient prognosis.

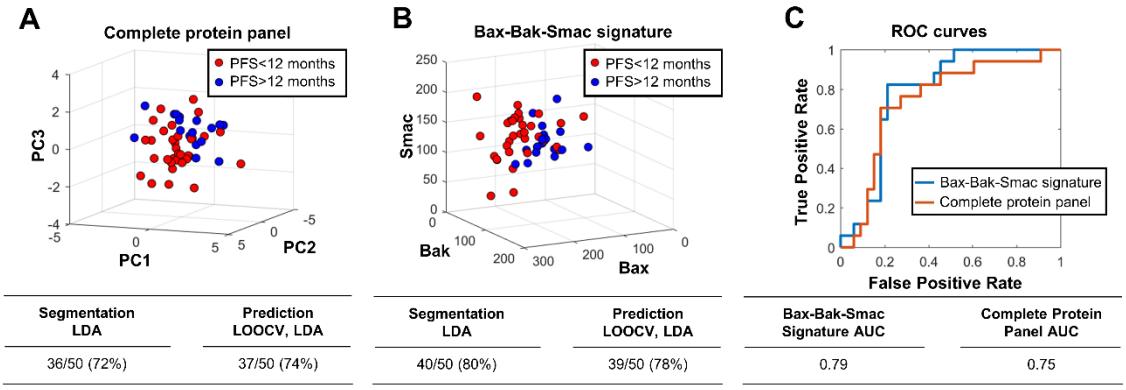

Segmentation LDA	Prediction LOOCV, LDA
36/50 (72%)	37/50 (74%)

Segmentation LDA	Prediction LOOCV, LDA
40/50 (80%)	39/50 (78%)

Bax-Bak-Smac Signature AUC	Complete Protein Panel AUC
0.79	0.75

Figure 2.2-5: Pattern recognition allows predicting patient prognosis. A A principal component analysis was performed on the H-Scores of nine apoptotic proteins. To provide a visualization of the spatial clustering, patients samples were positioned in a 3D scatter plot defined by the first three principal components and colour-coded according to their PFS time (red < 12 months, n = 33; blue > 12 months, n = 17). Linear discriminant analysis (LDA) correctly segmented 72% of the patients. Leave One Out Cross Validation (LOOCV) combined with LDA predicted the correct class for 74% of the patients. **B** 3D scatter plot showing the spatial clustering of patients with short and long PFS based on the H-Scores for Bax, Bak and Smac. LDA correctly segmented 80% of the patients and LOOCV-LDA achieved 78% prediction accuracy. **C** Comparison of the performance of the two classifiers shown in a and b. The receiver operating characteristic curves (ROCs) and respective areas under the curve (AUC) are shown.

2.2.5 Discussion

Apoptosis is the major cell death modality by which anti-cancer therapies eliminate malignant neoplastic cells. In this study, we assessed if proteins that regulate the two major apoptosis decision hubs, namely the apoptotic engagement of mitochondria and the terminal execution phase of apoptosis (Taylor *et al.*, 2008), alone or in combination can serve to prognosticate PFS in metastatic melanoma patients undergoing dacarbazine-based chemotherapy. We found that low rather than high expression of the pro-apoptotic proteins Bax, Bak and Smac correlates with higher PFS, and that these three proteins in combination can serve as a combinatorial prognostic marker with a promising AUC of 0.79.

Due to the central role of apoptosis in tumour cell elimination, the finding that low expression of pro-apoptotic proteins correlated with better prognosis in metastatic melanoma contradicted our expectations. However, counter-intuitive relationships between the expression patterns of apoptosis inducers or anti-apoptotic genes or proteins were reported previously. For example, high expression of Bax was found to correlate with an increased risk for relapse in childhood acute lymphoblastic leukaemia (Hogarth and Hall, 1999). High expression of Bax, measured as transcript and protein amounts, respectively, has also been associated with poor prognosis in acute myeloid

leukaemia and non-Hodgkin lymphoma (Bairey *et al.*, 1999; Köhler *et al.*, 2002). Similarly, studies in which high expression of the Bax antagonist Bcl-2 has been reported to correlate with better prognosis can be found for colorectal, breast, glioma, gastric and non small cell lung cancer (Ichim and Tait, 2016; Inada *et al.*, 1998; Labi and Erlacher, 2015; McDonald *et al.*, 2002; Meterissian *et al.*, 2001; Renouf *et al.*, 2009; Vargas-Roig *et al.*, 2008). Bax and Bcl-2 are the best characterized members of the Bcl-2 protein family, which controls mitochondrial engagement in apoptosis signal transduction (Hantusch *et al.*, 2018; Kale *et al.*, 2018), whereas Bak has been less thoroughly studied. Bak functions as a Bax-like protein and upon activation likewise is able to form pores in the outer mitochondrial membrane, thereby triggering apoptosis execution (Hantusch *et al.*, 2018; Kale *et al.*, 2018). Links between low Bak expression and an improved outcome have not been reported in metastatic melanoma so far, but reduced *BAK* mRNA amounts were associated with better overall survival in hepatocellular carcinoma (Kong *et al.*, 2018). Similarly, a counter-intuitive prognostic value of Smac has not yet been reported in melanoma, but high expression was found to correlate with early local disease recurrence in cervical cancer (Arellano-Llamas *et al.*, 2006). It needs, however, be stated that in reverse a large body of literature associates high expression of pro-apoptotic or a low expression of anti-apoptotic genes or proteins with better outcome, as would intuitively be expected (see e.g. (Baekelandt *et al.*, 2000; Dobrzycka *et al.*, 2010; Endo *et al.*, 2009; Grzybowska-Izydorczyk *et al.*, 2010; Jeong *et al.*, 2008; Kupryjańczyk *et al.*, 2003; Leverkus and Gollnick, 2006; Luo *et al.*, 2015; Ma *et al.*, 2019; Pluta *et al.*, 2011; Del Poeta *et al.*, 2003; Seok *et al.*, 2007)). Overall, it therefore appears that signatures indicative of apoptosis competency or resistance need to be interpreted or studied within the specific disease setting and context. For example, it was suggested that expression patterns indicative of high apoptosis responsiveness may correlate with poor outcome if dormant, stem-like cancer cells that may reside within tumor tissues re-populate tumors and promote further spread and progression of the disease after the bulk population of cells has been eliminated by apoptosis-inducing therapy (Ichim and Tait, 2016; Labi and Erlacher, 2015). In line with this, apoptotic cell loss can drive the proliferation of surrounding cells, for example through caspase-dependent prostaglandin signaling and secretion of other proliferation stimulating factors from dying cells (Huang *et al.*, 2011; Zhao *et al.*, 2018). These signaling processes indeed might be of relevance in melanoma treatment responsiveness and disease relapse (Donato *et al.*, 2014).

Since apoptosis resistance is a hallmark of cancer (Hanahan and Weinberg, 2011), it nevertheless appears puzzling that reduced expression of apoptosis drivers correlates with better prognosis in a treatment scenario that is clearly geared towards apoptosis induction. In addition to the above line of thoughts, the very high mutation burden of cutaneous melanoma (Lawrence *et al.*, 2013) might provide the basis for an additional explanation. While unfavorable expression of key apoptosis regulators in many cases may cause apoptotic cell death to be suppressed during cell transformation, tumor development and disease progression, and as such could be considered causative for the disease, such low basal apoptosis susceptibilities might nevertheless be overcome by elevated apoptosis-inducing stress in chemotherapy settings. In contrast, where low apoptosis susceptibility is not causative for the disease (and hence protein expression profiles would indicate "normal" susceptibility), other alterations and mutations might drive the development and progression of the disease. Many of these could prevent therapy-induced stress signals to be channeled towards apoptosis induction. Indeed, low expression of Bax and Bak might be linked to disease progression in earlier stages of melanoma. While Bax protein expression tends to be higher in melanoma tissues than in benign nevi (Tang *et al.*, 1998), low expression of Bax within primary superficial-spreading melanoma was associated with poor prognosis and therefore could indicate a role in disease development and progression (Fecker *et al.*, 2006). Similar findings were reported for Bak expression in the same study. Also in stage IIa melamoma, low Bax and Bak protein expression was associated with poor prognosis, with the majority of such patients developing metastatic disease (Tchernev and Orfanos, 2007). Taken together, these prior reports combined with our findings therefore suggest that low expression of pro-apoptotic players could be causative for early stage tumor formation and melanoma disease progression by lowering basal apoptosis susceptibility, and that this reduced susceptibility can be overcome once pro-apoptotic stress is elevated externally, for example by dacarbazine-based chemotherapy. It will be interesting to see if similar relationships can also be found in other cancer (sub)types in the future.

2.2.6 Acknowledgements and funding information

The authors kindly acknowledge support by the European Union's Horizon 2020 research and innovation programme under the Marie Skłodowska-Curie grant agreement #642295 (MEL-PLEX) and by the European Union's FP7 Marie Skłodowska-Curie Industry-Academia Partnership and Pathways research programme under the grant agreement #611107 (SYS-MEL). MR and CG receive support from the

Cluster of Excellence in Simulation Technology (EXC 2075) at the University of Stuttgart. MR also receives support from the German Research Foundation (FOR2036 (MO 3226/1-1)) and the Health Research Board Ireland (HRA POR 2015 1091). JW received a postdoctoral research fellowship from *Kom op tegen Kanker* (Stand up to Cancer), the Flemish Cancer Society, and is currently funded by a postdoctoral fellowship from *Stichting tegen Kanker* (Foundation against Cancer), the Belgian Cancer Society.

2.2.7 Supplementary material

The clinical information and IHC datasets are available as digital supplementary material at: https://www.nature.com/articles/s41419-020-2309-3#Sec21. Direct links are provided below.

Supplementary Table 2.2-1: Patient demographics, histopathology and staging, treatment and follow-up information of the cohort.
https://static-content.springer.com/esm/art%3A10.1038%2Fs41419-020-2309-3/MediaObjects/41419_2020_2309_MOESM6_ESM.xlsx

Supplementary Table 2.2-2: IHC digital and manual image analysis results and cores quality control.
https://static-content.springer.com/esm/art%3A10.1038%2Fs41419-020-2309-3/MediaObjects/41419_2020_2309_MOESM7_ESM.xlsx

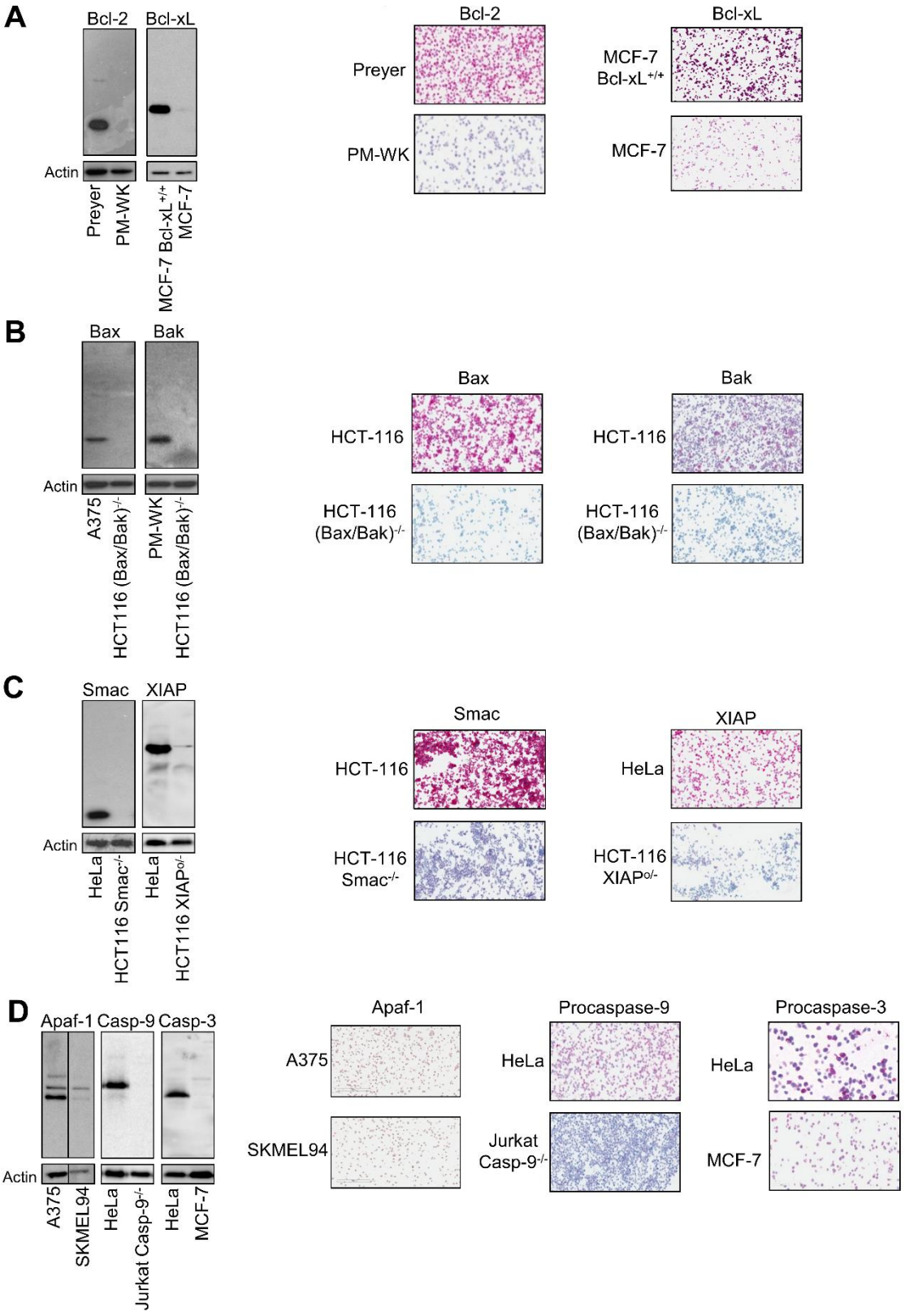

Supplementary Figure 2.2-1: Antibody validation. Commercially available antibodies for all markers to be studied were tested for specificity by Western blotting and by IHC on cell line pellets. Only results for antibodies passing quality assessment are shown. In Western blotting experiments, cell lines with known high or low/absent expression of the marker of interest were compared. Antibodies were required to yield single or clearly dominant specific bands at reported apparent molecular weights of marker proteins and/or their splice variants. IHC-based validation were required to clearly differentiate between cell line pellets with high or low/absent expression of the markers and to yield homogeneous staining across the isogenic populations. Subsequently, stained full face tissue sections were assessed by pathologists before staining protocols were approved for TMA stainings. **A** Validation results for anti-

apoptotic Bcl-2 family members Bcl-2 and Bcl-xL; **B** Validation results for pro-apoptotic Bcl-2 family members Bax and Bak; **C** Validation results for Smac and its antagonist XIAP; **D** Validation results for Apaf-1 and the zymogens of caspases-9 and -3.

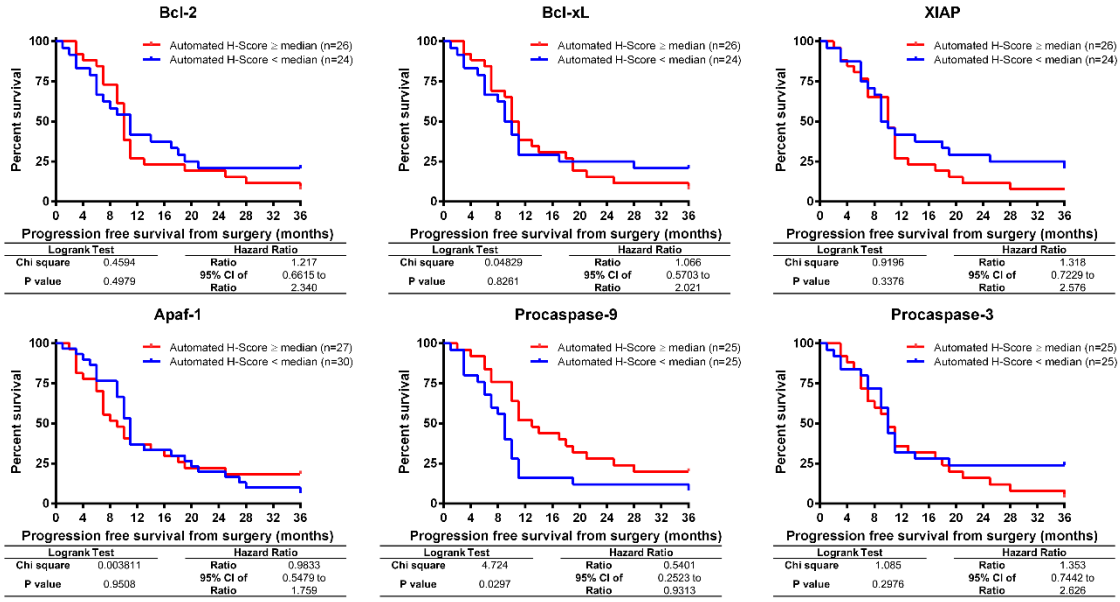

Supplementary Figure 2.2-2: Survival analysis for the cohort based on automated H-Score of Bcl-2, Bcl-xL, XIAP, Apaf-1, Procaspase-9 and Procaspase-3. Survival analysis based on automated H-Scores for Bcl-2, Bcl-xL, XIAP, Apaf-1, Procaspase-9 and Procaspase-3. Median H-Scores were used as cut-off to separate the patients with high (red line) and low (blue line) expression of each protein. Log-rank test was used to compare the Kaplan-Meier curves for progression free survival from the date of sample procurement.

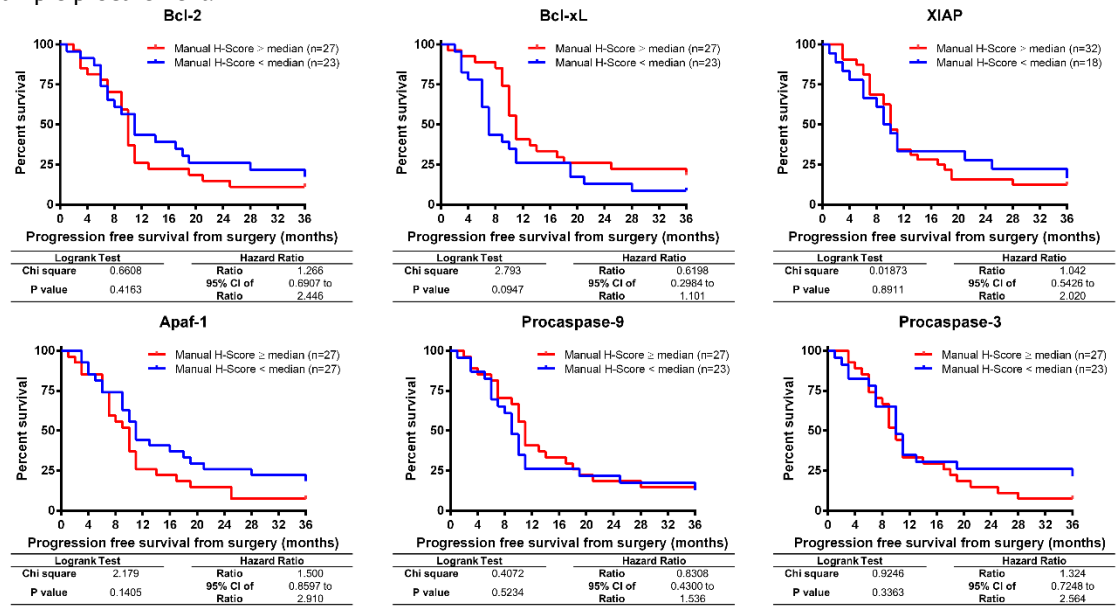

Supplementary Figure 2.2-3: Survival analysis for the cohort based on manual H-Score of Bcl-2, Bcl-xL, XIAP, Apaf-1, Procaspase-9 and Procaspase-3. Survival analysis based on manual H-Scores for Bcl-2, Bcl-xL, XIAP, Apaf-1, Procaspase-9 and Procaspase-3. Median H-Scores were used as cut-off to separate the patients with high (red line) and low (blue line) expression of each protein. Log-rank test was used to compare the Kaplan-Meier curves for progression free survival from the date of sample procurement.

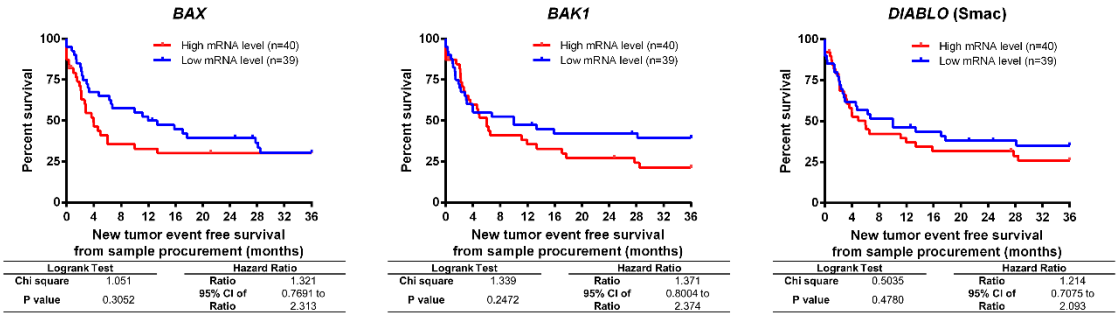

Supplementary Figure 2.2-4: Survival analysis in the metastatic TCGA-SKCM sub-cohort. Survival analysis based on *BAX*, *BAK1* and *DIABLO* (Smac) mRNA expression. Median normalized mRNA amount (log_2(FPKM-UQ+1)) was used as cut-off to separate the patients with high (red line) and low (blue line) expression of each transcript. Log-rank test was used to compare the Kaplan-Meier curves for progression free survival from the date of sample procurement.

2.3 Applying GAN-based data augmentation to improve transcriptome-based prognostication in breast cancer

The following manuscript was submitted to *PLOS Computational Biology* in October 2022 and is in revision at the date of submission of this dissertation. A preprint version is available on *medRxiv* and licensed under a Creative Commons Attribution 4.0 International License (http://creativecommons.org/licenses/by/4.0/).

Guttà, C.✉, Morhard, C., Rehm, M.✉ (2022) Applying GAN-based data augmentation to improve transcriptome-based prognostication in breast cancer. *medRxiv*. https://doi.org/10.1101/2022.10.07.22280776

✉ Corresponding authors

Author contributions:

CG: Conceptualized the study, integrated and curated the data, analysed the model results, assisted in the pipeline implementation, generated the figures and drafted the manuscript.
CM: Developed the pipeline and drafted the manuscript
MR: Supervised the project and drafted the manuscript

Code availability:

The scripts and input data used to generate the results of this work are available on Zenodo under a Creative Commons Attribution 4.0 International License (http://creativecommons.org/licenses/by/4.0/).

Guttà, C., Morhard, C. and Rehm, M. (2022) T-GAN-D: a GAN-based classifier for breast cancer prognostication. https://doi.org/10.5281/ZENODO.7151831

Research article

Applying GAN-based data augmentation to improve transcriptome-based prognostication in breast cancer

Cristiano Guttà[1, ✉], Christoph Morhard[2], Markus Rehm[1, 3, ✉]

1 Institute of Cell Biology and Immunology, University of Stuttgart, Allmandring 31, 70569 Stuttgart, Germany

2 ProKanDo GmbH, Elfriede-Breitenbach-Straße 38a, 71640 Ludwigsburg, Germany

3 Stuttgart Research Center Systems Biology, University of Stuttgart, Nobelstrasse 15, 70569 Stuttgart, Germany

Working title: Data augmentation for improved breast cancer prognostication

Keywords: Breast cancer; prognosis; mRNA expression; generative adversarial networks; artificial intelligence.

Competing interests: The authors declare that they have no conflict of interests.

✉ **To whom correspondence should be addressed.**

Prof. Dr. Markus Rehm

Institute for Cell Biology and Immunology

University of Stuttgart

Allmandring 31, 70569 Stuttgart, Germany

E-mail: markus.morrison@izi.uni-stuttgart.de

ORCID ID: 0000-0001-6149-9261

Cristiano Guttà

Institute for Cell Biology and Immunology

University of Stuttgart

Allmandring 31, 70569 Stuttgart, Germany

E-mail: cristiano.gutta@izi.uni-stuttgart.de

2.3.1 Abstract

Established prognostic tests based on limited numbers of transcripts can identify high-risk breast cancer patients yet are approved only for individuals presenting with specific clinical features or disease characteristics. Deep learning algorithms could hold potential for stratifying patient cohorts based on full transcriptome data, yet the development of robust classifiers is hampered by the number of variables in omics datasets typically far exceeding the number of patients. To overcome this hurdle, we propose a classifier based on a data augmentation pipeline consisting of a Wasserstein generative adversarial network (GAN) with gradient penalty and an embedded auxiliary classifier to obtain a trained GAN discriminator (T-GAN-D). Applied to 1244 patients of the METABRIC breast cancer cohort, this classifier outperformed established breast cancer biomarkers in separating low- from high-risk patients (disease specific death, progression or relapse within 10 years from initial diagnosis). Importantly, the T-GAN-D also performed across independent, merged transcriptome datasets (METABRIC and TCGA-BRCA cohorts), and merging data improved overall patient stratification. In conclusion, GAN-based data augmentation therefore allowed generating a robust classifier capable of stratifying low- vs high-risk patients based on full transcriptome data and across independent and heterogeneous breast cancer cohorts.

2.3.2 Introduction

Breast cancer is the tumor with the highest incidence in women, accounting for 2.3 million new diagnoses and 685,000 deaths worldwide in 2020. According to the World Health Organization, nearly eight million patients were diagnosed with breast cancer in the five years before 2020, making it the most prevalent tumor disease worldwide (WHO, 2021). In current clinical practice, the expression of estrogen receptor (ER), progesterone receptor (PR), and human epidermal growth factor receptor 2 (HER2) is determined by immunohistochemistry (IHC), with the expression patterns defining to which molecular subtype (luminal A, luminal B, HER2 positive or enriched and triple-negative breast cancer) individual tumors belong. Prognosis differs between these subtypes, and subtyping informs treatment plans in patients in which surgical resection of the tumor alone is insufficient (Yersal and Barutca, 2014). However, substantial response heterogeneities to the current standard of care treatments can be observed in populations of breast cancer patients (Turashvili and Brogi, 2017), highlighting the need for additional prognostic markers that could serve to identify high risk patients that

could instead benefit from alternative treatments or for which the burden from inefficient standard of care treatments could be avoided (Cardoso *et al.*, 2016).

Various multi-gene activity tests based on transcript abundance have been developed to assist in the clinical management of breast cancer (e.g. Oncotype DX (Syed, 2020), MammaPrint (Van't Veer *et al.*, 2002; van de Vijver *et al.*, 2002), Prosigna (Bernard *et al.*, 2009; Xia *et al.*, 2019), OncoMasTR (Buus *et al.*, 2020)) and received regulatory approval as prognostic tests (Ross *et al.*, 2008). Despite the prognostic value of these assays, their use is restricted to only subsets of patients with specific clinical characteristics (e.g. cancer stage, receptor or lymph node status, tumor size, menopause state, age group) (Jensen *et al.*, 2018; Kelly *et al.*, 2018; Yao *et al.*, 2022). It would therefore be desirable if more generally applicable prognostic tests based on transcriptome data could be developed.

The rapid advances in high-throughput sequencing technologies make tumor transcriptome data from larger patient cohorts increasingly available. The accessibility of -omics databases and companion clinical information now also encourages the application of deep learning (DL) methods to the oncology field, with the aim of learning and extracting features within large scale data that are not readily accessible by classical statistical and pattern recognition approaches. It is hoped that from DL-based methods tools can be developed that can aid in further advancing cancer diagnosis, prognosis or predicting treatment efficacy in the future (Tran *et al.*, 2021).

DL algorithms such as convolutional neural networks (CNN) were originally applied for image analysis but could be successfully repurposed to take non-image objects as input, such as RNA-seq data (Sharma *et al.*, 2019). One of the major pitfalls when applying DL models to transcriptome datasets is the typical imbalance between the number of quantified mRNAs (high) and the number of patients (low), which can lead to overfitting when solving classification tasks (Liu and Gillies, 2016). In addition, low numbers of samples or patients that represent one category (e.g. good prognosis) come at the risk of capturing patterns that are not robust when applied to larger populations (Barandela *et al.*, 2004). Feature selection strategies (Raghu *et al.*, 2017), under- and over-sampling (Chawla *et al.*, 2011) are three strategies that may help mitigating effects arising from imbalanced source data. An alternative strategy lies in novel data augmentation approaches, such as generative adversarial networks (GANs), by which source datasets can be enriched with artificially generated additional data. GANs are typically applied to imaging data and are composed of two subnetworks, the generator

and the discriminator. While the former produces synthetic images, the latter is challenged to discriminate fake vs. real images. Reiterating this process, the generator learns to produce images with features that can no longer be separated from the real images by the discriminator, with these generated images then enriching the source dataset (Goodfellow *et al.*, 2014). In comparison to other generative models, GANs are currently preferred due to their computational speed and the quality of the generated images (Shorten and Khoshgoftaar, 2019). In addition, they exhibit a lower risk of overfitting classifiers and are less susceptible to the impact of non-pertinent image features (such as brightness) when enriching training data with synthetic images (Bowles *et al.*, 2018). For example, GANs have been applied in the medical field to generate synthetic magnetic resonance, computed tomography or positron emission tomography images (Li *et al.*, 2021). Aside from image-data, different GAN implementations were also successfully applied to transcriptome data for cancer diagnosis (Wei *et al.*, 2021; Xiao *et al.*, 2021), staging (Kwon *et al.*, 2021) and subtyping (Yang *et al.*, 2021).

The Molecular Taxonomy of Breast Cancer International Consortium (METABRIC, hereafter MB) (Mukherjee *et al.*, 2018) and The Cancer Genome Atlas [3] – Breast Invasive Carcinoma (TCGA-BRCA, hereafter TCGA) cohorts represent two of the largest and most exhaustively annotated breast cancer datasets, including, in addition to mRNA expression data, features such as patient demographics, cancer staging, receptor statuses, and follow-up information such as survival times. Despite not being directly interoperable due to different sequencing technologies, these datasets can serve as use cases to test new DL-based prognostication approaches.

In this study, we therefore set out to develop a prognostication framework that used the trained discriminator of a GAN architecture as a standalone classifier and compared its performance to classical breast cancer biomarkers and a classical CNN.

[3] The Cancer Genome Atlas Program – National Cancer Institute: https://www.cancer.gov/about-nci/organization/ccg/research/structural-genomics/tcga

2.3.3 Materials and methods

2.3.3.1 Data integration

The METABRIC (MB) dataset was used to develop the prototype network implementation. Transcriptome data (median Z-scores), overall survival (OS), disease specific survival (DSS) and associated clinical records were downloaded from cbioportal.org (Cerami *et al.*, 2012; Gao *et al.*, 2013). The dataset was integrated with locoregional and distant recurrence information retrieved from Rueda et al. (Rueda *et al.*, 2019) and *Risk of Recurrence – Proliferation* (ROR-P) scores reported by Xia et al (Xia *et al.*, 2019). Clinical records, OS, DSS and progression free interval (PFI) of the validation TCGA-BRCA cohort (TCGA) were integrated from cbioportal.org (Cerami *et al.*, 2012; Gao *et al.*, 2013) and Liu et al. 2018 (Liu *et al.*, 2018), respectively. To merge the mRNA expression data of the two cohorts, normalized transcriptome datasets were downloaded using the R package MetaGxBreast (Gendoo *et al.*, 2019). The transcript amounts were rescaled as described by Gendoo et al. (Gendoo *et al.*, 2019) so that the 2.5 percentile corresponds to -1 and the 97.5 percentile corresponds to +1. Subsequently, transcripts overlapping between the two cohorts and with quantitative information missing in not more than five patients were retained, resulting in transcripts for m = 14042 genes. The R script used to download and rescale the datasets is available in the Zenodo repository (Guttà *et al.*, 2022).

2.3.3.2 Inclusion criteria and category definition

Both cohorts were filtered to exclude normal-like subtype samples (Sweeney *et al.*, 2014; Troester *et al.*, 2018; Xia *et al.*, 2019) and patients for which less than 10 years of follow-up time from diagnosis were available. Low and high risk categories were defined according to published clinical records(Bernard *et al.*, 2009; Xia *et al.*, 2019) as follows:

- high risk patients:
    - MB cohort: disease specific death, locoregional or distant recurrence event recorded before 10 years from initial diagnosis;
    - TCGA cohort: disease specific death, progression, local recurrence or distant metastases before 10 years from initial diagnosis.
- low risk patients: none of the above-mentioned events recorded before 10 years from initial diagnosis.

In total, 1248 patients of the MB cohort (n = 567 high risk, n = 681 low risk) and 165 patients of the TCGA cohort (n = 132 high risk, n = 33 low risk) satisfied the inclusion criteria. Four patients from each cohort were excluded after merging due to insufficient expression data.

2.3.3.3 Survival analysis and accuracy

Log-rank testing was used to compare predicted low vs high risk patients over a follow-up time of 10 years. Kaplan-Meier (KM) survival curves were computed using GraphPad Prism 8 (GraphPad Software, San Diego, CA). The area between the curves (ABC) displayed on the KM graphs for the pooled predictions was calculated as follows:

- Low risk AUC minus Predicted low risk AUC;
- Predicted low risk AUC minus Predicted high risk AUC;
- Predicted high risk AUC minus High risk AUC.

The ABCs values are shown on the graphs in the abovementioned order top to bottom. The AUC was computed using GraphPad Prism 8 (GraphPad Software, San Diego, CA).

Univariate and multivariate hazard ratios were calculated using the function *coxph* from the R's library *survival* (v. 3.4.0, https://www.r-project.org/).

2.3.3.4 GAN architecture

The architecture was based on a Wasserstein (Arjovsky *et al.*, 2017) GAN (Goodfellow *et al.*, 2014) with gradient penalty (Gulrajani *et al.*, 2017) and an auxiliary classifier (Odena *et al.*, 2016) as a variant of a conditional GAN implementation (Mirza and Osindero, 2014), yielding a AC-WGAN-GP architecture. The Wasserstein loss was implemented to reduce vanishing gradients and mode collapse (Kodali *et al.*, 2017) in the early phases of the training when the discriminator outperformed the generator. Stability was improved by exchanging the weights clipping approach described in Arjovsky et al. (Arjovsky *et al.*, 2017), with the gradient penalty described in Gulrajani et al. (Gulrajani *et al.*, 2017). To create a conditional GAN, an auxiliary classifier network was implemented (Odena *et al.*, 2016), resulting in a more stable training process and reduced mode collapse compared to the standard conditional GAN approach, supplying labels to both discriminator and generator (Kodali *et al.*, 2017). A z-vector of size 250 was fed as input for the generator. Following good training practice (Radford *et al.*, 2015), strided convolutions with step size 2, batch normalization and

LeakyRELU as activation function were used. Since using batch normalization in the discriminator and/or the ADAM optimizer led to an unstable training process, batch normalization (Ioffe and Szegedy, 2015) was only used in the generator, and RMSprop was selected as the activation function. A shallow network consisting of two layers in both the discriminator and the generator led to the most stable training process, due to the smaller number of trainable parameters compared to deeper networks. Hyperparameters were tuned empirically, selecting 1000 epochs for the training process. Three "discriminator-only" training runs were performed before each full network training run, and the generated pictures were subsequently smoothed with a final convolution layer with one filter and stride size of 1. The GAN architecture generated expression data of size 144x144 when using the entire transcriptome dataset of the MB cohort alone (m = 18543 genes) and 120x120 when merging the MB and TCGA cohorts (m = 14042 genes). In the latter setting, expression profiles with less than 14,440 transcripts were filled with random values, leading to better convergence. The resulting trained GAN Discriminator (T-GAN-D) was then used as an independent classifier to discriminate low and high risk patients. The Python code and the input files used to generate the predictions are available in the Zenodo repository (Guttà *et al.*, 2022).

2.3.3.5 CNN architecture

As the performance of the CNN implemented as the GAN's discriminator showed satisfactory performance, a similar architecture was used as a benchmark classifier. Batch normalization was employed to ensure shorter training periods and RELU was used as the activation function. A fixed training length of 1250 epochs was set due to the limited sample size and to generate comparable iterations.

The accuracy of both classifiers was calculated dividing the number of correct classifications by the total number of classifications performed.

2.3.4 Results

2.3.4.1 The METABRIC and BRCA-TCGA cohorts lend themselves as use cases for data augmentation and development of prognostication classifiers

One of the major challenges of machine learning applied to -omics data and companion medical records is the imbalance between the high amounts of variables compared to the limited number of patients available. Even in the case of breast cancer, one of the most frequent and widely studied malignant neoplasms, this limitation is apparent in the two major public transcriptome datasets, namely the MB cohort (n = 1904 patients, m =

A

METABRIC sub-cohort (n = 1248)		
Age at diagnosis (years)	**# cases**	**%**
<40	83	6.7
40-49	188	15.1
50-59	288	23.1
60-69	392	31.4
70-79	235	18.8
80+	62	5.0
Disease Stage	**# cases**	**%**
Stage I	303	24.3
Stage II	514	41.2
Stage III	88	7.1
Stage IV	8	0.6
Not available	335	26.8
Survival (months)	**Median**	
Overall survival	163.2	
Relapse or disease specific death	160.2	

B

BRCA-TCGA sub-cohort (n = 165)		
Age at diagnosis (years)	**# cases**	**%**
<40	20	12.1
40-49	38	23.0
50-59	29	17.6
60-69	44	26.7
70-79	22	13.3
80+	12	7.3
Disease Stage	**# cases**	**%**
Stage I	22	13.3
Stage II	72	43.6
Stage III	50	30.3
Stage IV	14	8.5
Not available	7	4.2
Survival (months)	**Median**	
Overall survival	92	
Progression or disease specific death	35.5	

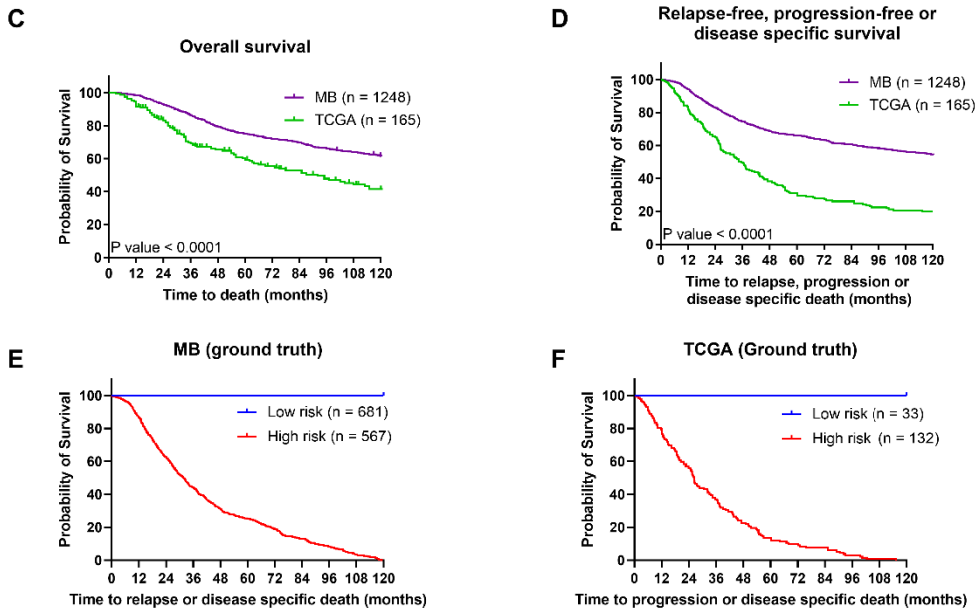

Figure 2.3-1: MB and TCGA patient demographics and survival. A Patients demographics of the MB subcohort. **B** Patients demographics of the TCGA subcohort. **C** Overall and **D** relapse-free, progression-free or disease specific survival of the MB and TCGA cohorts. **E** Kaplan Meier curves comparing low vs high risk patients of the MB and **F** the TCGA cohorts.

18543 transcripts) and the TCGA cohort (n = 1101 patients, m = 20532 transcripts). This imbalance is exacerbated for prognostic analyses that require long-term (10 years) follow-up information and the application of further exclusion criteria (see methods), reducing cohort sizes to n = 1248 and n = 165, respectively (**Figure 2.3-1A, B**). Both cohorts behaved notably different, with patients in the MB cohort on average having an overall substantially better prognosis in overall survival and relapse-free, progression-free or disease specific survival (**Figure 2.3-1C, D**). This is likely attributable to the MB dataset largely consisting of stage I and stage II patients (89.5% of patients with reported disease stage at diagnosis), whereas stage III and IV patients are more prominent in the TCGA dataset (40.4% of individuals with available disease stage at diagnosis). Despite these differences, the high risk subgroups of both cohorts showed

comparable median survival times (MB = 31.9 months [**Figure 2.3-1E**], TCGA = 26.3 months [**Figure 2.3-1F**]). Due to the limited sizes of these cohorts, they lend themselves as suitably challenging use-cases for applying and testing data augmentation for improving prognostication. In particular, we set out to implement a classifier based on a data augmentation network for improved patient stratification in the MB cohort, to subsequently validate robustness and transferability by integrating the independent TCGA cohort.

2.3.4.2 A trained GAN discriminator robustly identifies low and high risk breast cancer patients

To tackle the problem of data scarcity, we implemented a GAN architecture to augment transcriptomic data of the MB cohort and tested the performance of a trained discriminator in stratifying breast cancer patients. First, individual patient transcriptome profiles were rescaled and converted into arrays of pixels (**Figure 2.3-2A i**) in order to use these images as an input for the GAN. Independent of these true patient data, the generator created images representing the transcript profiles of synthetic hypothetical patients together with their category (low or high risk) (**Figure 2.3-2A ii**). After being exposed to a fraction of the real transcriptome images and associated categories, its adversary, the discriminator network then tried to distinguish fake from real transcriptome images for high or low risk patients (**Figure 2.3-2A iii**). Reiterating this training process over 1000 epochs, the generator learned to create realistic synthetic transcriptome images for high and low risk categories, which then could be used to augment the original MB cohort data. Associated characteristics of this process (discriminator loss, discriminator class loss, generator loss) are shown in **Supplementary Figure 2.3-1**. Using this approach, the discriminator learned to identify features relevant for the risk category definition, aided by the synthetic profiles that enriched the real training data at each epoch. The trained GAN discriminator (T-GAN-D) resulting from this process then was used as a standalone classifier to categorize images from the test fraction of the cohort into the high or low risk categories (**Figure 2.3-2A iv**), thus prognosticating patient outcome.

We first implemented and tested the T-GAN-D for its prognostic capability using follow-up and mRNA expression data of the prototyping MB cohort, consisting of n = 1248 individuals and m = 18543 genes. Within this cohort, we independently cross-validated (CV) five-fold with randomly composed training data. Kaplan-Meier curves

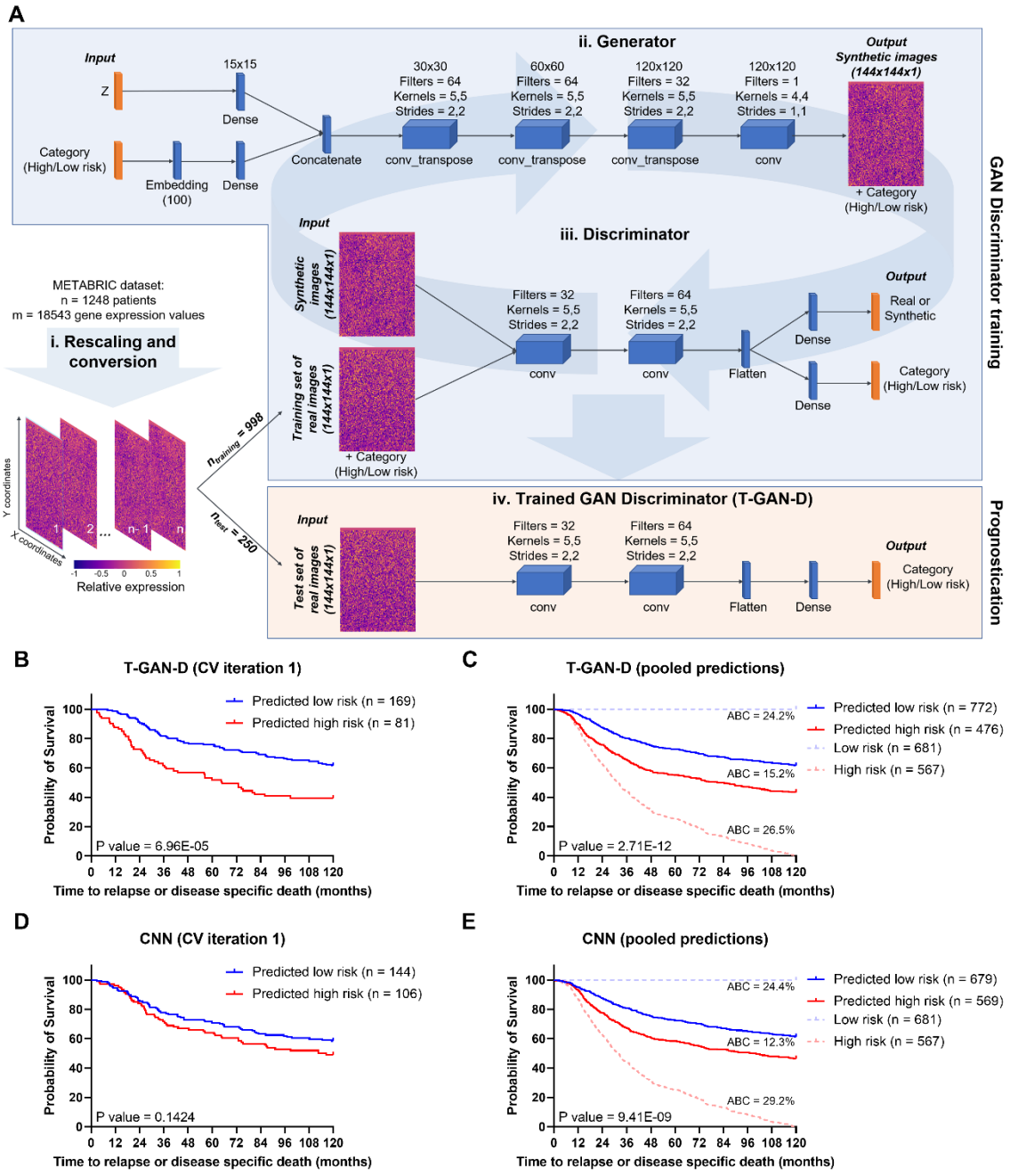

Figure 2.3-2: The T-GAN-D robustly stratifies low and high risk breast cancer patients. A Workflow of the data processing, including the schematics of the generator network and its adversary, the discriminator network. Together these result in an AC-WGAN-GP architecture. After the conversion of patient transcriptome profiles into images, 4/5 of the MB dataset was used to train the GAN's discriminator. After 1000 epochs, the trained discriminator was used as a standalone classifier to separate the remaining 1/5 patients of the dataset into low and high risk categories. **B** Kaplan-Meier curves separating low vs. high risk patients as predicted with the T-GAN-D (iteration 1 of the 5-fold CV shown as representative). **C** Kaplan-Meier curves generated pooling the category predictions obtained for all patients of the MB dataset after five independent CV runs. **D** Separation of low vs. high risk patients predicted with a classical CNN on the same subset used in **B** and **E** comparison obtained pooling the predictions of five independent CV runs. The area between the curves (ABC) between Low risk (blue dashed line) and Predicted low risk (solid blue line), Predicted low risk and Predicted high risk (solid red line), Predicted high risk and High risk groups (dashed red line) are shown top to bottom in **D** and **E**.

and log rank testing for each run yielded significant class separations in 4 out of 5 iterations (**Figure 2.3-2, Supplementary Figure 2.3-2A**). Pooling the results so that each patient of the MB dataset was present once in the survival analysis, the T-GAN-D separated high and low risk patients with high statistical significance (p-value = 2.71E-12) (**Figure 2.3-2C**). To obtain a reference performance baseline, a classical CNN was challenged with the same task, using the same training and test sets for each iteration. The CNN yielded class separations with a $p<0.05$ in only two out of five iterations (**Figure 2.3-2D, Supplementary Figure 2.3-2B)**. In the pooled comparison, the CNN performed well yet failed to outperform the T-GAN-D in separating low vs. high risk patients (**Figure 2.3-2E, Supplementary Table 2.3-1**). These results therefore demonstrate that the reiterative learning process of a GAN to train its discriminator and use it as an independent classifier provides a more robust and slightly improved patient stratification than a classical DL approach.

2.3.4.3 Introducing and independent cohort improves MB patient classification

A common limitation of predictors and classifiers is their limited robustness and transferability to independent datasets. This might arise from overfitting or overtraining within the initial cohort but also from heterogeneity and batch effects between source datasets. For validating our approach further, we therefore merged the mRNA expression data of the MB and TCGA cohorts, which originally were quantified with bead-based microarray technology (Illumina Human V3) or RNA-Seq (Illumina HiSeq) platforms respectively (Craven *et al.*, 2021), by rescaling the expression of transcripts overlapping between the two cohorts (m = 14042). We then retrained the discriminator using the entire TCGA data plus a fraction of the MB data from the merged dataset and generated predictions on an independent subset of MB patients (**Figure 2.3-3A**), using five-fold cross-validation. The T-GAN-D again separated patients into low and high-risk categories with high statistical significance (**Figure 2.3-3B, Supplementary Figure 2.3-3A**). The CNN trained and tested with the same data performed similarly well (**Figure 2.3-3C, Supplementary Figure 2.3-3B**). The T-GAN-D trained on the merged and reduced dataset also showed improved accuracy when compared to all settings where both a CNN or the GAN were trained on the full or reduced MB dataset alone (**Supplementary Table 2.3-1, Supplementary** Table 2.3-2). Therefore, in our setting, rescaling and converting transcriptome profiles into images was sufficient to successfully merge the two cohorts without the need for further preprocessing steps and allowed to stratify patients into high and low risk classes.

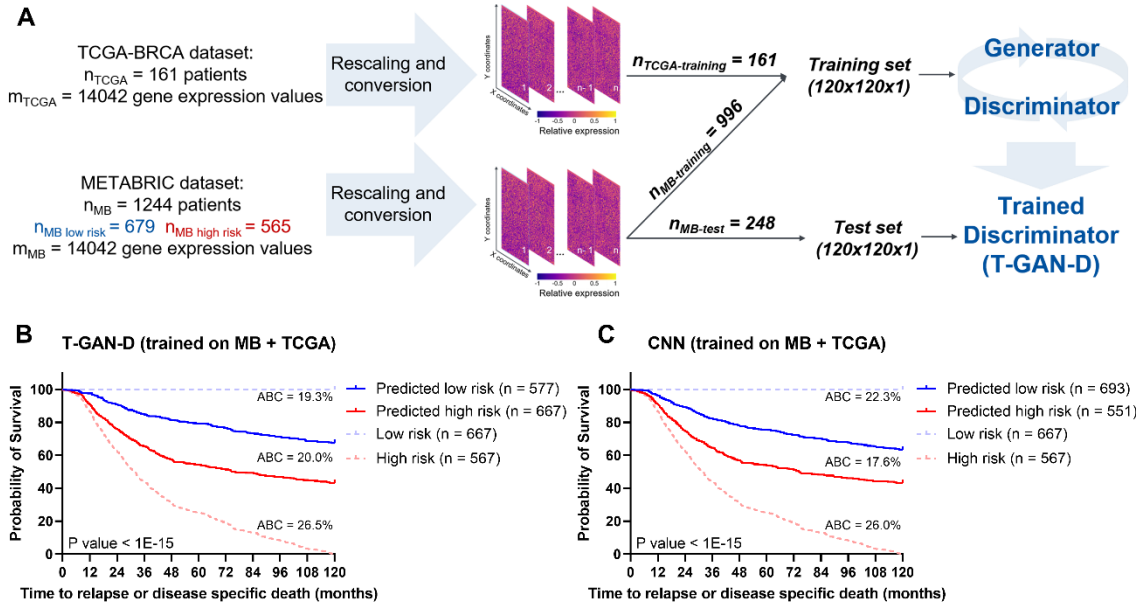

Figure 2.3-3: Introducing the independent TCGA cohort improves MB patient classification. **A** Schematic representing the training strategy: rescaled data from the entire TCGA cohort were merged with 4/5 of the MB cohort to train the T-GAN-D, which was subsequently used to predict the risk class of the remaining 1/5 of MB patients. The process was iterated 5 times. **B** Kaplan-Meier curves based on the pooled predictions of the T-GAN-D trained on both cohorts. **C** Kaplan-Meier curves separating low vs. high risk patients predicted with the CNN that was trained after merging the MB and the TCGA cohorts. The area between the curves (ABC) between Low risk (blue dashed line) and Predicted low risk (solid blue line), Predicted low risk and Predicted high risk (solid red line), Predicted high risk and high risk groups (dashed red line) are shown top to bottom in **B** and **C**.

2.3.4.4 The T-GAN-D outperforms classical outcome predictors and accurately stratifies early stage patients into risk categories

We next compared the performance of CNN and GAN based classifications to other established clinical markers in breast cancer. These included a scoring system based on a multi-transcript signature (Risk-of-recurrence - proliferation, [ROR-P]), estrogen receptor status (ER), human epidermal growth factor receptor 2 status (HER2), and progesterone receptor status (PR). Likewise, tumor staging was included, yet was available for only 911 out of 1248 patients of the MB cohort. The hazard ratios (HR) obtained from a univariate analysis were comparable for ROR-P, HER2 or tumor staging as classifiers, and similar HRs were also obtained for the CNN and T-GAN-D classifiers developed from only the MB transcriptome dataset (**Figure 2.3-4A**). Interestingly, the T-GAN-D classifier resulting from the merged cohort data returned a mean HR>2.0 (+/- 0.4), thereby surpassing all other markers. This feature was even more pronounced in a multivariate analysis including ER, HER2 and PR biomarkers (**Figure 2.3-4B**). When reducing the MB cohort to those patients for which staging information was available, HRs based on staging and T-GAN-D were comparable (**Figure 2.3-4C**). To test whether both classifiers might be redundant, we performed a

T-GAN-D based survival analysis within the tumor stage I and stage II subcohorts, which dominate the MB dataset. T-GAN-D based classification allowed separating high and low risk patients within both tumor stages (**Figure 2.3-4D, E**), indicating non-redundancy of the T-GAN-D classification to tumor staging information.

Taken together, these results show that training through data augmentation can enhance the prognostic performance of DL classifiers, and in this case surpasses individual classical biomarkers. In addition, the T-GAN-D performed well in prognostication of early stage breast cancer cases.

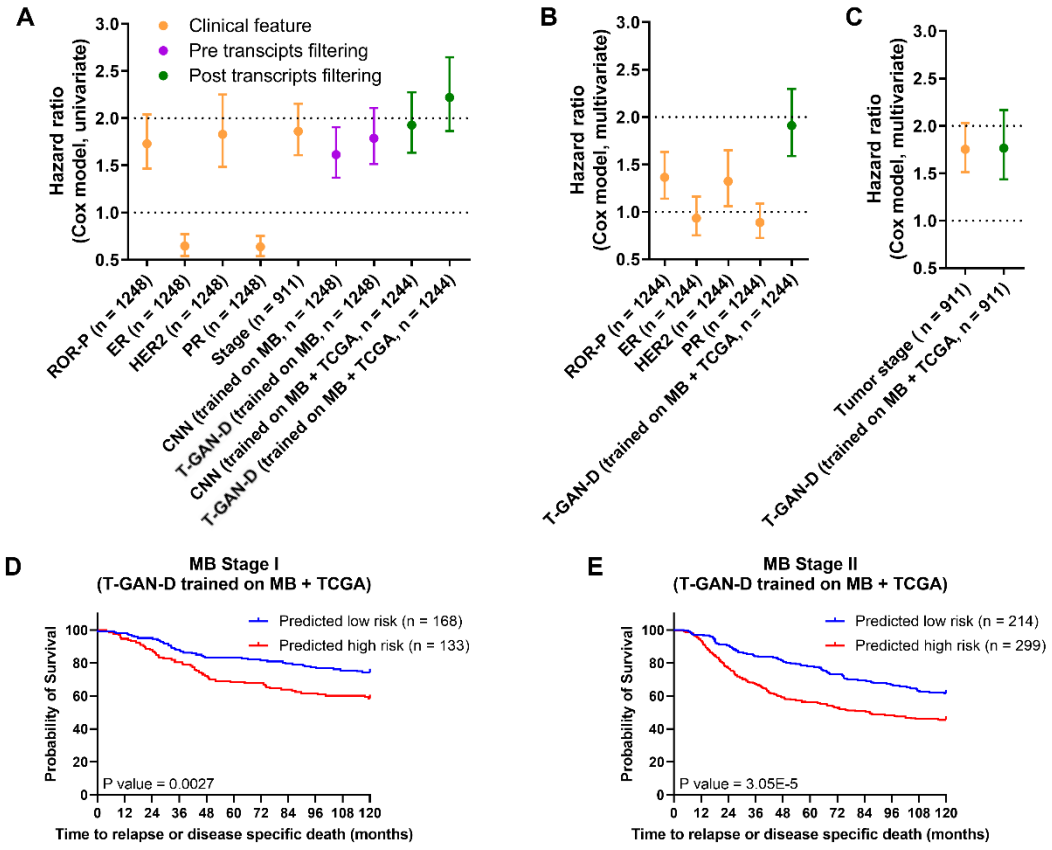

Figure 2.3-4: The T-GAN-D outperforms classical biomarkers after merging the MB and TCGA cohorts and significantly stratifies early stage MB patients. A Comparison of the hazard ratios (Cox model, univariate) of a multi-transcript signature (ROR-P) and established prognostic biomarkers (ER, HER2, PR) vs. the CNN and the T-GAN-D before and after cohort merging. **B** Multivariate Cox hazard ratio of the T-GAN-D compared to ROR-P and receptor status and (**C**) disease stage. (**D**) Kaplan -Meier curves of Stage I and (**E**) Stage II patients stratified by the T-GAN-D into low and high risk categories.

2.3.4.5 The T-GAN-D stratifies TCGA patients despite these being scarcely represented

After observing that introducing TCGA patients into the training set of the T-GAN-D did not degrade, but improved the stratification of MB patients, we tested the performance of the classifier on the smaller TCGA dataset. To do this, we trained the discriminator using the entire MB data plus a fraction of the TCGA data from the

merged dataset and generated predictions on an independent subset of TCGA patients (**Figure 2.3-5A**), using five-fold cross-validation. The T-GAN-D correctly predicted 78% of the cases (**Figure 2.3-5B**, **Supplementary Figure 2.3-4**, **Supplementary Table 2.3-3**). In contrast, when trained on the MB dataset alone, the T-GAN-D was not able to separate high and low risk patients (**Figure 2.3-5C**, **Supplementary Figure 2.3-4**), achieving an overall accuracy of only 43% (Supplementary Table 3). Therefore, the addition to the training set of a comparably small number of TCGA patients (n = 129) to the larger MB cohort (n = 1244) was sufficient to drastically improve the performance of the T-GAN-D predicting TCGA patient outcome. This demonstrates that even if the training set is largely dominated by patients belonging to one cohort, the introduction of a limited number of samples of a second, differently balanced dataset appears sufficient to possibly capture relevant patterns that contribute to achieving improved prognostic performance.

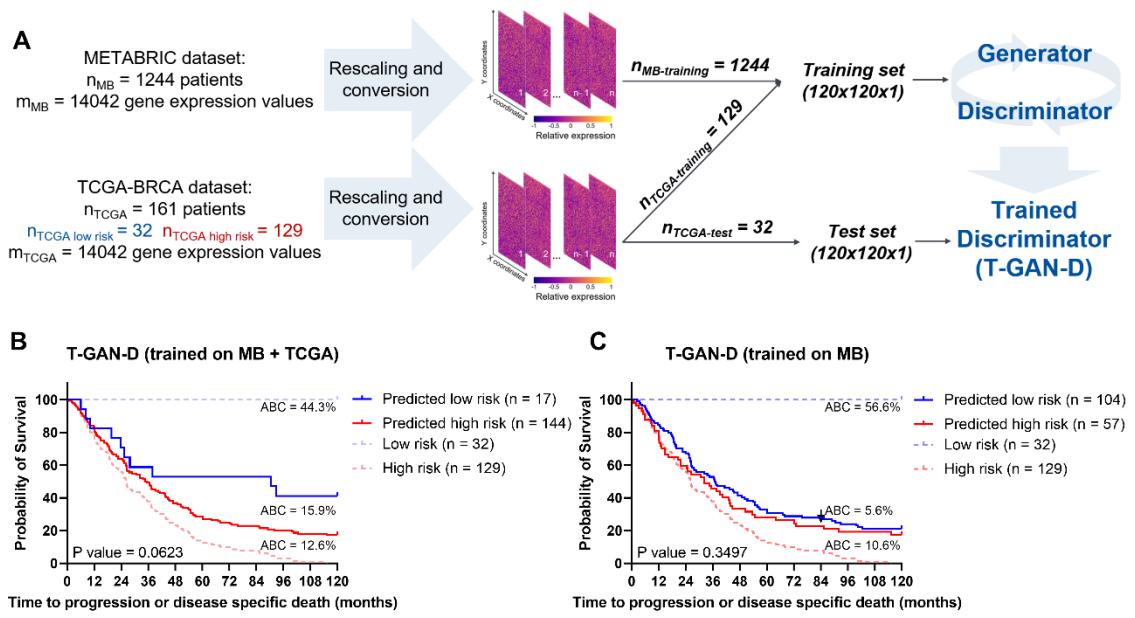

Figure 2.3-5: The T-GAN-D stratifies TCGA patients despite these being scarcely represented in the merged training set. A Schematic representing the training strategy: rescaled data from the entire MB cohort were merged with 4/5 of the TCGA cohort to train the T-GAN-D, which was subsequently used to predict the risk class of the remaining 1/5 of TCGA patients. The process was iterated 5 times. **B** Stratification of the TCGA patients by T-GAN-D trained on the merged dataset and **C** the MB dataset alone. Kaplan-Meier curves were generated pooling the predictions of all iterations of the 5-fold CV. The area between the curves (ABC) between Low risk (blue dashed line) and Predicted low risk (solid blue line), Predicted low risk and Predicted high risk (solid red line), Predicted high risk and High risk groups (dashed red line) are shown top to bottom in **B** and **C**.

2.3.5 Discussion

The increasing availability and routine acquisition of large scale genomic data encourage the repurposing and application of AI to the field of oncology in order to identify novel means for improved and personalized prediction of prognosis (Wallis, 2019). In this study, we developed a DL-based tool to stratify high vs. low risk breast cancer patients according to full transcriptome profiles. Using the MB and TCGA cohorts as use cases, we converted expression data into images and used the trained discriminator of our GAN architecture as a standalone prognostic classifier. Our results show that the T-GAN-D performed better than classical outcome predictors and maintained robust performance when merging the two cohorts.

AI has already been applied to breast cancer based on different classes of data, to inform diagnosis, treatment planning and prognosis (Jia *et al.*, 2021; Zhang *et al.*, 2020). For example, pattern recognition and data augmentation proved to be promising approaches to assist in generating accurate diagnoses from mammography images (Desai *et al.*, 2020; McKinney *et al.*, 2020). Transcriptome data were also employed to develop ML-based analysis pipelines for breast cancer subtyping, diagnosis, patient stratification and identification of altered pathways (Liñares-Blanco *et al.*, 2021), and these techniques may improve the accuracy of cancer prognosis in the future. However, shortcomings must be taken into account, as applicable also to currently available breast cancer datasets. When dealing with low sample size - high dimension datasets such as the MB and TCGA cohorts, common DL classification algorithms such as neural networks may be prone to overfitting (Liu, Wei, *et al.*, 2017). Multi-gene signatures based on the expression of a lower number of transcripts may circumvent this problem, but are applicable only to subsets of patients with specific clinical characteristics (Jensen *et al.*, 2018; Kelly *et al.*, 2018; Ross *et al.*, 2008; Yao *et al.*, 2022). To tackle these problems, we aimed at developing a more universally applicable algorithm that takes advantage of GAN's data augmentation and generalizing capability. In our training strategy, the T-GAN-D was exposed not only to a subset of original data, but also to the synthetic patients generated by the generator in each epoch. This approach for the augmentation of training data was demonstrated before to aid a discriminator in learning hidden features and correlations (He *et al.*, 2015; Shams *et al.*, 2018). When compared to a classic CNN, the T-GAN-D showed comparable, yet slightly improved performance. Other GAN implementations have been applied to the MB or TCGA cohorts in the past, addressing different aims such as the generation of missing data (Arya and Saha, 2022),

the identification of multi -omics signatures (Kim *et al.*, 2018) and prognostication (Hsu and Lin, 2020). While showing encouraging results, these prior works limited the follow up time to 5 years and focused on death events only. Besides considering longer follow up times, the inclusion of progression or recurrence events in the class definition can be considered a more exhaustive assessment of a patient´s risk category, since OS or DSS alone may be insufficient especially in early stage screenings (Kourou *et al.*, 2015). In addition, short follow up times were shown to affect the prognostication performance of ML algorithms leading to low sensitivity, mostly due to the insufficient occurrence of recurrence or death events (Boeri *et al.*, 2020).

We demonstrated that the conversion of transcriptome profiles into images allowed the integration of independent transcriptome datasets. To date, the majority of gene expression databases cannot be directly integrated due to different sequencing technologies, protocols or batch effects, with the consequence of producing merely qualitative results in a meta-analysis fashion or unveiling evidences that remain cohort-specific (Carnielli *et al.*, 2018). To test if our conversion strategy could allow a straightforward integration of heterogenous datasets, we challenged the T-GAN-D in assessing the risk category of MB patients, training the network with a subset of MB patients plus the entire TCGA cohort. Introducing patients belonging to a different cohort improved the performance of the classifier, which in our case outperformed established clinical biomarkers and a published ROR-P signature (Xia *et al.*, 2019) in uni- and multi-variate analyses. The T-GAN-D classifier also stratified early stage breast cancer patients into low and high risk groups, even though no additional factors such as treatment regimens, age, subtype or other clinical features were considered when composing the training datasets. Early stage patients expected to experience recurrence or progression may benefit from more frequent screenings, yet it remains to be assessed if the transcriptome-based classifier operates independently of or correlates with other established risk factors.

High accuracy in predicting the risk class of the smaller and imbalanced TCGA cohort was achieved when training the T-GAN-D with a subset of TCGA patients plus the whole MB dataset. Classical ML algorithms (SVM and random forest, among others) were also shown to benefit from the combination of TCGA RNA-Seq and MB microarray data, which in a previous study improved 5 years OS prognostication (Dubourg-Felonneau *et al.*, 2018), but lead to misleadingly high accuracy due to highly imbalanced classes. Taken together, our results suggest that the T-GAN-D remains

robust when merging cohorts differently balanced between positive and negative outcomes, and that the network is still able to capture relevant risk patterns when one cohort is heavily underrepresented in the training dataset. Therefore, our classification framework may allow the integration of new, smaller datasets, lending itself as a suitable prototype for generating prospective personalized outcome predictions for scarce *de novo* data.

In conclusion, our proof-of-concept study represents an avenue for developing a scalable data augmentation-based tool that could be a stepping stone towards individualized prognosis in the future. Molecular high throughput techniques are increasing in quality, resolution and amount of data produced and are more and more commonly captured in clinical research and diagnostic environments. It was estimated that within the next decade, between 2 and 40 exabytes of genomic data will be generated every year (Stephens *et al.*, 2015), with large quantities being related to human health and disease. GAN-based approaches therefore could become a meaningful approach to exploit such data for the benefit of patients. In addition, -omics domains other than transcriptomics likewise have the potential to enter the clinical arena as part of routine analytical practice, including proteome, metabolome or lipidome data. Such data classes can readily be integrated with clinical-pathological information (Karczewski and Snyder, 2018), and could be processed with the assistance of GAN based approaches to improve patient-tailored interventions or prognostication.

2.3.6 Data availability

Transcriptome data (median Z-scores), OS, DSS and associated clinical records of the METABRIC cohort were downloaded from cbioportal.org. Locoregional and distant recurrence records and ROR-P scores of the MB cohort were retrieved from Rueda et al. 2019 (DOI: 10.1038/s41586-019-1007-8) and Xia et al. 2019 (DOI: 10.1038/s41467-019-13588-2) respectively. Clinical records, OS, DSS and PFI of the TCGA-BRCA cohort were integrated from cBioportal.org and Liu et al. 2018 (DOI: 10.1016/j.cell.2018.02.052). Curated METABRIC and BRCA-TCGA expression data were downloaded using the MetaGxBreast R package (Gendoo et al. 2019, DOI: 10.1038/s41598-019-45165-4). The input files and scripts used to generate the results are available in the Zenodo repository (DOI: 10.5281/zenodo.7151831).

2.3.7 Acknowledgements and funding information

MR and CG receive funding by the Deutsche Forschungsgemeinschaft (DFG, German Research Foundation) under Germany's Excellence Strategy - EXC 2075 – 390740016 and acknowledge the support by the Stuttgart Center for Simulation Science (SimTech).

2.3.8 Supplementary material

Supplementary Tables: Accuracy and Log-rank P value of each CV iteration and pooled category predictions for all experimental settings.

Supplementary Table 2.3-1: MB risk class prediction (Figure 2.3-2, Supp. Figure 2.3-2).

	T-GAN-D		*CNN*	
Run no.	***Accuracy***	***Log-rank P value***	***Accuracy***	***Log-rank P value***
1	61.2%	6.96E-05	55.2%	0.1424
2	62.0%	1.89E-05	66.0%	7.77E-09
3	62.0%	0.0003	55.6%	0.0444
4	58.2%	0.0076	56.6%	0.0667
5	55.0%%	0.0995	55.8%	0.0570
Mean accuracy and pooled Log-Rank P value	**59.7%**	**2.71E-12**	**57.9%**	**9.41E-09**

Supplementary Table 2.3-2: MB risk class prediction (Figure 2.3-3, Supp. Figure 2.2-3).

	T-GAN-D (trained on MB + TCGA)		*CNN (trained on MB + TCGA)*	
Run no.	***Accuracy***	***Log-rank P value***	***Accuracy***	***Log-rank P value***
1	64.5%	1.59E-07	57.3%	0.0317
2	60.2%	4.40E-05	64.3%	3.13E-07
3	57.8%	0.0004	61.4%	0.0001
4	63.5%	1.47E-06	58.2%	0.0023
5	62.7%	0.0009	61.0%	0.0005
Mean accuracy and pooled Log-Rank P value	**61.7%**	**< 1E-15**	**60.5%**	**< 1E-15**

Supplementary Table 2.3-3: TCGA risk class prediction (Figure 2.3-5, Supp. Figure 2.3-4).

	T-GAN-D (trained on MB + TCGA)		*T-GAN-D (trained on MB)*	
Run no.	***Accuracy***	***Log-rank P value***	***Accuracy***	***Log-rank P value***
1	78.8%	0.1455	39.4%	0.1970
2	75.0%	0.2526	65.6%	0.2035
3	81.3%	0.3514	40.6%	0.5831
4	81.3%	0.1116	46.9%	0.3030
5	75.0%	0.0103	21.9%	0.4676
Mean accuracy and pooled Log-Rank P value	**78.3%**	**0.0623**	**42.9%**	**0.3497**

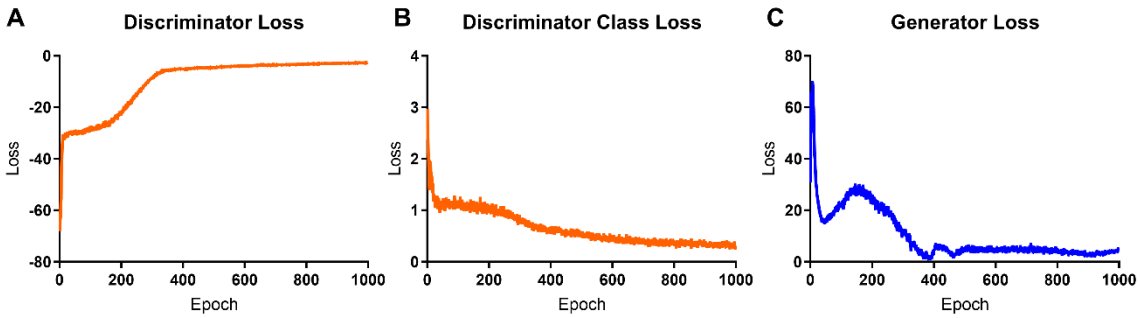

Supplementary Figure 2.3-1: AC-WGAN-GP loss functions. A Loss functions of the discriminator identifying real vs fake patients and **B** risk category. **C** Loss function of the generator. Loss functions were computed over 1000 training epochs.

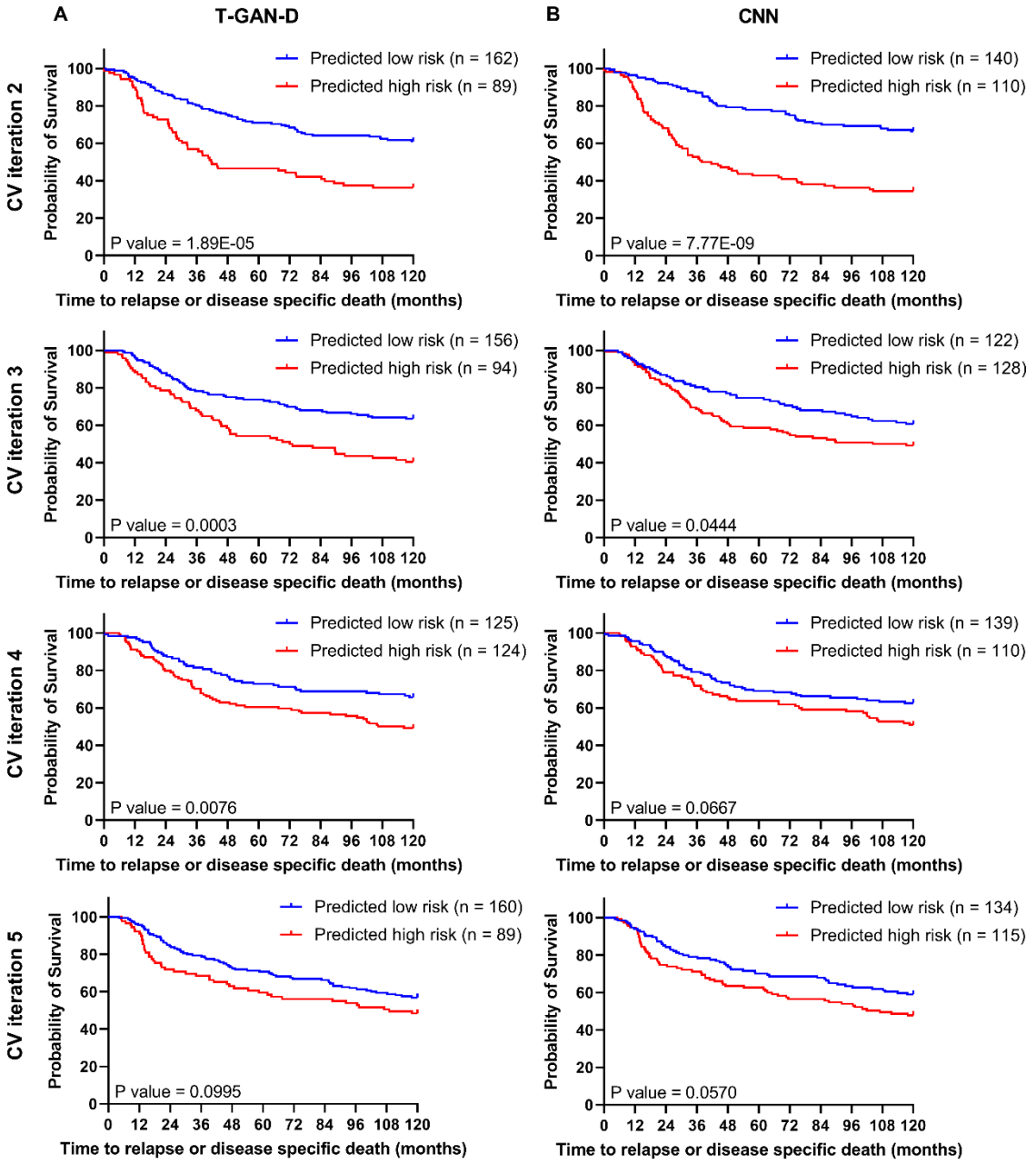

Supplementary Figure 2.3-2: Kaplan-Meier curves generated with the risk categories predicted in the CV iterations not shown in Figure 2.3-2. The prototyping MB cohort with all available transcriptomic data was used to compare the patient stratification obtained with the **A** T-GAN-D and **B** a classic CNN.

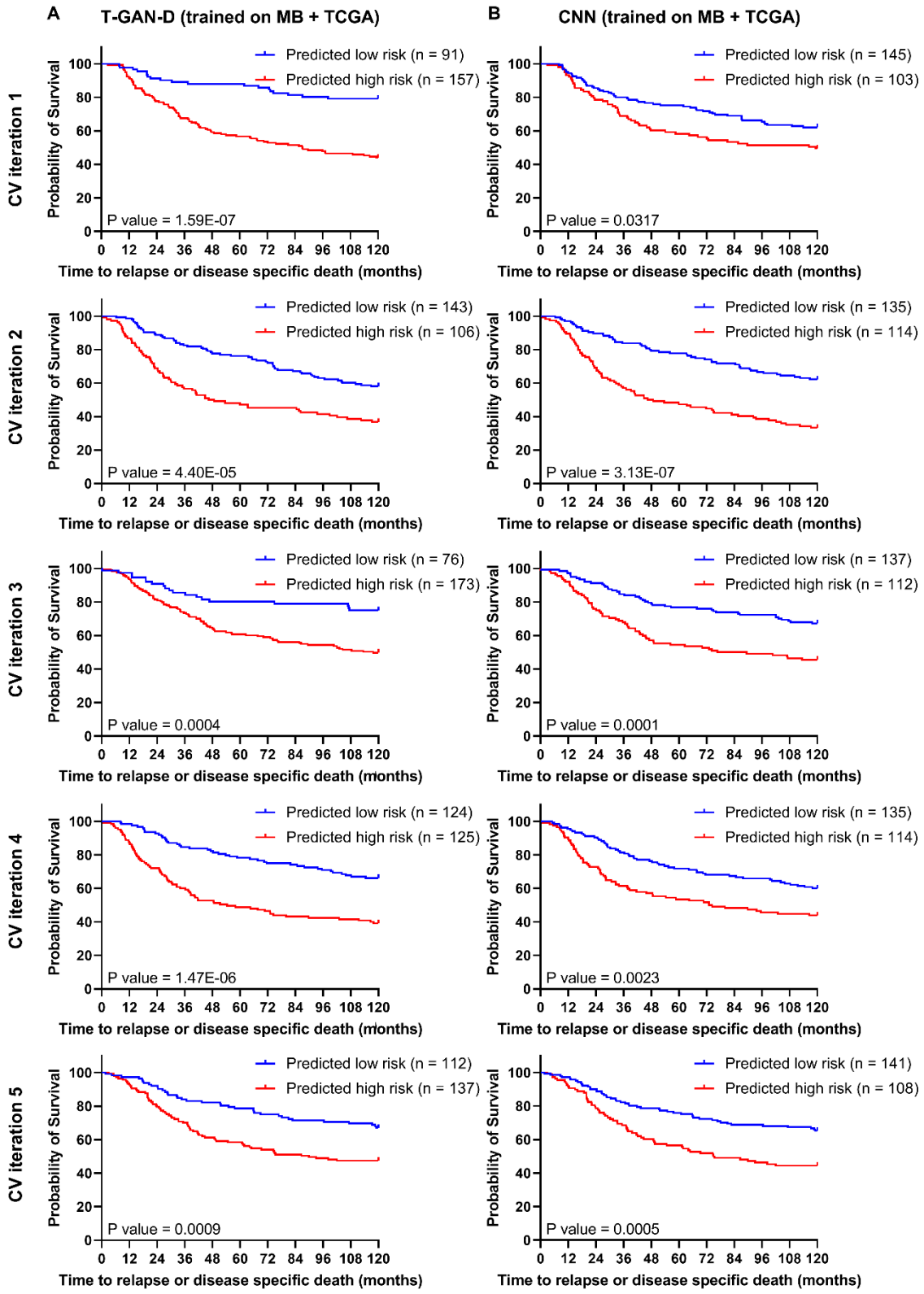

Supplementary Figure 2.3-3: Kaplan-Meier curves of individual CV iterations pooled in Figure 2.3-3. A fraction of the MB and the full TCGA cohorts were integrated to train **A** the T-GAN-D and **B** the CNN. After rescaling both datasets and filtering out the genes not available in both cohorts the risk class of the MB patients was predicted.

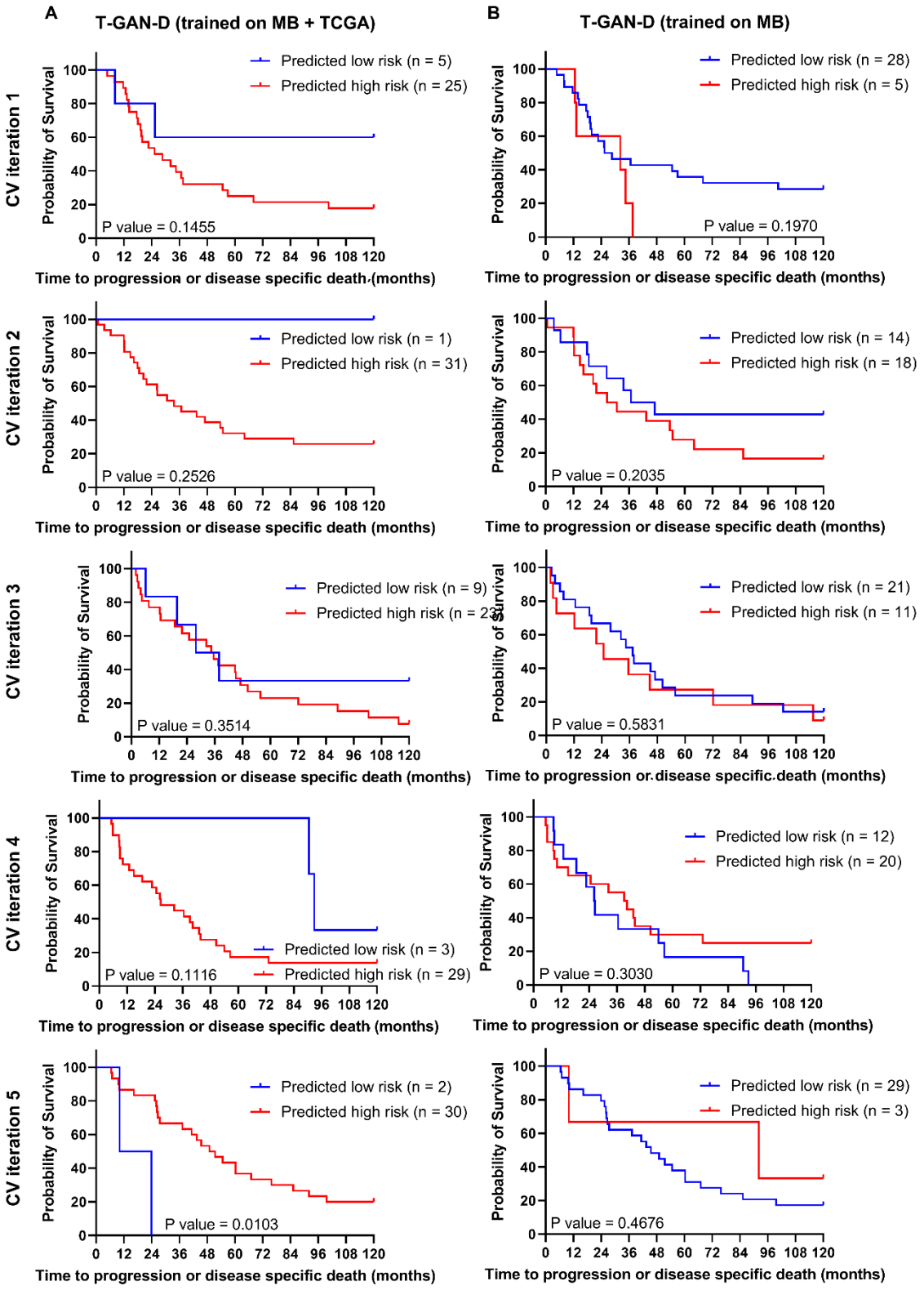

Supplementary Figure 2.3-4: Kaplan-Meier curves of individual CV iterations pooled in Figure 2.3-5. The T-GAN-D was trained **A** on the merged dataset and **B** on the MB dataset alone. After rescaling both datasets and filtering out the genes not available in both cohorts the risk class of the TCGA patients was predicted.

3 DISCUSSION

3.1 Artificial Intelligence: a technological and social phenomenon

The work presented in this thesis positions itself in the rapid changing field of AI. While the interest for data-driven automated tools has been limited to the research environment for a long time, AI recently forced its way in the mainstream news. On the 30th of November 2022 the attention of the general public was captured by the release of a new chatbot, named ChatGPT, developed by the AI research and deployment company OpenAI[4]. Within just one week from its release, over one million users interacted with the virtual interlocutor, generating mixed reactions. On the one side, enthusiastic comments highlighted the high quality and level of detail of the conversations, reported as "human-like". To reach such performance, the natural language processing (NLP) model was trained by human trainers using both supervised and reinforcement learning. The chatbot does not only interact with the user providing information on specific topics, but can write or debug code and generate texts, like poems, song lyrics or assays, even emulating a specific style. Most importantly, ChatGPT is stateful, meaning that it can remember previous statements from the same conversation and proceed interacting with the user in a logical manner. Such a powerful technology raised great interest but also serious ethical concerns. Elon Musk referred to ChatGPT as "scary good"[5] to the point that even the concept of creativity itself may

[4] https://openai.com/blog/chatgpt/%5C/

[5] https://fortune.com/2022/12/11/elon-musk-history-with-chatgpt-maker-openai-as-told-by-the-ai-chatbot-itself/

need to be redefined[6] . Despite several limitations still to be addressed, the release of ChatGPT raised the awareness of the general public towards AI. NLP and several other AI-based technologies have already penetrated the clinical environment with mixed success, attracting tech firms (e.g. Google and Microsoft), pharmaceutical companies (e.g. Roche) and several startups (Davenport and Kalakota, 2019) in a market that reached in 2020 a worth of over 29 billion USD[7]. For example, IBM's Watson has been recently featured in the news for its "Oncology Expert Advisor" project, aimed at providing personalized treatment indications based on patient electronic health records and clinical databases. Despite the high expectations of the developers, the NLP model did not perform satisfactorily when tested in the clinics: Watson was reported to achieve very high accuracy when solving diagnostic tasks (90-96%) but obtained inconsistent percentages of concordance (49-83%) with human experts when dealing with time-dependent information like therapy timelines (Strickland, 2019). Even though NLP models still show substantial limitations applied to the medical domain, several devices and software based on different AI paradigms were developed and FDA approved. To date, 521 AI/ML-enabled medical devices are authorized and marketed in the US, 75% of which are used to analyze radiology images, whilst -omics-oriented technologies lag behind [8]. A historic milestone was set in 2021 by "Paige Prostate", the first approved digital pathology-based tool to detect prostate cancer from patient biopsies. The fact that the majority of marketed AI-based technologies are currently geared towards images is not surprising. In order to perform satisfactorily, the algorithms need sufficient training data and digitalized medical images are routinely generated in the clinics. The interest for AI applied to image analysis has also been fueled by the advances in the algorithm designs and the use of graphical processing units. A revolutionary event has been the

[6] https://www.vox.com/future-perfect/2022/12/15/23509014/chatgpt-artificial-intelligence-openai-language-models-ai-risk-google

[7] https://www.gminsights.com/industry-analysis/precision-medicine-market?utm_source=prnewswire.com&utm_medium=referral&utm_campaign=Paid_prnewswire

[8] https://www.fda.gov/medical-devices/software-medical-device-samd/artificial-intelligence-and-machine-learning-aiml-enabled-medical-devices

2012 ImageNet Large Scale Visual Recognition Challenge (Russakovsky *et al.*, 2015), where a CNN halved the error rate of the previous winner of the image classification contest (Krizhevsky *et al.*, 2012), approaching human-like recognition abilities. With such a result, the potential of DL ended in the spotlights, capturing the attention not only of the AI experts, but of the entire technology industry [9], making CNNs the new "*workhorse for image classification*" (Bhinder *et al.*, 2021). In addition to image acquisition technologies, novel high-throughput platforms can generate high dimensional -omics datasets (e.g. whole-exome, whole-genome and targeted panels; transcription profiles from microarrays, RNA-seq, methylation profiles). Since the early 2000s various ML learning approaches have been used to analyze separate molecular datasets and progressed in order to integrate multi-omics data (Bhinder *et al.*, 2021). The availability of both data and algorithms, together with the combined efforts of experts from different knowledge domains, produced a rise in life science publications related to AI from 596 in 2010 to 12,422 in 2019 (Benjamens *et al.*, 2020). Currently, at least one diagnostic or predictive AI/big data-based study is published per week, claiming equal or greater accuracy than humans (Davenport and Kalakota, 2019). This thesis places itself in this rapidly evolving scenario, in which AI strongly gained the general public's attention. In particular, this work aimed at developing ML frameworks to solve prognostic or predictive classification tasks. Different ML paradigms were used to analyze data representing increasing levels of complexity, ranging from the expression of a limited number of markers in melanoma cell lines to full transcriptome profiles of breast cancer patients.

3.2 Apoptosis-based data-driven models accurately predict treatment outcome and melanoma patient prognosis

The first two studies presented in this dissertation focused on melanoma as a case study. Two different but complementary problems were addressed: prediction of treatment outcomes and prognostication. The skin represents an ideal organ for the development of novel AI-based approaches. Compared to other malignancies, obtaining samples

[9] https://www.economist.com/special-report/2016/06/23/from-not-working-to-neural-networking

from primary tumors and loco-regional metastases requires less invasive procedures, given the accessibility of the organ. Moreover, the introduction of novel targeted and immunotherapies in 2011 fostered the research of biomarkers and response signatures to predict treatment responses. (Vera *et al.*, 2022). Advances in sequencing technologies improved the decision making, identifying those patients bearing the BRAF V600 mutation. In these cases, treatment with BRAF and MEK inhibitors achieved high response rates (Ascierto *et al.*, 2012; Caunt *et al.*, 2015). More recently, immune checkpoint inhibitors entered the clinics improving overall survival at the expense of severe adverse effects (Livingstone *et al.*, 2020). Unfortunately, the benefits of targeted- and immune-therapies can be transient with the cancer acquiring resistance (Gide *et al.*, 2018; Kakadia *et al.*, 2018), therefore identifying novel therapeutic options is still a priority. In chapter 2.1 it was shown that targeting the apoptosis pathway with the TRAIL receptor agonist IZI1551 in combination with the Smac mimetic birinapant in a panel of melanoma cell lines represents a promising treatment strategy to induce cell death. Nevertheless, the responses were highly heterogenous with 12 out of 16 probed cell lines exhibiting synergistic responses. Therefore, a predictive pipeline was developed to identify case-specifically responders and non-responders based on the expression of 19 apoptosis proteins, representing the key regulators of the intrinsic and the extrinsic pathway. The framework consisted of a dimensionality reduction step performed through PCA, followed by LDA to separate the two classes. Even though in other settings these two algorithms may be considered redundant, PCA prior to LDA circumvents the problem of small datasets with features outnumbering samples. Applying PCA to the initial dataset reduces the number of variables while retaining the majority of the variance of the initial dataset (Yang and Yang, 2003). Similar PCA plus LDA pipelines were implemented to classify breast cancer vs. normal samples from the expression of 34 differentially expressed proteins (Liang *et al.*, 2010) or hepatocellular carcinoma vs. healthy donors from intense label-free surface-enhanced Raman scattering spectra of serum samples (Gurian *et al.*, 2021). To test the generalization capability of the pipeline, the LDA classifier trained with the expression patterns of the cell lines grown in 2D was challenged to discriminate responders and resistant samples. To do this, the protein expression of five cell lines grown in 3D and of cells derived from five melanoma metastases was measured and fed into the model in a transfer learning fashion, obtaining 100% and 80% classification accuracy respectively. These results confirmed that the patterns identified in cell lines were sufficiently robust to be

transferred to independent test samples and held true in higher scale settings. In addition, this demonstrated that the selected cell line panel was diverse enough to capture the heterogeneity of real-world patient profiles (Bhinder *et al.*, 2021). Comparable prediction performance was obtained after ranked feature selection, reducing the number of markers to 11 with XIAP scoring first. A pivotal role of XIAP in the response to a similar combination treatment was reported in breast cancer cell lines that developed TRAIL resistance. In this case, birinapant restored sensitivity due to its activity towards XIAP (Morrish *et al.*, 2020). The reduced marker panel was additionally used to estimate the response rates of metastatic melanoma patients from their mRNA expression profiles retrieved from the TCGA repository. Thirty percent of patients were predicted as putative responders, a result in line with the ABBV-261 (also known as eftozanermin alfa) phase I clinical trial response rates. Similarly to IZI1551, ABBV-261 contains six TRAIL-R binding sites per molecule to maximize receptor clustering. In a first-in-human phase 1 study (NCT03082209), ABBV-261 was administered as a monotherapy to colorectal and pancreatic cancer patients showing acceptable safety and anticancer activity. In the dose optimization cohort, stable disease was recorded in 42% and partial response in 6% of patients respectively (LoRusso et al., 2022). The recorded response rates confirm the potential of hexavalent TRAIL receptor agonist-based interventions and highlight the need for tools allowing the selection of those patients more likely to respond to the treatment. In conclusion, the first study described the successful implementation of a binary classifier to identify responders to IZI1551 and birinapant combination treatment. This tool could serve as a prototype for the development of apoptosis-based frameworks to identify potential responders.

A similar data-driven modelling approach was described in chapter 2.2 to classify long- vs short-term melanoma survivors from the expression of nine regulators of the intrinsic apoptosis pathway. Combining digital image analysis, survival analysis and pattern recognition, a putative prognostic signature for metastatic melanoma based on the expression of Bax, Bak and Smac was identified. Prognosis assessment of melanoma patients relied on morphological features and follow-up of the primary tumor for a long time (Gershenwald *et al.*, 2017). These parameters are often insufficient to identify potential high-risk individuals, with two out of three patients dying from melanoma even though being initially diagnosed with stage I or II disease (Morton *et al.*, 2014). Therefore, signatures indicative of increased risk of recurrence or relapse can improve patient handling, especially for those individuals who do not qualify for or developed

resistance to novel targeted or immune therapies. In these cases, chemotherapeutic agents like DTIC are still in use, even if improvements in terms of disease progression and survival were observed only in a limited subset of patients (Guida *et al.*, 2018). In order to identify a prognostic signature informative for advanced stage patients treated with chemotherapy, the expression of nine apoptosis proteins was quantified from biopsies of 58 patients assembled in TMAs. Following extensive antibody validation, an automated imaging pipeline was fine tuned to quantify protein abundances from the immunohistochemically stained tissue sections. The H-Scores generated by the digital pipeline correlated well with pathologists' visual evaluation and provided higher granularity across the entire dynamic range. In the clinical practice, quantitative scoring of IHC samples is not routinely performed. Typically, a trained expert performs a qualitative evaluation of the tissue cores often with diagnostic rather than quantitative purpose. Visual quantitative scoring is time consuming, therefore is rarely performed on large scale studies, it is influenced by the experience level of the observer and has limited dynamic range. Digital image analysis overcomes these limitations, producing fast, objective and highly reproducible quantifications (Ram *et al.*, 2021). Based on the H-Scores, survival analyses revealed that high expression of the proapoptotic proteins Bax, Bak and Smac significantly correlated with reduced PFS. These trends were further validated at transcript level in the independent TCGA-SKCM cohort. These results may seem counter-intuitive, given the assumption that apoptosis represents an obstacle to cancer development and high expression of pro-apoptotic proteins should facilitate cancer cells elimination. This may not always be the case, since an increasing body of literature showed that apoptosis may drive oncogenesis in certain conditions and that elevated expression of anti-apoptotic or reduced expression of pro-apoptotic proteins correlates with favorable prognosis (Castillo Ferrer *et al.*, 2021). For example, high expression levels of Bcl-2 correlated with good prognosis in colorectal and breast cancer (Huang *et al.*, 2017; Vargas-Roig *et al.*, 2008), while high expression of Bax correlated with poor outcome in acute myeloid leukemia (Kulsoom *et al.*, 2018). In addition, overexpression of Caspase-3 was reported in various cancers and was associated with shortened overall survival in several disease settings (Hu *et al.*, 2014), suggesting noncanonical oncogenic roles (Boudreau *et al.*, 2019). Given the results of the survival analysis, it can be speculated that chemotherapy treatment could exert a more potent effect on those tumors driven by lower apoptosis susceptibility, while being insufficient to induce cell death in tumors driven by other alterations that reduce

treatment efficacy through other mechanisms. Finally, the PCA plus LDA framework was adapted to take as input the H-Scores generated by the digital imaging pipeline. The expression of the nine markers was sufficient to correctly classify 74% of the patients into long- and short-term survivors (PFS > 12 months and PFS < 12 months, respectively). The classification performance was further improved when reducing the input to Bax, Bak and Smac expression, without performing dimensionality reduction prior to LDA, achieving an AUC = 0.79. Taken together, these results point towards the integration of classification methods as an additional module for IHC digital image analysis pipelines. Albeit the number of markers in this study was limited to nine, novel multiplex IHC (mIHC) have the capability of measuring tens of biomarkers at the same time. These technologies require less material compared to classical IHC, that allows the detection of only one marker per slide, thereby retaining additional information such as colocalization and relative spatial distribution of different markers. Multiplex IHC relies on full image digitalization and can be coupled with DL techniques aimed at discovering hidden combinations of features impossible to be captured by the human eye, that can be correlated with clinical outcomes (Van Herck *et al.*, 2021). The reliability of primary antibodies against specific antigens plays a crucial role in mIHC and the protocols have to be finely optimized to preserve the epitopes between staining cycles. High-throughput proteomic technologies such as mass spectrometry (MS) can circumvent these limitations. MS was successfully applied to FFPE tissue sections, yielding results comparable to fresh or frozen specimens (Fowler *et al.*, 2011). As a result, millions of long-term stored FFPE cancer samples associated with long-term follow-up information could be potentially analyzed with in-depth proteomic methods (Coscia *et al.*, 2020). In order to retain the spatial information, laser capture miscrodissection of FFPE tissues can be coupled with MS and applied to sample voxels as small as 10 μm × 50 μm × 50 μm (equivalent to the protein content of 10 cells with a radius of ∼8 μm), allowing high-resolution, in-depth proteome tissue mapping (Nwosu *et al.*, 2022).

In summary, the two data-driven models presented here were successfully applied to apoptosis expression profiles to identify predictive and prognostic signatures. These proof-of-concept tools can potentially be extended to higher-dimensional data or embedded in quantification pipelines to assist case-specific clinical decision making.

3.3 Transcriptomic data-to-image conversion coupled with DL-based classification improves breast cancer prognostication

In the third study, the object of the analysis was not limited to a specific pathway, but upscaled to high-dimensional, full transcriptome datasets. A DL-based architecture was developed to identify low- and high-risk breast cancer patients according to their mRNA expression profiles. These were converted into arrays of pixels and used as input to train the discriminator of an AC-WGAN-GP architecture. The trained discriminator (T-GAN-D) was subsequently used as a standalone prognostic classifier, showing improved stratification when compared to routinely used clinical biomarkers.

Breast cancer was identified as an ideal use case given the availability of public datasets, namely the METABRIC and the TCGA-BRCA. These are among the largest and best curated cancer cohorts and have been extensively used to test classic ML applications (Liñares-Blanco *et al.*, 2021). However, when dealing with such low sample size - high dimension datasets, classic ML algorithms are prone to severe overfitting and may require additional steps such as feature selection or dimensionality reduction to decrease the number of input variables (Liu, Wei, *et al.*, 2017). While feature selection may be useful in some settings (e.g. biomarker discovery) significant hidden multi-variable patterns may be lost when discarding variables. Similarly, combining variables through dimensionality reduction leads to some degree of loss of information (Jia *et al.*, 2022). Deep neural networks can overcome this limitation since the extraction of discriminative features is embedded in the architecture itself. Thus, DL algorithms can outperform ML techniques when analyzing large-scale and noisy datasets (Janiesch *et al.*, 2021). In addition, risk predictors based on the expression of a limited number of transcripts can circumvent these problems and have already entered the clinics. GES are generally used to inform patient managing decisions when anatomo-pathological criteria alone are not conclusive. In particular, patients predicted at high-risk of recurrence or progression may receive neoadjuvant or adjuvant chemotherapy, while low-risk patients are spared from the adverse effects of potentially unnecessary chemotherapy (Foulon et al., 2020). Commercialized GES are approved for use in sub-cohorts of patients with specific characteristics (e.g. tumor subtype, stage at diagnosis, age, menopausal state), therefore more generalized prognostic tools are still needed. In order to benchmark the stratification potential of T-GAN-D, the low- and high-risk classes were defined using the same criteria of published ROR-P categories, a research-based implementation of the Prosigna GES (Xia *et al.*, 2019).

According to this classification system, patients are categorized as high-risk if they experience recurrence, progression, metastases or cancer-related death within ten years from initial diagnosis. Applied to the METABRIC cohort, T-GAN-D outperformed well established clinical biomarkers (ER, PR and HER2 expression) and ROR-P. The performance of the classifier was further improved by adding to the training dataset patients from the independent TCGA-BRCA cohort. Despite different sequencing technologies used to generate the data and the different composition of the TCGA cohort, skewed towards advanced stage cancers, the T-GAN-D was able to extract and generalize features that improved patient stratification. High accuracy in indicating high-risk patients was also obtained when predicting the class of the smaller and imbalanced TCGA-BRCA dataset, combining the METABRIC cohort for training. These results were achieved without any batch-effect correction or normalization procedure, usually required by classic ML methods (Wang *et al.*, 2018). This indicated that, in this case study, the conversion of mRNA expression profiles into images was sufficient for the T-GAN-D to achieve satisfactory generalization. The potential of the prototype tool can still be explored in future validation studies with transfer learning approaches. To this end, the standalone trained classifier could be used to predict the risk class of unseen samples retrieved from smaller public datasets or implemented in prospective studies with *de novo* generated data. Moreover, it would be interesting to test the influence of the arrangement of pixels into the converted images. Transcriptomic data are unstructured, meaning that spatial relationships between the variables do not exist. Classical ML algorithms are generally used in this case, since the features are considered to be independent, and their order of appearance in the input feature vector is not relevant. Algorithms like GANs and CNNs do consider the order of neighboring pixels to extract patterns, therefore the element arrangement has an impact on determining a class. While CNNs were already applied to gene expression data (Mostavi *et al.*, 2020), very few studies explored the possibility of organizing the pixels in a biological meaningful way. Two studies aimed at discriminating tumor from normal samples of the TCGA PanCancer dataset using CNN architectures. Transcripts were organized according to their location on the chromosomes (Lyu and Haque, 2018) or to their similarity computed with t-distributed stochastic neighbor embedding (t-SNE) and kernel PCA (kPCA) (Sharma *et al.*, 2019) . Finally, multiple layers representing multi -omics data may be embedded in a single image. A concept idea could be considering the transcriptomic data as an image in grayscale, but additional channels and -omics

domains may be added, for example red for genomics, green for proteomics and blue for metabolomics. This visionary example is clearly limited by the availability of matching data, number of samples and, last but not least, computing power.

3.4 From the desk to the bedside: AI's challenges and perspectives

The application of AI to a plethora of oncology related tasks has proven immense potential in research studies. Therefore, the question is not anymore *if*, but *when* AI will be fully integrated into clinical practice (Bhinder *et al.*, 2021). To reach this goal, several obstacles still need to be overcome, both technical, and, equally relevant, ideological. One of the main concerns regarding AI models is their interpretability. While basic ML models (e.g. linear regression), are fully explainable, advanced DL algorithms rely on several hidden layers of data interactions. This lack of transparency makes it almost impossible to identify those features contributing to an output definition (e.g. the risk class of a patient) (Shao *et al.*, 2022). Novel model implementations have been employed aiming to alleviate the "black box" effect, such as interpretable DL frameworks (Fortelny and Bock, 2020) or explanation techniques (Ribeiro *et al.*, 2016). Improved interpretability contributes to increase the perceived level of trust of the user towards an algorithm, especially when a clinical decision needs to be informed by the model (Antoniadi *et al.*, 2021). A second major limitation of AI algorithms is robustness. An algorithm's training procedure relies inevitably on available training data and may underperform when applied to test cohorts of individuals representing different ethnicities, genders or even socioeconomic backgrounds (Obermeyer *et al.*, 2019). For example, publicly available datasets commonly used for testing and validating AI models in cancer, such as the TCGA datasets, are biased towards patients with European ancestry, who possess race-specific genomic aberrations and may not be suited to draw general conclusions (Yuan *et al.*, 2018). The healthcare environment represents another layer of intrinsic bias, since prevention initiatives, access to novel therapeutics and more frequent follow-ups heavily influence patient outcomes (Shreve *et al.*, 2022). While methods to identify sources of bias are currently being developed (Vokinger *et al.*, 2021), the construction of inclusive, diverse, interoperable datasets represents theoretically the ideal solution. To this end, anonymization and pseudonymization systems compatible with automated multi-institution integration have been proposed to comply with the European General Data Protection Regulation (Forti, 2021) and the United States' Health Insurance Portability and Accountability Act

(Stadler, 2021). The use of these data protection techniques though, may increase the complexity of the models and impact their explainability (Kourou *et al.*, 2021). While data protection laws are currently well defined, a specific legislation to regulate AI, ML and big data is still lacking. In particular, specific rules that regulate legal responsibilities and accountability for potentially harmful, AI-informed decisions need to be established in order to protect patient rights (Shreve *et al.*, 2022). Another critical aspect that needs updated regulations is model monitoring and maintenance. Currently, the FDA does not allow any modification of an algorithm after approval, "locking" the models. On the one side, "locked" models are safer because no potentially deleterious features can be added. On the other hand, these models cannot be updated to integrate novel rules (e.g. the introduction of new treatment options or clinical practice patterns) potentially leading to a decay of performance over time. Therefore, in order to take full advantage of AI algorithms in the clinic, these should be object of quality assurance (QA) and quality improvement (QI) efforts comparable to existing hospital QI initiatives (Feng *et al.*, 2022). In addition to technical and ethical reasons, AI is also treated with skepticism due to concerns about the healthcare workforce displacement. To date, considering also the limited implementation of AI in the clinical practice, no jobs were reported to be eliminated due to AI. It is extremely unlikely that any task involving direct patient contact and especially empathy can be automated and replaced by a machine, while jobs involving analysis of digital information, such as radiology or pathology, may be automated to a certain extent in the future. First, these professionals do not just "read" images, but interact with other physicians and synergize to provide the optimal care. In addition, the models need labelled data provided by humans and need constant training and update, especially when new imaging technologies enter the market. Taking all of this into account, in the near future AI will be a tool to assist decision making, but will not be a replacement for a human expert. On the contrary, it is possible that new professional profiles oriented at working with AI may be created (Davenport and Kalakota, 2019).

In conclusion, even though concepts like "digital twins" (Björnsson *et al.*, 2019) and the full integration of AI tools in the clinics are still at their dawn, the pivotal role of data-driven oncology is universally recognized. The technology improves constantly and has proven its potential in several use-cases and environments and will slowly but steadily be implemented into the clinical practice. With all due respect to the skeptics, let the machines learn.

4 REFERENCES

Abu-Mostafa, Y.S. (1989), "The Vapnik-Chervonenkis Dimension: Information versus Complexity in Learning", *Neural Computation*, MIT Press - Journals, Vol. 1 No. 3, pp. 312–317, doi: 10.1162/NECO.1989.1.3.312.

Akbani, R., Akdemir, K.C., Aksoy, B.A., Albert, M., Ally, A., Amin, S.B., Arachchi, H., *et al.* (2015), "Genomic Classification of Cutaneous Melanoma", *Cell*, Vol. 161 No. 7, pp. 1681–1696, doi: 10.1016/j.cell.2015.05.044.

Aldausari, N., Sowmya, A., Marcus, N. and Mohammadi, G. (2022), "Video Generative Adversarial Networks: A Review", *ACM Computing Surveys (CSUR)*, Vol. 55 No. 2, doi: 10.1145/3487891.

Aldridge, B.B., Gaudet, S., Lauffenburger, D.A. and Sorger, P.K. (2011), "Lyapunov exponents and phase diagrams reveal multi-factorial control over TRAIL-induced apoptosis", *Molecular Systems Biology*, Vol. 7, p. 553, doi: 10.1038/msb.2011.85.

Allensworth, J.L., Sauer, S.J., Lyerly, H.K., Morse, M.A. and Devi, G.R. (2013), "Smac mimetic Birinapant induces apoptosis and enhances TRAIL potency in inflammatory breast cancer cells in an IAP-dependent and TNF-α-independent mechanism", *Breast Cancer Research and Treatment*, Vol. 137 No. 2, pp. 359–371, doi: 10.1007/s10549-012-2352-6.

Amaravadi, R.K., Schilder, R.J., Martin, L.P., Levin, M., Graham, M.A., Weng, D.E. and Adjei, A.A. (2015), "A Phase I study of the SMAC-mimetic birinapant in adults with refractory solid tumorsor lymphoma", *Molecular Cancer Therapeutics*, American Association for Cancer Research Inc., Vol. 14 No. 11, pp. 2569–2575, doi: 10.1158/1535-7163.MCT-15-0475/175510/AM/A-PHASE-1-STUDY-OF-THE-SMAC-MIMETIC-BIRINAPANT-IN.

Antoniadi, A.M., Du, Y., Guendouz, Y., Wei, L., Mazo, C., Becker, B.A. and Mooney, C. (2021), "Current Challenges and Future Opportunities for XAI in Machine Learning-Based Clinical Decision Support Systems: A Systematic Review",

Applied Sciences, Vol. 11 No. 11, p. 5088, doi: 10.3390/APP11115088.

Anvekar, R.A., Asciolla, J.J., Lopez-Rivera, E., Floros, K. V., Izadmehr, S., Elkholi, R., Belbin, G., *et al.* (2012), "Sensitization to the mitochondrial pathway of apoptosis augments melanoma tumor cell responses to conventional chemotherapeutic regimens", *Cell Death and Disease*, Nature Publishing Group, Vol. 3 No. 11, pp. 1–11, doi: 10.1038/cddis.2012.161.

Anvekar, R.A., Asciolla, J.J., Missert, D.J. and Chipuk, J.E. (2011), "Born to be Alive: A Role for the BCL-2 Family in Melanoma Tumor Cell Survival, Apoptosis, and Treatment", *Frontiers in Oncology*, Vol. 1 No. October, pp. 1–16, doi: 10.3389/fonc.2011.00034.

Arellano-Llamas, A., Garcia, F.J., Perez, D., Cantu, D., Espinosa, M., De la Garza, J.G., Maldonado, V., *et al.* (2006), "High Smac/DIABLO expression is associated with early local recurrence of cervical cancer", *BMC Cancer*, Vol. 6 No. 1, p. 256, doi: 10.1186/1471-2407-6-256.

Arjovsky, M., Chintala, S. and Bottou, L. (2017), "Wasserstein GAN", 26 January, available at: https://arxiv.org/abs/1701.07875v3 (accessed 1 March 2022).

Arya, N. and Saha, S. (2022), "Generative Incomplete Multi-View Prognosis Predictor for Breast Cancer: GIMPP", *IEEE/ACM Transactions on Computational Biology and Bioinformatics*, Institute of Electrical and Electronics Engineers (IEEE), Vol. 19 No. 4, pp. 2252–2263, doi: 10.1109/TCBB.2021.3090458.

Ascierto, P.A., Kirkwood, J.M., Grob, J.-J., Simeone, E., Grimaldi, A.M., Maio, M., Palmieri, G., *et al.* (2012), "The role of BRAF V600 mutation in melanoma.", *Journal of Translational Medicine*, Vol. 10, p. 85, doi: 10.1186/1479-5876-10-85.

Ashkenazi, A. (2015), "Targeting the extrinsic apoptotic pathway in cancer : lessons learned and future directions", *J Clin Invest.*, Vol. 125 No. 2, pp. 487–489, doi: 10.1172/JCI80420.normal.

Atkins, M.B., Hsu, J., Lee, S., Cohen, G.I., Flaherty, L.E., Sosman, J.A., Sondak, V.K., *et al.* (2008), "Phase III Trial Comparing Concurrent Biochemotherapy With Cisplatin, Vinblastine, Dacarbazine, Interleukin-2, and Interferon Alfa-2b With Cisplatin, Vinblastine, and Dacarbazine Alone in Patients With Metastatic Malignant Melanoma (E3695): A Trial Coordinated by the Eastern Cooperative Oncology Group", *Journal of Clinical Oncology*, Vol. 26 No. 35, pp. 5748–5754,

doi: 10.1200/JCO.2008.17.5448.

Awada, H., Durmaz, A., Gurnari, C., Kishtagari, A., Meggendorfer, M., Kerr, C.M., Kuzmanovic, T., *et al.* (2021), "Machine learning integrates genomic signatures for subclassification beyond primary and secondary acute myeloid leukemia", *Blood*, Vol. 138 No. 19, pp. 1885–1895, doi: 10.1182/BLOOD.2020010603.

Baekelandt, M., Holm, R., Nesland, J.M., Tropé, C.G. and Kristensen, G.B. (2000), "Expression of apoptosis-related proteins is an independent determinant of patient prognosis in advanced ovarian cancer", *Journal of Clinical Oncology*, Vol. 18 No. 22, pp. 3775–3781, doi: 10.1200/JCO.2000.18.22.3775.

Bairey, O., Zimra, Y., Shaklai, M., Okon, E. and Rabizadeh, E. (1999), "Bcl-2, Bcl-X, Bax, and Bak expression in short- and long-lived patients with diffuse large B-cell lymphomas.", *Clinical Cancer Research : An Official Journal of the American Association for Cancer Research*, Vol. 5 No. 10, pp. 2860–6.

Bansal, M.A., Sharma, D.R. and Kathuria, D.M. (2022), "A Systematic Review on Data Scarcity Problem in Deep Learning: Solution and Applications", *ACM Computing Surveys (CSUR)*, Vol. 54 No. 10s, pp. 1–29, doi: 10.1145/3502287.

Barandela, R., Valdovinos, R.M., Salvador Sánchez, J. and Ferri, F.J. (2004), "The imbalanced training sample problem: under or over sampling?", *Lecture Notes in Computer Science (Including Subseries Lecture Notes in Artificial Intelligence and Lecture Notes in Bioinformatics)*, Springer Verlag, Vol. 3138, pp. 806–814, doi: 10.1007/978-3-540-27868-9_88/COVER.

Batistatou, A., Zioga, A., Panelos, J., Massi, D., Agnantis, N.J. and Charalabopoulos, K. (2007), "A new concept of melanocytic neoplasia pathogenesis based on the phenotype of common acquired nevi", *Medical Hypotheses*, Vol. 69 No. 6, pp. 1334–1339, doi: 10.1016/J.MEHY.2007.03.004.

Bedikian, A.Y., Millward, M., Pehamberger, H., Conry, R., Gore, M., Trefzer, U., Pavlick, A.C., *et al.* (2006), "Bcl-2 Antisense (oblimersen sodium) Plus Dacarbazine in Patients With Advanced Melanoma: The Oblimersen Melanoma Study Group", *Journal of Clinical Oncology*, Vol. 24 No. 29, pp. 4738–4745, doi: 10.1200/JCO.2006.06.0483.

Benetatos, C.A., Mitsuuchi, Y., Burns, J.M., Neiman, E.M., Condon, S.M., Yu, G., Seipel, M.E., *et al.* (2014), "Birinapant (TL32711), a bivalent SMAC mimetic,

targets TRAF2-associated cIAPs, abrogates TNF-induced NF-κB activation, and is active in patient-derived xenograft models", *Molecular Cancer Therapeutics*, Vol. 13 No. 4, pp. 867–879, doi: 10.1158/1535-7163.MCT-13-0798.

Benjamens, S., Dhunnoo, P. and Meskó, B. (2020), "The state of artificial intelligence-based FDA-approved medical devices and algorithms: an online database", *Npj Digital Medicine 2020 3:1*, Nature Publishing Group, Vol. 3 No. 1, pp. 1–8, doi: 10.1038/s41746-020-00324-0.

Bernard, P.S., Parker, J.S., Mullins, M., Cheung, M.C.U., Leung, S., Voduc, D., Vickery, T., *et al.* (2009), "Supervised risk predictor of breast cancer based on intrinsic subtypes", *Journal of Clinical Oncology*, American Society of Clinical Oncology, Vol. 27 No. 8, pp. 1160–1167, doi: 10.1200/JCO.2008.18.1370.

Bertsimas, D. and Wiberg, H. (2020), "Machine Learning in Oncology: Methods, Applications, and Challenges", *JCO Clinical Cancer Informatics*, American Society of Clinical Oncology (ASCO), No. 4, pp. 885–894, doi: 10.1200/cci.20.00072.

Bhinder, B., Gilvary, C., Madhukar, N.S. and Elemento, O. (2021), "Artificial Intelligence in Cancer Research and Precision Medicine", *Cancer Discovery*, American Association for Cancer Research, Vol. 11 No. 4, pp. 900–915, doi: 10.1158/2159-8290.CD-21-0090.

Bishop, C.M. (2006), "Pattern Recogniton and Machine Learning", *Information Science and Statistics*, Springer-Verlag New York, p. 738.

Björnsson, B., Borrebaeck, C., Elander, N., Gasslander, T., Gawel, D.R., Gustafsson, M., Jörnsten, R., *et al.* (2019), "Digital twins to personalize medicine", *Genome Medicine*, Vol. 12 No. 1, pp. 1–4, doi: 10.1186/S13073-019-0701-3/FIGURES/1.

Boeri, C., Chiappa, C., Galli, F., De Berardinis, V., Bardelli, L., Carcano, G. and Rovera, F. (2020), "Machine Learning techniques in breast cancer prognosis prediction: A primary evaluation", *Cancer Medicine*, Wiley-Blackwell, Vol. 9 No. 9, p. 3234, doi: 10.1002/CAM4.2811.

Bollard, S.M., Casalou, C. and Potter, S.M. (2021), "Gene expression profiling in melanoma: A view from the clinic", *Cancer Treatment and Research Communications*, Elsevier, Vol. 29, p. 100447, doi: 10.1016/J.CTARC.2021.100447.

Bombonati, A. and Sgroi, D.C. (2011), “The molecular pathology of breast cancer progression”, *The Journal of Pathology*, Vol. 223 No. 2, pp. 308–318, doi: 10.1002/PATH.2808.

Boudreau, M.W., Peh, J. and Hergenrother, P.J. (2019), “Procaspase-3 Overexpression in Cancer: A Paradoxical Observation with Therapeutic Potential”, *ACS Chemical Biology*, American Chemical Society, Vol. 14 No. 11, pp. 2335–2348, doi: 10.1021/ACSCHEMBIO.9B00338/ASSET/IMAGES/MEDIUM/CB-2019-003389_0008.GIF.

Bowles, C., Chen, L., Guerrero, R., Bentley, P., Gunn, R., Hammers, A., Dickie, D.A., *et al.* (2018), “GAN Augmentation: Augmenting Training Data using Generative Adversarial Networks”, doi: 10.48550/arxiv.1810.10863.

Bray, F., Ferlay, J., Soerjomataram, I., Siegel, R.L., Torre, L.A. and Jemal, A. (2018), “Global cancer statistics 2018: GLOBOCAN estimates of incidence and mortality worldwide for 36 cancers in 185 countries”, *CA: A Cancer Journal for Clinicians*, Vol. 68 No. 6, pp. 394–424, doi: 10.3322/CAAC.21492.

Broad Institute TCGA Genome Data Analysis Center. (2016), “Analysis-ready standardized TCGA data from Broad GDAC Firehose 2016_01_28 run”, *Broad Institute of MIT and Harvard*, doi: https://doi.org/10.7908/C11G0KM9.

Broussard, L., Howland, A., Ryu, S., Song, K., Norris, D., Armstrong, C.A. and Song, P.I. (2018), “Melanoma Cell Death Mechanisms”, *Chonnam Medical Journal*, Chonnam National University Medical School, Vol. 54 No. 3, p. 135, doi: 10.4068/CMJ.2018.54.3.135.

Brouwer, J.M., Westphal, D., Dewson, G., Robin, A.Y., Uren, R.T., Bartolo, R., Thompson, G. V., *et al.* (2014), “Bak Core and Latch Domains Separate during Activation, and Freed Core Domains Form Symmetric Homodimers”, *Molecular Cell*, Cell Press, Vol. 55 No. 6, pp. 938–946, doi: 10.1016/J.MOLCEL.2014.07.016.

Buus, R., Sestak, I., Barron, S., Loughman, T., Fender, B., Ruiz, C.L., Dynoodt, P., *et al.* (2020), “Validation of the OncoMASTR risk score in estrogen receptor–positive/HER2-negative patients: A TransATAC study”, *Clinical Cancer Research*, American Association for Cancer Research Inc., Vol. 26 No. 3, pp. 623–631, doi: 10.1158/1078-0432.CCR-19-0712/75352/AM/VALIDATION-OF-THE-

ONCOMASTR-RISK-SCORE-IN-ESTROGEN.

Caberlotto, L. and Lauria, M. (2015), “Systems biology meets -omic technologies: Novel approaches to biomarker discovery and companion diagnostic development”, *Expert Review of Molecular Diagnostics*, Vol. 15 No. 2, pp. 255–265, doi: 10.1586/14737159.2015.975214.

Cardoso, F., van’t Veer, L.J., Bogaerts, J., Slaets, L., Viale, G., Delaloge, S., Pierga, J.-Y., *et al.* (2016), “70-Gene Signature as an Aid to Treatment Decisions in Early-Stage Breast Cancer”, *New England Journal of Medicine*, Vol. 375 No. 8, pp. 717–729, doi: 10.1056/NEJMOA1602253/SUPPL_FILE/NEJMOA1602253_DISCLOSURES.PDF.

Carneiro, B.A. and El-Deiry, W.S. (2020), “Targeting apoptosis in cancer therapy”, *Nature Reviews. Clinical Oncology*, NIH Public Access, Vol. 17 No. 7, p. 395, doi: 10.1038/S41571-020-0341-Y.

Carnielli, C.M., Macedo, C.C.S., De Rossi, T., Granato, D.C., Rivera, C., Domingues, R.R., Pauletti, B.A., *et al.* (2018), “Combining discovery and targeted proteomics reveals a prognostic signature in oral cancer”, *Nature Communications*, Nature Publishing Group, Vol. 9 No. 1, p. 3598, doi: 10.1038/s41467-018-05696-2.

Castillo Ferrer, C., Berthenet, K. and Ichim, G. (2021), “Apoptosis – Fueling the oncogenic fire”, *The FEBS Journal*, John Wiley & Sons, Ltd, Vol. 288 No. 15, pp. 4445–4463, doi: 10.1111/FEBS.15624.

Caunt, C.J., Sale, M.J., Smith, P.D. and Cook, S.J. (2015), “MEK1 and MEK2 inhibitors and cancer therapy: the long and winding road”, *Nature Reviews Cancer*, Nature Publishing Group, Vol. 15 No. 10, pp. 577–592, doi: 10.1038/nrc4000.

Cerami, E., Gao, J., Dogrusoz, U., Gross, B.E., Sumer, S.O., Aksoy, B.A., Jacobsen, A., *et al.* (2012), “The cBio cancer genomics portal: an open platform for exploring multidimensional cancer genomics data.”, *Cancer Discovery*, American Association for Cancer Research, Vol. 2 No. 5, pp. 401–4, doi: 10.1158/2159-8290.CD-12-0095.

Charles, E.M. and Rehm, M. (2014), “Key regulators of apoptosis execution as biomarker candidates in melanoma.”, *Molecular & Cellular Oncology*, Vol. 1 No. 3, p. e964037, doi: 10.4161/23723548.2014.964037.

Chawla, N. V., Bowyer, K.W., Hall, L.O. and Kegelmeyer, W.P. (2011), "SMOTE: Synthetic Minority Over-sampling Technique", *Journal Of Artificial Intelligence Research*, American Association for Artificial Intelligence, Vol. 16, pp. 321–357, doi: 10.1613/jair.953.

Choi, E., Biswal, S., Malin, B., Duke, J., Stewart, W.F. and Sun, J. (2017), "Generating Multi-label Discrete Patient Records using Generative Adversarial Networks", *Machine Learning in Health Care*, doi: 10.48550/arxiv.1703.06490.

Clarke, P.G.H. and Clarke, S. (1996), "Nineteenth century research on naturally occurring cell death and related phenomena", *Anatomy and Embryology*, Vol. 193 No. 2, pp. 81–99, doi: 10.1007/BF00214700.

Condon, S.M., Mitsuuchi, Y., Deng, Y., Laporte, M.G., Rippin, S.R., Haimowitz, T., Alexander, M.D., *et al.* (2014), "Birinapant, a smac-mimetic with improved tolerability for the treatment of solid tumors and hematological malignancies", *Journal of Medicinal Chemistry*, American Chemical Society, Vol. 57 No. 9, pp. 3666–3677, doi: 10.1021/JM500176W/SUPPL_FILE/JM500176W_SI_001.PDF.

Coscia, F., Doll, S., Bech, J.M., Schweizer, L., Mund, A., Lengyel, E., Lindebjerg, J., *et al.* (2020), "A streamlined mass spectrometry–based proteomics workflow for large-scale FFPE tissue analysis", *The Journal of Pathology*, John Wiley & Sons, Ltd, Vol. 251 No. 1, pp. 100–112, doi: 10.1002/PATH.5420.

Craven, K.E., Gökmen-Polar, Y. and Badve, S.S. (2021), "CIBERSORT analysis of TCGA and METABRIC identifies subgroups with better outcomes in triple negative breast cancer", *Scientific Reports 2021 11:1*, Nature Publishing Group, Vol. 11 No. 1, pp. 1–19, doi: 10.1038/s41598-021-83913-7.

Crawford, N., Salvucci, M., Hellwig, C.T., Lincoln, F.A., Mooney, R.E., O'Connor, C.L., Prehn, J.H., *et al.* (2018), "Simulating and predicting cellular and in vivo responses of colon cancer to combined treatment with chemotherapy and IAP antagonist Birinapant/TL32711", *Cell Death & Differentiation*, doi: 10.1038/s41418-018-0082-y.

Cummins, J.M., Kohli, M., Rago, C., Kinzler, K.W., Vogelstein, B. and Bunz, F. (2004), "X-linked inhibitor of apoptosis protein (XIAP) is a nonredundant modulator of tumor necrosis factor-related apoptosis-inducing ligand (TRAIL)-mediated apoptosis in human cancer cells.", *Cancer Research*, Vol. 64 No. 9, pp.

3006–8.

Czabotar, P.E., Lessene, G., Strasser, A. and Adams, J.M. (2014), "Control of apoptosis by the BCL-2 protein family: implications for physiology and therapy", *Nature Reviews Molecular Cell Biology*, Vol. 15 No. 1, pp. 49–63, doi: 10.1038/nrm3722.

Darding, M., Feltham, R., Tenev, T., Bianchi, K., Benetatos, C., Silke, J. and Meier, P. (2011), "Molecular determinants of Smac mimetic induced degradation of cIAP1 and cIAP2", *Cell Death and Differentiation*, Vol. 18 No. 8, pp. 1376–1386, doi: 10.1038/cdd.2011.10.

Davenport, T. and Kalakota, R. (2019), "The potential for artificial intelligence in healthcare", *Future Healthcare Journal*, Royal College of Physicians, Vol. 6 No. 2, p. 94, doi: 10.7861/FUTUREHOSP.6-2-94.

Davids, M.S., Von Keudell, G., Portell, C.A., Cohen, J.B., Fisher, D.C., Foss, F., Roberts, A.W., *et al.* (2018), "Revised Dose Ramp-Up to Mitigate the Risk of Tumor Lysis Syndrome When Initiating Venetoclax in Patients With Mantle Cell Lymphoma", *Journal of Clinical Oncology : Official Journal of the American Society of Clinical Oncology*, J Clin Oncol, Vol. 36 No. 35, pp. 3525–3527, doi: 10.1200/JCO.18.00359.

Davis, L.E., Shalin, S.C. and Tackett, A.J. (2019), "Current state of melanoma diagnosis and treatment", *Cancer Biology & Therapy*, Taylor & Francis, Vol. 20 No. 11, p. 1366, doi: 10.1080/15384047.2019.1640032.

Denault, J.B., Eckelman, B.P., Shin, H., Pop, C. and Salvesen, G.S. (2007), "Caspase 3 attenuates XIAP (X-linked inhibitor of apoptosis protein)-mediated inhibition of caspase 9", *The Biochemical Journal*, Biochem J, Vol. 405 No. 1, pp. 11–19, doi: 10.1042/BJ20070288.

Desai, S.D., Giraddi, S., Verma, N., Gupta, P. and Ramya, S. (2020), "Breast Cancer Detection Using GAN for Limited Labeled Dataset", *Proceedings - 2020 12th International Conference on Computational Intelligence and Communication Networks, CICN 2020*, Institute of Electrical and Electronics Engineers Inc., pp. 34–39, doi: 10.1109/CICN49253.2020.9242551.

Deveraux, Q.L., Leo, E., Stennicke, H.R., Welsh, K., Salvesen, G.S. and Reed, J.C. (1999), "Cleavage of human inhibitor of apoptosis protein XIAP results in fragments with distinct specificities for caspases", *EMBO Journal*, Vol. 18 No. 19,

pp. 5242–5251, doi: 10.1093/emboj/18.19.5242.

Díaz-Uriarte, R. and Alvarez de Andrés, S. (2006), "Gene selection and classification of microarray data using random forest", *BMC Bioinformatics*, Vol. 7, doi: 10.1186/1471-2105-7-3.

Dickens, L.S., Powley, I.R., Hughes, M.A. and MacFarlane, M. (2012), "The 'complexities' of life and death: Death receptor signalling platforms", *Experimental Cell Research*, Vol. 318 No. 11, pp. 1269–1277, doi: 10.1016/J.YEXCR.2012.04.005.

Dineen, S.P., Roland, C.L., Greer, R., Carbon, J.G., Toombs, J.E., Gupta, P., Bardeesy, N., *et al.* (2010), "Smac mimetic increases chemotherapy response and improves survival in mice with pancreatic cancer", *Cancer Research*, Vol. 70 No. 7, pp. 2852–2861, doi: 10.1158/0008-5472.CAN-09-3892.

Dobrzycka, B., Terlikowski, S.J., Bernaczyk, P.S., Garbowicz, M., Niklinski, J., Chyczewski, L. and Kulikowski, M. (2010), "Prognostic significance of smac/DIABLO in endometrioid endometrial cancer", *Folia Histochemica et Cytobiologica*, Vol. 48 No. 4, pp. 678–681, doi: 10.2478/v10042-010-0091-2.

Domingues, B., Lopes, J., Soares, P. and Populo, H. (2018), "Melanoma treatment in review", *ImmunoTargets and Therapy*, Vol. 7, pp. 35–49, doi: 10.2147/itt.s134842.

Donato, A.L., Huang, Q., Liu, X., Li, F., Zimmerman, M.A. and Li, C.-Y. (2014), "Caspase 3 promotes surviving melanoma tumor cell growth after cytotoxic therapy.", *The Journal of Investigative Dermatology*, Nature Publishing Group, Vol. 134 No. 6, pp. 1686–92, doi: 10.1038/jid.2014.18.

Dubourg-Felonneau, G., Cannings, T., Cotter, F., Thompson, H., Patel, N., Cassidy, J.W. and Clifford, H.W. (2018), "A Framework for Implementing Machine Learning on Omics Data", doi: 10.48550/arxiv.1811.10455.

Eckardt, J.N., Wendt, K., Bornhäuser, M. and Middeke, J.M. (2021), "Reinforcement Learning for Precision Oncology", *Cancers*, Vol. 13 No. 18, doi: 10.3390/CANCERS13184624.

Elemento, O., Leslie, C., Lundin, J. and Tourassi, G. (2021), "Artificial intelligence in cancer research, diagnosis and therapy", *Nature Reviews Cancer*, Nature Publishing Group, Vol. 21 No. 12, pp. 747–752, doi: 10.1038/s41568-021-00399-1.

Elmore, S. (2007), “Apoptosis: A Review of Programmed Cell Death”, *Toxicologic Pathology*, NIH Public Access, Vol. 35 No. 4, p. 495, doi: 10.1080/01926230701320337.

Elston, C.W. and Ellis, I.O. (1991), “Pathological prognostic factors in breast cancer. I. The value of histological grade in breast cancer: experience from a large study with long-term follow-up”, *Histopathology*, Vol. 19 No. 5, pp. 403–410, doi: 10.1111/j.1365-2559.1991.tb00229.x.

Endo, K., Kohnoe, S., Watanabe, A., Tashiro, H., Sakata, H., Morita, M., Kakeji, Y., *et al.* (2009), “Clinical significance of Smac/DIABLO expression in colorectal cancer.”, *Oncology Reports*, Vol. 21 No. 2, pp. 351–5.

Eytan, D.F., Snow, G.E., Carlson, S., Derakhshan, A., Saleh, A., Schiltz, S., Cheng, H., *et al.* (2016), “SMAC mimetic birinapant plus radiation eradicates human head and neck cancers with genomic amplifications of cell death genes FADD and BIRC2”, *Cancer Research*, American Association for Cancer Research Inc., Vol. 76 No. 18, pp. 5442–5454, doi: 10.1158/0008-5472.CAN-15-3317/652366/AM/SMAC-MIMETIC-BIRINAPANT-PLUS-RADIATION-ERADICATES.

Fairlie, W.D. and Lee, E.F. (2021), “Co-Operativity between MYC and BCL-2 Pro-Survival Proteins in Cancer”, *International Journal of Molecular Sciences*, Vol. 22 No. 6, p. 2841, doi: 10.3390/IJMS22062841.

Falschlehner, C., Ganten, T.M., Koschny, R., Schaefer, U. and Walczak, H. (2009), “TRAIL and other TRAIL receptor agonists as novel cancer therapeutics”, *Advances in Experimental Medicine and Biology*, Vol. 647, pp. 195–206, doi: 10.1007/978-0-387-89520-8_14.

Falschlehner, C., Schaefer, U. and Walczak, H. (2009), “Following TRAIL’s path in the immune system”, *Immunology*, Vol. 127 No. 2, pp. 145–154, doi: 10.1111/J.1365-2567.2009.03058.X.

Fang, Y. and Eglen, R.M. (2017), “Three-Dimensional Cell Cultures in Drug Discovery and Development”, *SLAS Discovery*, Vol. 22 No. 5, pp. 456–472, doi: 10.1177/1087057117696795.

Fecker, L.F., Geilen, C.C., Tchernev, G., Trefzer, U., Assaf, C., Kurbanov, B.M., Schwarz, C., *et al.* (2006), “Loss of proapoptotic Bcl-2-related multidomain proteins in primary melanomas is associated with poor prognosis.”, *The Journal of*

Investigative Dermatology, Vol. 126 No. 6, pp. 1366–1371, doi: 10.1038/sj.jid.5700192.

Feng, J., Phillips, R. V., Malenica, I., Bishara, A., Hubbard, A.E., Celi, L.A. and Pirracchio, R. (2022), "Clinical artificial intelligence quality improvement: towards continual monitoring and updating of AI algorithms in healthcare", *Npj Digital Medicine 2022 5:1*, Nature Publishing Group, Vol. 5 No. 1, pp. 1–9, doi: 10.1038/s41746-022-00611-y.

Feoktistova, M., Geserick, P., Kellert, B., Dimitrova, D.P., Langlais, C., Hupe, M., Cain, K., *et al.* (2011), "CIAPs Block Ripoptosome Formation, a RIP1/Caspase-8 Containing Intracellular Cell Death Complex Differentially Regulated by cFLIP Isoforms", *Molecular Cell*, Vol. 43 No. 3, pp. 449–463, doi: 10.1016/j.molcel.2011.06.011.

Fortelny, N. and Bock, C. (2020), "Knowledge-primed neural networks enable biologically interpretable deep learning on single-cell sequencing data", *Genome Biology*, Genome Biol, Vol. 21 No. 1, doi: 10.1186/S13059-020-02100-5.

Forti, M. (2021), "The Deployment of Artificial Intelligence Tools in the Health Sector: Privacy Concerns and Regulatory Answers within the GDPR", *European Journal of Legal Studies*, Vol. 13.

Foulon, A., Theret, P., Rodat-Despoix, L. and Kischel, P. (2020), "Beyond Chemotherapies: Recent Strategies in Breast Cancer Treatment", *Cancers*, Vol. 12 No. 9, pp. 1–20, doi: 10.3390/CANCERS12092634.

Fowler, C.B., O'Leary, T.J. and Mason, J.T. (2011), "Protein mass spectrometry applications on FFPE tissue sections.", *Methods in Molecular Biology (Clifton, N.J.)*, Humana Press, Vol. 724, pp. 281–295, doi: 10.1007/978-1-61779-055-3_18/TABLES/1.

Frank, E., Hall, M., Trigg, L., Holmes, G. and Witten, I.H. (2004), "Data mining in bioinformatics using Weka", *Bioinformatics*, Vol. 20 No. 15, pp. 2479–2481, doi: 10.1093/bioinformatics/bth261.

Fraser, C., Ryan, J. and Sarosiek, K. (2019), "BH3 Profiling: A Functional Assay to Measure Apoptotic Priming and Dependencies", *Methods in Molecular Biology*, Humana Press Inc., Vol. 1877, pp. 61–76, doi: 10.1007/978-1-4939-8861-7_4/FIGURES/10.

Frey, N. V., Luger, S., Mangan, J., Zebrowski, A., Loren, A.W., Minderman, H., Baird, J., *et al.* (2014), "A Phase I Study Using Single Agent Birinapant in Patients with Relapsed Myelodysplastic Syndrome and Acute Myelogenous Leukemia", *Blood*, American Society of Hematology, Vol. 124 No. 21, pp. 3758–3758, doi: 10.1182/BLOOD.V124.21.3758.3758.

Fulda, S. (2010), "Evasion of apoptosis as a cellular stress response in cancer", *International Journal of Cell Biology*, doi: 10.1155/2010/370835.

Fulda, S. (2015), "Promises and challenges of Smac mimetics as cancer therapeutics", *Clinical Cancer Research*, Vol. 21 No. 22, pp. 5030–5036, doi: 10.1158/1078-0432.CCR-15-0365.

Fulda, S. and Vucic, D. (2012), "Targeting IAP proteins for therapeutic intervention in cancer", *Nature Reviews Drug Discovery*, Vol. 11 No. 4, p. 331, doi: 10.1038/nrd3698.

Gao, J., Aksoy, B.A., Dogrusoz, U., Dresdner, G., Gross, B., Sumer, S.O., Sun, Y., *et al.* (2013), "Integrative analysis of complex cancer genomics and clinical profiles using the cBioPortal", *Science Signaling*, Vol. 6 No. 269, doi: 10.1126/scisignal.2004088.

Garman, B., Anastopoulos, I.N., Krepler, C., Brafford, P., Sproesser, K., Jiang, Y., Wubbenhorst, B., *et al.* (2017), "Genetic and Genomic Characterization of 462 Melanoma Patient-Derived Xenografts, Tumor Biopsies, and Cell Lines", *Cell Reports*, Vol. 21 No. 7, pp. 1936–1952, doi: 10.1016/j.celrep.2017.10.052.

Gendoo, D.M.A., Zon, M., Sandhu, V., Manem, V.S.K., Ratanasirigulchai, N., Chen, G.M., Waldron, L., *et al.* (2019), "MetaGxData: Clinically Annotated Breast, Ovarian and Pancreatic Cancer Datasets and their Use in Generating a Multi-Cancer Gene Signature", *Scientific Reports*, Nature Publishing Group, Vol. 9 No. 1, doi: 10.1038/S41598-019-45165-4.

Gerdes, M.J., Sevinsky, C.J., Sood, A., Adak, S., Bello, M.O., Bordwell, A., Can, A., *et al.* (2013), "Highly multiplexed single-cell analysis of formalinfixed, paraffin-embedded cancer tissue", *Proceedings of the National Academy of Sciences of the United States of America*, Vol. 110 No. 29, pp. 11982–11987, doi: 10.1073/pnas.1300136110.

Gershenwald, J.E., Scolyer, R.A., Hess, K.R., Sondak, V.K., Long, G. V., Ross, M.I.,

Lazar, A.J., *et al.* (2017), "Melanoma staging: Evidence-based changes in the American Joint Committee on Cancer eighth edition cancer staging manual", *CA: A Cancer Journal for Clinicians*, American Cancer Society, Vol. 67 No. 6, pp. 472–492, doi: 10.3322/caac.21409.

Geserick, P., Drewniok, C., Hupe, M., Haas, T.L., Diessenbacher, P., Sprick, M.R., Schön, M.P., *et al.* (2008), "Suppression of cFLIP is sufficient to sensitize human melanoma cells to TRAIL- and CD95L-mediated apoptosis", *Oncogene*, Nature Publishing Group, Vol. 27 No. 22, pp. 3211–3220, doi: 10.1038/sj.onc.1210985.

Gide, T.N., Wilmott, J.S., Scolyer, R.A. and Long, G. V. (2018), "Primary and acquired resistance to immune checkpoint inhibitors in metastatic melanoma", *Clinical Cancer Research*, American Association for Cancer Research Inc., 15 March, doi: 10.1158/1078-0432.CCR-17-2267.

Gieffers, C., Kluge, M., Merz, C., Sykora, J., Thiemann, M., Schaal, R., Fischer, C., *et al.* (2013), "APG350 induces superior clustering of trail receptors and shows therapeutic antitumor efficacy independent of cross-Linking via fcγ receptors", *Molecular Cancer Therapeutics*, Vol. 12 No. 12, pp. 2735–2747, doi: 10.1158/1535-7163.MCT-13-0323.

Gnip, P., Vokorokos, L. and Drotár, P. (2021), "Selective oversampling approach for strongly imbalanced data", *PeerJ Computer Science*, Vol. 7, pp. 1–22, doi: 10.7717/PEERJ-CS.604.

Goldman, M., Craft, B., Hastie, M., Repečka, K., McDade, F., Kamath, A., Banerjee, A., *et al.* (2019), "The UCSC Xena platform for public and private cancer genomics data visualization and interpretation", *BioRxiv*, Cold Spring Harbor Laboratory, 26 September, doi: 10.1101/326470.

Goodfellow, I., Pouget-Abadie, J., Mirza, M., Xu, B., Warde-Farley, D., Ozair, S., Courville, A., *et al.* (2014), "Generative Adversarial Networks", *Communications of the ACM*, Association for Computing Machinery, Vol. 63 No. 11, pp. 139–144, doi: 10.1145/3422622.

Goossens, N., Nakagawa, S., Sun, X. and Hoshida, Y. (2015), "Cancer biomarker discovery and validation", *Translational Cancer Research*, Vol. 4 No. 3, pp. 256–269, doi: 10.3978/j.issn.2218-676X.2015.06.04.

Green, D.R. and Llambi, F. (2015), "Cell Death Signaling", *Cold Spring Harbor*

Perspectives in Biology, Cold Spring Harb Perspect Biol, Vol. 7 No. 12, doi: 10.1101/CSHPERSPECT.A006080.

Grissa, D., Pétéra, M., Brandolini, M., Napoli, A., Comte, B. and Pujos-Guillot, E. (2016), "Feature selection methods for early predictive biomarker discovery using untargeted metabolomic data", *Frontiers in Molecular Biosciences*, Frontiers Media S.A., Vol. 3 No. JUL, p. 30, doi: 10.3389/FMOLB.2016.00030/BIBTEX.

Grossman, R.L., Heath, A.P., Ferretti, V., Varmus, H.E., Lowy, D.R., Kibbe, W.A. and Staudt, L.M. (2016), "Toward a Shared Vision for Cancer Genomic Data", *New England Journal of Medicine*, Vol. 375 No. 12, pp. 1109–1112, doi: 10.1056/NEJMp1607591.

Grzybowska-Izydorczyk, O., Cebula, B., Robak, T. and Smolewski, P. (2010), "Expression and prognostic significance of the inhibitor of apoptosis protein (IAP) family and its antagonists in chronic lymphocytic leukaemia", *European Journal of Cancer*, Vol. 46 No. 4, pp. 800–810, doi: 10.1016/j.ejca.2009.11.023.

Guida, M., Tommasi, S., Strippoli, S., Natalicchio, M.I., De Summa, S., Pinto, R., Cramarossa, A., *et al.* (2018), "The search for a melanoma-tailored chemotherapy in the new era of personalized therapy: A phase II study of chemo-modulating temozolomide followed by fotemustine and a cooperative study of GOIM (Gruppo Oncologico Italia Meridionale)", *BMC Cancer*, Vol. 18 No. 1, pp. 1–8, doi: 10.1186/s12885-018-4479-2.

Gulrajani, I., Ahmed, F., Arjovsky, M., Dumoulin, V. and Courville, A. (2017), "Improved Training of Wasserstein GANs", *Advances in Neural Information Processing Systems*, Neural information processing systems foundation, Vol. 2017-December, pp. 5768–5778.

Gupta, A., Gomes, F. and Lorigan, P. (2017), "The role for chemotherapy in the modern management of melanoma", *Melanoma Management*, Vol. 4 No. 2, pp. 125–136, doi: 10.2217/mmt-2017-0003.

Gurian, E., Di Silvestre, A., Mitri, E., Pascut, D., Tiribelli, C., Giuffrè, M., Crocè, L.S., *et al.* (2021), "Repeated double cross-validation applied to the PCA-LDA classification of SERS spectra: a case study with serum samples from hepatocellular carcinoma patients", *Analytical and Bioanalytical Chemistry*, Springer Science and Business Media Deutschland GmbH, Vol. 413 No. 5, pp.

1303–1312, doi: 10.1007/S00216-020-03093-7/FIGURES/6.

Guttà, C., Morhard, C. and Rehm, M. (2022), “T-GAN-D: a GAN-based classifier for breast cancer prognostication”, doi: 10.5281/ZENODO.7151831.

Guyon, I., Weston, J., Barnhill, S. and Vapnik, V. (2002), “Gene Selection for Cancer Classification using Support Vector Machines”, *Machine Learning*, Springer, Vol. 46 No. 1, pp. 389–422, doi: 10.1023/A:1012487302797.

Han, S.S., Kim, M.S., Lim, W., Park, G.H., Park, I. and Chang, S.E. (2018), “Classification of the Clinical Images for Benign and Malignant Cutaneous Tumors Using a Deep Learning Algorithm”, *Journal of Investigative Dermatology*, Elsevier, Vol. 138 No. 7, pp. 1529–1538, doi: 10.1016/J.JID.2018.01.028.

Hanahan, D. and Weinberg, R.A. (2011), “Hallmarks of cancer: The next generation”, *Cell*, Elsevier Inc., Vol. 144 No. 5, pp. 646–674, doi: 10.1016/j.cell.2011.02.013.

Hantusch, A., Rehm, M. and Brunner, T. (2018), “Counting on Death – Quantitative aspects of Bcl-2 family regulation”, *FEBS Journal*, Vol. 285 No. 22, pp. 4124–4138, doi: 10.1111/febs.14516.

Harbeck, N., Penault-Llorca, F., Cortes, J., Gnant, M., Houssami, N., Poortmans, P., Ruddy, K., *et al.* (2019), “Breast cancer”, *Nature Reviews Disease Primers 2019 5:1*, Nature Publishing Group, Vol. 5 No. 1, pp. 1–31, doi: 10.1038/s41572-019-0111-2.

He, K., Zhang, X., Ren, S. and Sun, J. (2015), “Delving deep into rectifiers: Surpassing human-level performance on imagenet classification”, *Proceedings of the IEEE International Conference on Computer Vision*, Vol. 2015 Inter, pp. 1026–1034, doi: 10.1109/ICCV.2015.123.

Hellwig, C.T., Passante, E. and Rehm, M. (2011), “The molecular machinery regulating apoptosis signal transduction and its implication in human physiology and pathophysiologies.”, *Current Molecular Medicine*, Vol. 11 No. 1, pp. 31–47.

Heppt, M. V., Dietrich, C., Graf, S.A., Ruzicka, T., Tietze, J.K. and Berking, C. (2016), “The Systemic Management of Advanced Melanoma in 2016”, *Oncology Research and Treatment*, Vol. 39 No. 10, pp. 635–642, doi: 10.1159/000448904.

Van Herck, Y., Antoranz, A., Andhari, M.D., Milli, G., Bechter, O., De Smet, F. and Bosisio, F.M. (2021), “Multiplexed Immunohistochemistry and Digital Pathology as the Foundation for Next-Generation Pathology in Melanoma: Methodological

Comparison and Future Clinical Applications", *Frontiers in Oncology*, Frontiers Media S.A., Vol. 11, p. 1012, doi: 10.3389/FONC.2021.636681/BIBTEX.

Hira, M.T., Razzaque, M.A., Angione, C., Scrivens, J., Sawan, S. and Sarkar, M. (2021), "Integrated multi-omics analysis of ovarian cancer using variational autoencoders", *Scientific Reports*, Nature Publishing Group, Vol. 11 No. 1, pp. 1–16, doi: 10.1038/s41598-021-85285-4.

Hogan, S.A., Levesque, M.P. and Cheng, P.F. (2018), "Melanoma Immunotherapy: Next-Generation Biomarkers", *Frontiers in Oncology*, Vol. 8 No. MAY, doi: 10.3389/FONC.2018.00178.

Hogarth, L.A. and Hall, A.G. (1999), "Increased BAX expression is associated with an increased risk of relapse in childhood acute lymphocytic leukemia.", *Blood*, Vol. 93 No. 8, pp. 2671–8.

Holcik, M. and Korneluk, R.G. (2001), "XIAP, the guardian angel", *Nature Reviews Molecular Cell Biology*, Vol. 2 No. 7, pp. 550–556, doi: 10.1038/35080103.

Hsu, T.C. and Lin, C. (2020), "Generative Adversarial Networks for Robust Breast Cancer Prognosis Prediction with Limited Data Size", *Proceedings of the Annual International Conference of the IEEE Engineering in Medicine and Biology Society, EMBS*, Institute of Electrical and Electronics Engineers Inc., Vol. 2020-July, pp. 5669–5672, doi: 10.1109/EMBC44109.2020.9175736.

Hsu, Y.L., Huang, P.Y. and Chen, D.T. (2014), "Sparse principal component analysis in cancer research", *Translational Cancer Research*, NIH Public Access, Vol. 3 No. 3, p. 182, doi: 10.3978/J.ISSN.2218-676X.2014.05.06.

Hu, Q., Peng, J., Liu, W., He, X., Cui, L., Chen, X., Yang, M., *et al.* (2014), "Elevated cleaved caspase-3 is associated with shortened overall survival in several cancer types", *International Journal of Clinical and Experimental Pathology*, e-Century Publishing Corporation, Vol. 7 No. 8, p. 5057.

Huang, D., Quan, Y., He, M. and Zhou, B. (2009), "Comparison of linear discriminant analysis methods for the classification of cancer based on gene expression data", *Journal of Experimental & Clinical Cancer Research*, Vol. 28 No. 1, p. 149, doi: 10.1186/1756-9966-28-149.

Huang, Q., Li, F., Liu, X., Li, W., Shi, W., Liu, F.-F., O'Sullivan, B., *et al.* (2011), "Caspase 3–mediated stimulation of tumor cell repopulation during cancer

radiotherapy", *Nature Medicine*, Vol. 17 No. 7, pp. 860–866, doi: 10.1038/nm.2385.

Huang, Q., Li, S., Cheng, P., Deng, M., He, X., Wang, Z., Yang, C.H., *et al.* (2017), "High expression of anti-apoptotic protein Bcl-2 is a good prognostic factor in colorectal cancer: Result of a meta-analysis", *World Journal of Gastroenterology*, Baishideng Publishing Group Co, Vol. 23 No. 27, pp. 5018–5033, doi: 10.3748/wjg.v23.i27.5018.

Hughes, M.A., Powley, I.R., Jukes-Jones, R., Horn, S., Feoktistova, M., Fairall, L., Schwabe, J.W.R., *et al.* (2016), "Co-operative and Hierarchical Binding of c-FLIP and Caspase-8: A Unified Model Defines How c-FLIP Isoforms Differentially Control Cell Fate", *Molecular Cell*, Vol. 61 No. 6, pp. 834–849, doi: 10.1016/J.MOLCEL.2016.02.023.

Hutt, M., Fellermeier-Kopf, S., Seifert, O., Schmitt, L.C., Pfizenmaier, K. and Kontermann, R.E. (2018), "Targeting scFv-Fc-scTRAIL fusion proteins to tumor cells", *Oncotarget*, Vol. 9 No. 13, pp. 11322–11335, doi: 10.18632/oncotarget.24379.

Hutt, M., Marquardt, L., Seifert, O., Siegemund, M., Müller, I., Kulms, D., Pfizenmaier, K., *et al.* (2017), "Superior properties of Fc-comprising scTRAIL fusion proteins", *Molecular Cancer Therapeutics*, Vol. 16 No. 12, pp. 2792–2802, doi: 10.1158/1535-7163.MCT-17-0551.

Ichim, G. and Tait, S.W.G. (2016), "A fate worse than death: apoptosis as an oncogenic process", *Nature Reviews Cancer*, Vol. 16 No. 8, pp. 539–548, doi: 10.1038/nrc.2016.58.

Inada, T., Kikuyama, S., Ichikawa, A., Igarashi, S. and Ogata, Y. (1998), "Bcl-2 expression as a prognostic factor of survival of gastric carcinoma", *Anticancer Research*, Vol. 18 No. 3 B, pp. 2003–2010.

Ioffe, S. and Szegedy, C. (2015), "Batch Normalization: Accelerating Deep Network Training by Reducing Internal Covariate Shift", *32nd International Conference on Machine Learning, ICML 2015*, International Machine Learning Society (IMLS), Vol. 1, pp. 448–456.

Jan, R. and Chaudhry, G. e. S. (2019), "Understanding Apoptosis and Apoptotic Pathways Targeted Cancer Therapeutics", *Advanced Pharmaceutical Bulletin*,

Tabriz University of Medical Sciences, Vol. 9 No. 2, p. 205, doi: 10.15171/APB.2019.024.

Janecek, A.G.K. and Gansterer, W.N. (2008), "A Comparison of Classification Accuracy Achieved with Wrappers, Filters and PCA", *Workshop on New Challenges for Feature Selection in Data Mining and Knowledge Discovery*.

Janiesch, C., Zschech, P. and Heinrich, K. (2021), "Machine learning and deep learning", *Electronic Markets*, Springer Science and Business Media Deutschland GmbH, Vol. 31 No. 3, pp. 685–695, doi: 10.1007/S12525-021-00475-2/TABLES/2.

Jensen, M.B., Lænkholm, A.V., Nielsen, T.O., Eriksen, J.O., Wehn, P., Hood, T., Ram, N., *et al.* (2018), "The Prosigna gene expression assay and responsiveness to adjuvant cyclophosphamide-based chemotherapy in premenopausal high-risk patients with breast cancer", *Breast Cancer Research*, Vol. 20 No. 1, doi: 10.1186/s13058-018-1012-0.

Jeong, S.H., Lee, H.W., Han, J.H., Kang, S.Y., Choi, J.H., Jung, Y.M., Choi, H., *et al.* (2008), "Low expression of bax predicts poor prognosis in resected non-small cell lung cancer patients with non-squamous histology", *Japanese Journal of Clinical Oncology*, Vol. 38 No. 10, pp. 661–669, doi: 10.1093/jjco/hyn089.

Jia, D., Chen, C., Chen, C., Chen, F., Zhang, N., Yan, Z. and Lv, X. (2021), "Breast Cancer Case Identification Based on Deep Learning and Bioinformatics Analysis", *Frontiers in Genetics*, Frontiers Media S.A., Vol. 12, p. 767, doi: 10.3389/FGENE.2021.628136/XML/NLM.

Jia, W., Sun, M., Lian, J. and Hou, S. (2022), "Feature dimensionality reduction: a review", *Complex & Intelligent Systems 2022 8:3*, Springer, Vol. 8 No. 3, pp. 2663–2693, doi: 10.1007/S40747-021-00637-X.

Jollife, I.T. and Cadima, J. (2016), "Principal component analysis: a review and recent developments", *Philosophical Transactions of the Royal Society A: Mathematical, Physical and Engineering Sciences*, The Royal Society Publishing, Vol. 374 No. 2065, doi: 10.1098/RSTA.2015.0202.

Jost, P.J., Grabow, S., Gray, D., McKenzie, M.D., Nachbur, U., Huang, D.C.S., Bouillet, P., *et al.* (2009), "XIAP discriminates between type i and type II FAS-induced apoptosis", *Nature*, Vol. 460 No. 7258, pp. 1035–1039, doi:

10.1038/nature08229.

Kaiser, H.F. (1960), “The Application of Electronic Computers to Factor Analysis”, *Educational and Psychological Measurement*, Vol. 20 No. 1, pp. 141–151, doi: 10.1177/001316446002000116.

Kakadia, S., Yarlagadda, N., Awad, R., Kundranda, M., Niu, J., Naraev, B., Mina, L., *et al.* (2018), “Mechanisms of resistance to BRAF and MEK inhibitors and clinical update of US Food and Drug Administration-approved targeted therapy in advanced melanoma.”, *OncoTargets and Therapy*, Dove Press, Vol. 11, pp. 7095–7107, doi: 10.2147/OTT.S182721.

Kale, J., Osterlund, E.J. and Andrews, D.W. (2018), “BCL-2 family proteins: changing partners in the dance towards death”, *Cell Death & Differentiation*, Vol. 25 No. 1, pp. 65–80, doi: 10.1038/cdd.2017.186.

Karczewski, K.J. and Snyder, M.P. (2018), “Integrative omics for health and disease”, *Nature Reviews. Genetics*, NIH Public Access, Vol. 19 No. 5, p. 299, doi: 10.1038/NRG.2018.4.

von Karstedt, S., Conti, A., Nobis, M., Montinaro, A., Hartwig, T., Lemke, J., Legler, K., *et al.* (2015), “Cancer cell-autonomous TRAIL-R signaling promotes KRAS-Driven cancer progression, invasion, and metastasis”, *Cancer Cell*, Vol. 27 No. 4, pp. 561–573, doi: 10.1016/j.ccell.2015.02.014.

Von Karstedt, S., Montinaro, A. and Walczak, H. (2017), “Exploring the TRAILs less travelled: TRAIL in cancer biology and therapy”, *Nature Reviews Cancer*, Nature Publishing Group, 1 June, doi: 10.1038/nrc.2017.28.

Kelly, C.M., Crown, J., Russell, N., Barron, S., Lynch, S., O’Grady, A., Sheehan, K., *et al.* (2018), “Comparison of the prognostic performance between OncoMasTR and OncotypeDX multigene signatures in hormone receptor-positive, HER2-negative, lymph node-negative breast cancer.”, *Journal of Clinical Oncology*, American Society of Clinical Oncology, Vol. 36 No. 15_suppl, pp. 12074–12074, doi: 10.1200/jco.2018.36.15_suppl.12074.

Kensler, K.H., Sankar, V.N., Wang, J., Zhang, X., Rubadue, C.A., Baker, G.M., Parker, J.S., *et al.* (2019), “PAM50 molecular intrinsic subtypes in the nurses’ health Study cohorts”, *Cancer Epidemiology Biomarkers and Prevention*, American Association for Cancer Research Inc., Vol. 28 No. 4, pp. 798–806, doi: 10.1158/1055-

9965.EPI-18-0863/70112/AM/PAM50-MOLECULAR-INTRINSIC-SUBTYPES-IN-THE-NURSES.

Kerr, J.F.R., Wyllie, A.H. and Currie, A.R. (1972), "Apoptosis: A Basic Biological Phenomenon with Wideranging Implications in Tissue Kinetics", *British Journal of Cancer 1972 26:4*, Nature Publishing Group, Vol. 26 No. 4, pp. 239–257, doi: 10.1038/bjc.1972.33.

Keung, E.Z. and Gershenwald, J.E. (2018), "The eighth edition American Joint Committee on Cancer (AJCC) melanoma staging system: implications for melanoma treatment and care", *Expert Review of Anticancer Therapy*, Vol. 18 No. 8, pp. 775–784, doi: 10.1080/14737140.2018.1489246.

Kim, M., Oh, I. and Ahn, J. (2018), "An Improved Method for Prediction of Cancer Prognosis by Network Learning", *Genes*, Multidisciplinary Digital Publishing Institute (MDPI), Vol. 9 No. 10, pp. 1. – 11, doi: 10.3390/GENES9100478.

Kodali, N., Abernethy, J., Hays, J. and Kira, Z. (2017), "On Convergence and Stability of GANs", 19 May, available at: https://arxiv.org/abs/1705.07215v5 (accessed 1 March 2022).

Köhler, T., Schill, C., Deininger, M., Krahl, R., Borchert, S., Hasenclever, D., Leiblein, S., *et al.* (2002), "High Bad and Bax mRNA expression correlate with negative outcome in acute myeloid leukemia (AML)", *Leukemia*, Vol. 16 No. 1, pp. 22–29, doi: 10.1038/sj.leu.2402340.

Kohli, M., Yu, J., Seaman, C., Bardelli, A., Kinzler, K.W., Vogelstein, B., Lengauer, C., *et al.* (2004), "SMAC/Diablo-dependent apoptosis induced by nonsteroidal antiinflammatory drugs (NSAIDs) in colon cancer cells.", *Proceedings of the National Academy of Sciences of the United States of America*, National Academy of Sciences, Vol. 101 No. 48, pp. 16897–902, doi: 10.1073/pnas.0403405101.

Kong, X., Xu, P., Cai, W.J., Wang, H.G., Li, B. Bin, Huang, G.L., He, Z.W., *et al.* (2018), "ZBP-89 and Sp1 contribute to Bak expression in hepatocellular carcinoma cells", *BMC Cancer*, Vol. 18 No. 1, p. 419, doi: 10.1186/s12885-018-4349-y.

Kourou, K., Exarchos, K.P., Papaloukas, C., Sakaloglou, P., Exarchos, T. and Fotiadis, D.I. (2021), "Applied machine learning in cancer research: A systematic review for patient diagnosis, classification and prognosis", *Computational and Structural Biotechnology Journal*, Research Network of Computational and Structural

Biotechnology, Vol. 19, p. 5546, doi: 10.1016/J.CSBJ.2021.10.006.

Kourou, K., Exarchos, T.P., Exarchos, K.P., Karamouzis, M. V. and Fotiadis, D.I. (2015), "Machine learning applications in cancer prognosis and prediction", *Computational and Structural Biotechnology Journal*, Elsevier, Vol. 13, pp. 8–17, doi: 10.1016/J.CSBJ.2014.11.005.

Krepler, C., Chunduru, S.K., Halloran, M.B., He, X., Xiao, M., Vultur, A., Villanueva, J., *et al.* (2013), "The novel SMAC mimetic birinapant exhibits potent activity against human melanoma cells", *Clinical Cancer Research*, Vol. 19 No. 7, pp. 1784–1794, doi: 10.1158/1078-0432.CCR-12-2518.

Krizhevsky, A., Sutskever, I. and Hinton, G.E. (2012), "ImageNet Classification with Deep Convolutional Neural Networks", *Advances in Neural Information Processing Systems*, Vol. 25.

Kulsoom, B., Shamsi, T.S., Afsar, N.A., Memon, Z., Ahmed, N. and Hasnain, S.N. (2018), "Bax, Bcl-2, and Bax/Bcl-2 as prognostic markers in acute myeloid leukemia: are we ready for Bcl-2-directed therapy?", *Cancer Management and Research*, Dove Press, Vol. 10, pp. 403–416, doi: 10.2147/CMAR.S154608.

Kupryjańczyk, J., Szymańska, T., Mądry, R., Timorek, A., Stelmachów, J., Karpińska, G., Rembiszewska, A., *et al.* (2003), "Evaluation of clinical significance of TP53, BCL-2, BAX and MEKI expression in 229 ovarian carcinomas treated with platinum-based regimen", *British Journal of Cancer*, Vol. 88 No. 6, pp. 848–854, doi: 10.1038/sj.bjc.6600789.

Kwon, C.H., Park, S., Ko, S. and Ahn, J. (2021), "Increasing prediction accuracy of pathogenic staging by sample augmentation with a GAN", *PLOS ONE*, Public Library of Science, Vol. 16 No. 4, p. e0250458, doi: 10.1371/JOURNAL.PONE.0250458.

Labi, V. and Erlacher, M. (2015), "How cell death shapes cancer", *Cell Death and Disease*, Nature Publishing Group, Vol. 6 No. 3, p. e1675, doi: 10.1038/cddis.2015.20.

Lafont, E., Kantari-Mimoun, C., Draber, P., De Miguel, D., Hartwig, T., Reichert, M., Kupka, S., *et al.* (2017), "The linear ubiquitin chain assembly complex regulates TRAIL -induced gene activation and cell death", *The EMBO Journal*, Vol. 36 No. 9, pp. 1147–1166, doi: 10.15252/embj.201695699.

Lavrik, I.N., Golks, A. and Krammer, P.H. (2005), “Caspases: pharmacological manipulation of cell death”, *The Journal of Clinical Investigation*, Vol. 115 No. 10, pp. 2665–2672, doi: 10.1172/JCI26252.

Lawrence, M.S., Stojanov, P., Polak, P., Kryukov, G. V, Cibulskis, K., Sivachenko, A., Carter, S.L., *et al.* (2013), “Mutational heterogeneity in cancer and the search for new cancer-associated genes”, *Nature*, Vol. 499 No. 7457, pp. 214–218, doi: 10.1038/nature12213.

Lemke, J., von Karstedt, S., Zinngrebe, J. and Walczak, H. (2014), “Getting TRAIL back on track for cancer therapy”, *Cell Death and Differentiation*, Nature Publishing Group, Vol. 21 No. 9, pp. 1350–1364, doi: 10.1038/cdd.2014.81.

Leonardi, G.C., Falzone, L., Salemi, R., Zanghì, A., Spandidos, D.A., Mccubrey, J.A., Candido, S., *et al.* (2018), “Cutaneous melanoma: From pathogenesis to therapy”, *International Journal of Oncology*, Spandidos Publications, Vol. 52 No. 4, pp. 1071–1080, doi: 10.3892/ijo.2018.4287.

LeQuang, J.A. (2022), “Using Gene Expression Profiling to Personalize Skin Cancer Management”, *The Journal of Clinical and Aesthetic Dermatology*, Matrix Medical Communications, Vol. 15 No. 11 Suppl 1, p. S3.

Lev, D.C., Onn, A., Melinkova, V.O., Miller, C., Stone, V., Ruiz, M., McGary, E.C., *et al.* (2004), “Exposure of Melanoma Cells to Dacarbazine Results in Enhanced Tumor Growth and Metastasis In Vivo”, *Journal of Clinical Oncology*, Vol. 22 No. 11, pp. 2092–2100, doi: 10.1200/JCO.2004.11.070.

Leverkus, M. and Gollnick, H. (2006), “‘Bak (and Bax) to the future’ - Of primary melanoma prognosis?”, *Journal of Investigative Dermatology*, Vol. 126 No. 6, pp. 1212–1214, doi: 10.1038/sj.jid.5700239.

Li, X., Jiang, Y., Rodriguez-Andina, J.J., Luo, H., Yin, S. and Kaynak, O. (2021), “When medical images meet generative adversarial network: recent development and research opportunities”, *Discover Artificial Intelligence*, Springer, Vol. 1 No. 1, pp. 1–20, doi: 10.1007/S44163-021-00006-0.

Liang, S., Singh, M., Dharmaraj, S. and Gam, L.H. (2010), “The PCA and LDA Analysis on the Differential Expression of Proteins in Breast Cancer”, *Disease Markers*, Hindawi, Vol. 29 No. 5, pp. 231–242, doi: 10.3233/DMA-2010-0753.

Liccardi, G., Ramos Garcia, L., Tenev, T., Annibaldi, A., Legrand, A.J., Robertson, D.,

Feltham, R., *et al.* (2019), “RIPK1 and Caspase-8 Ensure Chromosome Stability Independently of Their Role in Cell Death and Inflammation”, *Molecular Cell*, Vol. 73 No. 3, pp. 413-428.e7, doi: 10.1016/j.molcel.2018.11.010.

Liñares-Blanco, J., Pazos, A. and Fernandez-Lozano, C. (2021), “Machine learning analysis of TCGA cancer data”, *PeerJ Computer Science*, PeerJ, Inc, Vol. 7, pp. 1–47, doi: 10.7717/PEERJ-CS.584.

Liu, B., Wei, Y., Zhang, Y. and Yang, Q. (2017), “Deep neural networks for high dimension, low sample size data”, *IJCAI International Joint Conference on Artificial Intelligence*, pp. 2287–2293, doi: 10.24963/ijcai.2017/318.

Liu, J., Lichtenberg, T., Hoadley, K.A., Poisson, L.M., Lazar, A.J., Cherniack, A.D., Kovatich, A.J., *et al.* (2018), “An Integrated TCGA Pan-Cancer Clinical Data Resource to Drive High-Quality Survival Outcome Analytics”, *Cell*, Vol. 173 No. 2, pp. 400-416.e11, doi: 10.1016/j.cell.2018.02.052.

Liu, R. and Gillies, D.F. (2016), “Overfitting in linear feature extraction for classification of high-dimensional image data”, *Pattern Recognition*, Pergamon, Vol. 53, pp. 73–86, doi: 10.1016/J.PATCOG.2015.11.015.

Liu, R., Hall, L.O., Bowyer, K.W., Goldgof, D.B., Gatenby, R. and Ahmed, K. Ben. (2017), “Synthetic minority image over-sampling technique: How to improve AUC for glioblastoma patient survival prediction”, *2017 IEEE International Conference on Systems, Man, and Cybernetics, SMC 2017*, Institute of Electrical and Electronics Engineers Inc., Vol. 2017-January, pp. 1357–1362, doi: 10.1109/SMC.2017.8122802.

Liu, Y. and Sheikh, M.S. (2014), “Melanoma: Molecular Pathogenesis and Therapeutic Management”, *Molecular and Cellular Pharmacology*, NIH Public Access, Vol. 6 No. 3, p. 228, doi: 10.4255/mcpharmacol.14.03.

Livingstone, A., Agarwal, A., Stockler, M.R., Menzies, A.M., Howard, K. and Morton, R.L. (2020), “Preferences for Immunotherapy in Melanoma: A Systematic Review”, *Annals of Surgical Oncology*, Springer, 1 February, doi: 10.1245/s10434-019-07963-y.

Lopez, J. and Tait, S.W.G. (2015), “Mitochondrial apoptosis: killing cancer using the enemy within”, *British Journal of Cancer*, Nature Publishing Group, Vol. 112 No. 6, p. 957, doi: 10.1038/BJC.2015.85.

LoRusso, P., Ratain, M.J., Doi, T., Rasco, D.W., de Jonge, M.J.A., Moreno, V., Carneiro, B.A., *et al.* (2022), "Eftozanermin alfa (ABBV-621) monotherapy in patients with previously treated solid tumors: findings of a phase 1, first-in-human study", *Investigational New Drugs*, Springer, Vol. 40 No. 4, pp. 762–772, doi: 10.1007/S10637-022-01247-1/FIGURES/3.

Luebker, S.A., Zhang, W. and Koepsell, S.A. (2017), "Comparing the genomes of cutaneous melanoma tumors to commercially available cell lines", *Oncotarget*, Vol. 8 No. 70, pp. 114877–114893, doi: 10.18632/oncotarget.22928.

Lui, P., Cashin, R., Machado, M., Hemels, M., Corey-Lisle, P.K. and Einarson, T.R. (2007), "Treatments for metastatic melanoma: Synthesis of evidence from randomized trials", *Cancer Treatment Reviews*, Vol. 33 No. 8, pp. 665–680, doi: 10.1016/j.ctrv.2007.06.004.

Luo, Y., Wang, X., Wang, H., Xu, Y., Wen, Q., Fan, S., Zhao, R., *et al.* (2015), "High Bak expression is associated with a favorable prognosis in breast cancer and sensitizes breast cancer cells to paclitaxel", *PLoS ONE*, Vol. 10 No. 9, p. e0138955, doi: 10.1371/journal.pone.0138955.

Lyu, B. and Haque, A. (2018), "Deep Learning Based Tumor Type Classification Using Gene Expression Data", *ACM-BCB 2018 - Proceedings of the 2018 ACM International Conference on Bioinformatics, Computational Biology, and Health Informatics*, Association for Computing Machinery, Inc, pp. 89–96, doi: 10.1145/3233547.3233588.

Ma, J., Niu, W., Wang, X., Zhou, Y., Wang, H., Liu, F., Liu, Y., *et al.* (2019), "Bromodomain-containing protein 7 sensitizes breast cancer cells to paclitaxel by activating Bcl2-antagonist/killer protein", *Oncology Reports*, Vol. 41 No. 3, pp. 1487–1496, doi: 10.3892/or.2018.6951.

Margolin, K. (2016), "The Promise of Molecularly Targeted and Immunotherapy for Advanced Melanoma", *Current Treatment Options in Oncology*, Vol. 17 No. 9, pp. 1–14, doi: 10.1007/s11864-016-0421-5.

Marouf, M., Machart, P., Bansal, V., Kilian, C., Magruder, D.S., Krebs, C.F. and Bonn, S. (2020), "Realistic in silico generation and augmentation of single-cell RNA-seq data using generative adversarial networks", *Nature Communications*, Vol. 11 No. 1, pp. 1–12, doi: 10.1038/s41467-019-14018-z.

McCarthy, J., Minsky, M.L., Rochester, N. and Shannon, C.E. (2006), “A proposal for the Dartmouth summer research project on artificial intelligence”, *AI Magazine*, Vol. 27 No. 4, pp. 12–14.

McDonald, F.E., Ironside, J.W., Gregor, A., Wyatt, B., Stewart, M., Rye, R., Adams, J., *et al.* (2002), “The prognostic influence of bcl-2 in malignant glioma.”, *British Journal of Cancer*, Nature Publishing Group, Vol. 86 No. 12, pp. 1899–904, doi: 10.1038/sj.bjc.6600217.

McKinney, S.M., Sieniek, M., Godbole, V., Godwin, J., Antropova, N., Ashrafian, H., Back, T., *et al.* (2020), “International evaluation of an AI system for breast cancer screening”, *Nature 2020 577:7788*, Nature Publishing Group, Vol. 577 No. 7788, pp. 89–94, doi: 10.1038/s41586-019-1799-6.

Mehnert, J.M. and Kluger, H.M. (2012), “Driver Mutations in Melanoma: Lessons Learned From Bench-to-Bedside Studies”, *Current Oncology Reports 2012 14:5*, Springer, Vol. 14 No. 5, pp. 449–457, doi: 10.1007/S11912-012-0249-5.

Meterissian, S.H., Kontogiannea, M., Al-Sowaidi, M., Linjawi, A., Halwani, F., Jamison, B. and Edwardes, M. (2001), “Bcl-2 Is a Useful Prognostic Marker in Dukes’ B Colon Cancer”, *Annals of Surgical Oncology*, Vol. 8 No. 6, pp. 533–537, doi: 10.1007/s10434-001-0533-3.

Middleton, M.R., Grob, J.J., Aaronson, N., Fierlbeck, G., Tilgen, W., Seiter, S., Gore, M., *et al.* (2000), “Randomized Phase III Study of Temozolomide Versus Dacarbazine in the Treatment of Patients With Advanced Metastatic Malignant Melanoma”, *Journal of Clinical Oncology*, Vol. 18 No. 1, pp. 158–158, doi: 10.1200/JCO.2000.18.1.158.

de Miguel, D., Lemke, J., Anel, A., Walczak, H. and Martinez-Lostao, L. (2016), “Onto better TRAILs for cancer treatment”, *Cell Death & Differentiation*, Nature Publishing Group, Vol. 23 No. 5, pp. 733–747, doi: 10.1038/cdd.2015.174.

Milella, M., Falcone, I., Conciatori, F., Incani, U.C., Del Curatolo, A., Inzerilli, N., Nuzzo, C.M.A., *et al.* (2015), “PTEN: Multiple functions in human malignant tumors”, *Frontiers in Oncology*, Frontiers Research Foundation, Vol. 5 No. FEB, p. 24, doi: 10.3389/FONC.2015.00024/BIBTEX.

Mirza, M. and Osindero, S. (2014), “Conditional Generative Adversarial Nets”, 6 November, available at: https://arxiv.org/abs/1411.1784v1 (accessed 1 March

2022).

Moi, S.H., Lee, Y.C., Chuang, L.Y., Yuan, S.S.F., Ou-Yang, F., Hou, M.F., Yang, C.H., *et al.* (2018), "Cumulative receiver operating characteristics for analyzing interaction between tissue visfatin and clinicopathologic factors in breast cancer progression", *Cancer Cell International*, BioMed Central Ltd., Vol. 18 No. 1, pp. 1–8, doi: 10.1186/S12935-018-0517-Z/TABLES/5.

Morgan-Lappe, S.E. (2017), "ABBV-621: A best-in-class TRAIL-receptor agonist fusion protein that enhances optimal clustering for the treatment of solid and hematologic tumors", *Proceedings of the American Association for Cancer Research Annual Meeting 2017*, American Association for Cancer Research (AACR), Vol. 77 No. 13 Supplement, pp. DDT01-03-DDT01-03, doi: 10.1158/1538-7445.am2017-ddt01-03.

Morrish, E., Brumatti, G. and Silke, J. (2020), "Future Therapeutic Directions for Smac-Mimetics", *Cells 2020, Vol. 9, Page 406*, Multidisciplinary Digital Publishing Institute, Vol. 9 No. 2, p. 406, doi: 10.3390/CELLS9020406.

Morton, D.L., Thompson, J.F., Cochran, A.J., Mozzillo, N., Nieweg, O.E., Roses, D.F., Hoekstra, H.J., *et al.* (2014), "Final Trial Report of Sentinel-Node Biopsy versus Nodal Observation in Melanoma", *New England Journal of Medicine*, Massachusetts Medical Society, Vol. 370 No. 7, pp. 599–609, doi: 10.1056/NEJMOA1310460/SUPPL_FILE/NEJMOA1310460_DISCLOSURES.PDF.

Mostavi, M., Chiu, Y.C., Huang, Y. and Chen, Y. (2020), "Convolutional neural network models for cancer type prediction based on gene expression", *BMC Medical Genomics*, BioMed Central Ltd., Vol. 13 No. 5, pp. 1–13, doi: 10.1186/S12920-020-0677-2/FIGURES/5.

Mukherjee, A., Russell, R., Chin, S.F., Liu, B., Rueda, O.M., Ali, H.R., Turashvili, G., *et al.* (2018), "Associations between genomic stratification of breast cancer and centrally reviewed tumour pathology in the METABRIC cohort", *Npj Breast Cancer 2018 4:1*, Nature Publishing Group, Vol. 4 No. 1, pp. 1–9, doi: 10.1038/s41523-018-0056-8.

Navarrete-Dechent, C., Dusza, S.W., Liopyris, K., Marghoob, A.A., Halpern, A.C. and Marchetti, M.A. (2018), "Automated Dermatological Diagnosis: Hype

or Reality?", *Journal of Investigative Dermatology*, Elsevier, Vol. 138 No. 10, pp. 2277–2279, doi: 10.1016/J.JID.2018.04.040.

Ni, M., Zhou, X., Liu, J., Yu, H., Gao, Y., Zhang, X. and Li, Z. (2020), "Prediction of the clinicopathological subtypes of breast cancer using a fisher discriminant analysis model based on radiomic features of diffusion-weighted MRI", *BMC Cancer*, Vol. 20 No. 1, doi: 10.1186/S12885-020-07557-Y.

Noonan, A.M., Bunch, K.P., Chen, J.Q., Herrmann, M.A., Lee, J.M., Kohn, E.C., O'Sullivan, C.C., *et al.* (2016), "Pharmacodynamic markers and clinical results from the phase 2 study of the SMAC mimetic birinapant in women with relapsed platinum-resistant or -refractory epithelial ovarian cancer", *Cancer*, John Wiley & Sons, Ltd, Vol. 122 No. 4, pp. 588–597, doi: 10.1002/CNCR.29783.

Nwosu, A.J., Misal, S.A., Truong, T., Carson, R.H., Webber, K.G.I., Axtell, N.B., Liang, Y., *et al.* (2022), "In-Depth Mass Spectrometry-Based Proteomics of Formalin-Fixed, Paraffin-Embedded Tissues with a Spatial Resolution of 50-200 μm", *Journal of Proteome Research*, American Chemical Society, Vol. 21 No. 9, pp. 2237–2245, doi: 10.1021/ACS.JPROTEOME.2C00409/SUPPL_FILE/PR2C00409_SI_001.PDF.

Obermeyer, Z., Powers, B., Vogeli, C. and Mullainathan, S. (2019), "Dissecting racial bias in an algorithm used to manage the health of populations", *Science*, American Association for the Advancement of Science, Vol. 366 No. 6464, pp. 447–453, doi: 10.1126/SCIENCE.AAX2342/SUPPL_FILE/AAX2342_OBERMEYER_SM.PDF.

Odena, A., Olah, C. and Shlens, J. (2016), "Conditional Image Synthesis With Auxiliary Classifier GANs", *34th International Conference on Machine Learning, ICML 2017*, International Machine Learning Society (IMLS), Vol. 6, pp. 4043–4055.

Oltersdorf, T., Elmore, S.W., Shoemaker, A.R., Armstrong, R.C., Augeri, D.J., Belli, B.A., Bruncko, M., *et al.* (2005), "An inhibitor of Bcl-2 family proteins induces regression of solid tumours", *Nature*, Vol. 435 No. 7042, pp. 677–681, doi: 10.1038/NATURE03579.

Pan, S.T., Li, Z.L., He, Z.X., Qiu, J.X. and Zhou, S.F. (2016), "Molecular mechanisms for tumour resistance to chemotherapy", *Clinical and Experimental Pharmacology and Physiology*, John Wiley & Sons, Ltd, Vol. 43 No. 8, pp. 723–737, doi:

10.1111/1440-1681.12581.

Panis, C., Pizzatti, L., Souza, G.F. and Abdelhay, E. (2016), "Clinical proteomics in cancer: Where we are", *Cancer Letters*, Vol. 382 No. 2, pp. 231–239, doi: 10.1016/j.canlet.2016.08.014.

Passante, E., Würstle, M.L., Hellwig, C.T., Leverkus, M. and Rehm, M. (2013), "Systems analysis of apoptosis protein expression allows the case-specific prediction of cell death responsiveness of melanoma cells", *Cell Death and Differentiation*, Vol. 20 No. 11, pp. 1521–1531, doi: 10.1038/cdd.2013.106.

Petricoin, E.F., Zoon, K.C., Kohn, E.C., Barrett, J.C. and Liotta, L.A. (2002), "Clinical proteomics: Translating benchside promise into bedside reality", *Nature Reviews Drug Discovery*, Vol. 1 No. 9, pp. 683–695, doi: 10.1038/nrd891.

Pluta, P., Cebula-Obrzut, B., Ehemann, V., Pluta, A., Wierzbowska, A., Piekarski, J., Bilski, A., *et al.* (2011), "Correlation of Smac/DIABLO protein expression with the clinico-pathological features of breast cancer patients", *Neoplasma*, Vol. 58 No. 5, pp. 430–435, doi: 10.4149/neo_2011_05_430.

Del Poeta, G., Venditti, A., Del Principe, M.I., Maurillo, L., Buccisano, F., Tamburini, A., Cox, M.C., *et al.* (2003), "Amount of spontaneous apoptosis detected by Bax/Bcl-2 ratio predicts outcome in acute myeloid leukemia (AML)", *Blood*, Vol. 101 No. 6, pp. 2125–2131, doi: 10.1182/blood-2002-06-1714.

Prukova, D., Andera, L., Nahacka, Z., Karolova, J., Svaton, M., Klanova, M., Havranek, O., *et al.* (2019), "Cotargeting of BCL2 with Venetoclax and MCL1 with S63845 Is Synthetically Lethal In Vivo in Relapsed Mantle Cell Lymphoma", *Clinical Cancer Research*, American Association for Cancer Research, Vol. 25 No. 14, pp. 4455–4465, doi: 10.1158/1078-0432.CCR-18-3275.

Radford, A., Metz, L. and Chintala, S. (2015), "Unsupervised Representation Learning with Deep Convolutional Generative Adversarial Networks", *4th International Conference on Learning Representations, ICLR 2016*.

Raghu, V.K., Ge, X., Chrysanthis, P.K. and Benos, P. V. (2017), "Integrated Theory- and Data-driven Feature Selection in Gene Expression Data Analysis", *Proceedings. International Conference on Data Engineering*, NIH Public Access, Vol. 2017, p. 1525, doi: 10.1109/ICDE.2017.223.

Ram, S., Vizcarra, P., Whalen, P., Deng, S., Painter, C.L., Jackson-Fisher, A., Pirie-

Shepherd, S., *et al.* (2021), “Pixelwise H-score: A novel digital image analysis-based metric to quantify membrane biomarker expression from immunohistochemistry images”, *PLoS ONE*, Vol. 16 No. 9.

Ravichandran, K.S. (2010), “Find-me and eat-me signals in apoptotic cell clearance: progress and conundrums”, *Journal of Experimental Medicine*, The Rockefeller University Press, Vol. 207 No. 9, pp. 1807–1817, doi: 10.1084/JEM.20101157.

Rehm, M., Huber, H.J., Dussmann, H. and Prehn, J.H.M. (2006), “Systems analysis of effector caspase activation and its control by X-linked inhibitor of apoptosis protein”, *EMBO Journal*, Vol. 25 No. 18, pp. 4338–4349, doi: 10.1038/sj.emboj.7601295.

Renouf, D.J., Wood-Baker, R., Ionescu, D.N., Leung, S., Masoudi, H., Gilks, C.B. and Laskin, J. (2009), “BCL-2 expression is prognostic for improved survival in non-small cell lung cancer”, *Journal of Thoracic Oncology*, Vol. 4 No. 4, pp. 486–491, doi: 10.1097/JTO.0b013e318199e03a.

Ribeiro, M.T., Singh, S. and Guestrin, C. (2016), “‘Why should i trust you?’ Explaining the predictions of any classifier”, *Proceedings of the ACM SIGKDD International Conference on Knowledge Discovery and Data Mining*, Association for Computing Machinery, Vol. 13-17-August-2016, pp. 1135–1144, doi: 10.1145/2939672.2939778.

Roberts, A.W., Davids, M.S., Pagel, J.M., Kahl, B.S., Puvvada, S.D., Gerecitano, J.F., Kipps, T.J., *et al.* (2016), “Targeting BCL2 with Venetoclax in Relapsed Chronic Lymphocytic Leukemia”, *The New England Journal of Medicine*, Vol. 374 No. 4, pp. 311–322, doi: 10.1056/NEJMOA1513257.

Ross, J.S., Hatzis, C., Symmans, W.F., Pusztai, L. and Hortobágyi, G.N. (2008), “Commercialized Multigene Predictors of Clinical Outcome for Breast Cancer”, *The Oncologist*, Oxford Academic, Vol. 13 No. 5, pp. 477–493, doi: 10.1634/THEONCOLOGIST.2007-0248.

Rožanc, J., Sakellaropoulos, T., Antoranz, A., Guttà, C., Podder, B., Vetma, V., Rufo, N., *et al.* (2019), “Phosphoprotein patterns predict trametinib responsiveness and optimal trametinib sensitisation strategies in melanoma”, *Cell Death and Differentiation*, Nature Publishing Group, Vol. 26 No. 8, pp. 1365–1378, doi: 10.1038/s41418-018-0210-8.

Rueda, O.M., Sammut, S.J., Seoane, J.A., Chin, S.F., Caswell-Jin, J.L., Callari, M., Batra, R., *et al.* (2019), "Dynamics of breast-cancer relapse reveal late-recurring ER-positive genomic subgroups", *Nature*, Vol. 567 No. 7748, pp. 399–404, doi: 10.1038/S41586-019-1007-8.

Russakovsky, O., Deng, J., Su, H., Krause, J., Satheesh, S., Ma, S., Huang, Z., *et al.* (2015), "ImageNet Large Scale Visual Recognition Challenge", *International Journal of Computer Vision*, Springer New York LLC, Vol. 115 No. 3, pp. 211–252, doi: 10.1007/S11263-015-0816-Y/FIGURES/16.

Saeys, Y., Inza, I. and Larrañaga, P. (2007), "A review of feature selection techniques in bioinformatics", *Bioinformatics*, Oxford Academic, Vol. 23 No. 19, pp. 2507–2517, doi: 10.1093/BIOINFORMATICS/BTM344.

Saha, S. and Sheikh, N. (2021), "Ultrasound Image Classification using ACGAN with Small Training Dataset", *Advances in Intelligent Systems and Computing*, Springer Science and Business Media Deutschland GmbH, Vol. 1333 AISC, pp. 85–93, doi: 10.48550/arxiv.2102.01539.

Samraj, A.K., Keil, E., Ueffing, N., Schulze-Osthoff, K. and Schmitz, I. (2006), "Loss of Caspase-9 Provides Genetic Evidence for the Type I/II Concept of CD95-mediated Apoptosis", *Journal of Biological Chemistry*, Vol. 281 No. 40, pp. 29652–29659, doi: 10.1074/jbc.M603487200.

Sanada, M., Hidaka, M., Takagi, Y., Takano, T.Y., Nakatsu, Y., Tsuzuki, T. and Sekiguchi, M. (2007), "Modes of actions of two types of anti-neoplastic drugs, dacarbazine and ACNU, to induce apoptosis", *Carcinogenesis*, Vol. 28 No. 12, pp. 2657–2663, doi: 10.1093/carcin/bgm188.

Sandru, A., Voinea, S., Panaitescu, E. and Blidaru, A. (2014), "Survival rates of patients with metastatic malignant melanoma", *Journal of Medicine and Life*, Carol Davila - University Press, Vol. 7 No. 4, p. 572.

Savova, G.K., Danciu, I., Alamudun, F., Miller, T., Lin, C., Bitterman, D.S., Tourassi, G., *et al.* (2019), "Use of Natural Language Processing to Extract Clinical Cancer Phenotypes from Electronic Medical Records", *Cancer Research*, NIH Public Access, Vol. 79 No. 21, p. 5463, doi: 10.1158/0008-5472.CAN-19-0579.

Scaffidi, C., Fulda, S., Srinivasan, A., Friesen, C., Li, F., Tomaselli, K.J., Debatin, K.M., *et al.* (1998), "Two CD95 (APO-1/Fas) signaling pathways", *The EMBO*

Journal, Vol. 17 No. 6, pp. 1675–1687, doi: 10.1093/EMBOJ/17.6.1675.

Scatena, C., Murtas, D. and Tomei, S. (2021), "Cutaneous Melanoma Classification: The Importance of High-Throughput Genomic Technologies", *Frontiers in Oncology*, Frontiers Media S.A., Vol. 11, p. 1313, doi: 10.3389/FONC.2021.635488/BIBTEX.

Schubert, W., Bonnekoh, B., Pommer, A.J., Philipsen, L., Böckelmann, R., Malykh, Y., Gollnick, H., *et al.* (2006), "Analyzing proteome topology and function by automated multidimensional fluorescence microscopy", *Nature Biotechnology*, Vol. 24 No. 10, pp. 1270–1278, doi: 10.1038/nbt1250.

Seok, Y.K., Jae, H.H., Kwang, J.L., Choi, J.H., Jung, I.P., Hyoung, I.K., Lee, H.W., *et al.* (2007), "Low expression of bax predicts poor prognosis in patients with locally advanced esophageal cancer treated with definitive chemoradiotherapy", *Clinical Cancer Research*, Vol. 13 No. 14, pp. 4146–4153, doi: 10.1158/1078-0432.CCR-06-3063.

Shams, S., Platania, R., Zhang, J., Kim, J. and Park, S.J. (2018), "Deep generative breast cancer screening and diagnosis", *Lecture Notes in Computer Science (Including Subseries Lecture Notes in Artificial Intelligence and Lecture Notes in Bioinformatics)*, Vol. 11071 LNCS, Springer Verlag, pp. 859–867, doi: 10.1007/978-3-030-00934-2_95.

Shao, C., Li, G., Huang, L., Pruitt, S., Castellanos, E., Frampton, G., Carson, K.R., *et al.* (2020), "Prevalence of High Tumor Mutational Burden and Association With Survival in Patients With Less Common Solid Tumors", *JAMA Network Open*, American Medical Association, Vol. 3 No. 10, pp. e2025109–e2025109, doi: 10.1001/JAMANETWORKOPEN.2020.25109.

Shao, D., Dai, Y., Li, N., Cao, X., Zhao, W., Cheng, L., Rong, Z., *et al.* (2022), "Artificial intelligence in clinical research of cancers", *Briefings in Bioinformatics*, Oxford Academic, Vol. 23 No. 1.

Sharma, A., Vans, E., Shigemizu, D., Boroevich, K.A. and Tsunoda, T. (2019), "DeepInsight: A methodology to transform a non-image data to an image for convolution neural network architecture", *Scientific Reports 2019 9:1*, Nature Publishing Group, Vol. 9 No. 1, pp. 1–7, doi: 10.1038/s41598-019-47765-6.

Sharma, S., Kaufmann, T. and Biswas, S. (2017), "Impact of inhibitor of apoptosis

proteins on immune modulation and inflammation", *Immunology and Cell Biology*, John Wiley & Sons, Ltd, Vol. 95 No. 3, pp. 236–243, doi: 10.1038/ICB.2016.101.

Shi, Z., Wen, B., Gao, Q. and Zhang, B. (2021), "Feature Selection Methods for Protein Biomarker Discovery from Proteomics or Multiomics Data", *Molecular & Cellular Proteomics*, Elsevier, Vol. 20, p. 100083, doi: 10.1016/J.MCPRO.2021.100083.

Shorten, C. and Khoshgoftaar, T.M. (2019), "A survey on Image Data Augmentation for Deep Learning", *Journal of Big Data*, Springer Open, Vol. 6 No. 1, pp. 1–48, doi: 10.1186/S40537-019-0197-0/FIGURES/33.

Shreve, J.T., Khanani, S.A. and Haddad, T.C. (2022), "Artificial Intelligence in Oncology: Current Capabilities, Future Opportunities, and Ethical Considerations.", *American Society of Clinical Oncology Educational Book. American Society of Clinical Oncology. Annual Meeting*, American Society of Clinical Oncology Alexandria, VA , Vol. 42 No. 42, pp. 1–10, doi: 10.1200/EDBK_350652.

Soengas, M.S., Capodieci, P., Polsky, D., Mora, J., Esteller, M., Opitz-Araya, X., McCombie, R., *et al.* (2001), "Inactivation of the apoptosis effector Apaf-1 in malignant melanoma", *Nature*, Vol. 409 No. 6817, pp. 207–211, doi: 10.1038/35051606.

Soengas, M.S. and Lowe, S.W. (2003), "Apoptosis and melanoma chemoresistance", *Oncogene*, Vol. 22 No. 20, pp. 3138–3151, doi: 10.1038/sj.onc.1206454.

Souers, A.J., Leverson, J.D., Boghaert, E.R., Ackler, S.L., Catron, N.D., Chen, J., Dayton, B.D., *et al.* (2013), "ABT-199, a potent and selective BCL-2 inhibitor, achieves antitumor activity while sparing platelets", *Nature Medicine*, Vol. 19 No. 2, pp. 202–208.

Spitzer, M.H. and Nolan, G.P. (2016), "Mass Cytometry: Single Cells, Many Features", *Cell*, Vol. 165 No. 4, pp. 780–791, doi: 10.1016/j.cell.2016.04.019.

Stadler, A. (2021), "The Health Insurance Portability and Accountability Act and its Impact on Privacy and Confidentiality in Healthcare", *Senior Honors Theses*.

Stephens, Z.D., Lee, S.Y., Faghri, F., Campbell, R.H., Zhai, C., Efron, M.J., Iyer, R., *et al.* (2015), "Big Data: Astronomical or Genomical?", *PLoS Biology*, Public Library of Science, Vol. 13 No. 7, doi: 10.1371/JOURNAL.PBIO.1002195.

Strachey, C.S. (1952), "Logical or non-mathematical programmes", *Association for*

Computing Machinery (ACM), pp. 46–49, doi: 10.1145/800259.808992.

Strickland, E. (2019), "IBM Watson, heal thyself: How IBM overpromised and underdelivered on AI health care", *IEEE Spectrum*, Institute of Electrical and Electronics Engineers Inc., Vol. 56 No. 4, pp. 24–31, doi: 10.1109/MSPEC.2019.8678513.

Suárez-García, J.G., Hernández-López, J.M., Moreno-Barbosa, E. and de Celis-Alonso, B. (2020), "A simple model for glioma grading based on texture analysis applied to conventional brain MRI", *PLOS ONE*, Public Library of Science, Vol. 15 No. 5, p. e0228972, doi: 10.1371/JOURNAL.PONE.0228972.

Sweeney, C., Bernard, P.S., Factor, R.E., Kwan, M.L., Habel, L.A., Quesenberry, C.P., Shakespear, K., *et al.* (2014), "Intrinsic subtypes from PAM50 gene expression assay in a population-based breast cancer cohort: Differences by age, race, and tumor characteristics", *Cancer Epidemiology Biomarkers and Prevention*, NIH Public Access, Vol. 23 No. 5, pp. 714–724, doi: 10.1158/1055-9965.EPI-13-1023.

Switzer, B., Puzanov, I., Skitzki, J.J., Hamad, L. and Ernstoff, M.S. (2022), "Managing Metastatic Melanoma in 2022: A Clinical Review", *JCO Oncology Practice*, American Society of Clinical Oncology (ASCO), Vol. 18 No. 5, pp. 335–351, doi: 10.1200/op.21.00686.

Syed, Y.Y. (2020), "Oncotype DX Breast Recurrence Score: A Review of its Use in Early-Stage Breast Cancer", *Molecular Diagnosis and Therapy*, Vol. 24 No. 5, pp. 621–632, doi: 10.1007/S40291-020-00482-7/TABLES/6.

Tait, S.W.G. and Green, D.R. (2010), "Mitochondria and cell death: outer membrane permeabilization and beyond", *Nature Reviews Molecular Cell Biology*, Vol. 11 No. 9, pp. 621–632, doi: 10.1038/nrm2952.

Tang, L., Tron, V.A., Reed, J.C., Mah, K.J., Krajewska, M., Li, G., Zhou, X., *et al.* (1998), "Expression of apoptosis regulators in cutaneous malignant melanoma.", *Clinical Cancer Research*, Vol. 4 No. 8, pp. 1865–71.

Tapak, L., Shirmohammadi-Khorram, N., Amini, P., Alafchi, B., Hamidi, O. and Poorolajal, J. (2019), "Prediction of survival and metastasis in breast cancer patients using machine learning classifiers", *Clinical Epidemiology and Global Health*, Elsevier, Vol. 7 No. 3, pp. 293–299, doi: 10.1016/J.CEGH.2018.10.003.

Tasci, E., Zhuge, Y., Camphausen, K. and Krauze, A. V. (2022), "Bias and Class

Imbalance in Oncologic Data—Towards Inclusive and Transferrable AI in Large Scale Oncology Data Sets", *Cancers*, Multidisciplinary Digital Publishing Institute (MDPI), Vol. 14 No. 12, doi: 10.3390/CANCERS14122897.

Taylor, R.C., Cullen, S.P. and Martin, S.J. (2008), "Apoptosis: Controlled demolition at the cellular level", *Nature Reviews Molecular Cell Biology*, Vol. 9 No. 3, pp. 231–241, doi: 10.1038/nrm2312.

Tchernev, G. and Orfanos, C.E. (2007), "Downregulation of cell cycle modulators p21, p27, p53, Rb and proapoptotic Bcl-2-related proteins Bax and Bak in cutaneous melanoma is associated with worse patient prognosis: preliminary findings", *Journal of Cutaneous Pathology*, Vol. 34 No. 3, pp. 247–256, doi: 10.1111/j.1600-0560.2006.00700.x.

Tenev, T., Bianchi, K., Darding, M., Broemer, M., Langlais, C., Wallberg, F., Zachariou, A., *et al.* (2011), "The Ripoptosome, a Signaling Platform that Assembles in Response to Genotoxic Stress and Loss of IAPs", *Molecular Cell*, Vol. 43 No. 3, pp. 432–448, doi: 10.1016/j.molcel.2011.06.006.

Tran, K.A., Kondrashova, O., Bradley, A., Williams, E.D., Pearson, J. V. and Waddell, N. (2021), "Deep learning in cancer diagnosis, prognosis and treatment selection", *Genome Medicine 2021 13:1*, BioMed Central, Vol. 13 No. 1, pp. 1–17, doi: 10.1186/S13073-021-00968-X.

Trevethan, R. (2017), "Sensitivity, Specificity, and Predictive Values: Foundations, Pliabilities, and Pitfalls in Research and Practice", *Frontiers in Public Health*, Frontiers Media S.A., Vol. 5, p. 307, doi: 10.3389/FPUBH.2017.00307/BIBTEX.

Troester, M.A., Sun, X., Allott, E.H., Geradts, J., Cohen, S.M., Tse, C.K., Kirk, E.L., *et al.* (2018), "Racial Differences in PAM50 Subtypes in the Carolina Breast Cancer Study", *JNCI: Journal of the National Cancer Institute*, Oxford Academic, Vol. 110 No. 2, pp. 176–182, doi: 10.1093/JNCI/DJX135.

Tse, C., Shoemaker, A.R., Adickes, J., Anderson, M.G., Chen, J., Jin, S., Johnson, E.F., *et al.* (2008), "ABT-263: a potent and orally bioavailable Bcl-2 family inhibitor", *Cancer Research*, Vol. 68 No. 9, pp. 3421–3428, doi: 10.1158/0008-5472.CAN-07-5836.

Turashvili, G. and Brogi, E. (2017), "Tumor heterogeneity in breast cancer", *Frontiers in Medicine*, Frontiers Media S.A., Vol. 4 No. DEC, p. 227, doi:

10.3389/FMED.2017.00227/BIBTEX.

Turing, A.M. (1950), "Computing Machinery and Intelligence", *Mind*, Oxford Academic, Vol. LIX No. 236, pp. 433–460, doi: 10.1093/MIND/LIX.236.433.

Van't Veer, L.J., Dai, H., Van de Vijver, M.J., He, Y.D., Hart, A.A.M., Mao, M., Peterse, H.L., *et al.* (2002), "Gene expression profiling predicts clinical outcome of breast cancer", *Nature 2002 415:6871*, Nature Publishing Group, Vol. 415 No. 6871, pp. 530–536, doi: 10.1038/415530a.

Vargas-Roig, L.M., Cuello-Carrión, F.D., Fernández-Escobar, N., Daguerre, P., Leuzzi, M., Ibarra, J., Gago, F.E., *et al.* (2008), "Prognostic value of Bcl-2 in breast cancer patients treated with neoadjuvant anthracycline based chemotherapy.", *Molecular Oncology*, Wiley-Blackwell, Vol. 2 No. 1, pp. 102–11, doi: 10.1016/j.molonc.2008.01.004.

Vera, J., Lai, X., Baur, A., Erdmann, M., Gupta, S., Guttà, C., Heinzerling, L., *et al.* (2022), "Melanoma 2.0. Skin cancer as a paradigm for emerging diagnostic technologies, computational modelling and artificial intelligence", *Briefings in Bioinformatics*, doi: 10.1093/BIB/BBAC433.

van de Vijver, M.J., He, Y.D., van 't Veer, L.J., Dai, H., Hart, A.A.M., Voskuil, D.W., Schreiber, G.J., *et al.* (2002), "A Gene-Expression Signature as a Predictor of Survival in Breast Cancer", *New England Journal of Medicine*, Massachusetts Medical Society, Vol. 347 No. 25, pp. 1999–2009, doi: 10.1056/nejmoa021967.

Vokinger, K.N., Feuerriegel, S. and Kesselheim, A.S. (2021), "Mitigating bias in machine learning for medicine", *Communications Medicine*, Nature Publishing Group, Vol. 1 No. 1, pp. 1–3, doi: 10.1038/s43856-021-00028-w.

Vörsmann, H., Groeber, F., Walles, H., Busch, S., Beissert, S., Walczak, H. and Kulms, D. (2013), "Development of a human three-dimensional organotypic skin-melanoma spheroid model for in vitro drug testing", *Cell Death and Disease*, Vol. 4 No. 7, p. e719, doi: 10.1038/cddis.2013.249.

Vucic, D. (2018), "XIAP at the crossroads of cell death and inflammation", *Oncotarget*, Vol. 9 No. 44, pp. 27319–27320, doi: 10.18632/oncotarget.25363.

Wagner, K.W., Punnoose, E.A., Januario, T., Lawrence, D.A., Pitti, R.M., Lancaster, K., Lee, D., *et al.* (2007), "Death-receptor O-glycosylation controls tumor-cell sensitivity to the proapoptotic ligand Apo2L/TRAIL", *Nature Medicine*, Vol. 13

No. 9, pp. 1070–1077, doi: 10.1038/nm1627.

Waks, A.G. and Winer, E.P. (2019), "Breast Cancer Treatment: A Review", *JAMA*, American Medical Association, Vol. 321 No. 3, pp. 288–300, doi: 10.1001/JAMA.2018.19323.

Wallis, C. (2019), "How Artificial Intelligence Will Change Medicine", *Nature*, Vol. 576 No. 7787, p. S48, doi: 10.1038/D41586-019-03845-1.

Wang, C. and Youle, R.J. (2012), "Predominant requirement of Bax for apoptosis in HCT116 cells is determined by Mcl-1's inhibitory effect on Bak", *Oncogene*, Vol. 31 No. 26, pp. 3177–3189, doi: 10.1038/onc.2011.497.

Wang, L., Li, Q., Aushev, V.N., Neugut, A.I., Santella, R.M., Teitelbaum, S. and Chen, J. (2021), "PAM50- and immunohistochemistry-based subtypes of breast cancer and their relationship with breast cancer mortality in a population-based study", *Breast Cancer*, Springer Japan, Vol. 28 No. 6, pp. 1235–1242, doi: 10.1007/S12282-021-01261-W/FIGURES/4.

Wang, Q., Armenia, J., Zhang, C., Penson, A. V., Reznik, E., Zhang, L., Minet, T., *et al.* (2018), "Unifying cancer and normal RNA sequencing data from different sources", *Scientific Data*, Vol. 5.

Wei, K., Li, T., Huang, F., Chen, J. and He, Z. (2021), "Cancer classification with data augmentation based on generative adversarial networks", *Frontiers of Computer Science 2022 16:2*, Springer, Vol. 16 No. 2, pp. 1–11, doi: 10.1007/S11704-020-0025-X.

Weinstock, M.A., Colditz, G.A., Willett, W.C., Stampfer, M.J., Bronstein, B.R., Mihm, M.C. and Speizer, F.E. (1989), "Nonfamilial cutaneous melanoma incidence in women associated with sun exposure before 20 years of age.", *Pediatrics*, Vol. 84 No. 2, pp. 199–204, doi: 10.1542/peds.84.2.199.

Weiss, H.L., Niwas, S., Grizzle, W.E. and Piyathilake, C. (2003), "Receiver Operating Characteristic (ROC) to Determine Cut-Off Points of Biomarkers in Lung Cancer Patients", *Disease Markers*, Hindawi, Vol. 19 No. 6, pp. 273–278, doi: 10.1155/2004/856026.

Wertz, I.E., Kusam, S., Lam, C., Okamoto, T., Sandoval, W., Anderson, D.J., Helgason, E., *et al.* (2011), "Sensitivity to antitubulin chemotherapeutics is regulated by MCL1 and FBW7", *Nature*, Vol. 471 No. 7336, pp. 110–114, doi:

10.1038/NATURE09779.

Whiteman, D.C., Green, A.C. and Olsen, C.M. (2016), "The Growing Burden of Invasive Melanoma: Projections of Incidence Rates and Numbers of New Cases in Six Susceptible Populations through 2031", *Journal of Investigative Dermatology*, Vol. 136 No. 6, pp. 1161–1171, doi: 10.1016/j.jid.2016.01.035.

WHO. (2021), "Breast cancer", available at: https://www.who.int/news-room/fact-sheets/detail/breast-cancer (accessed 30 August 2022).

Wilson, N.S., Yang, B., Yang, A., Loeser, S., Marsters, S., Lawrence, D., Li, Y., *et al.* (2011), "An Fcγ receptor-dependent mechanism drives antibody-mediated target-receptor signaling in cancer cells", *Cancer Cell*, Vol. 19 No. 1, pp. 101–113, doi: 10.1016/j.ccr.2010.11.012.

Wilson, T.R., McEwan, M., McLaughlin, K., Le Clorennec, C., Allen, W.L., Fennell, D.A., Johnston, P.G., *et al.* (2009), "Combined inhibition of FLIP and XIAP induces Bax-independent apoptosis in type II colorectal cancer cells", *Oncogene*, Vol. 28 No. 1, pp. 63–72, doi: 10.1038/onc.2008.366.

Wolterink, J.M., Dinkla, A.M., Savenije, M.H.F., Seevinck, P.R., van den Berg, C.A.T. and Išgum, I. (2017), "Deep MR to CT synthesis using unpaired data", *Lecture Notes in Computer Science (Including Subseries Lecture Notes in Artificial Intelligence and Lecture Notes in Bioinformatics)*, Springer Verlag, Vol. 10557 LNCS, pp. 14–23, doi: 10.1007/978-3-319-68127-6_2/FIGURES/6.

Wu, C.C., Lee, S., Malladi, S., Chen, M. Der, Mastrandrea, N.J., Zhang, Z. and Bratton, S.B. (2016), "The Apaf-1 apoptosome induces formation of caspase-9 homo- and heterodimers with distinct activities", *Nature Communications*, Vol. 7.

Xia, Y., Fan, C., Hoadley, K.A., Parker, J.S. and Perou, C.M. (2019), "Genetic determinants of the molecular portraits of epithelial cancers", *Nature Communications 2019 10:1*, Nature Publishing Group, Vol. 10 No. 1, pp. 1–13, doi: 10.1038/s41467-019-13588-2.

Xiao, Y., Wu, J. and Lin, Z. (2021), "Cancer diagnosis using generative adversarial networks based on deep learning from imbalanced data", *Computers in Biology and Medicine*, Pergamon, Vol. 135, p. 104540, doi: 10.1016/J.COMPBIOMED.2021.104540.

Yang, H., Chen, R., Li, D. and Wang, Z. (2021), "Subtype-GAN: a deep learning

approach for integrative cancer subtyping of multi-omics data", *Bioinformatics*, Oxford Academic, Vol. 37 No. 16, pp. 2231–2237, doi: 10.1093/BIOINFORMATICS/BTAB109.

Yang, J. and Yang, J.Y. (2003), "Why can LDA be performed in PCA transformed space?", *Pattern Recognition*, Pergamon, Vol. 36 No. 2, pp. 563–566, doi: 10.1016/S0031-3203(02)00048-1.

Yao, K., Tong, C.Y. and Cheng, C. (2022), "A framework to predict the applicability of Oncotype DX, MammaPrint, and E2F4 gene signatures for improving breast cancer prognostic prediction", *Scientific Reports*, Nature Publishing Group, Vol. 12 No. 1, pp. 1–11, doi: 10.1038/s41598-022-06230-7.

Yersal, O. and Barutca, S. (2014), "Biological subtypes of breast cancer: Prognostic and therapeutic implications", *World Journal of Clinical Oncology*, Baishideng Publishing Group Inc, Vol. 5 No. 3, p. 412, doi: 10.5306/WJCO.V5.I3.412.

Yim, W.W., Yetisgen, M., Harris, W.P. and Sharon, W.K. (2016), "Natural Language Processing in Oncology: A Review", *JAMA Oncology*, Vol. 2 No. 6, pp. 797–804, doi: 10.1001/JAMAONCOL.2016.0213.

Yousefi, S., Shaban, A., Amgad, M., Chandradevan, R. and Cooper, L.A.D. (2019), "Learning Clinical Outcomes from Heterogeneous Genomic Data Sources", 2 April, doi: 10.48550/arxiv.1904.01637.

Yu, H., Lin, L., Zhang, Z., Zhang, H. and Hu, H. (2020), "Targeting NF-κB pathway for the therapy of diseases: mechanism and clinical study", *Signal Transduction and Targeted Therapy*, Vol. 5 No. 1.

Yu, Z., Wang, Z., Yu, X. and Zhang, Z. (2020), "RNA-Seq-Based Breast Cancer Subtypes Classification Using Machine Learning Approaches", *Computational Intelligence and Neuroscience*, Hindawi Limited.

Yuan, J., Hu, Z., Mahal, B.A., Zhao, S.D., Kensler, K.H., Pi, J., Hu, X., *et al.* (2018), "Integrated Analysis of Genetic Ancestry and Genomic Alterations across Cancers", *Cancer Cell*, Vol. 34 No. 4, pp. 549-560.e9, doi: 10.1016/J.CCELL.2018.08.019.

Zack, T.I., Schumacher, S.E., Carter, S.L., Cherniack, A.D., Saksena, G., Tabak, B., Lawrence, M.S., *et al.* (2013), "Pan-cancer patterns of somatic copy number alteration", *Nature Genetics*, Vol. 45 No. 10, pp. 1134–1140, doi:

10.1038/NG.2760.

Zakaria, Z., Tivnan, A., Flanagan, L., Murray, D.W., Salvucci, M., Stringer, B.W., Day, B.W., *et al.* (2016), "Patient-derived glioblastoma cells show significant heterogeneity in treatment responses to the inhibitor-of-apoptosis-protein antagonist birinapant", *British Journal of Cancer*, Vol. 114 No. 2, pp. 188–198, doi: 10.1038/bjc.2015.420.

Zhang, A., Wang, X., Fan, C. and Mao, X. (2021), "The Role of Ki67 in Evaluating Neoadjuvant Endocrine Therapy of Hormone Receptor-Positive Breast Cancer", *Frontiers in Endocrinology*, Frontiers Media S.A., Vol. 12, p. 1426, doi: 10.3389/FENDO.2021.687244/BIBTEX.

Zhang, C., Zhao, Y., Xu, X., Xu, R., Li, H., Teng, X., Du, Y., *et al.* (2020), "Cancer diagnosis with DNA molecular computation", *Nature Nanotechnology*, Nature Publishing Group, Vol. 15 No. 8, pp. 709–715, doi: 10.1038/S41565-020-0699-0.

Zhao, R., Kaakati, R., Lee, A.K., Liu, X., Li, F. and Li, C.Y. (2018), "Novel roles of apoptotic caspases in tumor repopulation, epigenetic reprogramming, carcinogenesis, and beyond", *Cancer and Metastasis Reviews*, Vol. 37 No. 2–3, pp. 227–236, doi: 10.1007/s10555-018-9736-y.

Ziegler, D.S., Keating, J., Kesari, S., Fast, E.M., Zawel, L., Ramakrishna, N., Barnes, J., *et al.* (2011), "A small-molecule IAP inhibitor overcomes resistance to cytotoxic therapies in malignant gliomas in vitro and in vivo", *Neuro-Oncology*, Vol. 13 No. 8, pp. 820–829, doi: 10.1093/neuonc/nor066.

References

5 PUBLISHED RESEARCH ARTICLES

In this section, the papers presented in chapters 2.1 and 2.2 are provided in the form edited by the respective publishers. At the date of submission of this dissertation, the study presented in chapter 2.3 is in revision, therefore no edited version is provided.

Cell Death & Differentiation (2020) 27:2417–2432
https://doi.org/10.1038/s41418-020-0512-5

Cell Death & Differentiation

ARTICLE

Convergence of pathway analysis and pattern recognition predicts sensitization to latest generation TRAIL therapeutics by IAP antagonism

Vesna Vetma[1,2] · Cristiano Guttà[1] · Nathalie Peters[1] · Christian Praetorius[3,4] · Meike Hutt[1] · Oliver Seifert[1] · Friedegund Meier[4,5,6] · Roland Kontermann[1,7] · Dagmar Kulms[3,4,8] · Markus Rehm[1,2,7,9,10]

Received: 5 March 2019 / Revised: 30 January 2020 / Accepted: 31 January 2020 / Published online: 21 February 2020

Abstract

Second generation TRAIL-based therapeutics, combined with sensitising co-treatments, have recently entered clinical trials. However, reliable response predictors for optimal patient selection are not yet available. Here, we demonstrate that a novel and translationally relevant hexavalent TRAIL receptor agonist, IZI1551, in combination with Birinapant, a clinically tested IAP antagonist, efficiently induces cell death in various melanoma models, and that responsiveness can be predicted by combining pathway analysis, data-driven modelling and pattern recognition. Across a panel of 16 melanoma cell lines, responsiveness to IZI1551/Birinapant was heterogeneous, with complete resistance and pronounced synergies observed. Expression patterns of TRAIL pathway regulators allowed us to develop a combinatorial marker that predicts potent cell killing with high accuracy. IZI1551/Birinapant responsiveness could be predicted not only for cell lines, but also for 3D tumour cell spheroids and for cells directly isolated from patient melanoma metastases (80–100% prediction accuracies). Mathematical parameter reduction identified 11 proteins crucial to ensure prediction accuracy, with x-linked inhibitor of apoptosis protein (XIAP) and procaspase-3 scoring highest, and Bcl-2 family members strongly represented. Applied to expression data of a cohort of $n = 365$ metastatic melanoma patients in a proof of concept in silico trial, the predictor suggested that IZI1551/Birinapant responsiveness could be expected for up to 30% of patient tumours. Overall, response frequencies in melanoma models were very encouraging, and the capability to predict melanoma sensitivity to combinations of latest generation TRAIL-based therapeutics and IAP antagonists can address the need for patient selection strategies in clinical trials based on these novel drugs.

Introduction

The immune system can eliminate cancer cells by activating cell surface apoptosis-inducing death receptors, such as tumour necrosis factor-related apoptosis-inducing ligand receptors 1 and 2 (also known as death receptors 4 and 5

These authors contributed equally: Vesna Vetma, Cristiano Guttà

Edited by D.R. Green

Supplementary information The online version of this article (https://doi.org/10.1038/s41418-020-0512-5) contains supplementary material, which is available to authorized users.

✉ Markus Rehm
markus.morrison@izi.uni-stuttgart.de

1 Institute of Cell Biology and Immunology, University of Stuttgart, Stuttgart, Germany

2 Department of Physiology & Medical Physics, Royal College of Surgeons in Ireland, Dublin, Ireland

3 Center for Regenerative Therapies, Technical University Dresden, Dresden, Germany

4 Skin Cancer Center at the University Cancer Centre, Department of Dermatology, Faculty of Medicine, University Hospital Carl Gustav Carus, Technical University Dresden, Dresden, Germany

5 National Center for Tumor Diseases (NCT), Dresden, Germany

6 German Cancer Research Center (DKFZ), Heidelberg, Germany

7 Stuttgart Research Center Systems Biology, University of Stuttgart, Stuttgart, Germany

8 Experimental Dermatology, Department of Dermatology, Technical University Dresden, Dresden, Germany

9 Stuttgart Centre for Simulation Science (SC SimTech), University of Stuttgart, Stuttgart, Germany

10 Centre for Systems Medicine, Royal College of Surgeons in Ireland, Dublin, Ireland

(DR4/5)). Many cancer cells, including melanoma, over-express these TRAIL-Rs, possibly due to an additional role these receptors can play in supporting cellular proliferation and invasion by autonomous TRAIL/TRAIL-R signalling [1]. Developing TRAIL-based therapeutics has been a highly active but only moderately successful translational research field for many years, but recent progress in designing superior TRAIL-based biologics and an improved mechanistic understanding of drug-induced TRAIL-sensitisation now provide novel avenues for new anti-cancer therapies [2]. Latest generation TRAIL-derived therapeutics overcome limitations of previous formulations by significantly improving TRAIL receptor oligomerisation and activation by higher valency, and by exerting significantly prolonged serum half-lives. Highly promising variants are hexavalent fusion proteins that couple two single-chain TRAIL trimers and that outperform soluble human TRAIL and TRAIL-R-targeting antibodies [3–5]. Cellular inhibitor of apoptosis proteins (cIAPs) 1 and 2 can prevent TRAIL-induced cell death by recruiting components of the linear ubiquitin chain assembly complex (LUBAC) to aggregated TRAIL-Rs. The activitiy of LUBAC promotes pro-survival signalling and suppresses both apoptosis and necroptosis signalling cascades [6]. Synthetic IAP antagonists, such as Birinapant (TL32711), BV6 or LCL-161, therefore potently sensitise cells to TRAIL-induced caspase-8 activation and apoptosis [7, 8]. IAP antagonists bind to cIAPs and cause conformational changes that allow dimerisation of cIAP RING domains, auto-ubiquitylation and subsequent proteasomal degradation [9]. In cells capable of activating caspase-8, the cleavage of the Bcl-2 family protein Bid initiates the formation of Bax/Bak pores in the outer mitochondrial membrane, followed by activation of downstream caspases-9, -3, -7 and subsequent cell death [10]. Birinapant also binds to and inhibits x-linked inhibitor of apoptosis protein (XIAP), a major antagonist of caspases-9, -3, -7 that is also involved in upstream regulation of cell death signalling, with nM affinity [11–13]. Inducing apoptosis through the TRAIL pathway can proceed without the need for transcriptional responses or protein neo-synthesis, processes required for cell death induction by the majority of cytotoxic therapeutics. This suggests that pre-treatment amounts of proteins regulating apoptotic TRAIL signalling might suffice to derive predictors for treatment responsiveness.

Especially in highly heterogeneous cancers, such malignant melanoma, predictive markers and validated companion diagnostic tests developed from such markers will be necessary to identify those patients likely to respond to treatment [14, 15]. The incidence of cutaneous melanoma continues to rise rapidly [16]. While chemotherapy-based treatments provide little benefit for patients with metastatic melanoma, more recent treatment options such as targeted immuno-therapeutics, BRAFV600 and MEK inhibitors, and combinations thereof in many cases can prolong survival or, less frequently, induce lasting disease remission [17, 18]. However, substantial numbers of patients do not qualify for these treatments or experience disease relapse, so that additional treatment options, for example those building on TRAIL-based therapeutics and IAP antagonists, can be attractive alternatives should it become possible to reliably predict treatment responsiveness.

Here we can report that expression profiles of TRAIL pathway regulators can serve to predict responsiveness to the combination of IZI1551, a prototypical example of a translationally relevant latest generation TRAIL-based biologic [3], and Birinapant (TL32711), a well-characterised example for a translationally relevant IAP antagonist [8]. Across a diverse and heterogeneous melanoma cell line panel, 3D multi-cellular tumour spheroids (MCTS) and melanoma cells isolated from patient metastases, we achieved >80% prediction accuracy. A proof of concept in silico trial based on a cohort of 365 metastatic melanoma patients indicates that IZI1551/Birinapant responsiveness could be expected for up to 30% of tumours.

Materials and methods

Materials

TL32711 (Birinapant) was obtained from Active Biochem, Germany. IZI1551 was produced and purified as described before (Hutt et al. 2017). Q-VD-OPh was bought from Selleckchem, Germany. cIAP1 and cIAP2 recombinant proteins, required to determine absolute expression amounts in melanoma cells, were bought from R&D, Germany.

Melanoma cell lines and freshly isolated melanoma cells

Melanoma cell lines SkMel5 (ATCC; HTB-70), Malme 3M (ATCC; HTB-64), SkMel2 (ATCC; HTB-68), SkMel147 (Memorial Sloan Kettering Cancer Center; NY), WM3060 (Wistar; WC00126), WM1791c (Wistar; WC00086), MeWo (ATCC; HTB-65), Mel Juso (DSMZ; ACC74), WM1366 (Wistar; WC00078), WM115 (ATCC; CRL-1675), WM35 (Wistar; WC00060), WM3211 (Wistar, WC00045), WM793 (Wistar, WC00062), WM852 (Wistar, WC00065), WM1346 (Wistar, WC00121) and WM3248 (Wistar, WC00081) were purchased from ATCC (Manassas, VA, USA), DSMZ (Braunschweig, Germany) or the Wistar Institute (Philadelphia, PA, USA). Six cell lines carried activating BRAF mutations (WM35, WM793, WM3248, WM115, SkMel5 and Malme 3M), six cell lines NRAS mutations (WM1366, WM1346, SkMel147,

SkMel2, Mel Juso, WM3060), one cell line a CDK4 mutation (WM1791c), one cell line carried a c-KIT mutation (WM3211), one cell line carried both NRAS and BRAF mutations (WM852) and one cell line was BRAF/NRAS/c-KIT/CDK4 wildtype (MeWo). All cell lines were purchased as authenticated STR-profiled stocks directly from the vendors. Freshly isolated melanoma cells (M10, M20, M32, M34, M45) were obtained from metastases and prepared for experiments by the Department of Dermatology, University of Dresden, Germany. Two metastases carried BRAF activating mutations (M10 and M45), while three carried activating NRAS mutations (M20, M32 and M34). Further materials (M51_1, M52_2 and M54) were obtained for extended validation (M54, BRAF/NRAS wildtype; M51_1, M51_2 carried BRAF activating mutations). Cell isolates were obtained as part of routine resections at University Hospital Dresden, under the auspices of the local Ethics Committee (ethical approval number EK335082018). Informed consent was obtained from all subjects. Cells were maintained in RPMI-1640 (Thermo Fisher Scientific, Germany) supplemented with 10% (v/v) FBS Brazil One (PAN Biotech, Germany) at 37 °C and 5% CO_2. Mycoplasma testing was regularly conducted.

Culturing of 3D spheroids

Cells were harvested and diluted to the concentration of 10^4 cells/mL in RPMI-1640/10% FBS with the addition of 0.24% Methyl Cellulose (Sigma Aldrich, Germany). 250 cells per drop were placed into the lid of a Petri dish filled with PBS. Spheroids were incubated for 10 days at 37 °C and 5% CO_2. The medium was exchanged every other day. Slower growing Malme 3M cells and freshly obtained metastatic melanoma cells (M34) were seeded at 500 cells per drop and incubated for 2 weeks.

Flow cytometry

Semi high-throughput cell death measurements

Cells were washed, trypsinised and stained with propidium iodide (PI, Sigma Aldrich, Germany) at 1.33 µg/mL for 10 min. The measurements were performed on a high throughput flow cytometer (BD LSRII SORP) using the 488 nm laser for excitation, while emission was recorded at 617 nm. Flow cytometry data were analysed using Cyflogic v. 1.2.1 (CyFlo Ltd, Finland). All experiments were performed in triplicates and in $n = 3$ independent repeats.

Annexin V-GFP or APC/PI staining

Cells were harvested and washed in PBS and Annexin V Binding buffer (Biolegend, Germany). Cells were stained with Annexin V-APC (Biolegend, Germany) (0.1%) or Annexin V-GFP (made in-house, 0.1%) and PI (Biolegend, Germany) (1 µg/mL). Measurements were conducted on a BD FACS Canto II flow cytometer using 561 nm excitation (emission from 600 to 620 nm) (PI) or 640 nm excitation (emission from 655 to 685 nm) (APC). Alternatively, measurements were conducted with a MacsQuant flow cytometer using 488 nm excitation (emission from 655 to 730 nm (PI), and emission from 500 to 550 nm (GFP)). Flow cytometry data were analysed either with the BD FACS Diva software (BD Biosciences, USA) or with Flowing software (Turku Centre for Biotechnology, Finland).

TRAIL receptor measurements

Cells were harvested and blocked in ice-cold PBA buffer (1 × PBS, 0.25% BSA and 0.02% Sodium Azide). Surface death receptors were probed with the following antibodies for 1 h at 4 °C: mouse anti-TRAIL R1/TNFRSF 10A (1:100, R&D Systems), mouse anti-TRAIL R2/TNFRSF 10B (1:100, R&D Systems), mouse anti-TRAIL R3/TNFRSF 10C (1:100, R&D Systems) mouse anti-TRAIL R4/TNFRSF 10D (1:100, R&D Systems), purified mouse IgG1 (1:100, R&D Systems) and purified mouse IgG2b (1:100, R&D Systems). Secondary goat anti-mouse FITC conjugated antibody (1:50, Dako, Biozol, Germany) was added for 45 min at 4 °C. Cells were analysed in a MacsQuant flow cytometer using 488 nm excitation (emission was recorded at 500-550 nm). The surface expression of death receptors was calculated by calibration against quantification beads (QIFIKIT, Biozol, Germany), comparing the mean FITC signal of cells to calibration signals. Data were analysed with Flowing Software.

Western blot analysis

Protein quantification

Cells were trypsinised, washed in PBS, centrifuged and lysed in lysis buffer (150 mM NaCl, 1 mM EDTA, 20 mM TRIS, 1% Triton x-100, pH = 7.6) with addition of phosphatase inhibitor (PhosSTOP, 20×, Roche, Germany) and protease inhibitor cocktails (cOmplete, 20×, Roche, Germany). Spheroids were additionally sonicated. The total protein concentration was determined with Bradford assay. 20 µg of protein were resolved on Nu-PAGE™ 4–12% Bis–Tris Midi gels (Invitrogen, Thermo Fisher Scientific, Germany) at 200 V, 400 mA for 40 min, followed by transfer to nitrocellulose membranes using an iBlot device (Invitrogen, Thermo Fisher Scientific, Germany). The membranes were blocked in 0.5× Blocking Solution (Roche, Germany) for 1 h at room temperature. The

following primary antibodies were used for overnight incubations at 4 °C: mouse anti-Apaf-1 (1:1000; BD Transduction Laboratories), rabbit anti-Bak (1:1000; CST), rabbit anti-Bax (1:1000, CST), mouse anti-Bcl2 (1:1000; BD Transduction Laboratories) rabbit anti-Bcl-xL (1:1000, CST), mouse anti-Bid (1:1000, BD Transduction Laboratories), rabbit anti-Caspase 3 (1:1000; CST), mouse anti-Caspase 8 (1:1000; CST), rabbit anti-Caspase 9 (1:1000, CST), rabbit anti-cIAP1 (1:1000, Abcam), rabbit anti-cIAP2 (1:1000, Abcam), mouse anti-cFLIP (1:500, Abcam), mouse anti-cFLIP (1:500, Enzo), mouse anti-Cytochrome C (1:1000, BD Transduction Laboratories), rabbit anti-FADD (1:1000, Santa Cruz), rabbit anti-Mcl1 (1:1000, CST), mouse anti-PARP (1:1000, BD Transduction Laboratories), mouse anti-SMAC/DIABLO (1:1000, BD Transduction Laboratories), mouse anti-XIAP (1:1000, BD Transduction Laboratories), mouse anti-XIAP (1:1000, CST), mouse anti-actin (1:10000, CST). Subsequently, membranes were washed 3 × 10 min in TBST and incubated with secondary antibody (goat anti-rabbit IRDye 680 (1:10000) or goat anti-mouse IRDye 800 (1:5000) (LI-COR Biosciences) for 15 min at room temperature, followed by 10 min washing with TBST. Signals were captured on an Odyssey LiCor Imaging System. The quantification of proteins was performed on raw 16 bit images using Odyssey V3.0 software (LI-COR Biosciences). The intensities of the fluorescent signals were corrected for loading.

Data processing and analysis for predictor identification

All data processing and analysis were performed using a customised version of a previously developed pipeline [19]. The script was developed for MATLAB 2017b (The Mathworks, UK), equipped with the statistical toolbox. Prior to statistical analysis, protein data were mean-centred and scaled, dividing by the respective standard deviation. A principal component analysis (PCA) was performed on the standardised dataset and the PCs with an eigenvalue >1 were used for subsequent analyses. Linear discriminant analysis (LDA) was applied to objectively assess the accuracy of response class separation in the space defined by the first six PCs. Then, leave-one-out cross-validation (LOOCV) was applied iteratively to the 16-cell line panel to assess predictive capacity. For each iteration, data from 15 cell lines were used as a training set to define the PC space, and one test cell line was subsequently positioned according to its protein expression profile. LDA was then applied to determine if the test cell line was placed in the correct responsiveness sub-space. The response of 3D grown and patients-derived primary cell lines was predicted with the same workflow, using the predictor obtained from the data set of the 16-cell lines panel. The optimal predictive protein subset (reduced predictor) was determined using the *Select attributes* panel of the WEKA workbench (Version 3.8.2 [20]). A ranking of the proteins was obtained using the *CorrelationAttributeEval* attribute evaluator with *Ranker* search method and 10-fold cross-validation mode. This attribute selection method evaluates the *merit* of each protein individually by calculating the Pearson's correlation between the individual protein and the responsiveness class. The attribute selection step was performed using the proteins quantified in the 2D cell lines panel. The complete prediction pipeline was iteratively applied taking into account the first six PCs, and removing the protein with the lowest rank at each iteration. Statistical analyses not described above were performed with GraphPad Prism 7 (GraphPad Software).

In silico trial

The protein expression patterns of the melanoma cell line panel were used to estimate the protein expression profiles in melanoma tumours of 472 patients for which transcriptome data are deposited in the cancer genome atlas melanoma cohort (TCGA-SKCM). Normalised mRNA expression data (Upper Quartile normalised Fragments per Kilobase of transcript per Million mapped reads, log2 (FPKM-UQ+1)) generated by the Genomic Data Commons (GDC-NIH) were downloaded from the UCSC-XENA browser (Available at: https://xena.ucsc.edu/. Accessed: 4 February 2019). Data interpolation was performed using *Point-to-point* curve creation in GraphPad Prism 7 (GraphPad Software). Standard curves were generated using minimum and maximum values of protein expression range (cell line panel) and TCGA-SKCM back transformed mRNA expression data. For response predictions, PCA was applied to the data for the $n = 11$ predictor proteins in the cell lines dataset, followed by LDA-based definition of responsiveness and resistant subspaces, and subsequent positioning of $n = 365$ TCGA derived melanoma metastases in the PC space according to their estimated protein values.

Results

IAP antagonist Birinapant sensitises a subset of melanoma cell lines to apoptosis induced by the 2nd generation TRAIL-based biologic IZI1551

To study the responsiveness and the response heterogeneities of melanoma cells to IZI1551, a novel and translationally relevant hexavalent TRAIL receptor agonist [3], to the IAP antagonist TL32711/Birinapant, a compound currently evaluated in clinical trials [21], or combinations

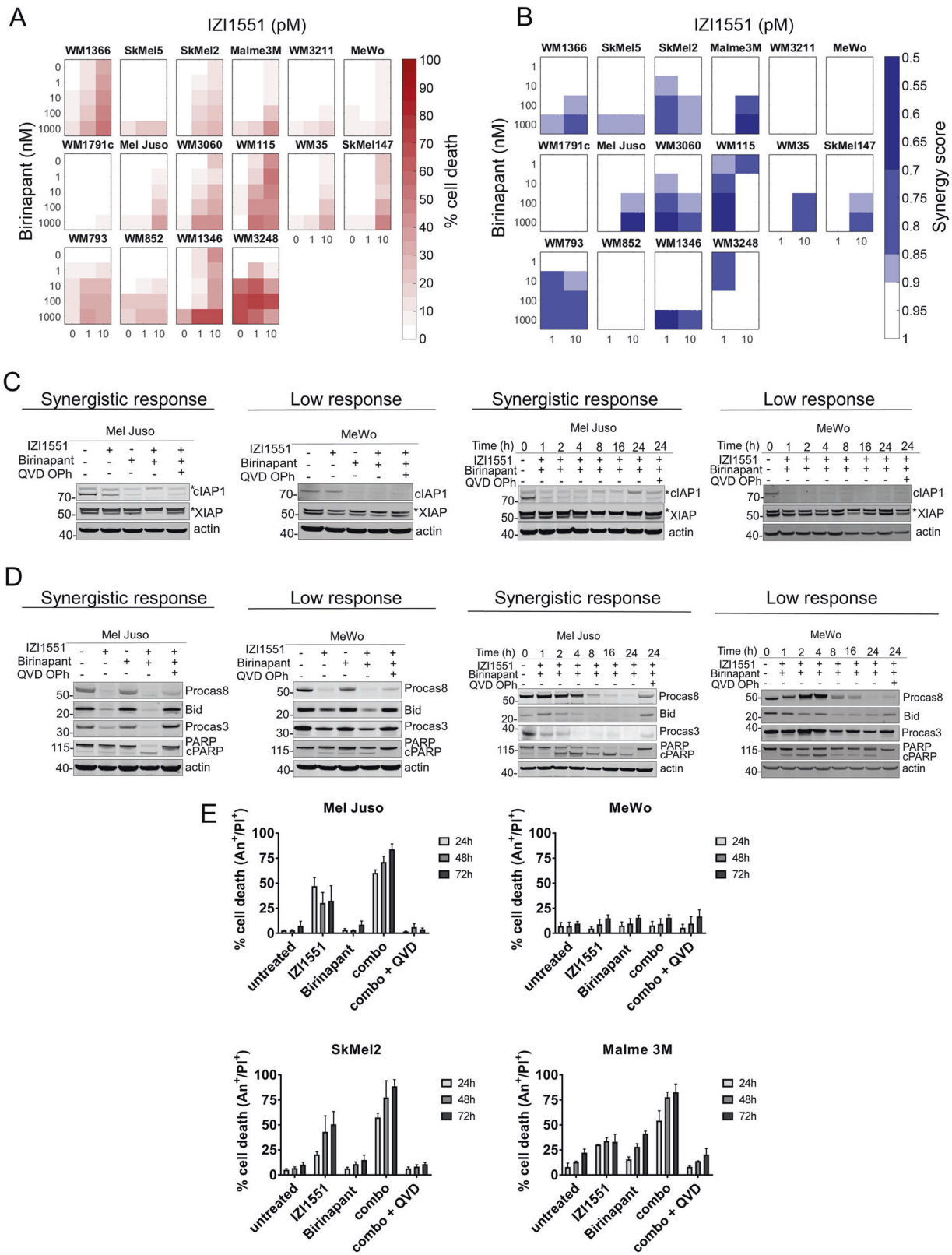

thereof, we employed a diverse set of sixteen cell lines (see materials and methods). For each cell line, cell death was determined at 15 treatment conditions, using semi-high throughput flow cytometry. Cell lines varied in their response to the treatments, ranging from high resistance to high sensitivity (Fig. 1a). Many cell lines responded

◀ **Fig. 1 IAP antagonist Birinapant sensitises a subset of melanoma cell lines to IZI1551-induced apoptosis.** **a** Melanoma cell lines respond heterogeneously to single and combination treatment of IZI1551 and Birinapant. Cells were treated for 72 h followed by flow cytometric determination of cell death (propidium iodide positivity). Data shown are means from $n = 3$ independent experiments. **b** Synergy scores for treatment combinations, as calculated by Webb's fractional product method. **c** Treatment-induced changes in IAP amounts, analysed by Western blotting. Actin served as loading control. Asterisks indicate unspecific bands. Representative results from $n = 3$ independent experiments are shown. **d** Apoptotic signalling was studied 24 h after single and combination treatment with IZI1551, Birinapant and Q-VD-OPh (30 μM). Actin served as a loading control. Representative results from $n = 3$ independent experiments are shown. **e** Melanoma cell lines die by apoptosis upon combination treatment. Cell lines were treated with 1 nM IZI1551, 1 μM Birinapant, with or without 30 μM Q-VD-OPh. Cells were stained with PI and Annexin V-APC and analysed by flow cytometry. Shown are mean values + SD of three independent experiments.

synergistically to the combination treatment (synergistic responders; WM1366, SkMel5, SkMel2, Malme3M, Mel Juso, WM3060, WM115, WM35, SkMel147, WM793, WM1346, WM3248), as determined using Webb's fractional product method, whereas others (WM3211, MeWo, WM1791c, WM852 cells) failed to do so (low responders) (Fig. 1b).

Birinapant had on-target activity in both synergistic responders and low responders, since cIAP1 protein amounts were efficiently and rapidly lost upon single agent and combination treatments (Fig. 1c). Neither single nor combination treatment induced detectable amounts of TNFα secretion (not shown), a response to IAP antagonists that in rare cases can contribute to autocrine cell death induction [22]. The amounts of XIAP remained largely unchanged, except for the combination treatment in synergistically responding Mel Juso cells (Fig. 1c). XIAP is a known caspase-3 substrate [23], and correspondingly caspase inhibitor Q-VD-OPh restored XIAP amounts, indicating that IZI1551/Birinapant induces apoptosis in responder cell lines such as Mel Juso (Fig. 1c). This was further supported by the processing of procaspases 8 and 3, and by the caspase-dependent cleavage of Bid and PARP in Mel Juso cells (Fig. 1d). In poorly responding MeWo cells, instead, PARP cleavage was modest and detectable only as a transient pulse (Fig. 1d, e). In line with these observations, caspase inhibitor Q-VD-OPh prevented IZI1551 and IZI1551/Birinapant induced cell death in Mel Juso cells and other synergistic responders, such as SkMel2 and Malme 3M (Fig. 1e).

Taken together, these results show that Birinapant sensitises a subset of human melanoma cell lines to cell death induced by IZI1551, a 2nd generation TRAIL-based therapeutic, and that apoptosis appears to be the primary cell death modality in synergistic responders.

Expression patterns of apoptosis proteins allow predicting IZI1551/Birinapant responsiveness

The combination of IZI1551/Birinapant can induce apoptotic cell death without the need for protein neosynthesis. We therefore next explored if baseline expression amounts of apoptosis proteins carry information on the responsiveness of melanoma cell lines to the combination of IZI1551/Birinapant. Pre-treatment amounts of 19 key pro- and anti-apoptotic players that regulate the apoptotic TRAIL signalling pathway was determined by quantitative immunoblotting at high dynamic range or, for death receptors, by cell surface staining (Fig. 2a; Supplemental Fig. 2). Expression patterns varied considerably between the proteins and across the cell lines. To explore possible correlations between protein expression patterns, we conducted a PCA. A total of six principle components (PCs), all with an eigenvalue >1 and thus fulfilling the Kaiser criterion [24], were required to capture approximately 80% of the data variance (Fig. 2b), highlighting that pre-treatment expression patterns were highly heterogeneous. Similarly, the associated weight coefficients indicated that individual proteins contributed heterogeneously to the first six PCs, without obvious positive or negative correlations between pro- and anti-apoptotic proteins (Fig. 2c). A visualisation of the cell line positions within the space defined by the first three PCs correspondingly failed to identify visually distinct clusters of cell lines (Fig. 2d). In conclusion, these data demonstrate high expression heterogeneity between proteins and between the cell lines.

Interestingly, colour coding the cell lines according to synergistic or low responsiveness indicated that synergistically responding and poorly responding cell lines occupy distinct regions within the plotted space (Fig. 2e). LDA confirmed this visual impression, with 14/16 cell lines (88%) correctly separated into their respective response categories. These results, therefore, indicate that even though apoptosis protein expression is highly heterogeneous across the cell lines, the expression patterns nevertheless carry information on the capability to respond synergistically to the combination of IZI1551/Birinapant.

We next tested if the protein expression patterns would be sufficient to predict responsiveness or resistance to IZI1551/Birinapant in melanoma cell lines. To this end, we performed LOOCV based on the approach described above. PCAs were conducted for sets of 15 cell lines, followed by LDAs to define the hyperspace regions of responsiveness and resistance. Missing cell lines were subsequently positioned into the LDA-segmented PC spaces according to their individual expression patterns of apoptosis regulators. If the tested cell line positioned into the correct response

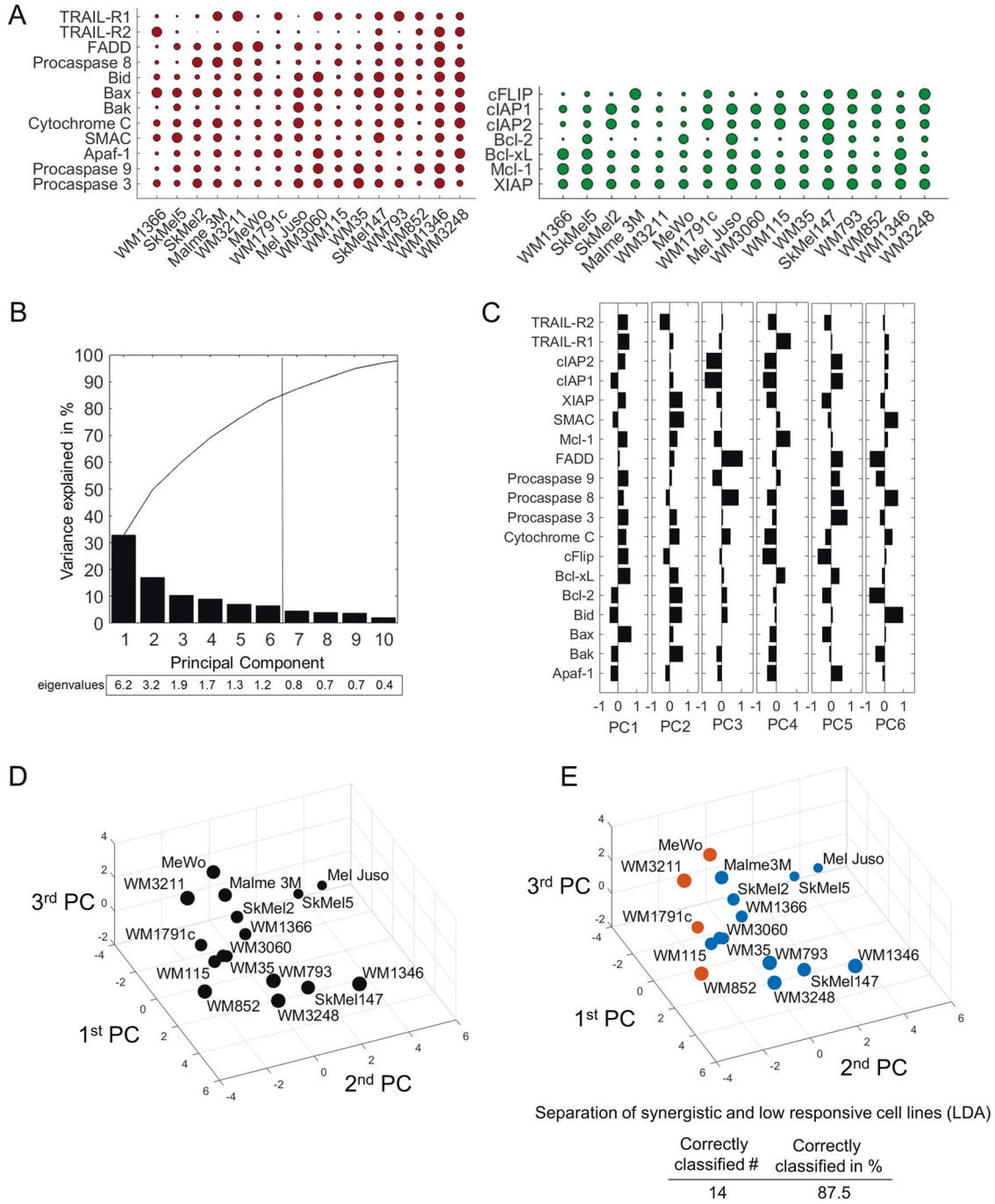

Fig. 2 Expression patterns of apoptosis proteins separate resistant from synergistically responding cell lines. a Baseline expression of pro- and anti-apoptotic proteins of the TRAIL pathway. Circles summarise 684 quantifications, and circle sizes represent relative expression amounts of the proteins between cell lines. Protein amounts are provided in Supplemental Table 1. **b** Percentage of the variance of the original dataset explained by PCs. PCs with an eigenvalue >1 were retained for further analysis. Accumulated "variance explained" is plotted in black. **c** Weight coefficient table. Bars represent the contributions of the respective proteins to the different PCs. **d** Cell lines positioned in a multidimensional space according to their individual protein expression profiles. The PC space shown was defined by the first three PCs. Circle sizes decrease with distance from the observer to aid 3D visualisation. **e** Colour coding indicates responsiveness of cell lines to IZI1551/Birinapant (orange = low response; blue = synergistic response). Table insert indicates accuracy of spatial segmentation between low and synergistic responders.

region, the prediction was considered successful (Fig. 3a). Overall, LOOCV was sufficient to correctly predict the responsiveness of 13 out of 16 cell lines (81%) (Fig. 3b), indicating that the measured protein panel allows predicting responsiveness to IZI1551/Birinapant on a case-by-case basis with high accuracy.

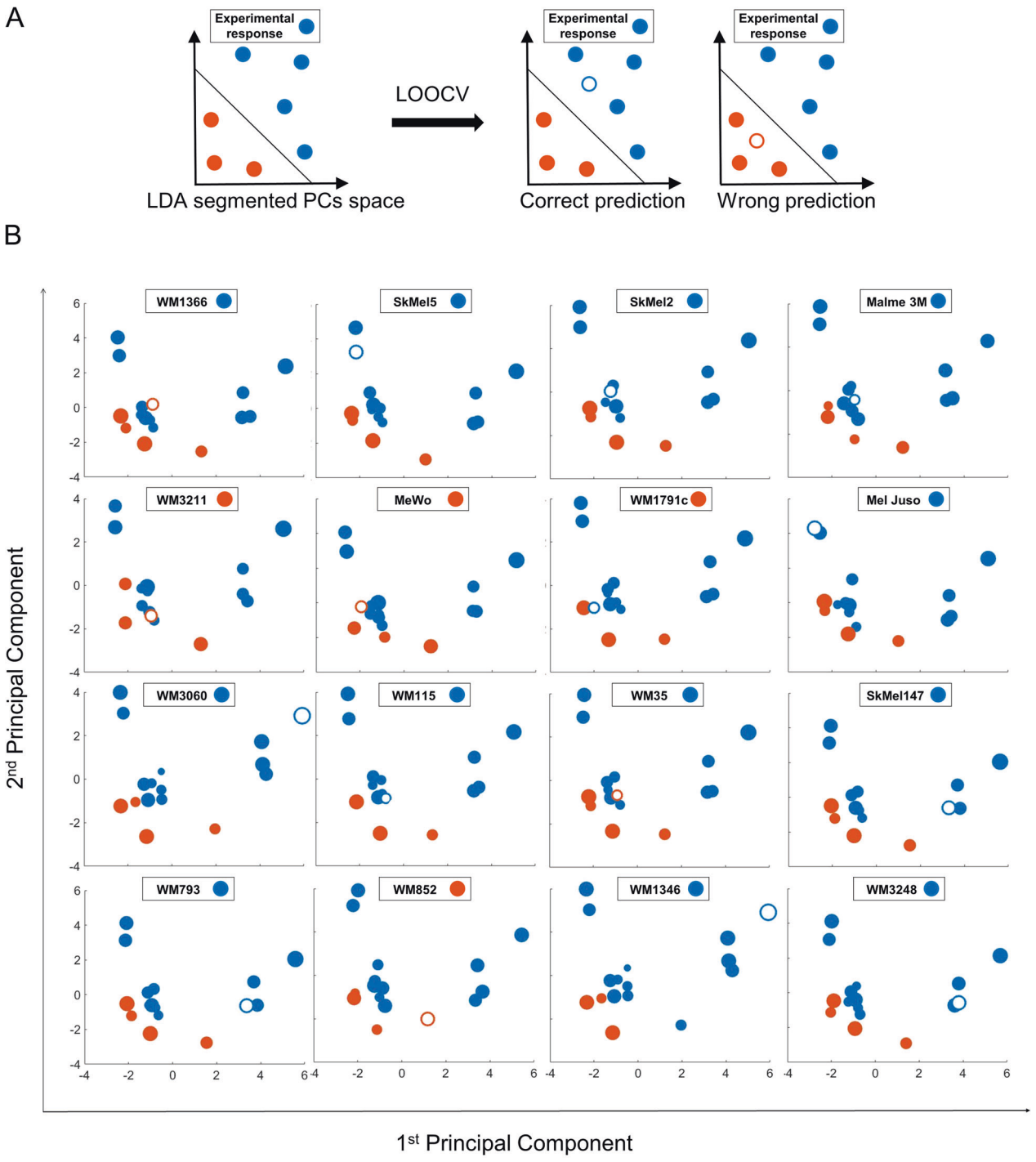

Leave One Out Cross Validation (LOOCV)

Correctly predicted #	Correctly predicted in %
13	81.25

◀ **Fig. 3 Expression patterns of apoptosis proteins allow predicting IZI1551/Birinapant responsiveness. a** Simplified 2D schematic showing the workflow for determining prediction accuracy by combined PCA/LDA/LOOCV. Following PCA, an LDA separates the PC space into areas for synergistic responsiveness and low responsiveness. A cell line of unknown responsiveness (empty circle) is then placed into the segmented PC space according to its protein expression profile, with the positioning serving as the response prediction. Experimental responsiveness data served to validate predictions. **b** 2D projection of LOOCV results for the 16 cell lines. The responsiveness of the test cell line was predicted (blue for synergistic, orange for low responsive). The empty circle represents the test cell line being placed into the PC space. Circle sizes decrease with distance from the observer to aid 3D visualisation. Table insert summarises prediction accuracy.

Responses to IZI1551/Birinapant can be predicted for 3D growth conditions

We next studied if responsiveness to IZI1551/Birinapant can be predicted for cells grown as MCTS. While more demanding as a cell culturing method, spheroids provide the advantage of higher microenvironmental complexity at nevertheless well-controlled experimental conditions [25]. Protein quantification from spheroids of five cell lines able to form MCTS demonstrated that the transition from 2D cell culture to 3D spheroid culture substantially affected protein expression patterns (Fig. 4a, b, Supplemental Fig. 3). A number of pro- as well as anti-apoptotic proteins were considerably downregulated, such as Bid, Bcl-2, Procaspase 3, FADD and Mcl-1. cFLIP and TRAIL-R1, instead, appeared to accumulate, and a number of other proteins changed heterogeneously in their expression amounts across spheroids of different cell lines (Fig. 4b). While a reductionist reasoning based on individual protein changes would intuitively suggest that IZI1551/Birinapant responsiveness of 3D MCTS should differ from 2D cultures, the combined complexity of altered protein expression prevents drawing conclusions prior to experimental validation. We therefore used the PCA/LDA-based approach to generate testable predictions on MCTS responsiveness. Positioning the MCTS forming cell lines into the PC space according to their respective pathway proteome revealed that their coordinates differed substantially from their 2D cultivated counterparts (Fig. 4c). Interestingly, despite the substantial changes in relative protein amounts, all cell lines were predicted to remain within their respective response class (Fig. 4c, colour-coded open circles). To test these in silico predictions, we measured cell death in spheroids treated with IZI1551, Birinapant or the combination thereof. Indeed, the predictions could be confirmed for all five cell lines, with SkMel2, WM1366, Mel Juso and Malme 3M responding to the combination treatment of IZI1551/Birinapant, and MeWo cells remaining resistant in the 3D growth scenario (Fig. 4d). TNFα was not secreted upon growth in 3D or in response to the treatments, as tested for Mel Juso and MeWo cells (not shown). Overall, we therefore conclude that a PCA/LDA-based prediction framework, parameterised with protein expression and treatment responsiveness data from 2D cell cultures, is sufficient to predict responses to IZI1551/Birinapant for 3D spheroid growth conditions.

Responses to IZI1551/Birinapant can be predicted for melanoma cells freshly isolated from metastases

For a translationally more relevant setting, we next tested if IZI1551/Birinapant responses can be predicted for melanoma cells freshly isolated from metastases. Following quantification of apoptosis regulatory proteins (Fig. 5a, Supplemental Fig. 4), cells were positioned into the PC space. Predictions were generated as described above and cells were colour coded according to their expected IZI1551/Birinapant responsiveness. M10, M20, M32 and M45 cells were predicted to respond to IZI1551/Birinapant combination treatment, whereas M34 cells were expected to respond poorly (Fig. 5b). Validation experiments confirmed the predictions on high responsiveness of M10, M32 and M20 cells and poor responsiveness of M34 cells (Fig. 5c). We therefore conclude that high predictions accuracies can also be achieved for cells freshly isolated from clinical materials.

A reduced predictor maintains performance and estimates response prevalence to IZI1551/Birinapant in metastatic melanoma

The framework to predict responsiveness to IZI1551/Birinapant builds on an otherwise unbiased selection of nineteen regulators known to be involved in canonical apoptosis signal transduction for this treatment combination. We next determined the contribution of the individual protein variables towards accurate predictions. To do so, we used the attribute selection feature of the WEKA workbench [20] to compute the "merit" of each protein, based on the protein expression profiles and the responsiveness data of the melanoma cell line panel. From this, we obtained a ranking of protein variables according to the degree of association with treatment responsiveness (in sequence of decreasing merit: XIAP, Procaspase 3, Cytochrome C, Mcl-1, cIAP1, Bax, Bid, Bcl-xL, Smac, FADD, Bak, cIAP2, TRAIL-R1, Procaspase 9, Apaf-1, TRAIL-R2, Procaspase 8, cFLIP and Bcl-2). We then iteratively performed predictions for the cell line panel, with the protein with the lowest merit removed upon each iteration. Performance was largely maintained (14/16 correct predictions for the cell line panel) when limiting the predictor to the eleven proteins with the highest merit (Fig. 6a). The reduced predictor correctly determined treatment responsiveness in 4/5 MCTS growth

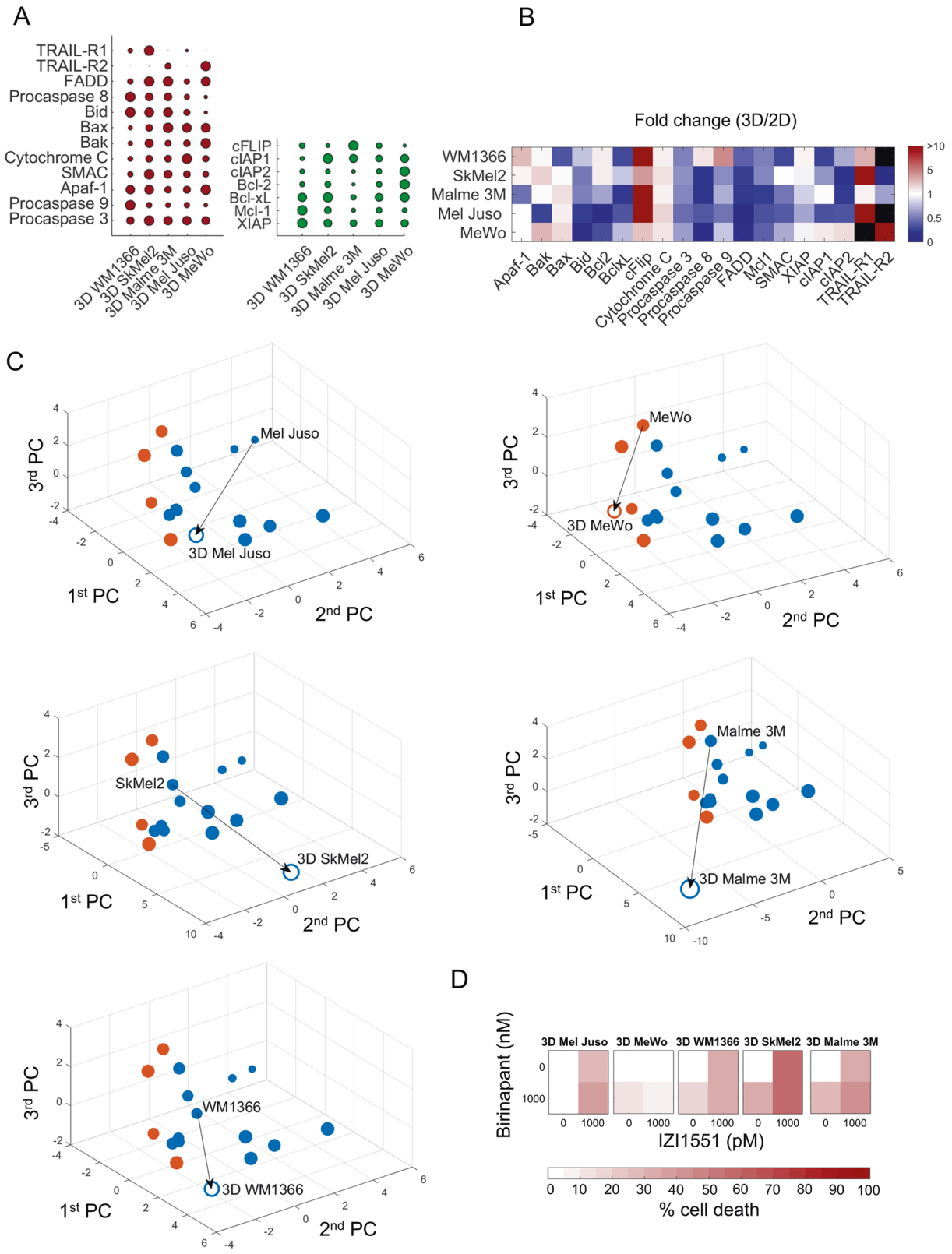

scenarios and in 4/5 biopsy-derived fresh melanoma cells (Fig. 6b, c). Further validation of the reduced predictor was conducted using nine additional and independently analysed samples, including three 2D and six 3D growth scenarios. Also in these samples prediction accuracies of approximately 80% were achieved (Fig. 6d–f, Supplemental

◀ **Fig. 4 Responses to IZI1551/Birinapant can be predicted for 3D growth conditions. a** Quantification of pro- and anti-apoptotic proteins in cell lines grown as MCTS (red and green, respectively). Circles summarise 285 quantifications and circle sizes represent mean protein quantities determined from at least $n = 3$ independent experiments. Protein amounts are provided in Supplemental table 1. **b** Heatmap showing the fold change in protein expression between 3D and 2D culture. Black colour indicates absence in either 2D or 3D conditions. **c** Positioning of cell lines grown in 3D in the PC space defined by 2D cultured cell lines. Empty circles indicate positions of cell lines grown in 3D. Arrows indicate the change of position in the PC space caused by altered protein expression between 2D to 3D growth conditions. Circle colours reflect expected responsiveness (blue) or resistance (orange), based on the LDA segmented PC space. The circle size decreases with distance from the observer to aid 3D visualisation. **d** Experimental validation of MCTS responsiveness to IZI1551/Birinapant treatment. MCTS of cell lines were treated with IZI1551 (1 nM) and Birinapant (1 μM) or their combination for 24 h. Cell death was measured by flow cytometry (PI uptake). Data show means of $n = 3$ measurements.

Fig. 5). Overall, we noted strong influences of XIAP and procaspase-3, direct interactors and regulators of type I signalling competency during extrinsic apoptosis [26, 27], and various members of the Bcl-2 family in the predictor (Fig. 6a). The ability to predict responsiveness to IZI1551/Birinapant in cell lines and ex vivo cultures raises the question if responses can be expected in patients, and if so, how frequent such responses might be. We therefore estimated the clinical response prevalence under the assumption that favourable drug pharmacokinetics and pharmacodynamics allow both drugs to reach their targets. Expression profiles of predictor variables were deduced from transcriptome data of metastatic melanoma patients ($n = 365$, TCGM-SKCM cohort, Supplemental Table 2) by mapping to protein expression ranges measured experimentally. Following positioning into the LDA segmented PC space defined by the predictor, 111 out of 365 patients were expected to respond to treatment (Fig. 6g). The expectation of approximately 30% responders needs to be interpreted in the context of predictor accuracy. The 80% prediction accuracy achieved in the cell line panel is composed of a predictor sensitivity of 92% and a specificity of 75%, so that the predictor strength lies in recalling true positives. Taken together, these results demonstrate that highly accurate predictions can be made for IZI1551/Birinapant responsiveness with a reduced set of input variables, and that in up to 30% of clinical cases an on target responsiveness could be expected, as estimated from a representative cohort of metastatic melanoma patients.

Discussion

Here, we report that protein expression signatures of TRAIL pathway regulators can serve to predict responsiveness to the combination of IZI1551 and Birinapant, targeted therapeutics with high translational relevance [7, 28]. High accuracies for response predictions were achieved for melanoma cell lines, for 3D multi-cellular melanoma spheroids and for cells newly isolated from melanoma metastases (approximately 80% prediction accuracy). Protein prioritisation resulted in a reduced marker that, when applied in a proof of concept in silico trial, suggests that IZI1551/Birinapant responsiveness could be expected in up to 30% of tumours in patients with metastatic melanoma.

Previous TRAIL-based therapeutics were tested in translational settings and performed unsatisfactorily [28]. Among the reasons for limited efficacy of TRAIL-R agonistic antibodies in the clinic were short serum half-lives and the requirement for immune cell-mediated, Fcγ-dependent clustering of therapeutic antibodies to induce efficient TRAIL-R1/R2 oligomerisation and caspase-8 activation [29]. 2nd generation TRAIL-based therapeutics address these problems, for example by increased valency and by using Fc regions as dimerisation and half-life extension modules [3, 4, 28]. IZI1551, consisting of two tri-valent single-chain TRAIL fragments cross-linked via the Fc part of an IgG antibody, is a prototypical example for this principle and potently induces apoptosis in vivo in cells moderately responsive to traditional TRAIL-based therapeutics [3]. However, in many cases sensitising co-treatments are required to ensure efficient apoptosis induction following TRAIL-R1/R2 activation. IAP antagonists are potent sensitisers to extrinsic apoptosis [21], suppressing the formation of LUBAC and the associated initiation of pro-survival signalling. IAP antagonists also sensitise to apoptosis induced by intrinsic cytotoxic stimuli, such as genotoxic therapeutics in pancreatic, colon and brain cancer [30–32], where cIAPs likely impair caspase-8 binding and activation on cytosolic ripoptosomes [33, 34].

While both 2nd generation TRAIL-R1/R2 agonists as well as IAP antagonists are currently tested in clinical trials (NCT03082209 [5, 21]), currently no studies test their combination. In addition, validated biomarkers predictive of treatment responsiveness do not exist for TRAIL-based therapeutics, IAP antagonists or the combination of both. The lack of reliable molecular markers to predict responses to TRAIL might indeed have contributed to the poor performance of TRAIL-based therapeutics in the clinical setting, since no patient selection could be performed [35]. The absence of response predictors for IAP antagonists likewise affects current clinical trials based on this class of therapeutics [21]. Notably, for both TRAIL-R1/R2 agonists as well as for IAP antagonists, the expression amounts of their direct molecular targets, i.e. TRAIL-R1/R2 amounts and cIAP

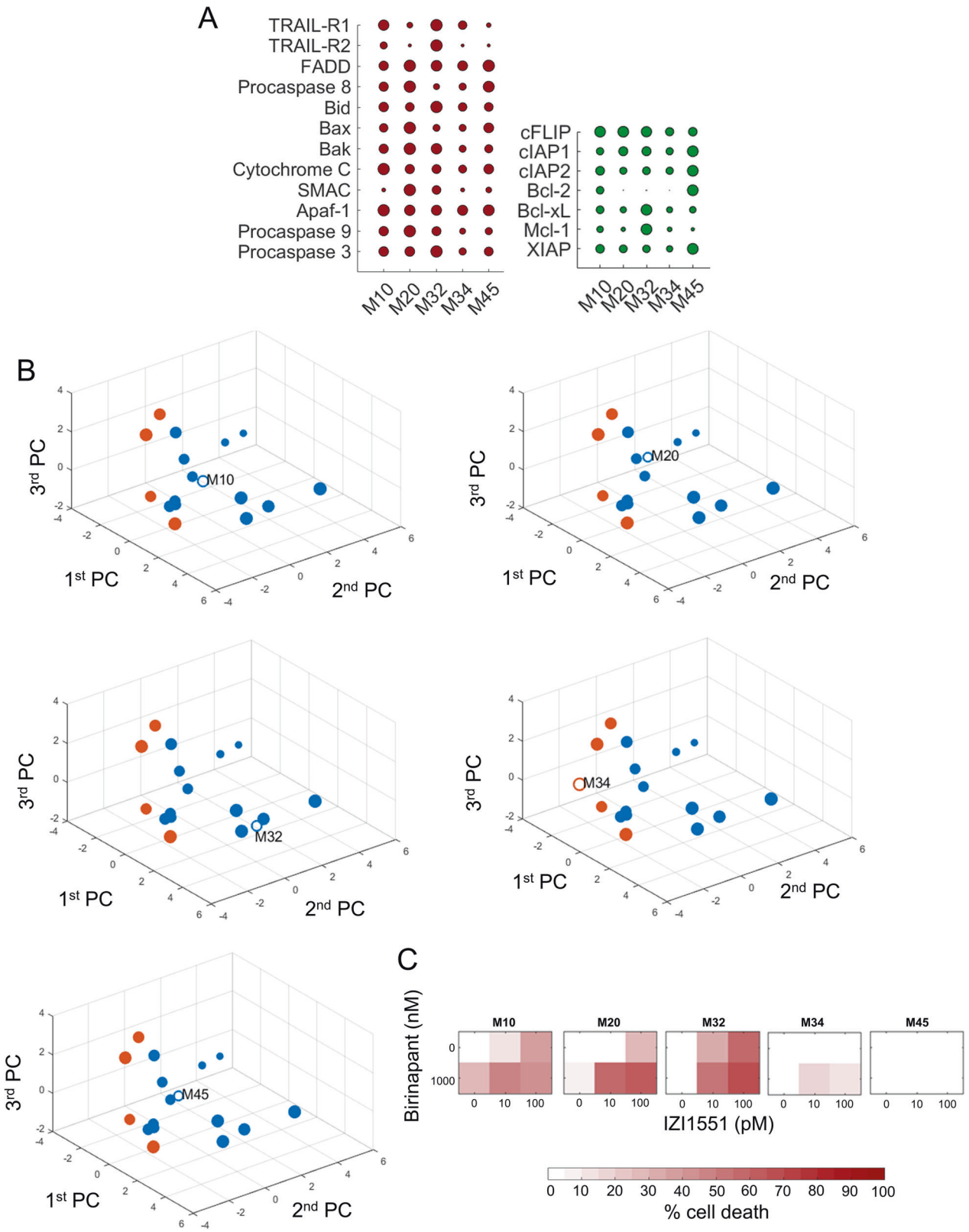

proteins, appear insufficient to derive response biomarkers [21, 36, 37]. This indicates that treatment efficacy is determined further downstream within the signal transduction network and/or too complex to be captured by traditional or reductionist biomarker discovery approaches.

◀ **Fig. 5 Responses to IZI1551/Birinapant can be predicted for cells isolated from melanoma metastases. a** Quantification of apoptosis regulatory proteins in cells derived from melanoma metastases. Red coloured circles represent pro-apoptotic and green circles anti-apoptotic proteins. Circles summarise 285 quantifications, and circle sizes represent mean protein quantities determined from at least $n = 3$ independent experiments. Protein amounts are shown in Supplemental table 1. **b** Positioning of melanoma cells from patient metastases in the PC space defined by 2D cultured cell lines. Empty circles indicate positions of patient cells. Circle colours reflect expected responsiveness (blue) or resistance (orange), based on the LDA segmented PC space. The circle size decreases with distance from the observer to aid 3D visualization. **c** Experimental validation of primary melanoma cell responsiveness to IZI1551/Birinapant treatment. Cells were treated as indicated for 24 h. Cell death was measured by flow cytometry (PI uptake). Heat maps show the mean of $n = 3$ independent experiments.

With IAP antagonists removing the apical suppression of extrinsic apoptosis induction, we hypothesised that the expression amounts of key regulatory proteins of the TRAIL signal transduction network can serve to predict responsiveness. Indeed, predictions on IZI1551/Birinapant responses, based on the expression patterns of key TRAIL pathway regulators, were highly accurate. Being able to predict responsiveness also in a micro-environmentally more complex 3D setting and in cells newly isolated from patients indicates that concerns about using continuously cultured cell lines to develop a predictor for IZI1551/Birinapant responsiveness can be alleviated, possibly because protein expression alone is sufficient to derive treatment responsiveness. Complex genetic characterisations and careful selection of cell line and in vivo models might, however, be warranted for studies on treatment scenarios that are highly dependent on disease-relevant mutations, and accordingly the genetic representation of the disease [38–40].

We initiated our study using 19 proteins considered key regulators of IZI1551/Birinapant induced signal transduction. We could reduce this panel to an 11 protein signature which, compared to traditional biomarkers, still seems rather large. However, this likely reflects the complexity of apoptosis signal transduction and regulation, as well as the disease heterogeneity observed in melanoma. The development of complex protein quantity-based biomarkers for routine clinical application still faces major technological challenges [41, 42]. Traditional immunohistochemical analyses of tumour biopsies typically provides insufficient dynamic range and limited calibration possibilities to derive reliable quantitative data. Alternative approaches, such as reverse phase protein arrays and mass spectrometric analyses of clinical specimen can overcome these hurdles, but are difficult to embed into routine pathology and laboratory workflows in the clinical environment. To take intra-tumour cell-to-cell heterogeneity into account, an aspect likely crucial to refine our predictor in a translational setting, technology such as mass cytometry could provide the possibility to capture multiplexed protein markers at the single cell level [43]. However, this technology is difficult to apply to tissue specimen. Developments in the field of high dynamic range fluorescence-based analysis of FFPE materials, coupled to multiplexing technologies that allow re-staining of tissue slices [44, 45], might more conveniently and routinely allow obtaining quantitative protein expression data, especially where entire cellular proteomes are not required.

It is noteworthy that none of the melanoma models studied lacked TRAIL-R1/R2 or caspase-8 expression, and TRAIL-Rs or caspase-8 amounts did not appear crucial to predict responsiveness. The amounts of these proteins therefore possibly do not limit IZI1551/Birinapant responsiveness in melanoma. A recent study in models of non-small-cell lung cancer and pancreatic ductal adenocarcinoma interestingly indicates that cancer cells might become addicted to TRAIL receptor expression, with autonomous TRAIL-R signalling contributing to disease progression [1]. Additionally, proliferating cells might rely on a cell death-independent role of caspase-8 in contributing to chromosome alignment during mitosis [46]. In the predictor, the expression of XIAP and caspase-3 strongly contributed to accurate response predictions. Both proteins play crucial roles in controlling cellular life/death decisions during apoptosis execution [10, 47]. XIAP additionally holds in check the "type I" link by which caspase-8 can activate caspase-3 [26, 27, 48]. However, kinetically the mitochondrial route still seems preferred in cells capable to die by type I signalling [26], most likely due to the strong amplification of apoptosis signalling by Bcl-2 family dependent mitochondrial outer membrane permeabilisation and apoptosome formation. Indeed, various Bcl-2 family members, such as Mcl-1, Bax, Bid, Bcl-xL and Bak, display prominently in the predictor. Mcl-1 and Bcl-xL negatively regulate Bax/Bak pore formation, while Bid is a primary substrate of both caspase-8 and caspase-3, with truncated Bid inhibiting Mcl-1 and Bcl-xL, and activating Bax and Bak [49]. Taken together, the interplay of caspases-3, XIAP and Bcl-2 family members, initiated by non-limiting amounts of TRAIL receptors and caspase-8, appears to play a central role in melanoma cell death upon exposure to IZI1551/Birinapant.

Taken together, this study represents a successful proof of concept for developing a stratification marker for malignant melanoma in response to a novel, clinically relevant combination treatment based on a 2nd generation hexavalent TRAIL variant (IZI1551) and a representative

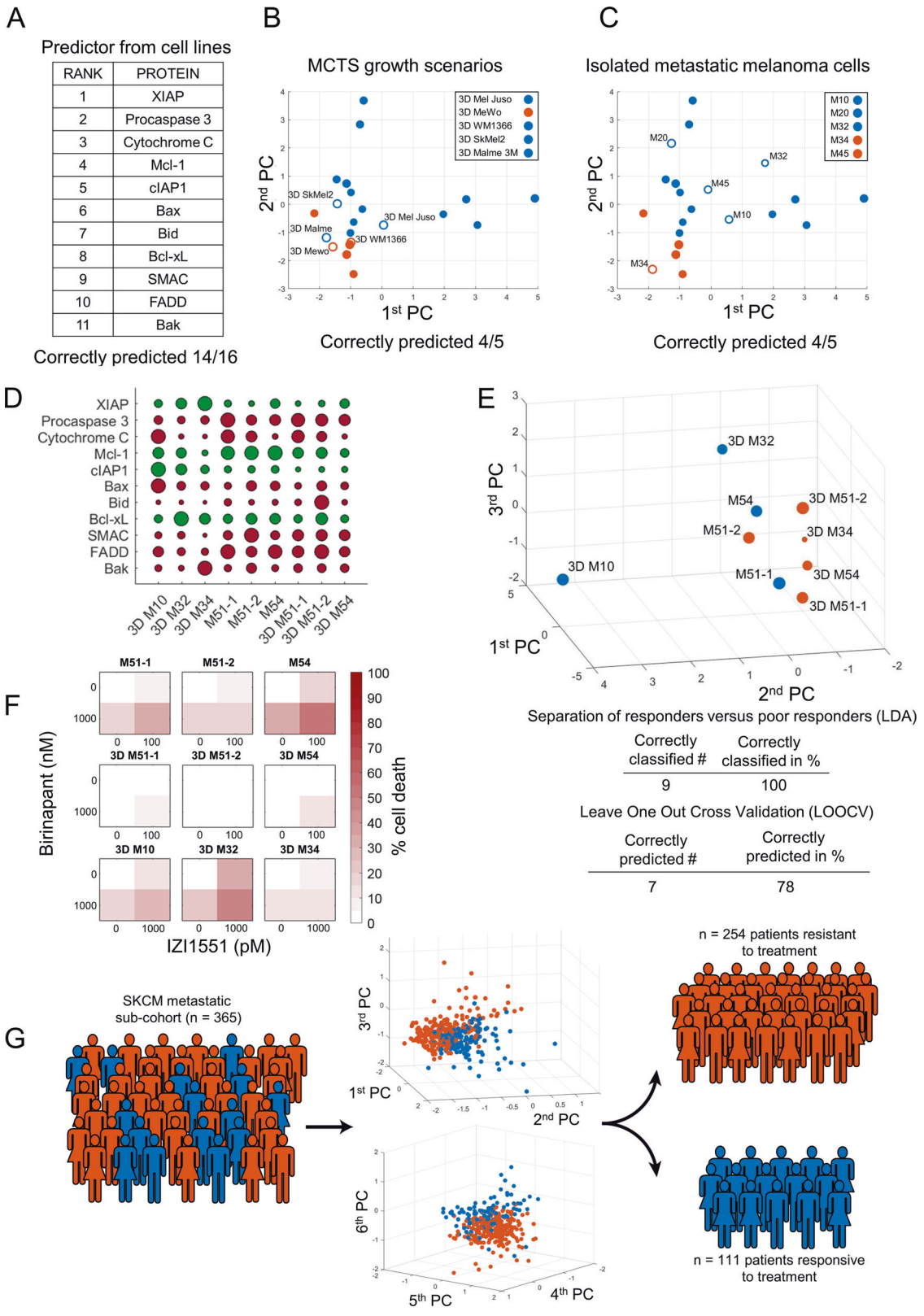

IAP antagonist, Birinapant. This can form the basis for future translational and clinical studies in which combination treatments of 2nd generation TRAIL-based therapeutics and IAP antagonists will be tested and for which optimal patient selection strategies are required.

◀ **Fig. 6 A reduced predictor maintains performance and estimates response prevalence to IZI1551/Birinapant in metastatic melanoma. a** Ranking of variables in a reduced predictor, as obtained by computed merit. **b**, **c** Responsiveness predictions and prediction accuracies for MCTS growth scenarios and for metastatic melanoma cells isolated from patients. The PC space is shown as a two-dimensional projection. Filled circles represent training data from the melanoma cell line panel. Open circles highlight positions of MCTS (**b**) or cells isolated from melanoma metastases (**c**). **d** Quantities of apoptosis regulators in additional validation samples. Circle sizes represent relative protein amounts. Protein amounts are listed in Supplemental table 1. Western blots are shown in Supplemental Fig. 5. **e** Validation samples positioned in the PC space obtained by the reduced predictor. Colour-coding indicates responsiveness. Table inserts display accuracy of spatial segmentation and prediction accuracy. **f** Experimental responsiveness of validation samples. Cells were treated as indicated for 24 h. Cell death was measured by flow cytometry (PI uptake). Heat maps show the mean of $n = 3$ independent experiments. **g** Estimation of response prevalence in a hypothetical trial. Estimated protein expression profiles of metastatic melanoma patients ($n = 365$) were used to predict responsiveness (blue, $n = 111$) or resistance (orange $n = 254$) to IZI1551/Birinapant combination treatment. 3D graphs show arrangement of predicted responders and non-responders in the predictor space.

Acknowledgements The authors kindly acknowledge support by the European Union's Horizon 2020 research and innovation programme under the Marie Skłodowska-Curie grant agreement #642295 (MELPLEX). MR and CG are funded by the Deutsche Forschungsgemeinschaft (DFG, German Research Foundation) under Germany's Excellence Strategy — EXC 2075 — 390740016. MR also receives support from the German Research Foundation (FOR2036 (MO 3226/1-1)) and the European Union's Horizon 2020 research and innovation programme (grant agreement #766069 (GLIO-TRAIN)) and the Health Research Board Ireland (HRA POR 2015 1091). The authors thank Doris Göttsch, Beatrice Reiser and Alexandra Kraske for technical assistance. Open access funding provided by Projekt DEAL.

Compliance with ethical standards

Conflict of interest R.E.K. is a named inventor on patent applications covering the scTRAIL technology (IZI1551). All remaining authors declare that they have no conflict of interest.

Publisher's note Springer Nature remains neutral with regard to jurisdictional claims in published maps and institutional affiliations.

References

1. von Karstedt S, Conti A, Nobis M, Montinaro A, Hartwig T, Lemke J, et al. Cancer cell-autonomous TRAIL-R signaling promotes KRAS-driven cancer progression, invasion, and metastasis. Cancer Cell. 2015;27:561–73.
2. von Karstedt S, Montinaro A, Walczak H. Exploring the TRAILs less travelled: TRAIL in cancer biology and therapy. Nat Rev Cancer. 2017;17:352–66.
3. Hutt M, Marquardt L, Seifert O, Siegemund M, Muller I, Kulms D, et al. Superior properties of Fc-comprising scTRAIL fusion proteins. Mol Cancer Ther. 2017;16:2792–802.
4. Gieffers C, Kluge M, Merz C, Sykora J, Thiemann M, Schaal R, et al. APG350 induces superior clustering of TRAIL receptors and shows therapeutic antitumor efficacy independent of cross-linking via Fcgamma receptors. Mol Cancer Ther. 2013;12:2735–47.
5. Morgan-Lappe SE. Abstract DDT01-03: ABBV-621: a best-in-class TRAIL-receptor agonist fusion protein that enhances optimal clustering for the treatment of solid and hematologic tumors. Cancer Res. 2017;77(13 Supplement):DDT01-03.
6. Lafont E, Kantari-Mimoun C, Draber P, De Miguel D, Hartwig T, Reichert M, et al. The linear ubiquitin chain assembly complex regulates TRAIL-induced gene activation and cell death. EMBO J. 2017;36:1147–66.
7. Fulda S, Vucic D. Targeting IAP proteins for therapeutic intervention in cancer. Nat Rev Drug Disco. 2012;11:109–24.
8. Benetatos CA, Mitsuuchi Y, Burns JM, Neiman EM, Condon SM, Yu G, et al. Birinapant (TL32711), a bivalent SMAC mimetic, targets TRAF2-associated cIAPs, abrogates TNF-induced NF-kappaB activation, and is active in patient-derived xenograft models. Mol Cancer Ther. 2014;13:867–79.
9. Darding M, Feltham R, Tenev T, Bianchi K, Benetatos C, Silke J, et al. Molecular determinants of Smac mimetic induced degradation of cIAP1 and cIAP2. Cell Death Differ. 2011;18:1376–86.
10. Taylor RC, Cullen SP, Martin SJ. Apoptosis: controlled demolition at the cellular level. Nat Rev Mol Cell Biol. 2008;9:231–41.
11. Allensworth JL, Sauer SJ, Lyerly HK, Morse MA, Devi GR. Smac mimetic Birinapant induces apoptosis and enhances TRAIL potency in inflammatory breast cancer cells in an IAP-dependent and TNF-alpha-independent mechanism. Breast Cancer Res Treat. 2013;137:359–71.
12. Vucic D. XIAP at the crossroads of cell death and inflammation. Oncotarget. 2018;9:27319–20.
13. Holcik M, Korneluk RG. XIAP, the guardian angel. Nat Rev Mol Cell Biol. 2001;2:550–6.
14. Caberlotto L, Lauria M. Systems biology meets-omic technologies: novel approaches to biomarker discovery and companion diagnostic development. Expert Rev Mol Diagn. 2015;15:255–65.
15. Goossens N, Nakagawa S, Sun X, Hoshida Y. Cancer biomarker discovery and validation. Transl Cancer Res. 2015;4:256–69.
16. Whiteman DC, Green AC, Olsen CM. The growing burden of invasive melanoma: projections of incidence rates and numbers of new cases in six susceptible populations through 2031. J Invest Dermatol. 2016;136:1161–71.
17. Hogan SA, Levesque MP, Cheng PF. Melanoma immunotherapy: next-generation biomarkers. Front Oncol. 2018;8:178.
18. Domingues B, Lopes JM, Soares P, Populo H. Melanoma treatment in review. Immunotargets Ther. 2018;7:35–49.
19. Rozanc J, Sakellaropoulos T, Antoranz A, Guttà C, Podder B, Vetma V, et al. Phosphoprotein patterns predict trametinib responsiveness and optimal trametinib sensitisation strategies in melanoma. Cell Death Differ. 2019;26:1365–78.
20. Frank E, Hall M, Trigg L, Holmes G, Witten IH. Data mining in bioinformatics using Weka. Bioinformatics. 2004;20:2479–81.
21. Fulda S. Promises and challenges of smac mimetics as cancer therapeutics. Clin Cancer Res. 2015;21:5030–6.
22. Krepler C, Chunduru SK, Halloran MB, He X, Xiao M, Vultur A, et al. The novel SMAC mimetic birinapant exhibits potent

activity against human melanoma cells. Clin Cancer Res. 2013;19:1784–94.
23. Deveraux QL, Leo E, Stennicke HR, Welsh K, Salvesen GS, Reed JC. Cleavage of human inhibitor of apoptosis protein XIAP results in fragments with distinct specificities for caspases. Embo J. 1999;18:5242–51.
24. Kaiser HF. The application of electronic computers to factor analysis. Educ Psychological Meas. 1960;20:141–51.
25. Vorsmann H, Groeber F, Walles H, Busch S, Beissert S, Walczak H, et al. Development of a human three-dimensional organotypic skin-melanoma spheroid model for in vitro drug testing. Cell death Dis. 2013;4:e719.
26. Aldridge BB, Gaudet S, Lauffenburger DA, Sorger PK. Lyapunov exponents and phase diagrams reveal multi-factorial control over TRAIL-induced apoptosis. Mol Syst Biol. 2011;7:553.
27. Wilson TR, McEwan M, McLaughlin K, Le Clorennec C, Allen WL, Fennell DA, et al. Combined inhibition of FLIP and XIAP induces Bax-independent apoptosis in type II colorectal cancer cells. Oncogene. 2009;28:63–72.
28. de Miguel D, Lemke J, Anel A, Walczak H, Martinez-Lostao L. Onto better TRAILs for cancer treatment. Cell Death Differ. 2016;23:733–47.
29. Wilson NS, Yang B, Yang A, Loeser S, Marsters S, Lawrence D, et al. An Fcgamma receptor-dependent mechanism drives antibody-mediated target-receptor signaling in cancer cells. Cancer Cell. 2011;19:101–13.
30. Crawford N, Salvucci M, Hellwig CT, Lincoln FA, Mooney RE, O'Connor CL, et al. Simulating and predicting cellular and in vivo responses of colon cancer to combined treatment with chemotherapy and IAP antagonist Birinapant/TL32711. Cell Death Differ. 2018;25:1952–66.
31. Dineen SP, Roland CL, Greer R, Carbon JG, Toombs JE, Gupta P, et al. Smac mimetic increases chemotherapy response and improves survival in mice with pancreatic cancer. Cancer Res. 2010;70:2852–61.
32. Ziegler DS, Keating J, Kesari S, Fast EM, Zawel L, Ramakrishna N, et al. A small-molecule IAP inhibitor overcomes resistance to cytotoxic therapies in malignant gliomas in vitro and in vivo. Neuro-Oncol. 2011;13:820–9.
33. Feoktistova M, Geserick P, Kellert B, Dimitrova DP, Langlais C, Hupe M, et al. cIAPs block ripoptosome formation, a RIP1/Caspase-8 containing intracellular cell death complex differentially regulated by cFLIP isoforms. Mol Cell. 2011;43:449–63.
34. Tenev T, Bianchi K, Darding M, Broemer M, Langlais C, Wallberg F, et al. The Ripoptosome, a signaling platform that assembles in response to genotoxic stress and loss of IAPs. Mol Cell. 2011;43:432–48.
35. Lemke J, von Karstedt S, Zinngrebe J, Walczak H. Getting TRAIL back on track for cancer therapy. Cell Death Differ. 2014;21:1350–64.
36. Wagner KW, Punnoose EA, Januario T, Lawrence DA, Pitti RM, Lancaster K, et al. Death-receptor O-glycosylation controls tumor-cell sensitivity to the proapoptotic ligand Apo2L/TRAIL. Nat Med. 2007;13:1070–7.
37. Zakaria Z, Tivnan A, Flanagan L, Murray DW, Salvucci M, Stringer BW, et al. Patient-derived glioblastoma cells show significant heterogeneity in treatment responses to the inhibitor-of-apoptosis-protein antagonist birinapant. Br J Cancer. 2016;114:188–98.
38. Fang Y, Eglen RM. Three-dimensional cell cultures in drug discovery and development. SLAS Discov. 2017;22:456–72.
39. Luebker SA, Zhang W, Koepsell SA. Comparing the genomes of cutaneous melanoma tumors to commercially available cell lines. Oncotarget. 2017;8:114877–93.
40. Garman B, Anastopoulos IN, Krepler C, Brafford P, Sproesser K, Jiang Y, et al. Genetic and genomic characterization of 462 melanoma patient-derived xenografts, tumor biopsies, and cell lines. Cell Rep. 2017;21:1936–52.
41. Panis C, Pizzatti L, Souza GF, Abdelhay E. Clinical proteomics in cancer: where we are. Cancer Lett. 2016;382:231–9.
42. Petricoin EF, Zoon KC, Kohn EC, Barrett JC, Liotta LA. Clinical proteomics: translating benchside promise into bedside reality. Nat Rev Drug Discov. 2002;1:683–95.
43. Spitzer MH, Nolan GP. Mass cytometry: single cells, many features. Cell. 2016;165:780–91.
44. Gerdes MJ, Sevinsky CJ, Sood A, Adak S, Bello MO, Bordwell A, et al. Highly multiplexed single-cell analysis of formalin-fixed, paraffin-embedded cancer tissue. Proc Natl Acad Sci USA. 2013;110:11982–7.
45. Schubert W, Bonnekoh B, Pommer AJ, Philipsen L, Bockelmann R, Malykh Y, et al. Analyzing proteome topology and function by automated multidimensional fluorescence microscopy. Nat Biotechnol. 2006;24:1270–8.
46. Liccardi G, Ramos Garcia L, Tenev T, Annibaldi A, Legrand AJ, Robertson D, et al. RIPK1 and Caspase-8 ensure chromosome stability independently of their role in cell death and inflammation. Mol Cell. 2019;73:413–28. e417.
47. Rehm M, Huber HJ, Dussmann H, Prehn JH. Systems analysis of effector caspase activation and its control by X-linked inhibitor of apoptosis protein. Embo J. 2006;25:4338–49.
48. Jost PJ, Grabow S, Gray D, McKenzie MD, Nachbur U, Huang DC, et al. XIAP discriminates between type I and type II FAS-induced apoptosis. Nature. 2009;460:1035–9.
49. Hantusch A, Rehm M, Brunner T. Counting on death—quantitative aspects of Bcl-2 family regulation. FEBS J. 2018;285:4124–38.

Guttà et al. *Cell Death and Disease* (2020)11:124
https://doi.org/10.1038/s41419-020-2309-3

Cell Death & Disease

ARTICLE Open Access

Low expression of pro-apoptotic proteins Bax, Bak and Smac indicates prolonged progression-free survival in chemotherapy-treated metastatic melanoma

Cristiano Guttà[1], Arman Rahman[2,3], Claudia Aura[2,3,4], Peter Dynoodt[2,5], Emilie M. Charles[4,6,7], Elodie Hirschenhahn[4,6,7], Jesuchristopher Joseph[2,6], Jasper Wouters[2,5,8,9], Ciaran de Chaumont[2,6], Mairin Rafferty[2], Madhuri Warren[4], Joost J. van den Oord[5], William M. Gallagher[2,3] and Markus Rehm[1,6,7,10,11]

Abstract

Despite the introduction of novel targeted therapies, chemotherapy still remains the primary treatment for metastatic melanoma in poorly funded healthcare environments or in case of disease relapse, with no reliable molecular markers for progression-free survival (PFS) available. As chemotherapy primarily eliminates cancer cells by apoptosis, we here evaluated if the expression of key apoptosis regulators (Bax, Bak, Bcl-2, Bcl-xL, Smac, Procaspase-9, Apaf-1, Procaspase-3 and XIAP) allows prognosticating PFS in stage III/IV melanoma patients. Following antibody validation, marker expression was determined by automated and manual scoring of immunohistochemically stained tissue microarrays (TMAs) constructed from treatment-naive metastatic melanoma biopsies. Interestingly and counter-intuitively, low expression of the pro-apoptotic proteins Bax, Bak and Smac indicated better prognosis (log-rank $p < 0.0001$, $p = 0.0301$ and $p = 0.0227$ for automated and $p = 0.0422$, $p = 0.0410$ and $p = 0.0073$ for manual scoring). These findings were independently validated in the cancer genome atlas (TCGA) metastatic melanoma cohort (TCGA-SKCM) at transcript level (log-rank $p = 0.0004$, $p = 0.0104$ and $p = 0.0377$). Taking expression heterogeneity between the markers in individual tumour samples into account allowed defining combinatorial Bax, Bak, Smac signatures that were associated with significantly increased PFS ($p = 0.0002$ and $p = 0.0028$ at protein and transcript level, respectively). Furthermore, combined low expression of Bax, Bak and Smac allowed predicting prolonged PFS (> 12 months) on a case-by-case basis (area under the receiver operating characteristic curve (ROC AUC) = 0.79). Taken together, our results therefore suggest that Bax, Bak and Smac jointly define a signature with potential clinical utility in chemotherapy-treated metastatic melanoma.

Introduction

Melanoma, an aggressive neoplasm originating from the malignant transformation of melanocytes, rapidly metastasises if not surgically removed at an early stage. Although novel and costly targeted treatment options and immunotherapies have significantly improved the management of metastatic disease[1–3], patients in poorly funded healthcare environments still rely on chemotherapy as the primary first-line treatment. Likewise, chemotherapy remains in frequent use as a second- or last-line treatment option in otherwise refractory or in recurrent disease. Even though treatments based on the DNA-alkylating

Correspondence: Markus Rehm (markus.morrison@izi.uni-stuttgart.de)
[1]Institute of Cell Biology and Immunology, University of Stuttgart, Stuttgart, Germany
[2]Oncomark Ltd., Nova UCD, Dublin 4, Ireland
Full list of author information is available at the end of the article.
Edited by T. Kaufmann

SPRINGER NATURE CDDpress

agent dacarbazine have been the chemotherapeutic standard of care for metastatic melanoma for > 30 years, chemotherapy may benefit only few patients[4,5]. The median survival of patients treated with dacarbazine-based chemotherapy lies in the range of 6–9 months[6–8], with no reliable molecular markers available that would allow to identify those patients in which disease progression is substantially delayed and which therefore might have benefited from this treatment.

Apoptosis is the main cell death mechanism by which the body tries to eliminate transformed and therefore potentially cancerous cells. Apoptosis likewise is the primary cell death modality induced by dacarbazine and other DNA-alkylating agents. DNA alkylation induces the intrinsic apoptosis pathway, as was shown experimentally in various melanoma model systems[9,10]. Pro- and anti-apoptotic Bcl-2 family members, such as Bax, Bak and Bcl-2, Bcl-xL, respectively, regulate the mitochondrial apoptosis signalling hub[11]. Activated Bax and Bak form pores in the outer mitochondrial membrane, leading to the release of pro-apoptotic factors, such as Smac, into the cytosol[12]. Subsequently, the execution phase of apoptosis is initiated, during which proteases such as initiator caspase-9 and effector caspase-3 are activated in an Apaf-1-dependent manner. These proteases then rapidly execute apoptotic death, but can be inhibited by the anti-apoptotic protein XIAP, which itself is targeted by Smac[13]. Impaired apoptosis signalling is a hallmark of cancer[14], based on which it is reasonable to assume that melanoma cells are highly apoptosis resistant. Indeed, experimental studies suggest that melanoma cells either are highly chemoresistant or acquire resistance and thereby evade apoptotic cell death[15,16]. However, it is less clear if perturbed expression of apoptosis regulators is indeed associated with patient prognosis in the clinical scenario. Various studies immunohistochemically assessed individual apoptosis regulators as potential protein biomarkers for melanoma progression and patient survival[17,18]. Unfortunately though, the majority of studies lack controls and validation information that would support the specificity of the used reagents and staining protocols. Not surprisingly, results obtained so far remained largely inconclusive or even contradictory[17]. Additionally, apoptosis regulators at key signalling hubs frequently act cooperatively and redundantly, so that it can be speculated that single molecule makers might not be sufficiently robust for clinical use.

In this study, we therefore assessed the expression of nine apoptosis regulators (Bax, Bak, Bcl-2, Bcl-xL, Smac, Procaspase-9, Apaf-1, Procaspase-3 and XIAP) in metastatic melanoma tissues by immunohistochemistry (IHC), using antibodies that passed rigorous validation. Interestingly, low expression of Bax, Bak and Smac associated with prolonged progression-free survival (PFS), a finding confirmed at transcriptional level in an independent cohort. Combining Bax, Bak and Smac expression with a pattern recognition approach allowed predicting individual patient PFS with high accuracy. Taken together, our results identified a putative combinatorial prognostic signature with potential clinical utility for chemotherapy-treated metastatic melanoma.

Materials and methods

Ethics approval and consent to participate

The use of the patient cohort was approved by the Medical Ethical Committee and Institutional Review Board (OG032) of the University Hospitals of KU Leuven (reference number ML10659) and by the UZ Leuven Biobank (reference number S56609).

Antibodies

The following antibodies were used for immunoblotting and immunohistochemistry. A rabbit polyclonal beta Actin antibody (Santa Cruz Biotechnology; sc-81178); Apaf-1 (Cell Signalling; D5C3), Bak (Abcam; ab32371), Bax (Millipore; ABC11), Bcl-2 (Dako; MO887), Bcl-xL (BD labs; 610212), Procaspase-3 (Cell Signalling; 9662), Procaspase-9 (Cell Signalling; 9502), Smac (Cell Signalling; 2954), XIAP (BD labs; 610762).

Cell culturing

For antibody validation, the following human cancer cell lines were used: A375, HCT-116, HCT-116 (Bax/Bak)$^{-/-}$, HCT-116 Smac$^{-/-}$, HCT-116 XIAP$^{o/-}$, HeLa, Jurkat Casp-9$^{-/-}$, MCF-7, PM-WK, Preyer, SK-Mel-94. Cell lines were obtained from ATCC, DSMZ or provided by colleagues (Professor Martin Leverkus, University of Heidelberg; Professor Richard Youle, National Institutes of Health, USA; Professor Richard Vogelstein, The Johns Hopkins University School of Medicine, USA; Professor Ingo Schmitz, University of Braunschweig, Germany; Professor Sebastian Wesselborg, University of Düsseldorf, Germany; Professor Maria Soengas, National Cancer Research Centre, Spain) and described before[19–24]. Cell lines were cultured in RPMI-1640 medium (Sigma-Aldrich) or Dulbecco's Modified Eagle Medium (DMEM; Lonza, Slough, UK) supplemented with 4 mM L-glutamine, 4.5 g/l glucose, 10% (w/v) heat-inactivated fetal bovine serum (Sigma-Aldrich), 100 U/ml penicillin and 100 µg/ml streptomycin (Sigma-Aldrich). Cells were grown at 5% CO_2 and 37°C.

Immunoblotting

For whole cell extracts, cells were collected at 400 *g* for 3 min and washed with phosphate-buffered saline. Cells were re-suspended in lysis buffer (62.5 mM Tris-HCl, pH 6.8, 10% (v/v) glycerine, 2% (w/v) sodium dodecyl sulfate (SDS), 1 mM phenylmethylsulfonyl fluoride, 1 µg/ml

Table 1 Summary of demographics and clinical information of the patients included in the study.

Characteristics		
Gender	*Value*	*%*
Male	30	51.7
Female	28	48.3
Age at surgery (years)	*Value*	*%*
< 65	44	75.9
≥ 65 and < 75	8	13.8
> 75	6	10.3
Metastatic melanoma location	*Value*	*%*
Distant skin site	10	17.2
Distant organ	17	29.3
Distant lymph node	28	48.3
Distant subcutaneous site	3	5.2
Metastasis stage	*Value*	*%*
M1a	8	13.8
M1b	8	13.8
M1c	42	72.4
Primary melanoma type	*Value*	*%*
Cutaneous	46	79.3
Mucosal	1	1.7
Ocular	2	3.4
Unknown	9	15.5
Treatment	*Value*	*%*
Dacarbazine	3	5.2
Dacarbazine, Cisplatin	54	93.1
Dacarbazine, Carboplatin	1	1.7
Overall survival	t_0 = *sample collection*	t_0 = *chemotherapy start*
Median (range) in months	19 (2–126)	11 (0–87)
Progression-free survival	t_0 = *sample collection*	t_0 = *chemotherapy start*
Median (range) in months	10 (1–100)	4 (0–83)

pepstatin A, 1 μg/ml leupeptin, and 5 μg/ml aprotinin) and heated at 95 °C for 20 min. Protein content was determined with the Pierce Micro-BCA protein assay (Pierce, Northumberland, UK). An equal amount of protein (20 μg) was loaded onto SDS-polyacrylamide gels. Proteins were separated at 100 V for 2.5 h and then blotted to nitrocellulose membranes (Protean BA 83; 2 μm; Schleicher & Schuell) in transfer buffer (25 mM Tris, 192 mM glycine, 20% methanol (v/v), and 0.01% SDS) at 18 V for 60 min. The blots were blocked with 5% non-fat dry milk in Tris-buffered saline with Tween 20 (TBST) (15 mM Tris-HCl, pH 7.5, 200 mM NaCl, and 0.1% Tween 20) at room temperature for 1 h. Membranes were incubated with the primary antibodies at room temperature for 2 h or overnight at 4°C. Membranes were washed with TBST three times for 5 min and incubated with peroxidase-conjugated secondary antibodies (Jackson Laboratories) for 1 h. Blots were washed and developed using the enhanced chemiluminescence detection reagent (Millipore, Ireland).

Preparation of cell pellets for IHC

Cells were grown to a confluence of 50–75%. Cells were then detached and suspended in 10% phosphate-buffered formalin at room temperature and fixed for 4–6 h. Fixed cells were centrifuged at 500 × *g* for 3 min, washed once with 1 × PBS and pelleted again. A 1% agarose solution was prepared in 1 × PBS and cooled down to 40 °C in a water bath. The cell/agarose mixtures were transferred into plugs and let solidify. The agarose plugs were processed into paraffin blocks using standard tissue processing. Cell pellet samples (typically 0.6 mm in diameter) were then used for analysis.

Tissue microarrays (TMAs)

TMAs of formalin-fixed paraffin-embedded (FFPE) tumour samples derived from 74 melanoma patients treated with Dacarbazine (alone or in combination with cisplatin or carboplatin), were generated. The TMA contained duplicate cores obtained from 14 primary melanomas, 62 metastatic melanomas and adjacent normal tissue. Demographics, clinical and follow-up information were available for the entire cohort. A total of $n = 58$ samples, representing untreated metastatic melanoma patients, were analysed for this study (Table 1).

Immunohistochemistry

IHC staining on FFPE cell pellets and tissue microarrays (TMA) was performed using an automated IHC platform (Link-48, Dako, Glostrup, Denmark) according to the manufacturer's instructions. Sections (4 μm in thickness) were deparaffinised and antigen retrieval was performed at 95 °C for 15 min in appropriate buffer (high pH buffer, pH 9.0; low pH buffer, pH 6.0) using the PT-Link module (Dako, Glostrup, Denmark). A polymer-based detection system (EnVision Flex, Dako) was used with Permanent Red as the chromogen, resulting in a red colour endpoint that contrasted well with brown melanin. Sections were counterstained with haematoxylin. Positive and negative controls (omission of the primary antibody and replacement with the IgG-2a isotype control, mouse-ab18443; IgG isotype control, rabbit-ab208334, Abcam, Cambridge,

UK) were included in each run. In addition, a Haematoxylin and Eosin (H&E) staining was performed for all slides of the TMAs, enabling pathologists to check for TMA core integrity, quality and tumour content.

Core quality assessment

A pathological review of the H&E-stained sections and TMA blocks was conducted to define the quality of individual tissue cores and to assess the percentage of tumour tissue in each core. Each core was individually observed to determine whether there were any tissue artifacts (poorly fixed tissue, folded tissue, no tumour present, no tissue present, foreign material introduced at embedding, poor tissue microscopic details) or staining artifacts (knife marks across section, holes, clumps of stain precipitate, air bubbles), which would have compromised either the manual or automated image analysis. All quality assessments were independently validated by a second pathologist. Cores with compromising artifacts or with insufficient percentage of tumour cells were excluded from further analyses.

Manual and automated scoring

IHC materials were first viewed at low power to judge overall quality and distribution of staining. Subsequently, staining frequency (total % stained cells) and staining intensity (intensity of stained cells; 0 = no staining, 1+ = weak staining, 2+ = moderate staining, 3+ = strong staining) were determined. Histoscores (*H* scores) were then calculated as follows:

$$H\text{score} = 1\times \%_{cells\ 1+} + 2\times \%_{cells\ 2+} + 3\times \%_{cells\ 3+}$$

The manual scoring was performed on images acquired with the Aperio ScanScope XT slide scanner (Aperio Technologies, Vista, CA) used at × 20 magnification with a maximum pixel resolution of 0.5 µm. ImageScope analysis software (Aperio Technologies, Vista, CA) was used for viewing and analysing digital images. Aperio Spectrum software was used to generate individual tissue spot images for automated analysis. The Colour Deconvolution algorithm (Aperio Technologies) was used to obtain quantitative values for average positive intensity (average intensity of pixels positively stained, graded from 0, 1, 2, 3) and total percent positive (percentage of positive stained area in relation to total area of the core). Histoscores were calculated as described above.

Survival analysis

PFS was calculated as the time between the surgery that procured the sample and the date of disease progression or of a new metastatic event in a different location. Pathologist's and automated *H* score were used to separate patients with high (above median) and low (below median) expression of each marker protein included in this study. In case more than one tissue core with satisfactory quality was available for a single patient, the average *H* score was considered. Log-rank testing was used to compare the two groups over a follow-up time of 36 months. Log-rank testing for trends was used when comparing three groups. Kaplan–Meier survival curves were generated and compared using GraphPad Prism (version 4.03). For analysis of data stored in the cancer genome atlas (TCGA), normalised mRNA expression data (upper quartile normalised Fragments per Kilobase of transcript per million mapped reads, $\log_2$(FPKM-UQ + 1)) generated by the Genomic Data Commons (GDC-NIH) were downloaded from the UCSC-XENA browser[25,26]. The SKCM cohort, unlike other TCGA data sets, contains mainly metastatic samples[27] (370 out of 477), some of which were collected a long time after initial diagnosis of the primary melanoma[28]. In order to correlate mRNA expression to progression of metastatic disease, the '*new tumour event free survival*' was calculated as the time between sample collection and the first new tumour event (in case of multiple new tumour events during the follow-up time) or, in case of no new tumour events, death. If a new tumour event was reported before the date of sample collection, the patient was excluded from the sub-cohort. Follow-up data and associated clinical records were downloaded from Broad GDAC Firehose[29] (new tumour event time from initial diagnosis) and UCSC-XENA browser[25,26] (overall survival from initial diagnosis), respectively. Sample collection information are available through the GDC data portal[30,31] (time from initial diagnosis to sample collection). As treatment information are not routinely available for all deposited metastatic melanoma cases, we downselected the cohort to stage III/IV melanoma patients diagnosed with metastatic melanoma before 2010, to ensure that chemotherapy-based treatment options would have been the standard first line of treatment ($n = 79$ patients). An optimised chi-square-based cutoff was determined to divide patients with high and low *BAX*, *BAK1* and *DIABLO* (Smac) mRNA amounts, and the two groups were compared by log-rank test. The cutoff for each marker was obtained by selecting the cohort separation that resulted in the highest chi-squared value with the function *survdiff* of the library *survival* in R (version 3.4.0). Median cutoff-based results are reported in Supplementary Fig. 4. Log-rank test for trend was used when comparing three groups. Kaplan–Meier survival curves were generated and compared using GraphPad Prism (version 4.03).

Data-driven modelling and pattern recognition

A data-driven modelling approach based on a previously published method[32] was developed to predict patients' PFS using *H* scores generated by automated image

analysis as input. The pipeline was developed for MATLAB (version 2016a, The Mathworks, UK), equipped with the statistical toolbox. Prior to the analysis, patients with a complete protein panel ($n = 50$) were divided into two PFS categories: PFS > 12 months ($n = 17$) and PFS < 12 months ($n = 33$). After standardisation of the initial data set, a principal component analysis (PCA) was performed and the principal components (PC) with an eigenvalue > 1 were considered for subsequent analyses. The patients were positioned in the 3D space defined by the first three PCs according to the scores computed by PCA, and linear discriminant analysis (LDA) was used to test the class segmentation accuracy. To evaluate the predictive potential of the framework, leave one out cross validation (LOOCV) followed by LDA was applied iteratively to the data set, using 49 patients as training set and one patient as test at each iteration. LDA was also applied to a data set reduced to three proteins (Bax, Bak and Smac), skipping the initial dimensionality reduction step. PCA and LDA were performed using the functions *pca* and *classify*, respectively. The predictive performance of the two classification models was compared by computing the area under the curve (AUC) with the function *perfcurve*.

Results

Low expression of pro-apoptotic proteins Bax, Bak and Smac correlates with increased PFS in chemotherapy-treated metastatic melanoma

Genotoxic chemotherapy based on DNA-alkylating agents such as dacarbazine induces intrinsic apoptosis, preferentially in proliferating cells such as cancer cells. Intrinsic apoptosis is governed by the family of Bcl-2 proteins and the subsequent signalling network of the apoptosis execution phase. We therefore tested key players of this apoptosis signalling modules as potential prognostic markers in metastatic melanoma. In total, we analysed the expression of six pro-apoptotic (Bax, Bak, Smac, Procaspase-9, Apaf-1, Procaspase-3) and three antiapoptotic proteins (Bcl-2, Bcl-xL, XIAP) in metastatic melanoma samples spotted on TMAs. Only treatment-naive samples from metastases were used for subsequent analyses. Information such as patient demographics, histopathology and staging, treatment and follow-up are provided as Supplementary Table 1 and are summarised in Table 1. Following comprehensive antibody validation (Supplementary Fig. 1A–D), IHC stains for $n = 58$ tumour metastases matching the inclusion criteria were analysed from the TMAs. Only tissue samples passing independent pathologist quality control for tissue integrity and staining artifacts were considered for subsequent analyses (Supplementary Table 2). TMAs scans were then used to generate mark-up images of the tissue cores, followed by automated quantification of staining intensities (see methods). The dynamic range of the staining intensities allowed to confidently define quartiles of negative, low, medium and high staining for protein expression (see Fig. 1a for examples for Bax, Bak and Smac). From these, *H* scores were calculated for each tumour sample (Fig. 1b), thereby allowing comparison with best practice manual scoring (see Fig. 2). To test if protein expression amounts and patient prognosis correlate, we performed survival analyses for all nine apoptosis regulatory proteins. Kaplan–Meier curves representing PFS from the date of sample procurement showed that low amounts of pro-apoptotic proteins Bax, Bak and Smac significantly correlated with better prognosis (Fig. 1c). With the exception of Procaspase-9, which associated with better prognosis in this analysis, none of the other proteins (Bcl-2, Bcl-xL, Apaf-1, XIAP and Procaspase-3) individually correlated with better or worse prognosis (Supplementary Fig. 2). Overall, these results surprisingly indicate that low amounts of apoptosis-inducing proteins Bax, Bak and Smac are linked to a better prognosis in chemotherapy-treated metastatic melanoma.

Manual scoring confirms association of low Bak, Bax and Smac protein expression with improved PFS

To further validate our findings, we next conducted best practice manual scoring of the stained TMAs. *H* scores for all marker candidates were obtained from two independent pathologists, both blinded to patient PFS. Plotting *H* scores obtained by automated analysis against manual *H* scores, we noted that manual scores strongly clustered at values of ~ 200, whereas automated scoring provided higher granularity across the entire dynamic range (Fig. 2a, Fig. 1b, Supplementary Table 2). This highlights that manual scoring appears limited in differentiating within the range of medium staining intensities and frequencies. Nevertheless, median separation of patient samples based on manual *H* scores provided survival curves for Bax, Bak and Smac staining that were very similar to those obtained by automated scoring (Fig. 2b). In contrast, the manual scores for all other proteins failed to separate patients with high and low PFS (Supplementary Fig. 3). These results therefore demonstrate that the Bax, Bak and Smac signatures are robust enough to also be captured in routine manual IHC-based biomarker discovery workflows.

Combined low expression of Bax, Bak and Smac is a combinatorial marker candidate for improved PFS

During apoptosis, Bax and Bak form pores in the outer mitochondrial membrane, leading to Smac release into the cytosol. Owing to the significant correlation of the single proteins with PFS and their direct relationship within the apoptosis signal transduction cascade, we checked if combinations of the three markers could

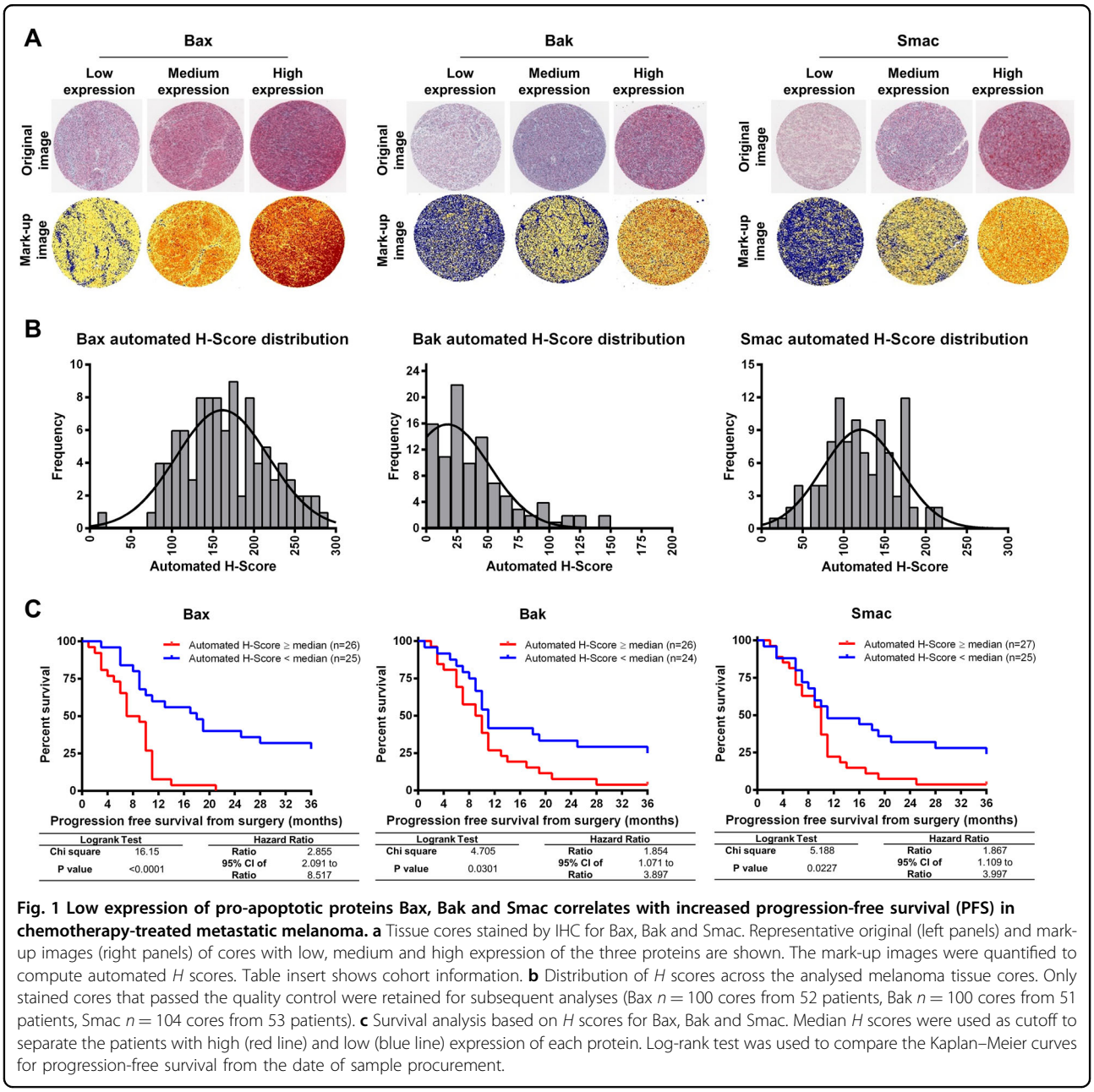

Fig. 1 Low expression of pro-apoptotic proteins Bax, Bak and Smac correlates with increased progression-free survival (PFS) in chemotherapy-treated metastatic melanoma. a Tissue cores stained by IHC for Bax, Bak and Smac. Representative original (left panels) and mark-up images (right panels) of cores with low, medium and high expression of the three proteins are shown. The mark-up images were quantified to compute automated *H* scores. Table insert shows cohort information. **b** Distribution of *H* scores across the analysed melanoma tissue cores. Only stained cores that passed the quality control were retained for subsequent analyses (Bax $n = 100$ cores from 52 patients, Bak $n = 100$ cores from 51 patients, Smac $n = 104$ cores from 53 patients). **c** Survival analysis based on *H* scores for Bax, Bak and Smac. Median *H* scores were used as cutoff to separate the patients with high (red line) and low (blue line) expression of each protein. Log-rank test was used to compare the Kaplan–Meier curves for progression-free survival from the date of sample procurement.

improve prognostication of PFS. For the $n = 50$ patients for which *H* scores for Bax, Bak and Smac were available, we noted that combined low or high staining for all three markers was restricted to subsets of the tumour samples (Fig. 3a). We therefore divided the cohort into three groups of combined high expression, heterogeneous expression and combined low expression. PFS-based survival analysis of the three groups demonstrated that patients harbouring tumours with combined low expression of Bax, Bak and Smac showed significantly improved PFS, extending beyond 36 months for 50% of this subgroup (Fig. 3b). In contrast, when only one or two markers where expressed in low amounts, PFS improved only slightly (median PFS = 10 months vs. 8.5 months when all three markers were highly expressed) (Fig. 3b). Overall, this shows that Bax, Bak and Smac could jointly define a signature that strongly associates with PFS, with combined low expression indicating improved PFS.

TCGA-SKCM-based analysis validates the prognostic Bax, Bak, Smac signature

To independently validate the prognostic potential of Bax, Bak and Smac expression, we analysed transcriptome data of $n = 79$ metastatic melanoma patients from the TCGA-SKCM cohort (Table 2). The survival analysis revealed that low *BAX*, *BAK1* and *DIABLO*

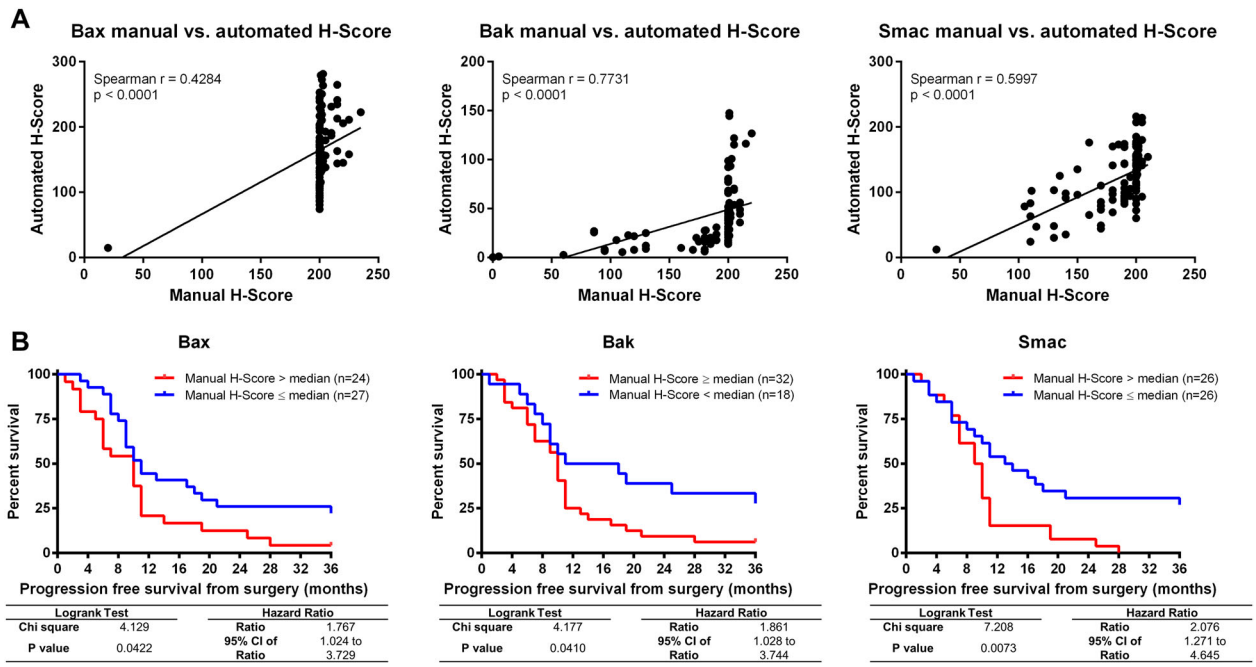

Fig. 2 Manual scoring confirms association of low Bak, Bax and Smac protein expression with improved PFS. a Correlation between automated and manual *H* scores. Manual scores were obtained from two independent pathologists blinded to patient follow-up. Correlation was analysed using Spearman's rank correlation coefficient. **b** Median *H* scores were used as cutoff to separate the patients with high (red line) and low (blue line) expression of each protein. Log-rank test was used to compare the Kaplan–Meier curves for progression-free survival from the date of sample procurement.

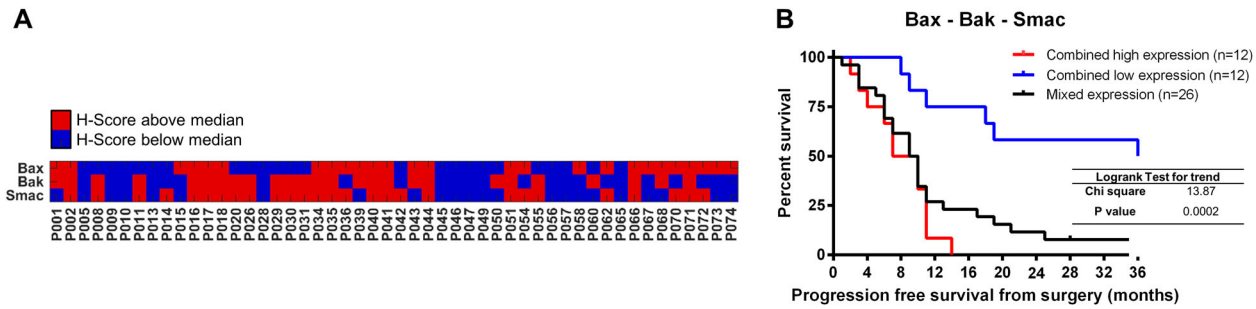

Fig. 3 Combined low expression of Bax, Bak and Smac is a combinatorial marker candidate for improved progression-free survival. **a** Expression profiles based on the *H* scores of Bax, Bak and Smac (blue: automated *H* score below median, red: above median) in $n = 50$ patients. **b** Survival analysis for the cohort based on the expression profiles shown in a. Log-rank test for trend was used to compare three Kaplan–Meier curves representing patients with low Bax, Bak and Smac *H* scores (blue) vs. mixed and high expression (black and red, respectively).

(*SMAC*) mRNA amounts significantly correlate with better prognosis (Fig. 4a). As previously observed at protein level, the expression pattern between *BAX*, *BAK1* and *DIABLO* was heterogeneous across the cohort (Fig. 4b). Patients with low tumour mRNA amounts across all three markers had a significantly better prognosis than patients in which at least one marker was highly expressed (Fig. 4c). Taken together, these results recapitulate in an independent cohort the trends observed at protein level, confirming the prognostic potential of Bax, Bak and Smac as a combinatorial marker in chemotherapy-treated metastatic melanoma.

Pattern recognition allows predicting patient prognosis

We next applied a data-driven pattern recognition approach to study if the Bax, Bak, Smac signature would be sufficiently strong to predict patient PFS from protein expression profiles[32]. First, *H* scores from automated TMA analysis for all marker candidates were subjected to

Table 2 Patient demographics and clinical information of the metastatic SKCM-TCGA sub-cohort.

Characteristics		
Gender	*Value*	*%*
Female	32	40.51
Male	47	59.49
Ethnicity	*Value*	*%*
White (non-Hispanic or Latino)	79	100
Disease stage at initial diagnosis	*Value*	*%*
Stage III	68	86.08
Stage IV	11	13.92
Age at diagnosis (years)		
Mean	55.5	
Median	55	
Range	18–87	
Overall survival from initial diagnosis (months)		
Mean	35.1	
Range	2.6–175.2	
Overall survival from sample procurement (months)		
Mean	15.9	
Range	1.1–64.9	

a PCA (applied to the 50 patient samples for which the complete nine protein panel was available). Patient tumours were positioned into a 3D space defined by the first three PCs and colour-coded to represent high or low PFS (PFS > 12 months and PFS < 12 months). Visually inspecting the scatter plot, we noticed a tendency of patients with high or low PFS to occupy distinct sub-regions of the PC space (Fig. 5a). To objectively assess the quality of this segregation, we applied LDA. LDA segmentation encouragingly separated 72% of the patients into their correct prognosis sub-space. Next, we tested if these patterns were sufficiently strong to also predict the PFS category on a case-by-case basis. To do so, we performed leave one out cross validation (LOOCV). At each iteration, the PFS category of one patient was predicted after using the remaining 49 patients as a training set that defined the PCA subspaces for high and low PFS. The panel of nine apoptosis regulatory proteins allowed to correctly predict high or low PFS in 74% of patients. Since our previous survival analyses (Fig. 1) showed that only Bax, Bak and Smac consistently correlated with PFS, we likewise tested if a similarly good or even better performing classifier can be derived from those three markers alone. Indeed, cluster segmentation and prediction accuracy tended to improve to 80% and 78% accuracy, respectively (Fig. 5b). In conclusion, as highlighted by the comparison of receiver operating characteristic (ROC) curves (Fig. 5c), classification based on the Bax-Bak-Smac signature alone is sufficient to obtain high prediction accuracies for patient PFS, whereas the remaining protein markers do not carry meaningful information to improve these predictions. Overall, this strengthens the evidence for low Bax, Bak and Smac expression being associated with better prognosis in metastatic melanoma and points out a route by which pattern recognition allows generating predictions for patient prognosis.

Discussion

Apoptosis is the major cell death modality by which anticancer therapies eliminate malignant neoplastic cells. In this study, we assessed if proteins that regulate the two major apoptosis decision hubs, namely the apoptotic engagement of mitochondria and the terminal execution phase of apoptosis[33], alone or in combination can serve to prognosticate PFS in metastatic melanoma patients undergoing dacarbazine-based chemotherapy. We found that low rather than high expression of the pro-apoptotic proteins Bax, Bak and Smac correlates with higher PFS, and that these three proteins in combination can serve as a combinatorial prognostic marker with a promising AUC of 0.79.

Owing to the central role of apoptosis in tumour cell elimination, the finding that low expression of pro-apoptotic proteins correlated with better prognosis in metastatic melanoma contradicted our expectations. However, counter-intuitive relationships between the expression patterns of apoptosis inducers or antiapoptotic genes or proteins were reported previously. For example, high expression of Bax was found to correlate with an increased risk for relapse in childhood acute lymphoblastic leukaemia[34]. High expression of Bax, measured as transcript and protein amounts, respectively, has also been associated with poor prognosis in acute myeloid leukaemia and non-Hodgkin lymphoma[35,36]. Similarly, studies in which high expression of the Bax antagonist Bcl-2 has been reported to correlate with better prognosis can be found for colorectal, breast, glioma, gastric and non small cell lung cancer[37–43]. Bax and Bcl-2 are the best-characterised members of the Bcl-2 protein family, which controls mitochondrial engagement in apoptosis signal transduction[44,45], whereas Bak has been less thoroughly studied. Bak functions as a Bax-like protein and upon activation likewise is able to form pores in the outer mitochondrial membrane, thereby triggering apoptosis execution[44,45]. Links between low Bak expression and an improved outcome have not been reported in metastatic melanoma so far, but reduced *BAK* mRNA amounts were associated with better overall survival in hepatocellular carcinoma[46]. Similarly, a counter-intuitive prognostic value of Smac has not yet been reported in melanoma, but

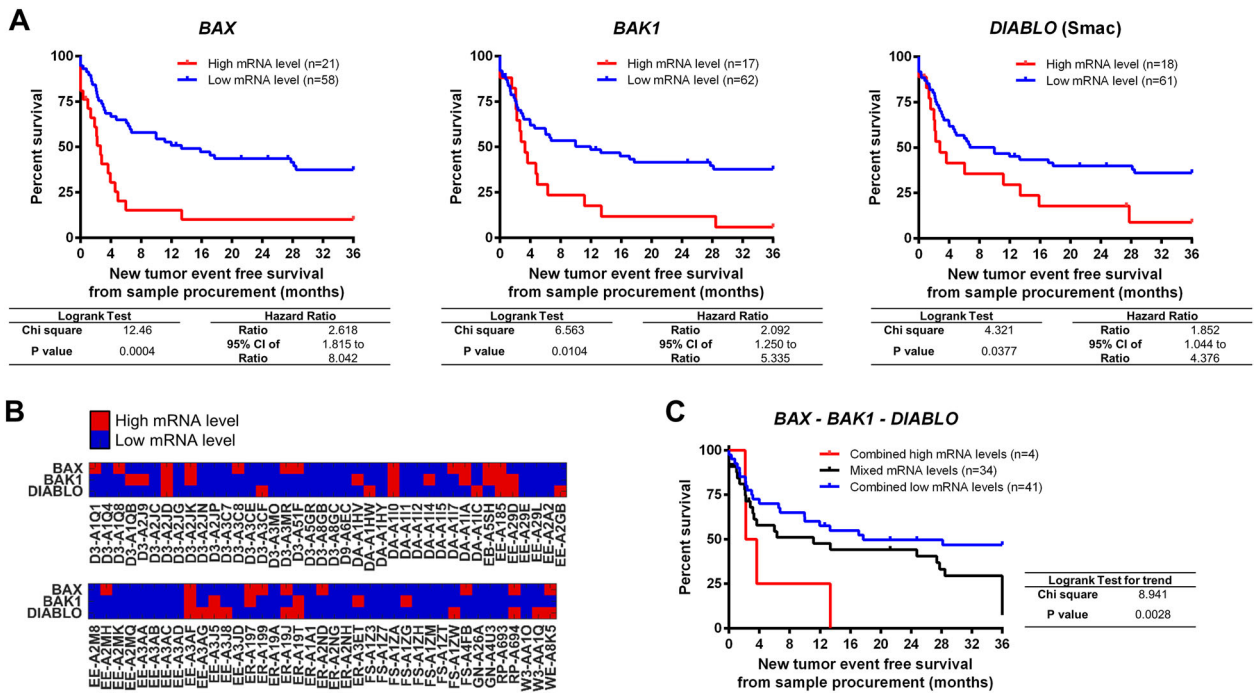

Fig. 4 TCGA-SKCM-based analysis validates the prognostic Bax, Bak, Smac signature. Independent validation of the prognostic signature at transcriptome level in the SKCM-TCGA metastatic sub-cohort. **a** Survival analysis in the SKCM-TCGA sub-cohort ($n = 79$ patients diagnosed with stage III or IV metastatic melanoma before 2010). An optimised chi-square-based cutoff was determined to divide patients with high (red) and low (blue) normalised *BAX*, *BAK1* and *DIABLO* (Smac) expression ($\log_2$(FPKM-UQ + 1)). Kaplan–Meier curves (follow-up from sample procurement) were compared by log-rank test. **b** mRNA amounts for *BAX*, *BAK1* and *DIABLO* (Smac) (blue: mRNA level below cutoff, red: mRNA level above cutoff). **c** Survival analysis in the metastatic TCGA-SKCM sub-cohort based on the expression profiles in Fig. 4b. Log-rank test for trend was used to compare three Kaplan–Meier curves representing patients with combined low *BAX*, *BAK1* and *DIABLO* (Smac) expression (blue), combined high expression (red) or with mixed expression (black).

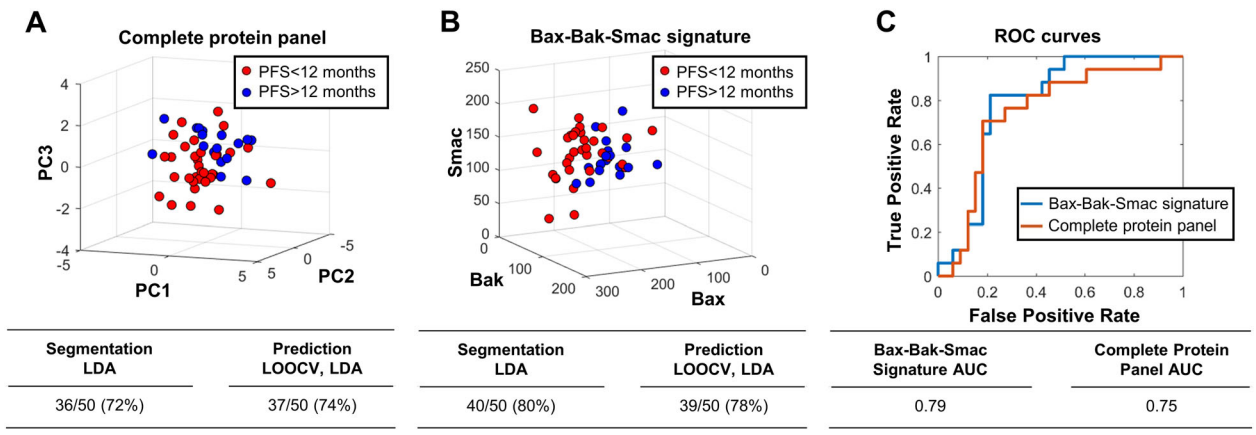

Segmentation LDA	Prediction LOOCV, LDA	Segmentation LDA	Prediction LOOCV, LDA	Bax-Bak-Smac Signature AUC	Complete Protein Panel AUC
36/50 (72%)	37/50 (74%)	40/50 (80%)	39/50 (78%)	0.79	0.75

Fig. 5 Pattern recognition allows predicting patient prognosis. a A principal component analysis was performed on the *H* scores of nine apoptotic proteins. To provide a visualisation of the spatial clustering, patients samples were positioned in a 3D scatter plot defined by the first three principal components and colour-coded according to their PFS time (red < 12 months, $n = 33$; blue > 12 months, $n = 17$). Linear discriminant analysis (LDA) correctly segmented 72% of the patients. Leave One Out Cross Validation (LOOCV) combined with LDA predicted the correct class for 74% of the patients. **b** 3D scatter plot showing the spatial clustering of patients with short and long PFS based on the *H* scores for Bax, Bak and Smac. LDA correctly segmented 80% of the patients and LOOCV-LDA achieved 78% prediction accuracy. **c** Comparison of the performance of the two classifiers shown in **a** and **b**. The receiver operating characteristic curves (ROCs) and respective areas under the curve (AUC) are shown.

high expression was found to correlate with early local disease recurrence in cervical cancer[47]. It needs to, however, be stated that in reverse a large body of literature associates high expression of pro-apoptotic or a low expression of antiapoptotic genes or proteins with better outcome, as would intuitively be expected (see e.g., ref. [48–59]). Overall, it therefore appears that signatures indicative of apoptosis competency or resistance need to be interpreted or studied within the specific disease setting and context. For example, it was suggested that expression patterns indicative of high apoptosis responsiveness may correlate with poor outcome if dormant, stem-like cancer cells that may reside within tumour tissues re-populate tumours and promote further spread and progression of the disease after the bulk population of cells has been eliminated by apoptosis-inducing therapy[42,43]. In line with this, apoptotic cell loss can drive the proliferation of surrounding cells, for example, through caspase-dependent prostaglandin signalling and secretion of other proliferation stimulating factors from dying cells[60,61]. These signalling processes indeed might be of relevance in melanoma treatment responsiveness and disease relapse[62].

As apoptosis resistance is a hallmark of cancer[63], it nevertheless appears puzzling that reduced expression of apoptosis drivers correlates with better prognosis in a treatment scenario that is clearly geared towards apoptosis induction. In addition to the above line of thoughts, the very high mutation burden of cutaneous melanoma[64] might provide the basis for an additional explanation. Although unfavourable expression of key apoptosis regulators in many cases may cause apoptotic cell death to be suppressed during cell transformation, tumour development and disease progression, and as such could be considered causative for the disease, such low basal apoptosis susceptibilities might nevertheless be overcome by elevated apoptosis-inducing stress in chemotherapy settings. In contrast, where low apoptosis susceptibility is not causative for the disease (and hence protein expression profiles would indicate "normal" susceptibility), other alterations and mutations might drive the development and progression of the disease. Many of these could prevent therapy-induced stress signals to be channelled towards apoptosis induction. Indeed, low expression of Bax and Bak might be linked to disease progression in earlier stages of melanoma. Although Bax protein expression tends to be higher in melanoma tissues than in benign nevi[65], low expression of Bax within primary superficial-spreading melanoma was associated with poor prognosis and therefore could indicate a role in disease development and progression[66]. Similar findings were reported for Bak expression in the same study. Also in stage IIa melamoma, low Bax and Bak protein expression was associated with poor prognosis, with the majority of such patients developing metastatic disease[67]. Taken together, these prior reports combined with our findings therefore suggest that low expression of pro-apoptotic players could be causative for early stage tumour formation and melanoma disease progression by lowering basal apoptosis susceptibility, and that this reduced susceptibility can be overcome once pro-apoptotic stress is elevated externally, for example by dacarbazine-based chemotherapy. It will be interesting to see if similar relationships can also be found in other cancer (sub)types in the future.

Acknowledgements
We kindly acknowledge support by the European Union's Horizon 2020 research and innovation programme under the Marie Skłodowska-Curie grant agreement #642295 (MEL-PLEX) and by the European Union's FP7 Marie Skłodowska-Curie Industry-Academia Partnership and Pathways research programme under the grant agreement #611107 (SYS-MEL). M.R. and C.G. are funded by the Deutsche Forschungsgemeinschaft (DFG, German Research Foundation) under Germany's Excellence Strategy - EXC 2075 – 390740016. M.R. also receives support from the German Research Foundation (FOR2036 (MO 3226/1–1)) and the Health Research Board Ireland (HRA POR 2015 1091). J. W. received a postdoctoral research fellowship from *Kom op tegen Kanker* (Stand up to Cancer), the Flemish Cancer Society, and is currently funded by a postdoctoral fellowship from *Stichting tegen Kanker* (Foundation against Cancer), the Belgian Cancer Society.

Author details
[1]Institute of Cell Biology and Immunology, University of Stuttgart, Stuttgart, Germany. [2]Oncomark Ltd., Nova UCD, Dublin 4, Ireland. [3]UCD School of Biomolecular and Biomedical Science, UCD Conway Institute, University College Dublin, Dublin 4, Ireland. [4]Pathology Diagnostics Ltd., Stirling House Business Centre, Waterbeach, Cambridge, UK. [5]Translational Cell and Tissue Research, KU Leuven (University of Leuven), Leuven, Belgium. [6]Department of Physiology and Medical Physics, Royal College of Surgeons in Ireland, Dublin 2, Ireland. [7]Centre for Systems Medicine, Royal College of Surgeons in Ireland, Dublin 2, Ireland. [8]VIB-KU Leuven Center for Brain & Disease Research, KU Leuven, Leuven, Belgium. [9]Department of Human Genetics, KU Leuven (University of Leuven), Leuven, Belgium. [10]Stuttgart Research Center Systems Biology, University of Stuttgart, Stuttgart, Germany. [11]Stuttgart Center for Simulation Science (SC SimTech), University of Stuttgart, Stuttgart, Germany

Competing interests
The authors declare that they have no conflict of interests.

Supplementary Information accompanies this paper at (https://doi.org/10.1038/s41419-020-2309-3).

Received: 5 December 2019 Revised: 29 January 2020 Accepted: 30 January 2020
Published online: 13 February 2020

References

1. Heppt, M. V. et al. The systemic management of advanced melanoma in 2016. *Oncol. Res. Treat.* **39**, 635–642 (2016).
2. Margolin, K. The promise of molecularly targeted and immunotherapy for advanced melanoma. *Curr. Treat. Options Oncol.* **17**, 1–14 (2016).
3. Domingues, B., Lopes, J., Soares, P. & Populo, H. Melanoma treatment in review. *ImmunoTargets Ther.* **7**, 35–49 (2018).
4. Lui, P. et al. Treatments for metastatic melanoma: synthesis of evidence from randomized trials. *Cancer Treat. Rev.* **33**, 665–680 (2007).

5. Gupta, A., Gomes, F. & Lorigan, P. The role for chemotherapy in the modern management of melanoma. *Melanoma Manag* **4**, 125–136 (2017).
6. Middleton, M. R. et al. Randomized phase III study of temozolomide versus dacarbazine in the treatment of patients with advanced metastatic malignant melanoma. *J. Clin. Oncol.* **18**, 158–158 (2000).
7. Bedikian, A. Y. et al. Bcl-2 antisense (oblimersen sodium) plus dacarbazine in patients with advanced melanoma: the oblimersen melanoma study group. *J. Clin. Oncol.* **24**, 4738–4745 (2006).
8. Atkins, M. B. et al. Phase III trial comparing concurrent biochemotherapy with cisplatin, vinblastine, dacarbazine, interleukin-2, and interferon alfa-2b with cisplatin, vinblastine, and dacarbazine alone in patients with metastatic malignant melanoma (e3695): a trial coordinated by the Eastern Cooperative Oncology Group. *J. Clin. Oncol.* **26**, 5748–5754 (2008).
9. Anvekar, R. A. et al. Sensitization to the mitochondrial pathway of apoptosis augments melanoma tumor cell responses to conventional chemotherapeutic regimens. *Cell Death Dis.* **3**, 1–11 (2012).
10. Sanada, M. et al. Modes of actions of two types of anti-neoplastic drugs, dacarbazine and ACNU, to induce apoptosis. *Carcinogenesis* **28**, 2657–2663 (2007).
11. Czabotar, P. E., Lessene, G., Strasser, A. & Adams, J. M. Control of apoptosis by the BCL-2 protein family: implications for physiology and therapy. *Nat. Rev. Mol. Cell Biol.* **15**, 49–63 (2014).
12. Tait, S. W. G. & Green, D. R. Mitochondria and cell death: outer membrane permeabilization and beyond. *Nat. Rev. Mol. Cell Biol.* **11**, 621–632 (2010).
13. Hellwig, C. T., Passante, E. & Rehm, M. The molecular machinery regulating apoptosis signal transduction and its implication in human physiology and pathophysiologies. *Curr. Mol. Med.* **11**, 31–47 (2011).
14. Hanahan, D. & Weinberg, R. A. Hallmarks of cancer: the next generation. *Cell* **144**, 646–674 (2011).
15. Soengas, M. S. & Lowe, S. W. Apoptosis and melanoma chemoresistance. *Oncogene* **22**, 3138–3151 (2003).
16. Lev, D. C. et al. Exposure of melanoma cells to dacarbazine results in enhanced tumor growth and metastasis in vivo. *J. Clin. Oncol.* **22**, 2092–2100 (2004).
17. Charles, E. M. & Rehm, M. Key regulators of apoptosis execution as biomarker candidates in melanoma. *Mol. Cell Oncol.* **1**, e964037 (2014).
18. Anvekar, R. A., Asciolla, J. J., Missert, D. J. & Chipuk, J. E. Born to be alive: a role for the BCL-2 family in melanoma tumor cell survival. *Apoptosis Treat. Front. Oncol.* **1**, 1–16 (2011).
19. Cummins, J. M. et al. X-linked inhibitor of apoptosis protein (XIAP) is a non-redundant modulator of tumor necrosis factor-related apoptosis-inducing ligand (TRAIL)-mediated apoptosis in human cancer cells. *Cancer Res.* **64**, 3006–3008 (2004).
20. Geserick, P. et al. Suppression of cFLIP is sufficient to sensitize human melanoma cells to TRAIL- and CD95L-mediated apoptosis. *Oncogene* **27**, 3211–3220 (2008).
21. Kohli, M. et al. SMAC/Diablo-dependent apoptosis induced by nonsteroidal antiinflammatory drugs (NSAIDs) in colon cancer cells. *Proc. Natl Acad. Sci. USA* **101**, 16897–16902 (2004).
22. Samraj, A. K., Keil, E., Ueffing, N., Schulze-Osthoff, K. & Schmitz, I. Loss of caspase-9 provides genetic evidence for the type I/II concept of CD95-mediated apoptosis. *J. Biol. Chem.* **281**, 29652–29659 (2006).
23. Soengas, M. S. et al. Inactivation of the apoptosis effector Apaf-1 in malignant melanoma. *Nature* **409**, 207–211 (2001).
24. Wang, C. & Youle, R. J. Predominant requirement of Bax for apoptosis in HCT116 cells is determined by Mcl-1's inhibitory effect on Bak. *Oncogene* **31**, 3177–3189 (2012).
25. UCSC Xena. Available at: https://xena.ucsc.edu/. (Accessed 24 Oct 2018).
26. Goldman, M. et al. The UCSC Xena platform for public and private cancer genomics data visualization and interpretation. *bioRxiv* 326470 (2019). https://doi.org/10.1101/326470.
27. Liu, J. et al. An integrated TCGA pan-cancer clinical data resource to drive high-quality survival outcome analytics. *Cell* **173**, 400–416.e11 (2018).
28. Akbani, R. et al. Genomic classification of cutaneous melanoma. *Cell* **161**, 1681–1696 (2015).
29. Broad Institute TCGA Genome Data Analysis Center. Analysis-ready standardized TCGA data from Broad GDAC Firehose 2016_01_28 run. *Broad Institute of MIT and Harvard* (2016). https://doi.org/10.7908/C11G0KM9.
30. GDC Data Portal. Available at: https://portal.gdc.cancer.gov/. (Accessed 25 Oct 2018).
31. Grossman, R. L. et al. Toward a shared vision for cancer genomic data. *N. Engl. J. Med.* **375**, 1109–1112 (2016).
32. Passante, E., Würstle, M. L., Hellwig, C. T., Leverkus, M. & Rehm, M. Systems analysis of apoptosis protein expression allows the case-specific prediction of cell death responsiveness of melanoma cells. *Cell Death Differ.* **20**, 1521–1531 (2013).
33. Taylor, R. C., Cullen, S. P. & Martin, S. J. Apoptosis: controlled demolition at the cellular level. *Nat. Rev. Mol. Cell Biol.* **9**, 231–241 (2008).
34. Hogarth, L. A., Hall, A. G. & Increased, B. A. X. expression is associated with an increased risk of relapse in childhood acute lymphocytic leukemia. *Blood* **93**, 2671–2678 (1999).
35. Köhler, T. et al. High Bad and Bax mRNA expression correlate with negative outcome in acute myeloid leukemia (AML). *Leukemia* **16**, 22–29 (2002).
36. Bairey, O., Zimra, Y., Shaklai, M., Okon, E. & Rabizadeh, E. Bcl-2, Bcl-X, Bax, and Bak expression in short- and long-lived patients with diffuse large B-cell lymphomas. *Clin. Cancer Res.* **5**, 2860–2866 (1999).
37. Meterissian, S. H. et al. Bcl-2 is a useful prognostic marker in Dukes' B colon cancer. *Ann. Surg. Oncol.* **8**, 533–537 (2001).
38. Vargas-Roig, L. M. et al. Prognostic value of Bcl-2 in breast cancer patients treated with neoadjuvant anthracycline based chemotherapy. *Mol. Oncol.* **2**, 102–111 (2008).
39. McDonald, F. E. et al. The prognostic influence of bcl-2 in malignant glioma. *Br. J. Cancer* **86**, 1899–1904 (2002).
40. Inada, T., Kikuyama, S., Ichikawa, A., Igarashi, S. & Ogata, Y. Bcl-2 expression as a prognostic factor of survival of gastric carcinoma. *Anticancer Res.* **18**, 2003–2010 (1998).
41. Renouf, D. J. et al. BCL-2 expression is prognostic for improved survival in non-small cell lung cancer. *J. Thorac. Oncol.* **4**, 486–491 (2009).
42. Labi, V. & Erlacher, M. How cell death shapes cancer. *Cell Death Dis.* **6**, e1675 (2015).
43. Ichim, G. & Tait, S. W. G. A fate worse than death: apoptosis as an oncogenic process. *Nat. Rev. Cancer* **16**, 539–548 (2016).
44. Hantusch, A., Rehm, M. & Brunner, T. Counting on death – quantitative aspects of Bcl-2 family regulation. *FEBS J.* **285**, 4124–4138 (2018).
45. Kale, J., Osterlund, E. J. & Andrews, D. W. BCL-2 family proteins: changing partners in the dance towards death. *Cell Death Differ.* **25**, 65–80 (2018).
46. Kong, X. et al. ZBP-89 and Sp1 contribute to Bak expression in hepatocellular carcinoma cells. *BMC Cancer* **18**, 419 (2018).
47. Arellano-Llamas, A. et al. High Smac/DIABLO expression is associated with early local recurrence of cervical cancer. *BMC Cancer* **6**, 256 (2006).
48. Leverkus, M. & Gollnick, H. 'Bak (and Bax) to the future' - of primary melanoma prognosis? *J. Investig. Dermatol.* **126**, 1212–1214 (2006).
49. Kupryjańczyk, J. et al. Evaluation of clinical significance of TP53, BCL-2, BAX and MEKI expression in 229 ovarian carcinomas treated with platinum-based regimen. *Br. J. Cancer* **88**, 848–854 (2003).
50. Baekelandt, M., Holm, R., Nesland, J. M., Tropé, C. G. & Kristensen, G. B. Expression of apoptosis-related proteins is an independent determinant of patient prognosis in advanced ovarian cancer. *J. Clin. Oncol.* **18**, 3775–3781 (2000).
51. Del Poeta, G. et al. Amount of spontaneous apoptosis detected by Bax/Bcl-2 ratio predicts outcome in acute myeloid leukemia (AML). *Blood* **101**, 2125–2131 (2003).
52. Jeong, S. H. et al. Low expression of bax predicts poor prognosis in resected non-small cell lung cancer patients with non-squamous histology. *Jpn. J. Clin. Oncol.* **38**, 661–669 (2008).
53. Seok, Y. K. et al. Low expression of bax predicts poor prognosis in patients with locally advanced esophageal cancer treated with definitive chemoradiotherapy. *Clin. Cancer Res.* **13**, 4146–4153 (2007).
54. Ma, J. et al. Bromodomain-containing protein 7 sensitizes breast cancer cells to paclitaxel by activating Bcl2-antagonist/killer protein. *Oncol. Rep.* **41**, 1487–1496 (2019).
55. Luo, Y. et al. High Bak expression is associated with a favorable prognosis in breast cancer and sensitizes breast cancer cells to paclitaxel. *PLoS ONE* **10**, e0138955 (2015).
56. Endo, K. et al. Clinical significance of Smac/DIABLO expression in colorectal cancer. *Oncol. Rep.* **21**, 351–355 (2009).
57. Dobrzycka, B. et al. Prognostic significance of smac/DIABLO in endometrioid endometrial cancer. *Folia Histochem. Cytobiol.* **48**, 678–681 (2010).
58. Grzybowska-Izydorczyk, O., Cebula, B., Robak, T. & Smolewski, P. Expression and prognostic significance of the inhibitor of apoptosis protein (IAP) family and its antagonists in chronic lymphocytic leukaemia. *Eur. J. Cancer* **46**, 800–810 (2010).

59. Pluta, P. et al. Correlation of Smac/DIABLO protein expression with the clinicopathological features of breast cancer patients. *Neoplasma* **58**, 430–435 (2011).
60. Huang, Q. et al. Caspase 3–mediated stimulation of tumor cell repopulation during cancer radiotherapy. *Nat. Med.* **17**, 860–866 (2011).
61. Zhao, R. et al. Novel roles of apoptotic caspases in tumor repopulation, epigenetic reprogramming, carcinogenesis, and beyond. *Cancer Metastasis Rev.* **37**, 227–236 (2018).
62. Donato, A. L. et al. Caspase 3 promotes surviving melanoma tumor cell growth after cytotoxic therapy. *J. Invest. Dermatol.* **134**, 1686–1692 (2014).
63. Hanahan, D. & Weinberg, R. A. Hallmarks of cancer: the next generation. *Cell* **144**, 646–674 (2011).
64. Lawrence, M. S. et al. Mutational heterogeneity in cancer and the search for new cancer-associated genes. *Nature* **499**, 214–218 (2013).
65. Tang, L. et al. Expression of apoptosis regulators in cutaneous malignant melanoma. *Clin. Cancer Res.* **4**, 1865–1871 (1998).
66. Fecker, L. F. et al. Loss of proapoptotic Bcl-2-related multidomain proteins in primary melanomas is associated with poor prognosis. *J. Invest. Dermatol.* **126**, 1366–1371 (2006).
67. Tchernev, G. & Orfanos, C. E. Downregulation of cell cycle modulators p21, p27, p53, Rb and proapoptotic Bcl-2-related proteins Bax and Bak in cutaneous melanoma is associated with worse patient prognosis: preliminary findings. *J. Cutan. Pathol.* **34**, 247–256 (2007).